



**REGIONAL UNIVERSITY OF CARIRI - URCA**  
**DEPARTMENT OF BIOLOGICAL CHEMISTRY - DQB**  
**GRADUATE PROGRAM IN BIOLOGICAL CHEMISTRY - PPQB**

**JAYZE DA CUNHA XAVIER**

**SYNTHESIS, SPECTROSCOPIC CHARACTERIZATION AND EVALUATION OF  
THE ANTIMICROBIAL AND ANXIOLYTIC EFFECT USING ADULT  
ZEBRAFISH (*Danio rerio*) SYNTHETIC CHALCONES**

**Crato**

**2022**



**REGIONAL UNIVERSITY OF CARIRI**  
**GRADUATE PROGRAM IN BIOLOGICAL CHEMISTRY**

Qualification Report of the Thesis presented to the Graduate Program in Biological Chemistry, of the Regional University of Cariri, as requirement to obtain the title of Doctor of Biological Chemistry.

Advisor: Hécio Silva dos Santos

Co-advisors: Alexandre Magno R. Teixeira  
Nitin Kumar

**Crato**

**2022**

---

Ficha catalográfica elaborada pelo autor através do sistema  
de geração automático da biblioteca central da universidade regional do cariri - URCA

Xavier, Jayze Da Cunha

X3s Synthesis, spectroscopic characterization and evaluation of the antimicrobial and anxiolytic effect using adult zebrafish (*Danio rerio*) synthetic chalcones Jayze da Cunha Xavier / Jayze Da Cunha Xavier. Crato-CE, 2022.

215p. il.

Tese. Programa de Pós-Graduação em Química Biológica da Universidade Regional do Cariri - URCA.

Orientador(a): Prof. Dr. Hécio Silva dos Santos

Coorientador(a): Prof. Dr. Alexandre Magno Rodrigues Teixeira e Nitin Kumar

1.Docking , 2.Microbiologia, 3.Bacteriano; I.Título.

CDD: 572

## Termo de Autorização para Publicação de Teses e Dissertações Eletrônicas

Na qualidade de titular dos direitos de autor da publicação abaixo identificada, autorizo à Universidade Regional do Cariri – URCA, a disponibilizar por tempo indeterminado ao alcance do público a obra abaixo citada, através do site <http://bdtd.ibict.br/bdtd/>, bem como da rede mundial de computadores – Internet, sem pagamento dos direitos autorais, de acordo com a Lei nº 9610/98, conforme permissões assinaladas, para fins de leitura, impressão e/ou download, a título de divulgação da produção científica brasileira, a partir desta data, atendendo à Portaria Nº 13 de 15/02/2006 da CAPES.

Identificação do Material Bibliográfico:	<input type="checkbox"/> Dissertação	<input checked="" type="checkbox"/> Tese
Autor: Jayze da Cunha Xavier		
CPF: 950189 133-04	RG:2008637205-4	
Nacionalidade: Brasileira	Estado Civil: solteira	
Endereço Completo: Rua Soriano Albuquerque, 166, Ap. 12.		
CEP: 63.105-195	Cidade: Crato	Estado: Ceará
Fone/Celular: (88)998006262	E-mail: jayzecx@gmail.com	
Título: Synthesis, Spectroscopic characterization and evaluation of the antimicrobial and anxiolytic effect using adult zebrafish ( <i>Danio rerio</i> ) synthetic chalcones		
Orientador: Hélcio Silva dos Santos		
Coorientadores: Alexandre Magno R. Teixeira and Nitin Kumar		
Membros da Banca: Sucheta		
Henrique Douglas Melo Coutinho		
Kirley Marques Canuto		
Carlos Emídio Sampaio Nogueira		
Emanuel Silva Marinho		
Data da Defesa: 29/07/2022	Curso: Química Biológica	
Área do Conhecimento: Microbiologia		
Palavras-Chave: docking, microbiologia, bacteriano		
3. Agência de Fomento: FUNCAP		
Informações de Acesso ao Documento: para publicação	<input checked="" type="checkbox"/> Acesso Total	<input type="checkbox"/> Acesso Parcial
Em caso de publicação parcial, especifique o(s) arquivo(s) e/ou capítulo(s) restrito(s):		

Crato, 29 de Julho de 2022.

Havendo concordância com a publicação eletrônica enviamos o(s) arquivo(s) em formato digital PDF da tese ou dissertação gerada a partir da versão final corrigida e aprovada pelo Orientador. A restrição (parcial ou total) poderá ser mantida por até dois anos a partir da data de autorização da publicação sob responsabilidade do Programa. A extensão deste prazo demandará justificativa formal apresentada será comunicada à CAPES

Assinatura do Autor:

Assinatura do Orientador:

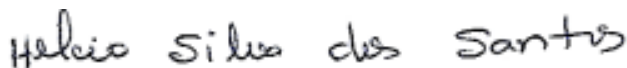
**JAYZE DA CUNHA XAVIER**

**SYNTHESIS, SPECTROSCOPIC CHARACTERIZATION AND EVALUATION OF  
THE ANTIMICROBIAL AND ANXIOLYTIC EFFECT USING ADULT ZEBRAFISH  
(*Danio rerio*) SYNTHETIC CHALCONES**

Qualification Report of the Thesis presented to the Graduate Program in Biological Chemistry, of the Regional University of Cariri, as requirement to obtain the title of Doctor of Biological Chemistry.

**The thesis report was defended and approved in: 29, July 2022**

**EXAMINATION BOARD**



---

**Prof. Dr. Hécio da Silva Santos**  
Orientador – (UVA).



---

**Prof. Dr. Henrique Douglas Melo Coutinho**  
Membro Titular Interno – URCA



---

**Prof. Dr. Carlos Augusto Nogueira**  
Membro Titular Interno - URCA



---

**Prof. Dr. Sucheta**  
Membro Titular Externo – KRMU

*Kirley Marques Canuto*

---

**Prof. Dr. Kirley Marques Canuto**  
**Membro Titular Externo – EMBRAPA**

*ESM*

---

**Prof. Dr. Emmanuel Silva Marinho**  
**Membro Externo – UECE**

---

**Prof. Diniz Maciel de Sena Junior**  
**Membro Suplente Interno -URCA**

I dedicate this work to God, my family for the encouragement, to the professors/advisors of the Biological Chemistry course, in which I am flattered to participate, for the perseverance and dedication, and to the friends for the support, all with their share of contribution somehow culminated in the successful conclusion of this.

---

## ACKNOWLEDGMENT

---

First of all, to God, for allowing the stage of my life to be with effort and dedication. To the parents Zélia and Jayme, who seem to have followed everything step by step, and in the greatest difficulties, they did not measure my exercises to be present and are at my side at a distance.

To my sibles Joyce, Junior, and Marcelino who are always present in my life despite the distance. You are very special! To my nephews Marina and Kayke who inspire me. Thanks to Professor Hécio who, from being a patient advisor, always respected them to teach us beyond and made me overcome the adjustment of adversities and unforeseen events. Thank you, especially for the trust and encouragement. To Professor Alexandre, for his constant cooperation during the co-orientation of this work. To my uncle and teacher Cunha for clarifying my day-to-day doubts and never losing my focus.

To Professor Henrique for the incentives and support since my course master's, his laboratory for carrying out the microbiological evaluations

To the postgraduate department in biological chemistry at URCA for technical support.

To Sunil, Sucheta, and Rakesh for the support with the English conversation, Gurpreet and Sukirt to reception and to Professor Nitin for supervising his teachers and following the effort to make my experience in Gurgaon-India possible, and for all the friends I made there.

To Funcap, for the financial support in Brazil, and to the Indian Program, scholarship number DCS/2019/000214, for the financial support during the period in India (March 2020 – September 2020) The Dean of Research and Graduate Studies at URCA for the course in biological chemistry for granting a scholarship from Funcap and for all the technical support to make part of the experiments carried out in the Thesis viable.

Thank you to all the friends who offered support as well as encouragement from all the friends who offered themselves directly or support for this work to come to fruition.

Thank you so much!



Title	Page
Table 1: Molecular structures of synthetic chalcones investigated in this thesis.	16
Figure 1: Fundamental structure of chalcones	20
Table 1. Antimicrobial activity of chalcones against <i>Staphylococcus aureus</i>	26
Scheme 1. Mechanism of the Claisen-Schmidt condensation reaction	30
Scheme 2. Types of bacterial resistance to antibiotics	31
Table 2- Interactions between <i>Staphylococcus aureus</i> TyrRS and chalcones	37
Figure 2: 2D maps of interactions between TyrRS-CHALSA1 (A), TyrRS-CHALSA2 (B), TyrRS-CHALSA3 (C), TyrRS-CHALSA4 (D) and TyrRS-CHALSA5 (E) complexes.	38
Fig. 3: TyrRS-CHALSA1 complex	38
Fig. 4: Three-dimensional structure of the TyrRS-SB239629 (A), TyrRS-CHALSA1 (B), TyrRS-CHALSA2 (C), TyrRS-CHALSA3 (D), TyrRS-CHALSA4 (E) and TyrRS-CHALSA5 (F) complexes.	39
Table 3. Predicted ADMET properties of the chalcone analogs A1-5.	40
Fig. 5: Ionized microspecies distribution of the Chalcones A1-5 analogs with the pH variation.	42
Scheme 1. Preparation of chalcone. a) NaOH 50 % w v <sup>-1</sup> , ethanol, t.a., 48 h.	60
Figure 1. Effect of Flumazenil (Fmz) under the anxiolytic effect of the Chalcone - Cinnamaldehyde in the Light & Dark Test. Chalcone - Cinnamaldehyde (0.5 mg / mL; 20 μL, i.p.). Dzp - Diazepam (1.0 mg / mL; 20 μL, i.p.). Fmz - flumazenil (0.1 mg / mL; 20 μL; i.p.). The values represent the mean ± standard error of the mean (E.P.M.) for 6 animals / group. ANOVA followed by Tukey (**** p<0.0001 vs. Naive or vehicle; #### p<0.0001 vs. Fmz + Dzp or Fmz + Chalcone).	63
Table 1. Interactions between the GABA <sub>A</sub> receptor and the chalcone ligand.	63
Figure 2. Interaction complex of inhibitor TE1 (A) and Chalcone (B) with the enzyme Carbonic Anhydrase II, and 2D map of interactions of the Carbonic Anhydrase II / chalcone complex (C).	64
Figure 3. Effect of cinnamaldehyde chalcone on pentylenetetrazole induced seizure in adult zebrafish, stage I (A), stage II (B), stage III (C). Dzp-Diazepam (1.0 mg/mL; 20 μL; p.o.); Vehicle – 3% DMSO (20 μL; p.o.). The values represent the mean ± standart error of the mean (E.P.M.) for 6 animals/group. ANOVA followed by Tukey (* p < 0.05, ** p < 0.01, *** p < 0.001, **** p < 0.0001 vs. Naive; ## p < 0.01 vs. Dzp).	65
Table 2. Interactions between the enzyme Carbonic Anhydrase II and the chalcone ligand	65
Figure 4. Diazepam (A) and Chalcone (B) interaction complex with the GABA <sub>A</sub> receptor, and 2D map of interactions of the GABA <sub>A</sub> / chalcone complex (C)	65
Scheme 1. Preparation of chalcone. a) NaOH 50% w v <sup>-1</sup> , ethanol, t.a., 48 h	67
Fig. 1. Optimized geometry of the title chalcone obtained at B3LYP/6-311++G(d,p) level	77

of theory.

**Fig. 2.** (a) Potential energy profiles of the title chalcone calculated at the B3LYP/6-311++G(d,p) level of theory for rotation around C6-C1-C $\beta$ -C $\alpha$  dihedral angle. The global and local minima for the optimized structures are indicated by means of open circle, and half open circle. In (b) and (c) are shown the conformers I and II, respectively, with their respective dihedral angle ( $\theta$ ), and potential energies (E), and with the blue planes containing the A ring, and the red planes containing the B ring 79

**Table 1.** <sup>1</sup>H and <sup>13</sup>C NMR data of the experimental and theoretical of title chalcone in CDCl<sub>3</sub>. Chemical shifts in  $\delta$ C and  $\delta$ H are in ppm. 80

**Table 2.** ATR-FTIR experimental frequencies (ATR-FTIR, in cm<sup>-1</sup>), calculated scaled vibrational wavenumbers (scal in cm<sup>-1</sup>) by the dual scale factor 0.983 (below 1700 cm<sup>-1</sup>) and 0.958 (above 1700 cm<sup>-1</sup>) and assignment for some of the vibrational modes for title chalcone (C<sub>19</sub>H<sub>20</sub>O<sub>6</sub>) associated with the bands of the infrared absorbance spectrum show in Figure 4. 81

**Fig. 3.** Experimental ATR-IR and theoretical Infrared spectrum obtained at B3LYP/6-311++G(d,p) level of theory. 82

**Fig. 4.** Frontier Molecular Orbitals (HOMO and LUMO) calculated for title chalcone at B3LYP/6-311++G(d,p) level of theory 85

**Table 3.** Calculated quantum reactivity descriptors for title chalcone computed at B3LYP/6-311++G(d,p) level of theory. 86

**Fig. 5.** The Electronic Fukui functions for the nucleophilic attack (f<sup>+</sup>), electrophilic attack (f<sup>-</sup>), and radical attack (f<sup>0</sup>) obtained with isodensity value 0.00072736 of the title chalcone. 88

**Table 4.** Condensed Fukui functions, the dual descriptor ( $\Delta f$ ), and the multiphilic index ( $\Delta\omega$ ) calculated from the Hirshfeld charge analysis for the anionic, neutral, and cationic species of the title chalcone. 88

**Fig. 6.** Calculated Molecular Electrostatic Potential (MEP) for title chalcone at B3LYP/6-311++G(d,p) level of theory 90

**Fig. 7.** Experimental UV-Vis spectrum of the title chalcone. 91

**Fig. 8.** Theoretical UV-Vis spectrum of the title chalcone using the TD-DFT method with the CAM-B3LYP/6-311++G(d,p) level of theory and ethanol as an implicit solven 91

**Fig. 9.** Graph of the distribution of chalcone micro species as a function of pH variation through the acid dissociation constant (pK<sub>a</sub>). 92

**Fig. 10.** Bioavailability radar of the title chalcone L by the druglikeness criteria (Lipophilicity (-0.7 < log P < 5.0), size (150 g/mol < MW < 500 g/mol), polarity (20 Å<sup>2</sup> < TPSA < 130 Å<sup>2</sup>), insolubility (-6 < log S < 0), insaturação (0.25 < Fraction Csp<sup>3</sup> < 1) and flexibility (0 < Num. Rotatable bonds < 9) 93

**Fig. 11.** Models of structure-activity relationship (QSAR) of chalcone: A - absorption represented by the log D and pH values, B - solubility class represented by the log S and pH values, C - water solubility represented by the concentration in mg/mL and pH values and D - Molecular fragments of the acute oral toxicity model. 94

**Fig. 12.** MICs of the Ciprofloxacin (Cip) and Ethidium Bromide (EB) in the absence or presence of binary mixture acetophenone (59.14%) and title chalcone (40.86%), as well as Chlorpromazine (CPZ) and carbonylcyanide m-chlorophenyl hydrazone (CCCP) against K2068 (MepA) 95

**Fig. 13.** The best pose of chalcone (pink) and the best pose of ciprofloxacin (blue) on the binding site of the MepA mode 95

**Table 5.** Physicochemical and pharmacokinetics properties by the ADMET parameters for title chalcone 96

<b>Fig. 14.</b> 2D ligand-protein interaction diagram of the title chalcone and the MepA model. Contact distances are shown in green	97
<b>Fig. 1.</b> Aerial parts of <i>C. Anisodontus</i> (a) 2-hydroxy-3,4,6-trimethoxyacetophenone (b)	110
<b>Fig. 2.</b> Fundamental structure of chalcone	111
<b>Table 1.</b> <sup>1</sup> H and <sup>13</sup> C NMR data of chalcone in CDCl <sub>3</sub> . Experimental and theoretical chemical shifts in δ <sub>C</sub> and δ <sub>H</sub> are in ppm	115
<b>Fig. 3.</b> Optimized geometry of the chalcone obtained at B3LYP/6-311++G(d,p) level of theory	117
<b>Table 2</b> Calculated bond lengths for the title chalcone at B3LYP/6-311++G(d,p) level of theory.	118
<b>Fig. 4.</b> Linear fitting of the experimental and theoretical chemical shifts for the structural characterization of the chalcone	119
<b>Fig. 5.</b> Experimental ATR-IR and theoretical Infrared spectrum obtained at B3LYP/6-311++G(d,p) level of theory.	120
<b>Table 3</b> ATR-FTIR experimental frequencies ( $\tilde{\nu}_{\text{ATR-FTIR}}$ , in cm <sup>-1</sup> ), calculated vibrational numbers ( $\tilde{\nu}_{\text{IR}}$ , in cm <sup>-1</sup> ), and scaled vibrational wavenumbers ( $\tilde{\nu}_{\text{scal}}$ , in cm <sup>-1</sup> ) by the dual scale (below 1700 cm <sup>-1</sup> ) and 0.958 (above 1700 cm <sup>-1</sup> ) and assignment for some of the vibrational modes of chalcone.	120
<b>Fig. 6.</b> Linear fitting using the experimental and calculated wavenumbers.	121
<b>Table 4</b> Calculated Quantum Reactivity Descriptors at B3LYP/6-311++G(d,p) level of theory	123
<b>Fig. 7.</b> Frontier Molecular Orbitals (HOMO and LUMO) calculated for the chalcone at B3LYP/6-311++G(d,p) level of theory.	123
<b>Fig. 8.</b> Isosurface for the Electronic Fukui functions for the nucleophilic attack ( $f^+$ ), electrophilic attack ( $f^-$ ), and radical attack ( $f^0$ ).	124
<b>Table 5</b> Calculated values for the Condensed Fukui functions for the nucleophilic attack ( $f^+$ ), electrophilic attack ( $f^-$ ), and radical attack ( $f^0$ ) using the Hirshfeld charge analysis, the dual descriptor ( $\Delta f$ ), and the multiphilic index ( $\Delta\omega$ )	125
<b>Fig. 9.</b> Calculated Molecular Electrostatic Potential (MEP).	126
<b>Fig. 10.</b> Experimental UV-Vis spectrum	126
<b>Fig. 11.</b> Theoretical UV-Vis spectrum.	128
<b>Fig. 12.</b> Effect of chalcone under the locomotor behavior of zebrafish ( <i>Danio rerio</i> ) adult in the Open Field Test (0-5 min). Dzp – Diazepam (1.0 mg/mL, i.p.); Vehicle– Control (DMSO 3%; 20 µl; i.p.). Values represent the mean ± standard error of the mean for 6 animals/group; ANOVA followed by Tukey ****p	129
<b>Fig. 13.</b> Effect of chalcone on adult zebrafish in the Light & Dark Test (0-5 min). The numbers above each column indicate percentage of permanence in the light zone. Naïve – group without treatment; Vehicle – Control (DMSO 3%; 20 µl; i.p.); Dzp – Diazepam (1.0 mg/mL; i.p.). Values represent the mean ± standard error of the mean for 6 animals/group	129
<b>Scheme 1.</b> Preparation of chalcone. a) NaOH 50% w v <sup>-1</sup> , ethanol, t.a., 48 h.	130
<b>Figure 1.</b> (a) Aerial parts of <i>C. anisodontus</i> ; (b) 2-hydroxy-3,4,6-trimethoxyacetophenone.	138
<b>Scheme 1.</b> Preparation of chalcone. a) NaOH 50 % w v <sup>-1</sup> , ethanol, t.a., 48 h.	139

<b>Figure 2.</b> MICs of the Ciprofloxacin (Cip) and Ethidium Bromide (EB) in the absence or presence of the cinnamaldehyde chalcone, as well as Chlorpromazine (CPZ) and carbonylcyanide m-chlorophenyl hydrazone (CCCP) against K2068 (MepA).	141
<b>Figure 3.</b> MICs of the Norfloxacin (NorA) and Ethidium Bromide (EtBr) in the absence or presence of the cinnamaldehyde chalcone, as well as, Chlorpromazine (CPZ) and Carbonylcyanide m-chlorophenyl hydrazone (CCCP) against SA1199-B (NorA).	143
<b>Figure 4.</b> Best pose of the chalcone docked on the binding site of the MepA model. Hydrogen bonds are depicted in green.	143
<b>Figure 5.</b> Superposition of the best poses of the chalcone (gold) and ciprofloxacin (pink).	144
<b>Table 1.</b> Experimental wavenumbers ( $\text{cm}^{-1}$ ) and normalized Raman intensity (in arbitrary unit) for some Raman bands of the six chalcones, and assignment of their vibrational modes.	158
<b>Fig. 1.</b> (a) FT-Raman of the six synthesized chalcones. Zoom of some Raman bands at different temperatures in the spectral range; (b) Raman bands for chalcones A1-A3 and A6 in the region $1800 - 1525 \text{ cm}^{-1}$ ; (c) Raman bands for chalcones A3, A4 and A5 in the region $1800 - 1525 \text{ cm}^{-1}$ ; (d) Raman bands for chalcones A1-A3 and A6 in the region $1050 - 750 \text{ cm}^{-1}$ ; (e) Raman bands for chalcones A3, A4 and A5 in the region $1050 - 750 \text{ cm}^{-1}$ .	159
<b>Fig. 2.</b> HOMO of the chalcones A1-A	160
<b>Fig. 3.</b> LUMO of the chalcones A1-A	160
<b>Table 2.</b> Quantum chemical parameters for the optimized geometries of the chalcones A1-A6.	161
<b>Fig. 4.</b> Experimental UV-Vis spectra of the chalcones A1-A6 in the region $190 - 240 \text{ nm}$	161
<b>Table 3.</b> Electronic absorption spectral data (experimental and theoretical) for three singlet states of the chalcones <b>A1-A6</b> .	161
<b>Table 4.</b> MIC of the six synthesized compounds.	163
<b>Fig. 5.</b> (a) MIC of Erythromycin, and (b) MIC of EB against the strain <i>S. aureus</i> RN4220.	165
<b>Fig. 6.</b> (a) MIC of Penicillin, and (b) MIC of EB against the strain <i>S. aureus</i> K4414	165
<b>Fig. 7.</b> (a) MIC of Norfloxacin, and (b) MIC of EB against the strain <i>S. aureus</i> 1199B	165
<b>Fig. 8.</b> (a) MIC of Ciprofloxacin, and (b) MIC of EB against the strain <i>S. aureus</i> K2068.	165
<b>Table 5.</b> Predicted ADMET properties of the chalcone analogs <b>A1-A6</b> .	166
<b>Fig. 9.</b> Microspecies distribution of the chalcone analogs A1-A6 with de pH variation.	166
<b>Fig. 10.</b> Distribution coefficient ( $\log D$ ) of the chalcone analogs A1-A6 with pH variation	167
<b>Table 6.</b> Predicted bioactivity of the chalcone analogs <b>A1-A6</b> through multi target classes.	168
<b>Fig. 11.</b> Best poses for the six synthesized chalcones, A1 (yellow), A2 (orange), A3 (light green), A4 (pink), A5 (light blue) and A6 (brown) on the binding site of the NorA model.	169
<b>Fig. 12.</b> Best poses for the six synthesized chalcones one the binding site of the model and its most important interactions. $\pi$ - $\pi$ interactions are depicted in bright pink, while $\pi$ -alkyl are in light pink. Hydrogen bonds are depicted in green and the fluorine bonding is in light	170

blue.

## SYMBOL, ACRONYM OR ABBREVIATION

---

Symbol, acronym or abbreviation	Means
CCD	Cromatografia em camada delgada (Thin layer chromatography)
NMR	Nuclear Magnetic Resonance
IR	Infrared
MS	Mass Spectrometry
CENAUREMN	Northeastern Center of Application and Use of Nuclear Magnetic Resonance
DFT	Density Functional Theory Nuclear
ADMET	Absorption, distribution, metabolism, excretion and toxicity
MRSA	Methicilin-resistant <i>Staphylococcus aureus</i>
MDR	Multi-drug-resistant
HIA	Heart infusion agar
BHI	Brain heart infusion
DMSO	Dimethyl sulfoxide
ANOVA	Analysis of variance
UVA	University Vale of Acaraú
CEUA	Ethics, Committee for the use of animals
MATE	Multidrugs and toxic compound extrusion
MFS	Main facilitator
MRS	Small resistance to multidrugs
RND	Resistance nodulation cell division
ABC	ATP binding
CPX	Ciprofloxacin
EtBr	Ethidium bromide
EPI	Efflux pump inhibitors
NSAIDS	Non-steroidal anti-inflammatory drugs
PL	Protein-binding complexes
QM	Quantum mechanics
Zfa	Zebrafish

**ABSTRACT**

<b>1. GENERAL INTRODUCTION.....</b>	<b>14</b>
1.1 RESEARSH STRATEGIES.....	14
<b>2 OBJECTIVES.....</b>	<b>20</b>
2.1 General Objective.....	20
2.2 Specific Objectives.....	20
2.3 2.3 Objectives and Questions.....	20
<b>3 THEORETICAL FOUNDATION.....</b>	<b>23</b>
Article review: Chalcones as potent agents against <i>Staphylococcus aureus</i> : A Computational Approach .....	23
<b>4 SCIENTIFIC PRODUCTION.....</b>	<b>43</b>
<b>CHAPTER 5</b> - Anticonvulsant, anxiolytic-like effect in adult zebrafish ( <i>Danio rerio</i> ) through GABAergic system of chalcone derived from natural products.....	57
.....	
<b>CHAPTER 6</b> - Structural characterization, DFT calculations, ADMET studies, antibiotic potentiating activity, evaluation of efflux pump inhibition and molecular docking of chalcone ( <i>E</i> )-1-(2-hydroxy-3,4,6-trimethoxyphenyl)-3-(4- methoxyphenyl) prop-2-en-1.....	70
<b>CHAPTER 7</b> - Structural characterization, electronic properties, and anxiolytic- like effect in adult zebrafish ( <i>Danio rerio</i> ) of cinnamaldehyde chalcone.....	109
<b>CHAPTER 8</b> -Antibacterial activity against multidrug-resistant <i>Staphylococcus aureus</i> and in the silica evaluation of the MepA efflux pump by cinnamaldehyde chalcone.....	137
<b>CHAPTER 9</b> - Spectroscopic analysis by NMR, FT-Raman, ATR-FTIR, and UV- Vis, evaluation of antimicrobial activity, and <i>in silico</i> studies of chalcones derived from 2- hydroxyacetophenone.....	147
<b>10 FINAL CONSIDERATIONS.....</b>	<b>176</b>
10.1 GENERAL DISCUSSION.....	176
10.2. GENERAL CONCLUSIONS.....	177
10.3 PERSPECTIVES FOR FUTURE INVESTIGATIONS.....	178
11 REFERENCES.....	179
<b>ATTACHMENTS.....</b>	<b>181</b>

---

**Caracterização espectroscópica e avaliação do potencial antimicrobiano e ansiolítico utilizando peixe-zebra adulto (*Danio rerio*) de chalconas sintéticas**

**RESUMO**

**Introdução:** Chalconas são compostos com atividades biológicas em diferentes espécies. Possuem uma estrutura simples e fácil de manusear devido à ponte  $\alpha$ - $\beta$ -insaturada que é responsável pela maioria das atividades biológicas facilitando a síntese de compostos mais eficazes no combate a infecções bacterianas graves, bem como outras patologias que, juntamente com antibióticos conhecidos, podem potencializar sua ação. **Objetivos:** O objetivo deste trabalho foi estudar chalconas por espectroscopia vibracional combinada com cálculos computacionais e docking como complementos para o entendimento da atividade antimicrobiana, bomba de efluxo e nocicepção pelo modelo alternativo de zebrafish. **Metodologia:** Foram sintetizadas oito chalconas caracterizadas por técnicas espectroscópicas. A identificação estrutural das chalconas e o estudo vibracional foram realizados por meio da técnica de Ressonância Magnética Nuclear (RMN), infravermelho (IV) e espectrometria de massas (E.M.). As propriedades farmacocinéticas foram previstas de acordo com o modelo de absorção, distribuição, metabolismo, excreção e toxicidade (ADMET). com base na mecânica quântica, simulações computacionais da interação entre *Staphylococcus aureus* Tyrosyl-tRNA sintetase e possíveis inibidores foram realizadas utilizando o código AutoDock Vina e cálculos da Teoria Funcional da Densidade (DFT) que permitem a previsão e o cálculo comportamental do material. cepas de *Staphylococcus aureus* foram usadas nos testes da Bomba de Efluxo. Além disso, os testes de nocicepção foram baseados no modelo de peixe-zebra. **Resultados e discussões:** As chalconas identificadas, testadas em combinação com antibióticos foram capazes de atenuar a resistência à penicilina contra K4414, norfloxacin contra 1199B e ciprofloxacina contra K2068. Outra chalcona combinada com flumazenil alterou os efeitos da chalcona (0,5 mg/mL) e do Diazepam (1,0 mg/mL) em peixes-zebra adultos. **Conclusão:** As chalconas estudadas são drogas eficazes e potenciais no combate a infecções bacterianas e efeito ansiolítico dependente do sistema GABAérgico. Novas evidências e destaques de que as chalconas podem potencialmente ser usadas para desenvolver compostos com propriedades ansiolíticas, um também possível inibidor da bomba de efluxo Mep A.

**Palavras-Chave:** microbiologia, chalconas, bioatividades, docking

**Agradecimentos:**

FUNCAP,

CNPq.



**SPECTROSCOPIC CHARACTERIZATION AND EVALUATION OF THE  
ANTIMICROBIAL AND ANTINOCICEPTIVE POTENTIAL USING ADULT  
ZEBRAFISH (*Danio rerio*) SYNTHETIC CHALCONAS**

**ABSTRACT**

**Introduction:** Chalcones are compounds with biological activities in different species. They have a simple and easy to handle structure due to the  $\alpha$ - $\beta$ -unsaturated bridge which is responsible for most biological activities facilitating the synthesis of more effective compounds in combating serious bacterial infections as well as other pathologies that, together with known antibiotics, can potentiate their action. **Objectives:** The objective of this work was to study chalcones by vibrational spectroscopy combined with computational calculations and docking as complements for the understanding of antimicrobial activity, efflux pump, and nociception by the alternative model of zebrafish. **Methodology:** Eight chalcones were synthesized characterized for spectroscopic techniques. The structural identification of chalcones and vibrational study were performed using technique Nuclear Magnetic Resonance (NMR), infrared (IV), and mass spectrometry (E.M.). The pharmacokinetic properties were predicted according to the model absorption, distribution, metabolism, excretion and toxicity (ADMET). based on quantum mechanics, computer simulations of the interaction between *Staphylococcus aureus* Tyrosyl-tRNA synthetase and possible inhibitors were performed using the AutoDock Vina code and Density Functional Theory (DFT) calculations that allow prediction and the behavioral calculation of the material. strains of *Staphylococcus aureus* were used in the Efflux Pump tests. In addition nociception tests were based zebrafish model. **Results and discussions:** Chalcones identified, tested in combination with antibiotics was able to attenuate penicillin resistance against K4414, norfloxacin against 1199B, and ciprofloxacin against K2068. Other chalcone combined with flumazenil altered the effects of chalcone (0.5 mg / mL) and Diazepam (1.0 mg / mL) in adult zebrafish. **Conclusion:** The chalcones studied are effective and potential drug in the fight against bacterial infections and anxiolytic effect dependent on the GABAergic system. New evidence and highlights that chalcones can potentially be used to develop compounds with anxiolytic properties, a also possible inhibitor of the Mep A efflux pump.

**Keywords:** microbiology, chalcones, bioactivities, docking

**Acknowledgment:**

FUNCAP,

CNPq.

Como entender como uma substância derivada da natureza pode interagir com um medicamento já existente e potencializar sua ação? Tudo depende da dose e da modificação precisa para que a interação proporcione um melhor resultado na eficiência do composto que isoladamente não teria. Esta pesquisa mostrou a possibilidade de prever quais mudanças nos compostos através de estudos computacionais sugere essa melhor interação e ação desta para uso terapêutico contra doenças infecciosas ou como ansiolítico. Ou seja, além de menos prejudiciais e devido sua fácil modificação, esses compostos proporcionam uma diminuição da dose de antibióticos e essa interação pode ajudar na questão da resistência microbiana e salvar vidas, pois impede que as bactérias expulsem o fármaco como defesa própria. Além de evitar o uso de mamíferos nestas pesquisas utilizando um modelo alternativo como o zebrafish que vem se mostrando bastante eficiente reduzindo também gastos e tempo.

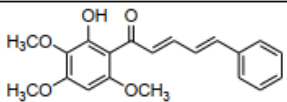
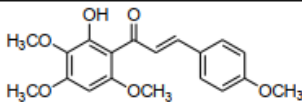
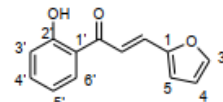
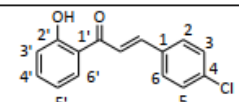
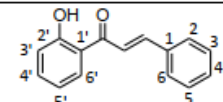
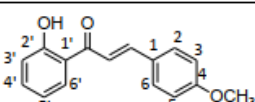
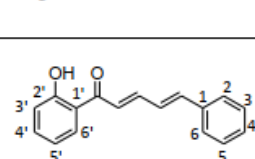
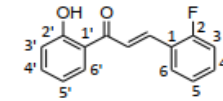
# 1 GENERAL INTRODUCTION

## 1.1 RESEARCH STRATEGIES

The chalcones were produced by the Claisen-Schmidt condensation reactions. The reaction was monitored by employing CCD (thin layer chromatography) and the purification of the final product was performed using silica gel column chromatography.

In this work, 8 chalcones were synthesized, two of which were derived from the natural product 2-hydroxy-3,4,6-trimethoxyacetophenone and 6 synthetic ones. The molecular structures of these chalcones are shown in the Frame 01.

Table 01: molecular structures of synthetic chalcones investigated in this thesis.

NOMENCLATURE IN THE POOL AND QUANTITY IN MILLIGRAM	FORMULA MOLECULAR CHEMICAL	NAME	
Cinnamaldehyde		(2E, 4E)-1-(2-hydroxy-3,4,6-trimethoxyphenyl)-5-phenylpenta-2,4-dien-1-one	semi-synthetic
Anisaldehyde		(E)-1-(2-hydroxy-3,4,6-trimethoxyphenyl)-3-(4-methoxyphenyl)prop-2-en-1-one	semi-synthetic
2HAF Furfural		(E)-3-(furan-2-yl)-1-(2-hydroxyphenyl)prop-2-en-1-one (A1)	synthetic
2HAF-4-Chlorobenzaldehyde		(E)-3-(4-chlorophenyl)-1-(2-hydroxyphenyl)prop-2-en-1-one (A2)	synthetic
2HAF-Benzaldehyde		(E)-1-(2-hydroxyphenyl)-3-phenylprop-2-en-1-one (A3)	synthetic
2HAF Anisaldehyde		(E)-1-(2-hydroxyphenyl)-3-(4-methoxyphenyl)prop-2-en-1-one (A4)	synthetic
2HAF Cinnamaldehyde		(2E, 4E)-1-(2-hydroxyphenyl)-5-phenylpenta-2,4-dien-1-one (A5)	synthetic
2HAF Fluorobenzaldehyde		(E)-3-(2-fluorophenyl)-1-(2-hydroxyphenyl)prop-2-en-1-one (A6)	synthetic

This work reveals the characteristic of the molecule synthesized from spectroscopic techniques. The structural identification of the chalcones and vibrational study were performed using the one-dimensional  $^1\text{H}$  and  $^{13}\text{C}$  NMR (Nuclear Magnetic Resonance) techniques, infrared (IR), and mass spectrometry (MS), at the Department of Organic and Inorganic Chemistry and at Northeastern Center of Application and Use of Nuclear Magnetic Resonance (CENAUREMN) at the Federal University of Ceará. These techniques are powerful tools to identify and compare the enhancement of the molecule and knowing which functional group would have a better result. Chalcones' analogs were selected using a version of the MarvinSketch® 20.15 software (CSIZMADIA et al, 1999) uploaded to the pkCSM web server (<https://biosig.lab.uq.edu.au/pkcsm/prediction>) (PIRES et al, 2015), where the pharmacokinetic properties were predicted by absorption, distribution, metabolism, excretion and toxicity (ADMET).

With regard to the interaction between *Staphylococcus aureus* Tyrosyl-tRNA synthetase and possible inhibitors, computer simulations for molecular docking were performed through the AutoDock Vina code (version 1.1.2), using 3-way multithreading, Lamarckian Genetic Algorithm (TROTT; OLSON, 2009).

These studies with the use of molecular docking allow a better approach, simplification, and low cost. The coupling together with the study of the extrusion activity allowing to know where the molecule is, where it fits, and its behavior, allowing a better understanding of the role of microorganisms in the adaptation process.

Strains of *Staphylococcus aureus* were used as carriers of the Efflux Pump and one considered wild was used in this study. The bacteria were kept in two different stocks (glycerol at  $-80\text{ }^\circ\text{C}$  and Heart Infusion Agar slants (HIA, Disco) at  $4\text{ }^\circ\text{C}$ ). The culture media used for the cultivation were: Heart Infusion Agar (HIA, Difco laboratories Ltda.), Brain Heart Infusion (BHI, difco Laboratories Ltda). Antibiotics were chosen according to specific bacterial efflux pumps. All antibiotics and chalcones were prepared with  $10\text{ mg / mL}$  of each substance diluted in  $1\text{ mL}$  of dimethylsulfoxide (DMSO) and then diluted in water, decreasing the concentration to  $1024\text{ }\mu\text{g / mL}$  (CLSI, 2012).

The analysis of the efflux pump allows to verify which pump a specific chalcone is acting, to suppose how and what is the best way to reverse this situation. The literature addresses 5 ways of inhibiting an efflux pump: 1) Reduction of expression bomb genetics; 2) Interruption of the pump assembly; 3) Reduction by competitive means or non-binding of the substrate; 4) Interruption of the pump's energy source (POOLE, 2007) and 5) Complex Epi-

substrate formation avoiding the extrusion of the cellular substrate when they have an affinity as p-glycoprotein protein (p-GP) (SRIVALLI; LAKSHMI, 2012).

For statistical analysis, the results were processed in triplicate and derived as a geometric mean. The analysis data were submitted using the GraphPad Prisma 6.0 statistical program. Using a geometric mean obtained from the triplicates as the central data  $\pm$  standard deviation from the mean, a two-way of analysis of variance (ANOVA) test will be performed. Then, a post hoc Bonferroni test was performed (where  $p < 0.05$  and  $p < 0.0001$  were evaluated and  $p > 0.05$  not significant).

For anxiety tests, wild zebrafish, aged 60 to 90 days ( $4.0 \pm 0.1$  g), of both sexes, were obtained through UVA (University Vale of Acaraú) - Sobral. Handling and acclimatization and maintenance in a glass aquarium with a temperature of 24-28°C, with tap water treated with anti-chlorine. The procedures of the experiments will be considered by the Ethics Committee for the Use of Animals (CEUA) No. 7210149/2016 and using the methodology Magalhães et al. (2017).

These animals have established themselves as good animal model to meet the physiological conditions and pathologies in vertebrates to the detriment of models with mammals (STEWART et al, 2014). Mainly as its advantages of use as optical transparency of the larvae, low maintenance cost, rapid proliferation and easy genetic modification in addition to its wide performance in several fields such as genetic study, developmental biology, toxicology, and preclinical experiments (SCHLEGEL, 2012).

The work structure starts with a general introduction that followed by the general objectives, survey and questions, the third chapter is the reference which is a review article submitted to the journal letters in drug design & discovery (LDDD), chapter 4 catalogs the scientific productions carried out in this work, followed by chapters 5 to 9 by the published articles:

5) Anxiolytic effect in adult zebrafish (*danio rerio*) through the gabaergic system and molecular docking study of chalcone (e) -1- (2-hydroxy-3,4,6-trimethoxyphenyl) - 3- (4-methoxyphenyl) prop-2-en-1-one, biointerface research in applied chemistry, biological sciences II qualis c.

6) Structural characterization, DFT calculations, ADMET studies, antibiotic potentiating activity, evaluation of inhibition of the efflux pump and molecular docking of chalcone (E) -1- (2-hydroxy-3,4,6-trimethoxyphenyl) -3- (4-methoxyphenyl) prop-2-en-1-one. Journal of Molecular Structure, biological sciences II, Qualis B2.

7) Structural characterization, electronic properties and anxiolytic effect in the adult zebrafish (*Danio rerio*) of cinnamaldehyde chalcone. Journal of Molecular Structure, Biological Sciences II, Qualis B2.

8) Antibacterial activity against multidrug-resistant *Staphylococcus aureus* and in the silica evaluation of the MepA efflux pump by cinnamaldehyde chalcone, submitted to the current Microbiology journal, Qualis B2 in the area of biological sciences II. In the seventh chapter, there will be the manuscript: Structural and spectroscopic analysis, evaluation of antimicrobial activity, and in silico studies of chalcones derived from 2-hydroxy acetophenone, submitted to the Journal of Molecular Structure, Qualis B2 in the area of Biological Sciences II.

9) Structural and spectroscopic analysis, evaluation of antimicrobial activity, and in silico studies of chalcones derived from 2-hydroxy acetophenone, biological sciences II, Qualis B2 too.

Finally the tenth chapter brings are as considerations divided into general discussion, general and perspectives for future investigations.

### 2.1. General Objective

The objective of this work was, therefore, to synthesize spectroscopic techniques and computational calculations of quantum chemistry as well as evaluate their antimicrobial potential using the microdilution technique, efflux pump-action, and anxiolytic effect.

### 2.2. Specifics Objectives

- Establish the structure-activity relationship of the molecules under study.
- To perform the molecular docking studies of the synthesized molecules with the target proteins for expression of antimicrobial activity and anxiolytic effect.
- Calculate the vibrational spectra of the chalcones used, to better assign their vibration modes.
- To perform in silico computational predictions in order to assess the drug likeness.

### 2.3 Objectives and Questions

Chalcones occur in flowers, leaves, fruits, roots, and stems, besides they can be synthetic or semi-synthetic. They can exist as two isomers, trans (E) and cis (Z), with the trans form being the most stable of them (RAMMOHAN et al, 2020). Its structure comprises at least two aromatic rings connected by an unsaturated  $\alpha$ - $\beta$  bridge, probably the most responsible for its biological activities (YADAV et al, 2018).

Chalcones are substances of widespread use in medicinal chemistry that are found naturally in some plants (ZHUANG, 2017), generally have no toxicity, and are bright yellow, responsible for their pigmentation (YADAV, 2011). These compounds with their synthetic derivatives present an opportunity to be used as chemopreventive drugs or as components in the treatment of cancer as they are highly tolerable and modifiable (ELIZABETH et al, 2015).

Chalcones can be adjusted naturally or synthesized by the Claisen-Schmidt Reaction, which is the condensation of a ketone with an aldehyde both aromatic in the presence of a catalyst, yielding a  $\alpha$ ,  $\beta$ -unsaturated ketone linked to two aromatic rings. Several activities biological has been reported for chalcones. (RITTER, 2015). Their antibacterial and antinociceptive potential can be enhanced when associated with the conventional methodology of synthesis by aldolic

condensation, thus providing greater structural diversity. And to differentiate biological activities of similar compounds when exhibiting different spectra, it is possible with the vibrational study of molecules to bind differently to the target and exhibit different Raman and infrared spectra (CAMPELO, 2017).

The microbial resistance that requires a constant conventional medicine, instigating the development of more efficient drugs. Studies show that 70% of bacteria are resistant to at least one antibiotic for clinical use. On the other hand, many microbial diseases are being treated with active molecules that are already used in other treatments (KATZ, 2006). Therefore, the need for new substances with pharmacological potential similar or greater than drugs on the market to combat bacterial resistance (RITTER, 2015). It has therefore become a challenge to prospect for new substances with a similar or even more active effect compared to conventional antimicrobials, since they are losing their effect due to misuse by hospitals and the general population, mainly due to indiscriminate use, self-medication, and interruption of treatment to combat pathologies.

This fight against microorganisms has become an increasingly frequent problem even with a wide variety of antimicrobials and the evolution of science in this field (LIVERMORE, 2005). Good results have been obtained with the use of natural products or associated with antibiotics to contain resistant pathogens (COUTINHO et al, 2008). This resistance, due to selectivity, adherence of the drug to the cell wall, expulsion of it by efflux pumps, and action of enzymes minimizing or inhibiting the action of the antibiotic (UTCHARIYAKIAT et al, 2016).

In view of this, this work aggregates the progressive development of new therapeutic agents from chalcones and the use of an alternative model with zebrafish that offers an effective study to the detriment of models with mammals. The use of zebrafish (*Danio rerio*) as an alternative model has become promising and has attracted a lot of researchers' attention (KALUEFF, 2017; TAYLOR et al, 2017; SNEDDON, 2019) as it makes it possible to ascertain host-pathogen interactions in the study. antimicrobial action and nociception. As well as in the study of infectious diseases, due to the easy visualization of its transparent body and because it has the potential for genetic manipulations (ELIZABETH et al, 2015). Analyzes with Gram-positive *Staphylococcus aureus* to check the action of chalcones in the inhibition of efflux pumps have also been showing efficacy (HOLLER et al 2012).

New methods of quantum calculations and couplings can also predict on the computer and detect the site of metabolism by making comparisons of the molecule with information from the literature. In addition to modifying a molecule at specific locations to design compounds with greater metabolic stability, because in silico methods in combination with previous metabolic identification studies can be synergistic in determining an activity (VAZ et al, 2010). Docking



techniques are important for the study of several areas, such as compounds that act on multiple targets against complex (multifactorial) diseases such as cancer, degenerative diseases, and infections by molecular coupling making it possible to observe the complexes formed between ligands and targets of certain diseases such as Alzheimer's (SCOTTI et al, 2016).

**Article:** Chalcones as potent agents against *Staphylococcus aureus*: A Computational Approach

**Authors:** Jayze da Cunha Xavier, Hécio Silva dos Santos, Márcia Machado Marinho, Matheus Nunes da Rocha, Alexandre Magno Rodrigues Teixeira, Henrique Douglas Melo Coutinho, Emmanuel Silva Marinho, Sucheta, Nitin Kumar, Raghav Mishra.

**Journal:** Letters in Drug Design & Discovery(LDDD)

**Situation:** submitted

#### Resumo

**Introdução:** Estudos com produtos naturais ou sintéticos de chalconas têm se mostrado bastante promissores devido à sua estrutura peculiar que permite diferentes possibilidades de realocações que definirão suas diversas bioatividades na criação de novas substâncias. Essa criação é facilitada pela síntese de substâncias em conjunto com o estudo molecular, o que permite um avanço considerável nas pesquisas, reduzindo o número de testes in vitro. **Objetivo:** Este trabalho tem como foco a atividade antibacteriana das chalconas contra o *Staphylococcus aureus*, causador de diversas doenças e é um dos principais microrganismos com crescente resistência aos medicamentos convencionais. **Métodos:** Foram considerados como análises complementares em chalconas artigos que estudaram atividade antibacteriana, bomba de efluxo ou docagem molecular. A partir dessas 29 chalconas encontradas, foi realizado o docking molecular e ADMET das cinco chalconas com a melhor atividade encontrada. **Resultados:** O resultado da atividade antimicrobiana contra *Staphylococcus aureus* foi confirmado através de estudo in silico e dados farmacocinéticos. **Conclusão:** Os resultados da atividade antimicrobiana das chalconas mais ativas contra *Staphylococcus aureus* foram corroborados pelo estudo in silico e farmacocinético que não só confirmou seu potencial de ação contra cepas resistentes, mas também estabeleceu na futura utilidade das chalconas como moléculas líderes ou protótipos para a síntese de novos agentes antimicrobianos potentes contra *Staphylococcus aureus*.

**Palavras-chave:** Claisen Schmidt, Bioatividade, MRSA, In-silico, ADMET, Antimicrobiano, Chalcones.

**1. Introduction:** Natural products have been selected over the years with the efficiency and selectivity needed to reach cellular targets and avoid resistance naturally, have characteristics that many pure synthetic molecules do not possess. [1]

That's why researchers have focused on molecules of natural origin. Among the huge variety of existing natural products, isolated or modified chalcones have been the target of chemical-pharmacological interest and have received great attention, mainly because of their simple structure. They are formed at least by two aromatic rings joined by an unsaturated  $\alpha$ - $\beta$  bond of three carbons. [2] This reactive keto-ethyl group - **CO-CH=CH-** is responsible for the pigmentation of yellow to brown in these compounds. [3]

They can be found in vegetables, fruits, teas and other plants, acting as precursors of flavonoids and isoflavonoids. [4] The basic structure of all chalcones is the formula 1-3-diaryl 2-propen-1-one [5] and can be easily manipulated by the Claisen-Schmidt reaction. Various substances can be formed from this base due to their relatively simple structure, thus enabling a wide range of pharmacological activities. [6-8]

Chalcones are bioactive compounds against virtually all eukaryotes and some Gram-negative and Gram-positive prokaryotes, as they have numerous molecular targets. [9] Their biological activities mainly include antimicrobial [10] and antibacterial. [11] In this 21<sup>st</sup> century, among gram-positive bacteria, multidrug resistant *Staphylococcus aureus* (MRSA) and multidrug-resistant *Mycobacterium tuberculosis* (MDR), and among Gram-negative bacteria, extended spectrum beta-lactamase (ESBLs) bacteria are main cause of serious global health problem in developing countries. Due to this resistance, there is tremendous increase in morbidity, mortality, hospitalization period and health expenses. [12-16]

Among bacterial pathogens, *Staphylococcus aureus* species despite being present in the skin and nasal mucosa as a normal flora is capable of causing many infections and diseases both in animals and in humans since skin infections [17], toxic shock syndrome [18] and sepsis. [19] Such opportunist infections reach debilitated people in hospitals and are difficult to treat. Fighting against *S. aureus* has become a difficult problem for health worldwide due to the growth of bacterial resistance to antibiotics. [20]

Bacteria strategies to resist antibiotics include antibiotic inactivation on enzyme action, modification of membrane permeability to control its internal concentration, or expel it by efflux pumps. [21] *Staphylococcus aureus* develops resistance to antimicrobials by different mechanisms. It is possible to use one or combinations of strategy, in addition to making horizontal transfers of this resistance through genes located in plasmids and transposons. [22-23] Other resistance mechanisms can be transmitted by genetic and phenotypic adaptation. [24] Therefore, the need arises to associate natural or modified substances with antibiotics to potentiate their action against

these pathogens. In view of this, a brief review on antibacterial activity, flow pump and donating in synthetic chalcones will be addressed in a general context.

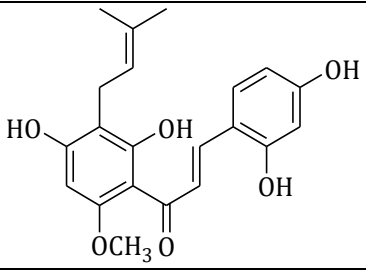
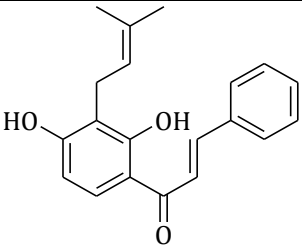
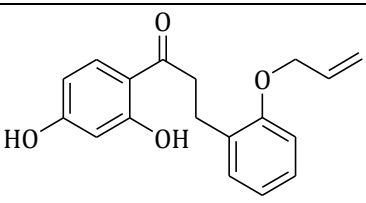
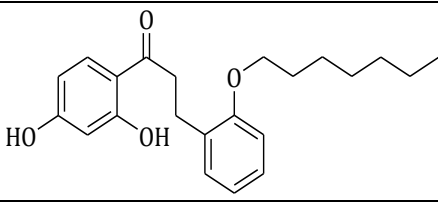
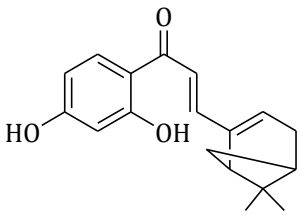
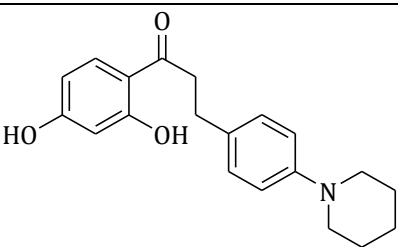
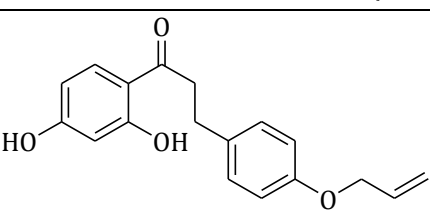
### 1.1 Chalcones and antibacterial activity against *Staphylococcus aureus*

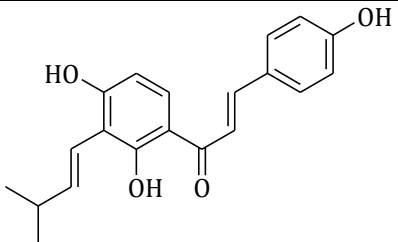
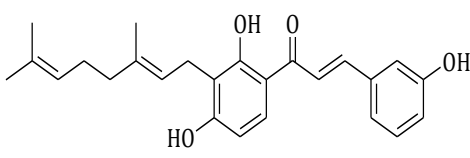
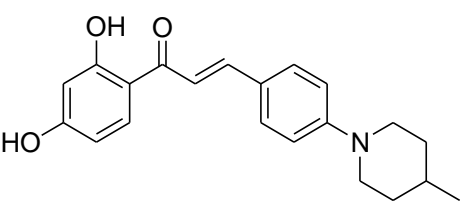
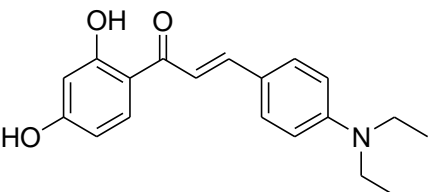
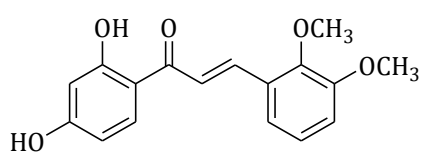
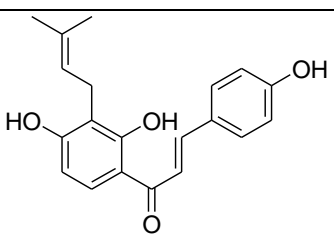
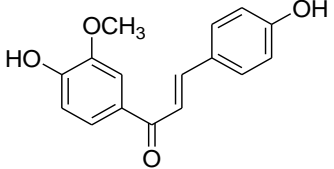
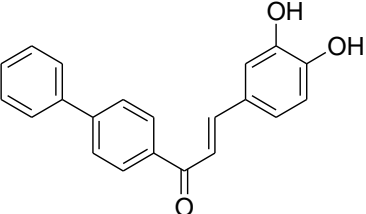
Chalcones have an open chain flavonoid structure in which the two aromatic rings are joined by a three carbon  $\alpha,\beta$ -unsaturated carbonyl linker. They can be obtained from natural sources or by synthesis, and are widely distributed in fruits, vegetables, and tea. [25-26]

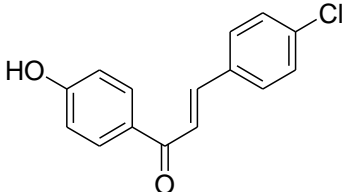
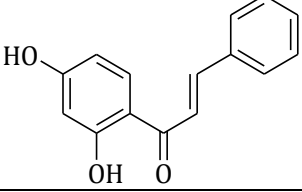
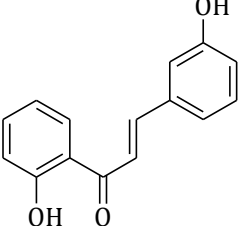
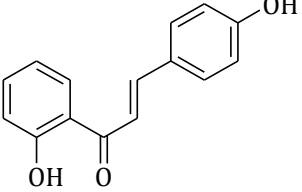
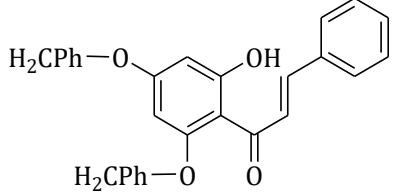
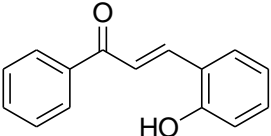
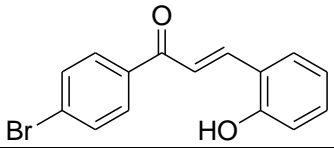
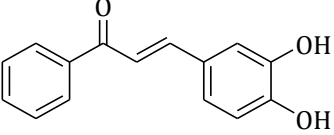
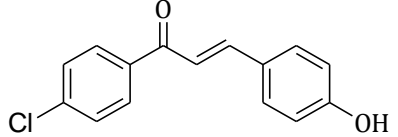
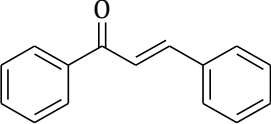
Due to its better bioavailability and high tolerance in the body, studies on chalcones and their derivatives have arisen worldwide interest for the development of therapeutic drugs. [3] Chalcones occur in flowers, leaves, fruits, roots and stems or can be synthesized. They can exist as two isomers, trans (E) and cis (Z), the trans form being the most stable of them. [27] Their structure comprises at least two aromatic rings connected by an unsaturated  $\alpha$ - $\beta$  bridge probably the most responsible for its biological activities. [28]

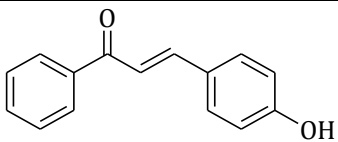
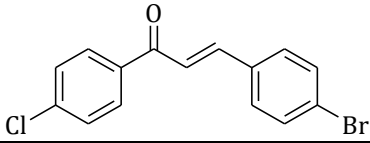
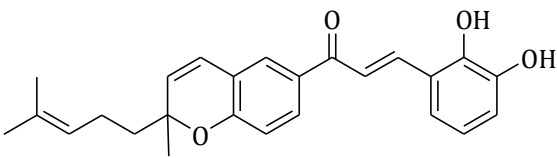
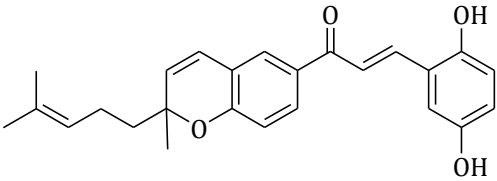
Natural chalcones appear with substitutions such as hydroxyls, methylation, dihydrochalcones, bichalcones and glycosides. They usually present as crystalline solids in shades of yellow to brown. They have diverse biological activities such as antibacterial activity [29] antioxidant [30], anti-inflammatory [31-32] and antiparasitic. The compounds that exhibit medium to significant antimicrobial effect against bacteria mainly *Staphylococcus aureus* could be extremely important as it is responsible for wide range of diseases [33] from mild skin infections to life-threatening diseases such as bacteremia, endocarditis, osteomyelitis, pneumonia and sepsis. [34] Its global burden increased and treatment for its infections has been complicated due to acquiring resistance to ample antibiotics including Methicillin and Vancomycin to become methicillin-resistant *Staphylococcus aureus*, leading to cause of infections in community and healthcare settings. [35-36] Belonging to the bacterial class “*Bacilli*”, it is the most notorious superbacterium in history. [37] The pathogenicity of *Staphylococcus aureus* is due to many virulence factors such as: enterotoxins, exfoliating toxins, and Panton-Valentine leucocidin (PVL). [38] The promising activity displayed by chalcones derivatives against *Staphylococcus aureus* (Table 1), make this class of compounds an important scaffold for the the discovery of new antibacterial agents with increased strength, low cost, superior pharmacokinetic properties, and minimum side effects.

Table 1. Antimicrobial activity of chalcones against *Staphylococcus aureus*

Structure	Strains	MICs *	Referenc e
	MRSA	0.188-0.375	[39]
	LMPO206U	0.3	[40]
	NRS 70 (MRSA)	0.39	[41]
	ATCC 29213(MSSA)	6.25	
	NRS 70 (MRSA)	0.625	
	ATCC 29213(MSSA)	25	
	NRS 70 (MRSA)	1.56	
	ATCC 29213(MSSA)	1.56	
	NRS 70 (MRSA)	3.13	
	ATCC 29213(MSSA)	3.13	
	NRS 70 (MRSA)	>200	
	ATCC 29213(MSSA)	25	

	ATCC 6538	1.95-7.8	[42]
	ATCC700699	3.1	[43]
	ATCC 25923	25	
	MRSA (USA 300')	3.125	[44]
	MSSA(ATTC 29213)	6.25	
	MRSA (USA 300')	>100	
	MSSA(ATTC 29213)	>100	
	NE*	62.5	[45]
	MSRAOM48 1	8	[46]
	MSRAOM58 4	8	
	MRSA	12.5-50	[47]
		25-50	
			

		25-50	
	ATCC 25 923	25.3	[48]
	ATCC 25 923	25.3	
	ATCC 25 923	25.3	
	ATCC 12600	63	
	MSSA	32-64	[50]
			
	Rosenbach 209	125	[51]
		125	
		125	

		125	
	NCIM 2079	1000	[52]
	ATCC 43300	32	[53]
	NRSA-NRS 17	>32	
	NRSA-NRS 1	32	
	ATCC 43300	32	
	NRSA-NRS 17	> 32	
	NRSA-NRS 1	32	

\*Minimum Inhibitory Concentration ( $\mu\text{g/mL}$ )

## 1.2 Structure- Activity Relationships (SAR)

The antibacterial activity data have showed that the presence at the ring A of hydroxyl groups located in the carbons C-2 and C-4; methoxy groups at C-3, C-4 and C-5 and aliphatic chain like prenyl and geranyl linked at C-3, phenyl at C-4, benzyl ether, allyloxy group and O-alkyl substituent at C-2, and halogens like chlorine and bromine atoms at C-4 of ring A together with hydroxyl groups at the C1' to C6', methoxy groups at the C-2', C-3' and C-4', piperidinic, piperidinyl methyl ring and amino group at the C4' are essential for antibacterial activity as well as the  $\alpha, \beta$ -unsaturated ketone moiety (Fig 1).

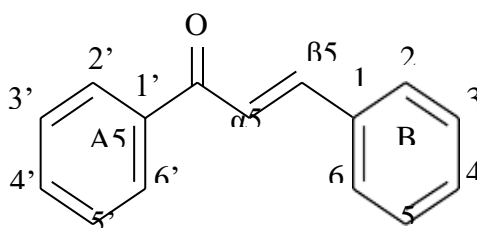


Fig. 1: Fundamental structure of chalcones

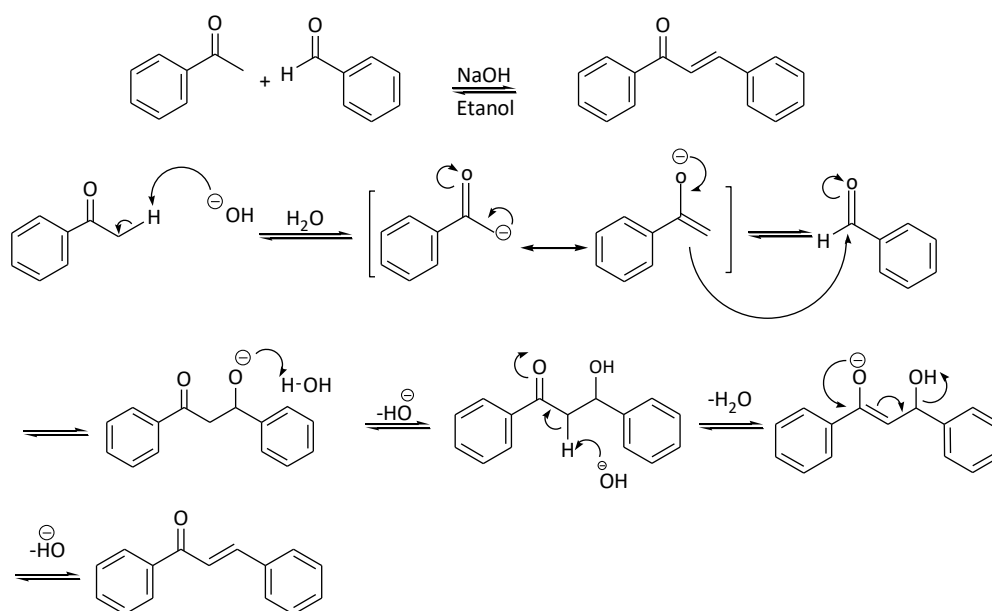
On the other hand, chalcones with ring B bearing only groups like hydroxyl, methoxy, methyl, chlorine atom, nitro, amino, and acetamide do not possess antimicrobial activity. The decreased activity for trihydroxy compounds is likely due to increased hydrophilicity and polarity properties and thus decreased bacterial membrane penetration. Taken together, these data suggest that two free phenol hydroxy groups on chalcones are optimal for Gram-positive antibacterial



activity. Additionally, chalcones with a lipophilic group such as isoprenoid and methoxy groups at positions 3', 5', and 2' of ring A are the most potent inhibitors of MRSA strains.

### 1.3 Chalcone synthesis

Some synthetics usually come from the Claisen- Schmidt reaction (Scheme 1) consisting of equal amounts of acetophenone and aldehyde both substituted that undergo condensation in the presence of alkaline with acid catalysts or based on polar solvents at 50-100°C for at least 12 hours. However, this method has the as disadvantages the probability of side-products and longer reaction time [3].



Scheme 1. Mechanism of the Claisen-Schmidt condensation reaction

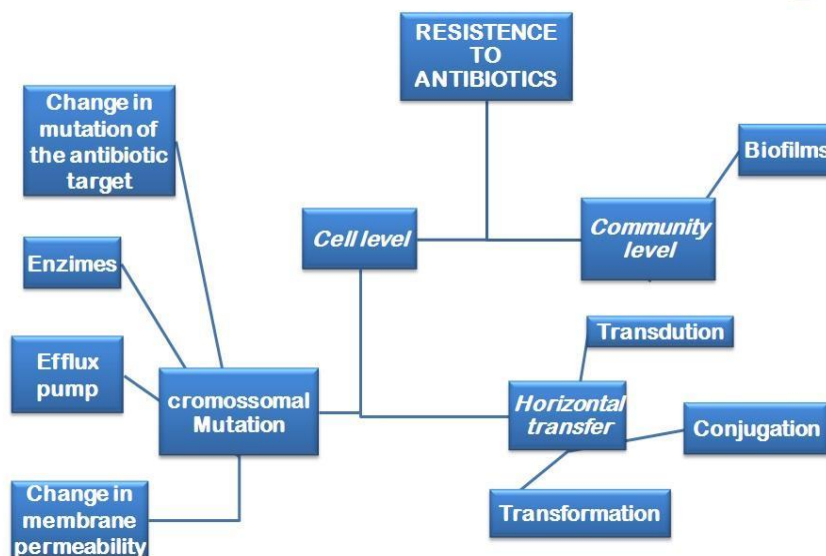
### 1.4 Resistance mechanisms

The treatment of nosocomial infections caused by the most common multidrug-resistant pathogens *Enterococcus faecium*, *Staphylococcus aureus*, *Klebsiella pneumoniae*, *Acinetobacter baumannii*, *Pseudomonas aeruginosa*, and *Enterobacter* spp., called “escape pathogens” is a major challenge. [21] Since the discovery of penicillin, antibiotics have played a crucial role in the control of infectious diseases, however, their inappropriate and abusive use over the years mainly due to early interrupted treatments, self-medication, use of drugs without specificity and lack of control of the use of antibiotics in the food industry has resulted in the emergence of pathogenic bacteria of difficult treatment. [54]

Inadequate use of broad-spectrum orally administered  $\beta$ -lactam antibiotics such as ampicillin, amoxicillin, or cefalexin provoke the selection of ESBLs producing  $\beta$ -Proteobacteria in hospitals and communities. Resistance to  $\beta$ -lactams in *Staphylococcus aureus*, different from Gram-negative, is often mediated by modified transpeptidases (target  $\beta$ -lactam proteins). The lactam ring is hydrolyzed by these enzymes that usually attack a wide spectrum of these antibiotics. [55]

The appearance of resistant superbug reduced the efficacy of the old drugs, becoming necessary the discovery of new and stronger antibacterial molecules. [55] Fluoroquinolones represent one of the most common drugs used nowadays in the treatment of bacterial infections, as well as several other diseases. [56] This group of antibiotics belongs to the second generation of quinolones including Ciprofloxacin and Norfloxacin. [57]

So, following this thought the creation of new antibiotics has to meet the requirements of low selectivity, specificity, neutralize biofilms and kill dormant bacteria. [58] As achieving these requirements is not a very easy task, a viable alternative is to act on the pathogen virulence factors, so directing research to create new inhibitors that combined with known drugs can restore their action i.e. to reduce the appearance of resistant strains, to enlarge the bacterial spectrum and to minimize the formation of biofilms and resistance. [59] In general, bacterial resistance can be summarized as shown in the Scheme 2 below:



Scheme 2. Types of bacterial resistance to antibiotics [58]

Antibiotic resistance can be developed at the cellular level owing to chromosomal mutation or horizontal transfer (transformation, transduction or conjugation) and at the community level (biofilm). At the cellular level, bacteria can become resistant to antibiotics by inactivation of the antibiotic through enzyme, chemical modification of the antibiotic target, change in cellular permeability or expression of efflux pumps. [58]

Analyzing otherwise there are two categories of antibacterial resistance mechanisms:

a) innate or intrinsic resistance and b) acquired resistance. Intrinsic resistance is related to biological properties of the own bacteria, while acquired resistance refers to the incorporation of bacteria resistance genes for bacteria or chromosomal mutation and combination of both. [60]

A previous study found that the increased expression of flotation pumps is often related to mutation in the regulatory network controlling expression and that these mutations may be within a local repressor gene, due to a global transcription factor or intergenic sites that alter the expression of the pump genes or their regulators. [61] Flow pumps are protein structures capable of expelling toxins, antibiotics and various compounds through primary and secondary active transporters out of the cell. The primers use ATP hydrolysis [62] and the secondary ones use ion gradient [63] both to catalyze transport through the membrane. In addition to these categories of active primary carriers and secondary active carriers, there is a third category of phosphotransferase system that catalyzes the transport of drugs with concomitant phosphorylation of the drug, usually for the cellular entry of the drug substrate. [64]

Researchers [65] showed results indicating that flavones are promising lead compounds to treat MRSA-associated infections through disrupting the proton motive force and membrane permeability. NorA, TetK and QacC are examples of proton motive force-dependent efflux pumps. [66]

The resistance mechanism mediated by efflux pumps has inspired several studies. Currently, they are the most prevalent mechanisms in multidrug-resistant bacteria. [67] More than 15 types of efflux pumps expressed by plasmids or chromosomes are known and 7 chromosomal efflux systems were encoded in *Staphylococcus aureus* (NorA, Norb, Norc, MdeA, SepA, MepA and SdrM) where only MepA belongs to the multidrug and toxic compound extrusion (MATE) and the others the superfamily of the main facilitator superfamily (MFS). [68]

In addition to these two, three other families that have been identified are important: the small resistance to multidrugs, the ATP-binding cassette (ABC) transporter superfamily and the resistance nodulation division (RND) superfamily. [69] All of them are found in both Gram-positive and Gram-negative, with the exception of RND, which is expressed exclusively by Gram-negative bacteria. [70]

Nora transmembrane protein usually encoded from the nor A gene is commonly more expressed in resistant strains of *Staphylococcus aureus*. It acts by anti-carrier mechanism under proton motive force, expelling toxic compounds, fluoroquinolone such as Ciprofloxacin and Ethidium bromide. [71] To try to reverse this situation, the literature addresses five forms of inhibition of the efflux pump:

- 1) Reduction of the genetic expression of the pump;
- 2) Interruption of the pump assembly;

- 3) Reduction by competitive means or not the binding of the substrate;
- 4) Interruption of the pump energy source [72] and
- 5) Epi-substrate complex formation preventing the extrusion of the cell substrate when they have affinity as p-glycoprotein protein. [73]

In summary efflux pumps expel structurally diverse compounds, including antibiotics from clinical environment that are even becoming therapeutically ineffective. In this sense, in addition to new antibiotics and resistance modifying agents, it is efflux pump inhibitor that are characterized.

## 1.5 Docking studies

3D structures of protein-ligand complexes (PL) for many years have opened paths. However, changes in theoretical developments, improvement of computational algorithms and more efficient computational resources, allowed the use of routine methods *in silico* to model this interaction PL. This relationship becomes increasingly explored, in the sense of describing the protein ligand and its interactions more precisely, as well as predicting the affinities of connection. [74-75] These affinities, very useful for the identification of binding sites in proteins. [76]

A reliable prediction of the affinity of receptor-molecules (1Gbinding) at the beginning of research is essential for the creation of new drugs. An accurate calculation depends on factors such as the system's energy model, protein flexibility count, the presence of water at the connection site, and the solvent model. [75]

On the other hand, quantum mechanics (QM) approaches have their limitations regarding the accuracy and predictability of these methods:

- i) additional validation and benchmarking are required;
- ii) need optimized codes especially those that use Graphics processing units;
- iii) flexibility of conformational sampling and proteins (for example, minimization with the possibility of cutting the system, and optimal combinations of these fully validated);
- iv) solvency contribution in charge systems;
- v) omission of entropic considerations. [75]

The purpose of anchoring simulations is to determine binding conformation (mode) and affinity (binding) between a ligand and a macromolecular receptor. [77-78] Molecular fitting predicts thermodynamic parameters based on molecular recognition between two or more molecules. [79] There are several methods for molecular coupling and virtual screening already developed such as AutoDOCK [80], DOCK [81], SLIDE [82], Rosette Ligand [83] but no method is better or worse than the other, assuming that for optimal performance different targets may require different combinations of approaches, sampling and scoring functions [84-85]. Davis and colleagues (2009) found that although the overall success rate varies dramatically between systems,

all targets were found in a collection of GlaxoSmithKline precise binding compounds and that no algorithm consistently outperformed the others in all tested systems. [86]

Coupling applications can be rigid body and flexible coupling. Rigid body ones are usually used as a fast method for initial screenings of small molecules. [87] Because they do not consider the binder or the flexibility of the receptor, therefore, they have reduced specificity and precision. Nevertheless, they can correctly predict the binding sites of the ligand for different proteins in relation to their co-crystallized complexes. [88] In contrast, flexible coupling methods, although they allow the flexibility of the side chain to be modeled, it can make it difficult to obtain reliable data, because the process of recognizing binders in proteins is complete and expensive. [89] Currently, most computational coupling programs, such as Autodock 3.0.5 and AutodockVina consider protein as a rigid body and ligand as a flexible molecule. [90]

In this thought, the hybrid methods one uses information based on (I) receptors such as some nuclear magnetic resonance (NMR) restrictions, (II) small molecules such as SARs or (III) the contacts of the protein receptor with the mini-molecule. These hybrid methods for coupling small molecules can be classified according to the data type and the integration point and the experimental information according to the structure of the receptors in the small molecules or the interface. [91]

The results are usually evaluated first with a visual observation of the predicted connection modes for correct answers followed by structural analysis, geometric grouping of predicted poses, re-scoring and cheminformatics approaches. The output of ligand coupling programs usually includes a Protein Data Bank (PDB) coordinate file and supplementary data such as predicted binding affinity, pose grouping options, etc. [92]

Docking is being widely applied in research in several areas, such as in the study of melatonin receptors [93], in the study of anti-cancer agents [94], in the development of new anti-leishmanial drugs [95], in the understanding of drug metabolism. [96] Docking techniques are important for the study of several areas such as compounds that act on multiple targets against complex (multifactorial) diseases such as cancer, degenerative diseases and infections from molecular coupling. Making it possible to observe the complexes formed between ligands and targets of certain diseases such as Alzheimer's. [97]

New methods from couplings can also predict in computer and detect the site of metabolism making comparisons of the molecule with information from the literature. As well as modifying a molecule in specific locations to design compounds with greater metabolic stability because *in silico* methods in combination with previous metabolic identification studies can be synergistic in determining an activity. [96]

Recent studies with molecular docking [98] evaluate the norAefflux pump expressed by *Staphylococcus aureus* describing the norfloxacin binding site of a NorA model to explain at the molecular level the interactions of aminoguanidine hydrants with the generated pump model and was observed by molecular docking [99] that thiophene DB hinders the binding of norfloxacin to NorA, being expelled from the bacteria in place of the antibiotic and probably functioning as a competitive inhibitor of the NorA efflux protein.

### 1.5.1 Methodology

The present review focuses on the recent developments in the antibacterial activity against *Staphylococcus aureus* of Chalcones in the last 13 years through databases such as Cyber Analytical Platform and Examination System (CAPES), Google scholar and Pubmed. We considered articles published from 2007 to 2020 that reported the MIC, flow pump as a mechanism of resistance and molecular docking analysis as a complementary analysis. Molecular Docking and absorption, distribution, metabolism, excretion and toxicity (ADMET) of five chalcones with better activity are discussed here. This work will be useful for future investigations on these multifaceted molecules.

### 1.5.2 Obtaining the 3D structure of the target protein

The structure of the *Staphylococcus aureus*, Tyrosyl-tRNA synthetase (TyrRS) protein was obtained from the Protein Data Bank database (<https://www.rcsb.org/>). The protein was prepared for molecular docking simulations by removing all residues and adding polar hydrogens [100] to produce favorable protonation states for docking. [101] *Staphylococcus aureus* TyrRS was identified in the repository as “Cristal structure of *Staphylococcus aureus*, TyrRS in complex with SB-239629” (PDB 1JIJ). The structure of TyrRS is deposited in Protein Data Bank with a resolution of 3.20 Å, determined by X-ray diffraction (R-Value Free: 0.305, R-Value Work: 0.257), classified as ligase, *Staphylococcus aureus* organism and expression system *Escherichia coli*.

### 1.5.3 Preparation of binders

For the study of molecular docking, MIC below 1µg/mL of reported chalcones were selected as ligands, being coded as: CHALSA1, CHALSA2, CHALSA3, CHALSA4 and CHALSA5. Seeking to use the ligands in their best potential energy state for docking simulations, CHALSA1-5 was optimized by the semi-empirical parametric method 7 (PM7) [102-103] using the MOPAC® software.

### 1.5.4 Molecular Docking

Computational simulations of interaction between *Staphylococcus aureus* TyrRS and possible inhibitors were performed using the AutoDock Vina code (version 1.1.2), using 3-way multithreading, Lamarckian Genetic Algorithm [90]. The grid box parameters were configured to fit the whole protein for a greater range in the selection of poses and as a standard procedure 100 independent simulations were performed for all protein targets, obtaining 10 poses each. As a criterion for selecting the simulations with the best poses, results that presented free binding energy ( $\Delta G$ ) below -6.0 kcal/mol [104] and Root Mean Square Deviation (RMSD) values less than 2 Å were considered. [105] The Discovery Studio Visualizer [106] and UCSF Chimera [107] codes were used to analyze the results and generate two-dimensional maps of chemical interactions. Based on the distances between the donor and acceptor atoms, the hydrogen bonds are classified as strong (between 2.5 and 3.1 Å), moderate (between 3.1 to 3.55 Å) and weak (> 3.55 Å).

### 1.5.5 ADMET

Chalcones 1-5 analogs were drawn using MarvinSketch® software version 20.15 [108], where the physicochemical properties used as bioavailability and pharmacokinetic descriptors were calculated, such as: acid ionization constant (pKa), partition coefficient (log P) and buffer (log D7.4) and polarity (TPSA). Then, the SMILES of the compounds were loaded on the pkCSM web server (<http://biosig.unimelb.edu.au/pkcsm/prediction>) [109], where the pharmacokinetic properties were predicted by the ADMET. After determining the bioavailability of the compounds, bioactivities were predicted through interactions with the target classes of GPCR ligand, Ion channel modulator, and Enzyme inhibitor on the Molinspiration web server (<https://molinspiration.com/cgi-bin/properties>), where values less than 0.02 indicate low activity and values greater than 0.05 indicate high activity.

## 2. Results

### 2.1 Docking Results of Chalcones

CHALSA1 presented RMSD in the 1.097 Å, CHALSA2 was 1.85 Å, CHALSA3 was 1.452 Å, CHALSA4 was 1.531 Å and CHALSA5 was 1.863 Å. CHALSA1 also presented an affinity energy of -7.4 kcal / mol, CHALSA2 of -7.6 kcal / mol, CHALSA3 of -6.0 kcal / mol and CHALSA 5 of -6.3 kcal / mol, CHALSA4 -5.8 kcal / mol. CHALSA1 showed hydrogen bonds with the residues GLY38, GLY193 stands out SER194, GLN196, and VAL224, with distances varying between 2.12 and 2.65 Å and three hydrophobic interactions with the HIS50A, PRO53A, VAL224A residues, with distances between 3.45 and 3.98 Å. CHALSA2 presented nine interactions with TyrRS, eight hydrophobic interactions varying between 3.49 and 3.81 Å with

residues VAL4, GLU7, ASP8, TRP11, ARG59, GLU62, PHE273, LYS276, and a hydrogen bond with the residue LYS276 (Table 2).

With respect to CHALSA3, it presented five interactions, all hydrophobic with distances between 3.62 and 3.99 Å, with residues ILE78, LEU128, LEU133, PHE136, and LEU173. Already CHALSA4 showed only hydrophobic interactions with residues PHE136, PHE136, THR169, and LEU173, in which a  $\pi$ -stacking interaction with residue PHE136 stands out, and all interactions were in the range of 3.49 and 3.90 Å. CHALSA5 presented seven interactions, three strong hydrogen bonds with distances varying between 2.05 and 2.69 Å with residues GLY74, LEU128, THR169, and four hydrophobic interactions varying between 3.26 and 3.87 Å with residues LEU133, PHE136, THR166 and LEU173 (Fig. 2).

Regarding the comparison with the co-crystallized inhibitor, only the CHALSA1 coupled in the region of the catalytic site of the inhibitor SB-239629, presenting hydrogen bonds with the residues GLY38, GLY193, and GLN196, highlighting that these bonds were classified as strong (Fig. 3). The chalcones CHALSA2-5, despite presenting favorable binding energy to the protein target, are coupled in different regions of the active site of the inhibitor SB-239629 (Fig. 4).

Table 2. Interactions between *Staphylococcus aureus* TyrRS and chalcones

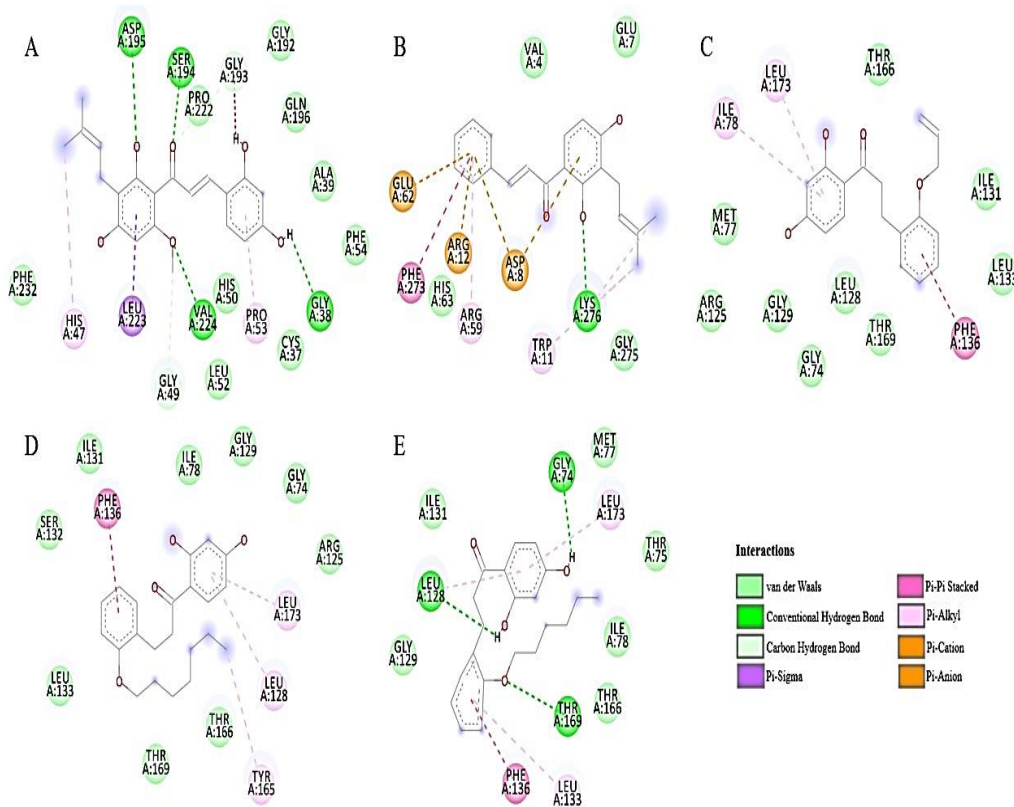
Ligand	Receptor	Interaction	Distance (Å)	
CHALSA1	*GLY38A	H-Bond	2.45	
	*GLY193A	H-Bond	2.26	
	SER194A	H-Bond	2.47	
	*GLN196A	H-Bond	2.65	
	VAL224A	H-Bond	2.12	
	HIS50A	Hydrophobic	3.98	
	PRO53A	Hydrophobic	3.47	
	VAL224A	Hydrophobic	3.45	
	VAL4A	Hydrophobic	3.58	
	GLU7A	Hydrophobic	3.81	
	ASP8A	Hydrophobic	3.57	
	TRP11A	Hydrophobic	3.51	
	CHALSA2	ARG59A	Hydrophobic	3.80
	GLU62A	Hydrophobic	3.63	
PHE273A	Hydrophobic	3.85		
LYS276A	Hydrophobic	3.49		
LYS276A	H-Bond	2.77		
ILE78A	Hydrophobic	3.84		
CHALSA3	LEU128A	Hydrophobic	3.99	
	LEU133A	Hydrophobic	3.62	
	PHE136A	Hydrophobic	3.75	
	LEU173A	Hydrophobic	3.68	
CHALSA4	PHE136A	Hydrophobic	3.52	
	PHE136A	$\pi$ -stacking	3.90	
	THR169A	Hydrophobic	3.79	
	LEU173A	Hydrophobic	3.49	
CHALSA5	GLY74A	H-Bond	2.05	
	LEU128A	H-Bond	2.45	
	THR169A	H-Bond	2.69	
	LEU133A	Hydrophobic	3.51	
	PHE136A	Hydrophobic	3.68	



THR166A	Hydrophobic	3.87
LEU173A	Hydrophobic	3.26

\*

to the  
site of  
SB-



Residues  
belonging  
catalytic  
inhibitor  
239629

Fig. 2: 2D maps of interactions between TyrRS-CHALSA1 (A), TyrRS-CHALSA2 (B), TyrRS-CHALSA3 (C), TyrRS-CHALSA4 (D) and TyrRS-CHALSA5 (E) complexes.

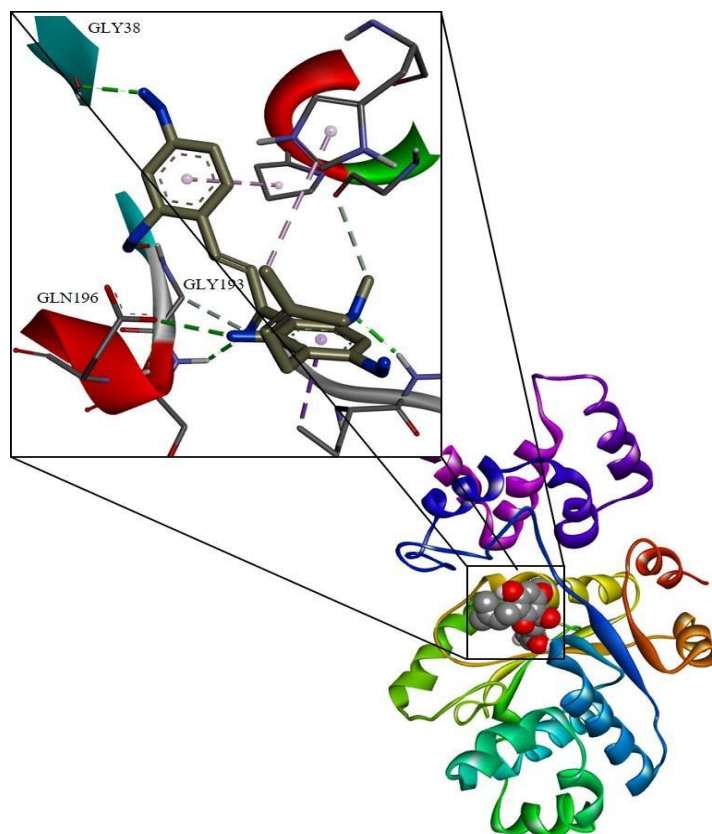


Fig. 3: TyrRS-CHALSA1 complex

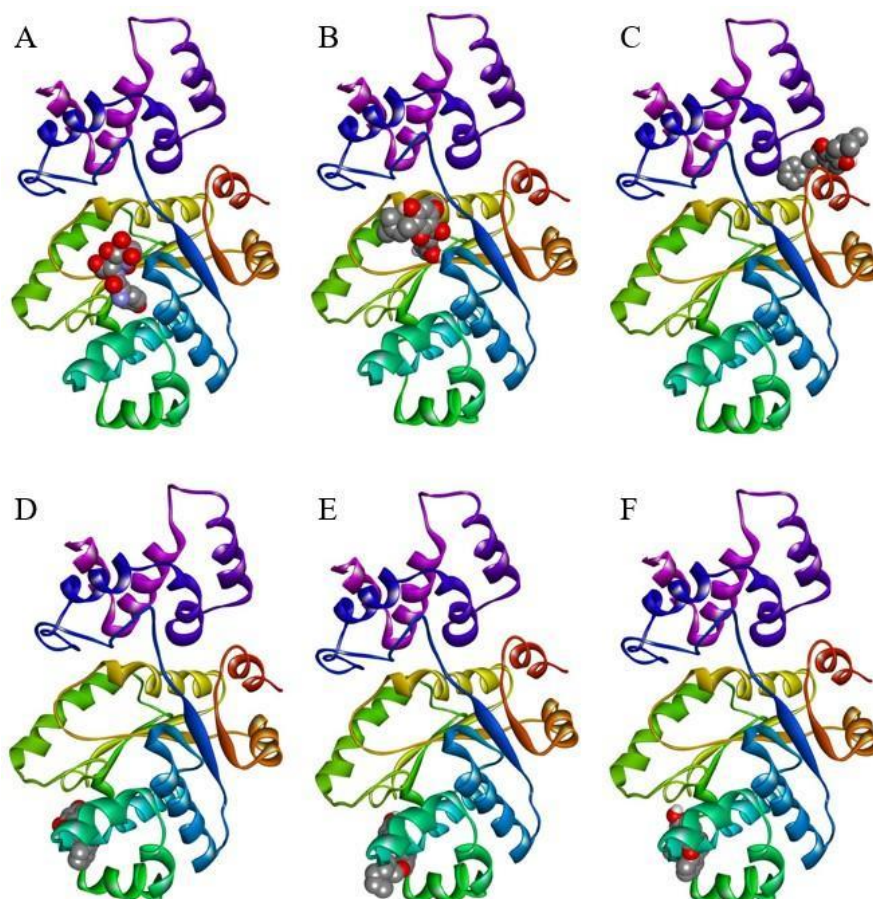


Fig. 4: Three-dimensional structure of the TyrRS-SB239629 (A), TyrRS-CHALSA1 (B), TyrRS-CHALSA2 (C), TyrRS-CHALSA3 (D), TyrRS-CHALSA4 (E) and TyrRS-CHALSA5 (F) complexes.

## 2.2 ADMET Results

Through the physicochemical properties calculated for Chalcones A1-5 analogues, such as ionization constant (pKa), partition coefficient (log P) and buffer (log D<sub>7.4</sub>) and polarity (TPSA), it was possible to make a quantitative structure relationship activity (QSAR) determinants of bioavailability and pharmacokinetics of these compounds (table 3) [110-114] .

Table 3. Predicted ADMET properties of the chalcone analogs A1-5.

Properties	A1	A2	A3	A4	A5
pKa	7.005	6.930	7.866	7.866	7.866
log P	4.897	5.662	4,426	6.353	5.908
log D <sub>7.4</sub>	4.330	5.053	4,299	6.225	5.781
TPSA	110.05	60.36	66.76	66.76	66.76
	0	0	0	0	0
<b>Absorption</b>					
Intestinal absorption (human, %)	72.647	96.40	93.25	89.54	89.64
		2	5	8	5

Absorbed)					
P-glycoprotein substrate	Yes	No	Yes	Yes	Yes
P-glycoprotein I inhibitor	Yes	Yes	Yes	Yes	Yes
<b>Distribution</b>					
VD <sub>ss</sub> * (human, log L/kg)	0	0.367	0.032	-0.013	-0.201
Blood Brain Barrier permeability (log BB)	-1.002	-0.378	-0.453	-0.284	-0.351
<b>Metabolism</b>					
CYP2D6 substrate	No	No	No	No	No
CYP3A4 substrate	No	Yes	No	No	No
<b>Excretion</b>					
Total Clearance (log ml/min/kg)	0.431	0.28	0.313	1.117	1.145
<b>Toxicity</b>					
G-protein-coupled receptors ligand	-0.01	0.01	-0.07	0.15	0.15
Ion channel modulator	-0.07	-0.00	-0.09	0.01	0.01
Enzyme inhibitor	0.16	<b>0.23</b>	0.09	<b>0.21</b>	<b>0.22</b>
AMES toxicity	No	No	Yes	No	No
hERG I inhibitor	No	No	No	No	No
Oral Rat Acute Toxicity (LD <sub>50</sub> **)	2.313	2.134	1.914	1.957	1.984
Hepatotoxicity	No	Yes	No	No	Yes

\* VD<sub>ss</sub>: volume of distribution. \*\*LD<sub>50</sub>, mol/kg

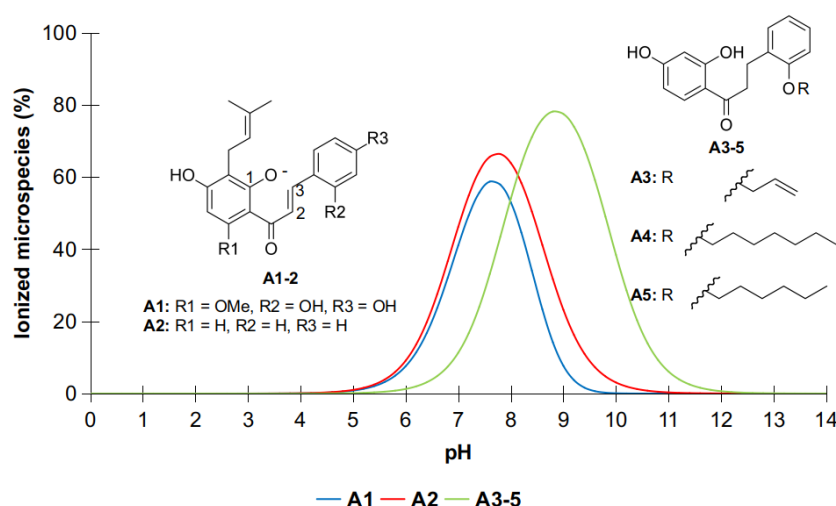


Fig. 5: Ionized microspecies distribution of the Chalcones A1-5 analogs with the pH variation.

### 3. Discussions

#### 3.1 Docking

With the accumulative rise in bacterial resistance to current drugs, the search for more efficient pharmacological tools that can specifically block proteins essential for bacterial replication has been encouraged. This line of research is reinforced by the success of the antibacterial drug Mupirocin, which targets bacterial isoleucyl-tRNA synthetases. [115] Aminoacyl-tRNA synthetases play an essential role in protein synthesis, producing charged tRNAs, the inhibition of these enzymes can interfere with the bacterial replicative process. [116]

In this context, molecules that have the ability to bind aminoacyl-tRNA synthetases have the potential for inhibition and therefore can become antibacterial drugs. [117] For the study of the inhibitory potential of *Staphylococcus aureus* TyrRS, the monocyclic inhibitor SB-239629 was used as a comparison, which has an IC<sub>50</sub> of 3nM [118] and is complexed with the enzyme through four hydrogen bonds and one hydrophobic interaction with His48.

After carrying out the docking simulations, it was possible to observe that chalcones 1 to 5 had an RMSD value within the ideal parameter, less than 2 Å [119]. As a fundamental parameter, affinity energy was used, which, according to the literature, values lower than -6.0 kcal/mol, indicate high affinity to interact with the protein target. [104] following these parameters, CHALSA4 presented a value slightly below the ideal parameter. Allowing us to infer that these chalcones have a good affinity with *Staphylococcus aureus* TyrRS, which corroborates the practical results found in the literature that presented lower MIC values at 1 µg / mL [117], thus reflecting a high affinity. Chalcones 1 to 5 showed interactions with the protein target forming complexes that showed interactions with distances between 2.05 and 3.99 Å (Table 2).

CHALSA1 presented connections that classify as strong [120]. The chalcones 1-5 showed favorable affinity energy for interaction with the TyrRS receptor, presenting hydrophobic interactions and hydrogen bonds, highlighting that CHALSA1 is coupled in a region similar to that of the SB-239629 inhibitor, which does not happen with the other analyzed chalcones (CHALSAs 2-5) that couple in different regions of the catalytic center, suggesting potential use in synergism with other molecules (Fig. 4).

#### 3.2 ADMET

When evaluating the main micro species of the compounds, it is possible to observe that the pK<sub>a</sub> values suggest that the substances A1-2 have a charge generated as a function of the ionization of the hydroxyl group attached to carbon 1 of the benzene pentasubstituted in physiological pH. At the same time, the modification of the alkyl radicals to the oxygen bonded to the bisubstituted

benzene of the A3-5 analogs suggests the predominance of its neutral species (Fig. 5). Although the neutral characteristic of the molecules is favorable for their respective pharmacokinetic phases, they are very lipophilic compounds, with log P values ranging from 4.4 to 6.3, in addition to being highly permeable in intestinal cells ( $\log D > 3$ ), which indicates which are highly absorbed compounds in the intestine, with absorption percentages  $> 70\%$  (Table 3).

Another limiting factor in the transport of drugs across cell membranes and the decrease in their bioavailability is the inhibition of intestinal P-glycoprotein. [114] The high polarity of the compounds, with TPSA values greater than  $60\text{\AA}$ , together with their high lipophilicity and permeability potentials, suggest that the compounds are potential Pgp inhibitors. As a consequence of this, we can highlight the analog A1 with  $\text{TPSA} = 110.05\text{\AA}^2$ , with VDss that tries to zero, after intestinal absorption.

In addition, the other A2-5 analogs have molecular volume available for transport and diffusion in cell membranes and for penetration into the various biological barriers, such as the Blood-Brain Barrier, where the log BB values between -0.4 and -0.2 indicate that they are compounds moderately absorbed in the central nervous system (Table 3).

As the main precursors of phase I metabolism, cytochrome P450 isoenzymes (CYP450) are responsible for the redox reactions of the drug. CYP3A4 is the enzyme responsible for O-dealkylation reactions, constituting more water-soluble compounds for renal elimination. [121-123] In this prediction, only compound A2 is a potential substrate for CYP3A4, this is due to the compound being predominantly lipophilic and little polar, where the two hydroxyl groups linked to the pentasubstituted benzene are subject to structural modifications, constituting more water-soluble radicals, with potential for release total log ml / min / kg in the order of 0.28 (Table 3).

Tumorigenic activity has led to an emphasis on studies of rational drug planning, where it is possible to detect carcinogenic activity caused by oral medication administration. The interaction with several biological targets can provide information about the toxicological activity of an oral drug candidate. [124-125] The low score of interaction with G-protein-coupled receptors indicates that the substances have poor interaction with proteins of cell membranes, while the prediction of AMES toxicity suggests that substance A2 may have carcinogenic activity.

In addition, the ligands have low interaction with ion transport channels, which means that they are not inhibitors of hERG channels, and do not present a cardiotoxic risk. Finally, the minimum oral dose of LD50 evaluated for compounds A2 and A5 in the order of 2.134 and 1.984 mol/kg, respectively, together with their enzyme inhibiting activity, suggests that the compounds may inhibit the activity of metabolizing enzymes in drugs, resulting in liver toxicity (Table 3).

Through the physicochemical properties, it was possible to justify the bioavailability and pharmacokinetics predicted for the Chalcones A1-5 analogs. Since they are predominantly

lipophilic compounds and highly absorbed in the intestine, substance A2 obtained greater bioavailability, following the highest order of VD<sub>ss</sub> in the bloodstream. Despite its hepatotoxic tendency, the substance has the best bioactivity with multi-biological targets, constituting an active ingredient as a promising oral drug.

#### 4. Conclusions

Chalcones are composed with primordial characteristics and relevant in chemistry-pharmacology, encompass multiple biological activities in both prokaryotes and eukaryotes. Their simple structure facilitates its manipulation in the synthesis of new compounds to enhance their bioactivities. These studies can be improved, streamlined and economically viable with the use of molecular docking.

The docking together with the study of extrusion-activity makes it possible to understand the molecule widely, the mechanisms involved in the actions of the molecule and the characteristics of the coupling of its receptors. It also makes it possible to develop new compounds, agonists and more selective antagonists.

The results of the antimicrobial activity of 29 chalcones and 5 most active chalcones against *Staphylococcus aureus* was supported by *in silico* and the pharmacokinetic study which not only confirmed their potential to act against resistant strains but also established in future utility of chalcones as lead molecules or prototypes for the synthesis of potent new antimicrobial agents against *Staphylococcus aureus*.

However, the main gap in this area of research is the scarcity of clinical trials. With them the results of the research could reach pharmacies and the consumption of the population to fight serious bacterial infections such as those caused by *Staphylococcus aureus*.

#### References

- 1 Wright, G. D. Opportunities for Natural Products in 21st Century Antibiotic Discovery. *Nat. Prod. Rep.* **2017**, *34* (7), 694–701. <https://doi.org/10.1039/c7np00019g>.
- 2 Mahapatra, D. K.; Bharti, S. K.; Asati, V. Anti-Cancer Chalcones: Structural and Molecular Target Perspectives. *Eur. J. Med. Chem.* **2015**, *98*, 69–114. <https://doi.org/10.1016/j.ejmech.2015.05.004>.
- 3 Gaonkar, S. L.; Vignesh, U. N. Synthesis and Pharmacological Properties of Chalcones: A Review. *Res. chem. intermed.* **2017**, *43* (11), 6043–6077. <https://doi.org/10.1007/s11164-017-2977-5>.

- 4 Ur Rashid, H.; Xu, Y.; Ahmad, N.; Muhammad, Y.; Wang, L. Promising Anti-Inflammatory Effects of Chalcones via Inhibition of Cyclooxygenase, Prostaglandin E2, Inducible NO Synthase and Nuclear Factor K $\beta$  Activities. *Bioorg. Chem.* **2019**, *87*, 335–365. <https://doi.org/10.1016/j.bioorg.2019.03.033>.
- 5 Sahu, N. K.; Balbhadra, S. S.; Choudhary, J.; Kohli, D. V. Exploring Pharmacological Significance of Chalcone Scaffold: A Review. *Curr. Med. Chem.* **2012**, *19* (2), 209–225.
- 6 Silva, C. F. M.; Pinto, D. C. G. A.; Silva, A. M. S. Chromones: A Promising Ring System for New Anti-Inflammatory Drugs. *ChemMedChem* **2016**, *11* (20), 2252–2260. <https://doi.org/10.1002/cmdc.201600359>.
- 7 Mujwar, S.; Deshmukh, R.; Harwansh, R. K.; Gupta, J. K.; Gour, A. Drug Repurposing Approach for Developing Novel Therapy against Mupirocin-Resistant *Staphylococcus aureus*. *Assay Drug Dev. Technol.* **2019**, *17* (7), 298–309. <https://doi.org/10.1089/adt.2019.944>.
- 8 8. Mishra I, Sachan N. Thiazole Scaffold: An Overview on Its Synthetic and Pharmaceutical Aspects. *ECS Transactions.* **2022**, *107* (1), 17745.
- 9 Zhou, B.; Xing, C. Diverse Molecular Targets for Chalcones with Varied Bioactivities. *Med. Chem. (Los Angeles)* **2015**, *5* (8), 388–404. <https://doi.org/10.4172/2161-0444.1000291>.
- 10 Baviskar, B. A.; Baviskar, B.; Shiradkar, M. R.; Deokate, U. A.; Khadabadi, S. S. Synthesis and Antimicrobial Activity of Some Novel Benzimidazolyl Chalcones. *E-J. Chem.* **2009**, *6* (1), 196–200. <https://doi.org/10.1155/2009/746292>.
- 11 Khan, S. A.; Asiri, A. M.; Alamry, K. A.; El-Daly, S. A.; Zayed, M. A. M. Eco-Friendly Synthesis and in Vitro Antibacterial Activities of Some Novel Chalcones. *Russ. J. Bioorganic Chem.* **2013**, *39* (3), 312–317. <https://doi.org/10.1134/s1068162013030072>.
- 12 Medina, E.; Pieper, D. H. Tackling Threats and Future Problems of Multidrug-Resistant Bacteria. *Curr. Top. Microbiol. Immunol.* **2016**, *398*, 3–33. [https://doi.org/10.1007/82\\_2016\\_492](https://doi.org/10.1007/82_2016_492).
- 13 Isha; Sachan, N. Design, Synthesis and Biological Assessment of Thiazole Derivatives as Possible Antioxidant and Antimicrobial Agents. *J. Pharm. Res. Int.* **2021**, 24–32. <https://doi.org/10.9734/jpri/2021/v33i53a33635>.
- 14 Pandit, N.; Shah, K.; Agrawal, N.; Upmanyu, N.; Shrivastava, S. K.; Mishra, P. Synthesis, Characterization and Biological Evaluation of Some Novel Fluoroquinolones. *Med. Chem. Res.* **2016**, *25* (5), 843–851. <https://doi.org/10.1007/s00044-016-1526-x>.
- 15 Mishra, R.; Sachan, N.; Kumar, N.; Mishra, I.; Chand, P. Thiophene Scaffold as Prospective Antimicrobial Agent: A Review: Thiophene as Antimicrobial Agent: A Review. *J. Heterocycl. Chem.* **2018**, *55* (9), 2019–2034. <https://doi.org/10.1002/jhet.3249>.



- 16 Mishra, I.; Mishra, R.; Mujwar, S.; Chandra, P.; Sachan, N. A Retrospect on Antimicrobial Potential of Thiazole Scaffold. *J. Heterocycl. Chem.* **2020**, *57* (6), 2304–2329. <https://doi.org/10.1002/jhet.3970>.
- 17 Krishna, S.; Miller, L. S. Host-Pathogen Interactions between the Skin and *Staphylococcus aureus*. *Curr. Opin. Microbiol.* **2012**, *15* (1), 28–35. <https://doi.org/10.1016/j.mib.2011.11.003>.
- 18 Dugourd, P. M.; Dupont, A.; Hubiche, T.; Chiaverini, C.; Alkhalifa, A.; Roudiere, L.; Tristan, A.; Gustave, C. A.; Del Giudice, P. *Staphylococcal* toxic shock syndrome should be considered in the event of diffuse erythema with fever and shock. *Ann Dermatol Vener.* **2019**, *146* (4), 287–291.
- 19 Bergin, S. P.; Holland, T. L.; Fowler, V. G., Jr; Tong, S. Y. C. Bacteremia, Sepsis, and Infective Endocarditis Associated with *Staphylococcus aureus*. *Curr. Top. Microbiol. Immunol.* **2017**, *409*, 263–296. [https://doi.org/10.1007/82\\_2015\\_5001](https://doi.org/10.1007/82_2015_5001).
- 20 Dantes, R.; Mu, Y.; Belflower, R.; Aragon, D.; Dumyati, G.; Harrison, L. H.; Lessa, F. C.; Lynfield, R.; Nadle, J.; Petit, S.; Ray, S. M.; Schaffner, W.; Townes, J.; Fridkin, S.; Emerging Infections Program-Active Bacterial Core Surveillance MRSA Surveillance Investigators. National Burden of Invasive Methicillin-Resistant *Staphylococcus aureus* Infections, United States, 2011. *JAMA Intern. Med.* **2013**, *173* (21), 1970–1978. <https://doi.org/10.1001/jamainternmed.2013.10423>.
- 21 Pendleton, J. N.; Gorman, S. P.; Gilmore, B. F. Clinical Relevance of the ESKAPE Pathogens. *Expert Rev. Anti. Infect. Ther.* **2013**, *11* (3), 297–308. <https://doi.org/10.1586/eri.13.12>.
- 22 Yılmaz, E. Ş.; Aslantaş, Ö. Antimicrobial Resistance and Underlying Mechanisms in *Staphylococcus aureus* Isolates. *Asian Pac. J. Trop. Med.* **2017**, *10* (11), 1059–1064. <https://doi.org/10.1016/j.apjtm.2017.10.003>.
- 23 van Hoek, A. H. A. M.; Mevius, D.; Guerra, B.; Mullany, P.; Roberts, A. P.; Aarts, H. J. M. Acquired Antibiotic Resistance Genes: An Overview. *Front. Microbiol.* **2011**, *2*, 203. <https://doi.org/10.3389/fmicb.2011.00203>.
- 24 Kohanski, M. A.; DePristo, M. A.; Collins, J. J. Sublethal Antibiotic Treatment Leads to Multidrug Resistance via Radical-Induced Mutagenesis. *Mol. Cell.* **2010**, *37* (3), 311–320. <https://doi.org/10.1016/j.molcel.2010.01.003>.
- 25 Dua, R.; Shrivastava, S.; Sonwane, S.; Srivastava, S. Pharmacological significance of synthetic heterocycles scaffold: A review. *Adv. Biol. Res.* **2011**, *5*, 120–144.
- 26 Kalirajan, R.; Sivakumar, S. U.; Jubie, S.; Gowramma, B.; Suresh, B. Synthesis and biological evaluation of some heterocyclic derivatives of chalcones. *Int. J. ChemTech Res.* **2009**, *1*, 27–34.

- 27 Rammohan, A.; Reddy, J. S.; Sravya, G.; Rao, C. N.; Zyryanov, G. V. Chalcone Synthesis, Properties and Medicinal Applications: A Review. *Environ. Chem. Lett.* **2020**, *18* (2), 433–458. <https://doi.org/10.1007/s10311-019-00959-w>.
- 28 Lal, K.; Yadav, P.; Kumar, A.; Kumar, A.; Paul, A. K. Design, Synthesis, Characterization, Antimicrobial Evaluation and Molecular Modeling Studies of Some Dehydroacetic Acid-Chalcone-1,2,3-Triazole Hybrids. *Bioorg. Chem.* **2018**, *77*, 236–244. <https://doi.org/10.1016/j.bioorg.2018.01.016>.
- 29 Qiu R.-L.; Li L.; Zhu M.-H.; Liu J. Study on the chemical constituents of *Psoralea corylifolia*. *Zhong Yao Cai* **2011**, *34* (8), 1211–1213.
- 30 Doan, T. N.; Tran, D. T. Synthesis, Antioxidant and Antimicrobial Activities of a Novel Series of Chalcones, Pyrazolic Chalcones, and Allylic Chalcones. *Pharmacol. Pharm.* **2011**, *02* (04), 282–288. <https://doi.org/10.4236/pp.2011.24036>.
- 31 Bandgar, B. P.; Patil, S. A.; Gacche, R. N.; Korbadi, B. L.; Hote, B. S.; Kinkar, S. N.; Jalde, S. S. Synthesis and Biological Evaluation of Nitrogen-Containing Chalcones as Possible Anti-Inflammatory and Antioxidant Agents. *Bioorg. Med. Chem. Lett.* **2010**, *20* (2), 730–733. <https://doi.org/10.1016/j.bmcl.2009.11.068>.
- 32 Vogel, S.; Barbic, M.; Jürgenliemk, G.; Heilmann, J. Synthesis, Cytotoxicity, Anti-Oxidative and Anti-Inflammatory Activity of Chalcones and Influence of A-Ring Modifications on the Pharmacological Effect. *Eur. J. Med. Chem.* **2010**, *45* (6), 2206–2213. <https://doi.org/10.1016/j.ejmech.2010.01.060>.
- 33 Kuete, V.; Alibert-Franco, S.; Eyong, K. O.; Ngameni, B.; Folefoc, G. N.; Nguemeving, J. R.; Tangmouo, J. G.; Fotso, G. W.; Komguem, J.; Ouahouo, B. M. W.; Bolla, J.-M.; Chevalier, J.; Ngadjui, B. T.; Nkengfack, A. E.; Pagès, J.-M. Antibacterial Activity of Some Natural Products against Bacteria Expressing a Multidrug-Resistant Phenotype. *Int. J. Antimicrob. Agents* **2011**, *37* (2), 156–161. <https://doi.org/10.1016/j.ijantimicag.2010.10.020>.
- 34 David, M. Z.; Daum, R. S. Community-Associated Methicillin-Resistant *Staphylococcus aureus*: Epidemiology and Clinical Consequences of an Emerging Epidemic. *Clin. Microbiol. Rev.* **2010**, *23* (3), 616–687. <https://doi.org/10.1128/CMR.00081-09>.
- 35 David, M. Z.; Daum, R. S. Treatment of *Staphylococcus aureus* Infections. *Curr. Top. Microbiol. Immunol.* **2017**, *409*, 325–383. [https://doi.org/10.1007/82\\_2017\\_42](https://doi.org/10.1007/82_2017_42).
- 36 DeLeo, F. R.; Otto, M.; Kreiswirth, B. N.; Chambers, H. F. Community-Associated Methicillin-Resistant *Staphylococcus aureus*. *Lancet* **2010**, *375* (9725), 1557–1568. [https://doi.org/10.1016/s0140-6736\(09\)61999-1](https://doi.org/10.1016/s0140-6736(09)61999-1).

- 37 Peacock, S. J.; Paterson, G. K. Mechanisms of Methicillin Resistance in *Staphylococcus aureus*. *Annu. Rev. Biochem.* **2015**, *84* (1), 577–601. <https://doi.org/10.1146/annurev-biochem-060614-034516>.
- 38 Powers, M. E.; Bubeck Wardenburg, J. Igniting the Fire: *Staphylococcus aureus* Virulence Factors in the Pathogenesis of Sepsis. *PLoS Pathog.* **2014**, *10* (2), e1003871. <https://doi.org/10.1371/journal.ppat.1003871>.
- 39 Lee, G.-S. Antibacterial and Synergistic Activity of Prenylated Chalcone Isolated from the Roots of *Sophora Flavescens*. *한국응용생명화학회지* **2010**, *53* (3), 290–296. <https://doi.org/10.3839/jksabc.2010.045>.
- 40 Mbaveng, A. T.; Ngameni, B.; Kuete, V.; Simo, I. K.; Ambassa, P.; Roy, R.; Bezabih, M.; Etoa, F.-X.; Ngadjui, B. T.; Abegaz, B. M.; Meyer, J. J. M.; Lall, N.; Beng, V. P. Antimicrobial Activity of the Crude Extracts and Five Flavonoids from the Twigs of *Dorstenia Barteri* (Moraceae). *J. Ethnopharmacol.* **2008**, *116* (3), 483–489. <https://doi.org/10.1016/j.jep.2007.12.017>.
- 41 Feng, L.; Maddox, M. M.; Alam, M. Z.; Tsutsumi, L. S.; Narula, G.; Bruhn, D. F.; Wu, X.; Sandhaus, S.; Lee, R. B.; Simmons, C. J.; Tse-Dinh, Y.-C.; Hurdle, J. G.; Lee, R. E.; Sun, D. Synthesis, Structure-Activity Relationship Studies, and Antibacterial Evaluation of 4-Chromanones and Chalcones, as Well as Olympicin A and Derivatives. *J. Med. Chem.* **2014**, *57* (20), 8398–8420. <https://doi.org/10.1021/jm500853v>.
- 42 Mariani, R.; Suganda, A.; Sukandar, E. Drug-drug interactions between Griseofulvin and a new prenylated chalcone from *Elatostema parasiticum* and its antibacterial activity nortriptyline at binding sites of bovine serum albumin. *PharmacologyOnline.* **2016**, *1*, 1–6.
- 43 Muharini, R.; Díaz, A.; Ebrahim, W.; Mándi, A.; Kurtán, T.; Rehberg, N.; Kalscheuer, R.; Hartmann, R.; Orfali, R. S.; Lin, W.; Liu, Z.; Proksch, P. Antibacterial and Cytotoxic Phenolic Metabolites from the Fruits of *Amorpha Fruticosa*. In *Phytotherapie 2017 „Von der Innovation zur Evidenz“*; Georg Thieme Verlag KG, 2017.
- 44 Zhang, M.; Prior, A. M.; Maddox, M. M.; Shen, W.-J.; Hevener, K. E.; Bruhn, D. F.; Lee, R. B.; Singh, A. P.; Reinicke, J.; Simmons, C. J.; Hurdle, J. G.; Lee, R. E.; Sun, D. Pharmacophore Modeling, Synthesis, and Antibacterial Evaluation of Chalcones and Derivatives. *ACS Omega* **2018**, *3* (12), 18343–18360. <https://doi.org/10.1021/acsomega.8b03174>.
- 45 Chen, J.; Li, Y.; Yang, L.-Q.; Li, Y.-Z.; Nan, Z.-B.; Gao, K. Biological Activities of Flavonoids from Pathogenic-Infected *Astragalus Adsurgens*. *Food Chem.* **2012**, *131* (2), 546–551. <https://doi.org/10.1016/j.foodchem.2011.09.021>.

- 46 Cui, Y.; Taniguchi, S.; Kuroda, T.; Hatano, T. Constituents of *Psoralea Corylifolia* Fruits and Their Effects on Methicillin-Resistant *Staphylococcus aureus*. *Molecules* **2015**, *20* (7), 12500–12511. <https://doi.org/10.3390/molecules200712500>.
- 47 Gaur, R.; Gupta, V. K.; Pal, A.; Darokar, M. P.; Bhakuni, R. S.; Kumar, B. In Vitro and in Vivo Synergistic Interaction of Substituted Chalcone Derivatives with Norfloxacin against Methicillin Resistant *Staphylococcus aureus*. *RSC Adv.* **2015**, *5* (8), 5830–5845. <https://doi.org/10.1039/c4ra10842f>.
- 48 Alvarez, M. A.; Debattista, N. B.; Pappano, N. B. Antimicrobial Activity and Synergism of Some Substituted Flavonoids. *Folia Microbiol. (Praha)* **2008**, *53* (1), 23–28. <https://doi.org/10.1007/s12223-008-0003-4>.
- 49 Drewes, S. E.; van Vuuren, S. F. Antimicrobial Acylphloroglucinols and Dibenzylxy Flavonoids from Flowers of *Helichrysum Gymnocomum*. *Phytochemistry* **2008**, *69* (8), 1745–1749. <https://doi.org/10.1016/j.phytochem.2008.02.022>.
- 50 Tran, T.-D.; Do, T.-H.; Tran, N.-C.; Ngo, T.-D.; Huynh, T.-N.-P.; Tran, C.-D.; Thai, K.-M. Synthesis and Anti Methicillin Resistant *Staphylococcus aureus* Activity of Substituted Chalcones Alone and in Combination with Non-Beta-Lactam Antibiotics. *Bioorg. Med. Chem. Lett.* **2012**, *22* (14), 4555–4560. <https://doi.org/10.1016/j.bmcl.2012.05.112>.
- 51 Batovska, D.; Parushev, S.; Stamboliyska, B.; Tsvetkova, I.; Ninova, M.; Najdenski, H. Examination of Growth Inhibitory Properties of Synthetic Chalcones for Which Antibacterial Activity Was Predicted. *Eur. J. Med. Chem.* **2009**, *44* (5), 2211–2218. <https://doi.org/10.1016/j.ejmech.2008.05.010>.
- 52 Prasad, S.; Radhakrishna, V.; Ravi, T. K. Synthesis, Spectroscopic and Antibacterial Studies of Some Schiff Bases of 4-(4-Bromophenyl)-6-(4-Chlorophenyl)-2-Aminopyrimidine. *Arab. J. Chem.* **2019**, *12* (8), 3943–3947. <https://doi.org/10.1016/j.arabjc.2016.03.003>.
- 53 Bush, K.; Fisher, J. F. Epidemiological Expansion, Structural Studies, and Clinical Challenges of New  $\beta$ -Lactamases from Gram-Negative Bacteria. *Annu. Rev. Microbiol.* **2011**, *65* (1), 455–478. <https://doi.org/10.1146/annurev-micro-090110-102911>.
- 54 Buffet-Bataillon, S.; Tattevin, P.; Bonnaure-Mallet, M.; Jolivet-Gougeon, A. Emergence of Resistance to Antibacterial Agents: The Role of Quaternary Ammonium Compounds--a Critical Review. *Int. J. Antimicrob. Agents* **2012**, *39* (5), 381–389. <https://doi.org/10.1016/j.ijantimicag.2012.01.011>.
- 55 Paphitou, N. I. Antimicrobial Resistance: Action to Combat the Rising Microbial Challenges. *Int. J. Antimicrob. Agents* **2013**, *42* Suppl., S25-8. <https://doi.org/10.1016/j.ijantimicag.2013.04.007>.

- 56 Sharma, P. C.; Alawadhi, N.; Sharma, A.; Pahwa, R.; Rajak, H. Fluoroquinolones in urinary tract infections: A study on perception analysis of prescribers. *Der Chemica Sinica*. **2010**, *1*(3), 84-90.
- 57 Koba, M.; Baczek, T.; Macur, K.; Bober, L.; Frackowiak, T.; Buciński, A.; Rystok-Grabska, D.; Stasiak, J.; Koba, K. Factor Analysis of Microbiological Activity Data and Structural Parameters of Antibacterial Quinolones. *J. Mol. Model.* **2010**, *16* (2), 327–335. <https://doi.org/10.1007/s00894-009-0549-3>.
- 58 Schillaci, D.; Spanò, V.; Parrino, B.; Carbone, A.; Montalbano, A.; Barraja, P.; Diana, P.; Cirrincione, G.; Cascioferro, S. Pharmaceutical Approaches to Target Antibiotic Resistance Mechanisms. *J. Med. Chem.* **2017**, *60* (20), 8268–8297. <https://doi.org/10.1021/acs.jmedchem.7b00215>.
- 59 Kvist, M.; Hancock, V.; Klemm, P. Inactivation of Efflux Pumps Abolishes Bacterial Biofilm Formation. *Appl. Environ. Microbiol.* **2008**, *74* (23), 7376–7382. <https://doi.org/10.1128/AEM.01310-08>.
- 60 Frieri, M.; Kumar, K.; Boutin, A. Antibiotic Resistance. *J. Infect. Public Health* **2017**, *10* (4), 369–378. <https://doi.org/10.1016/j.jiph.2016.08.007>.
- 61 Blair, J. M. A.; Webber, M. A.; Baylay, A. J.; Ogbolu, D. O.; Piddock, L. J. V. Molecular Mechanisms of Antibiotic Resistance. *Nat. Rev. Microbiol.* **2015**, *13* (1), 42–51. <https://doi.org/10.1038/nrmicro3380>.
- 62 Higgins, C. F. Multiple Molecular Mechanisms for Multidrug Resistance Transporters. *Nature* **2007**, *446* (7137), 749–757. <https://doi.org/10.1038/nature05630>.
- 63 Lekshmi, M.; Ammini, P.; Adjei, J.; Sanford, L. M.; Shrestha, U.; Kumar, S.; Varela, M. F. Modulation of Antimicrobial Efflux Pumps of the Major Facilitator Superfamily in *Staphylococcus aureus*. *AIMS Microbiol.* **2018**, *4* (1), 1–18. <https://doi.org/10.3934/microbiol.2018.1.1>.
- 64 Kumar, S.; Smith, K. P.; Floyd, J. L.; Varela, M. F. Cloning and Molecular Analysis of a Mannitol Operon of Phosphoenolpyruvate-Dependent Phosphotransferase (PTS) Type from *Vibrio Cholerae* O395. *Arch. Microbiol.* **2011**, *193* (3), 201–208. <https://doi.org/10.1007/s00203-010-0663-8>.
- 65 Wu, S.-C.; Han, F.; Song, M.-R.; Chen, S.; Li, Q.; Zhang, Q.; Zhu, K.; Shen, J.-Z. Natural Flavones from *Morus Alba* against Methicillin-Resistant *Staphylococcus aureus* via Targeting the Proton Motive Force and Membrane Permeability. *J. Agric. Food Chem.* **2019**, *67* (36), 10222–10234. <https://doi.org/10.1021/acs.jafc.9b01795>.
- 66 Schindler, B. D.; Frempong-Manso, E.; DeMarco, C. E.; Kosmidis, C.; Matta, V.; Seo, S. M.; Kaatz, G. W. Analyses of Multidrug Efflux Pump-like Proteins Encoded on the *Staphylococcus*

- aureus* Chromosome. *Antimicrob. Agents Chemother.* **2015**, *59* (1), 747–748. <https://doi.org/10.1128/AAC.04678-14>.
- 67 Coêlho, M. L.; Ferreira, J. H. L.; de Siqueira Júnior, J. P.; Kaatz, G. W.; Barreto, H. M.; de Carvalho Melo Cavalcante, A. A. Inhibition of the NorA Multi-Drug Transporter by Oxygenated Monoterpenes. *Microb. Pathog.* **2016**, *99*, 173–177. <https://doi.org/10.1016/j.micpath.2016.08.026>.
- 68 Schindler, B. D.; Jacinto, P. L.; Buensalido, J. A. L.; Seo, S. M.; Kaatz, G. W. Clonal Relatedness Is a Predictor of Spontaneous Multidrug Efflux Pump Gene Overexpression in *Staphylococcus aureus*. *Int. J. Antimicrob. Agents* **2015**, *45* (5), 464–470. <https://doi.org/10.1016/j.ijantimicag.2014.11.007>.
- 69 Chambers, C. S.; Viktorová, J.; Řehořová, K.; Biedermann, D.; Turková, L.; Macek, T.; Křen, V.; Valentová, K. Defying Multidrug Resistance! Modulation of Related Transporters by Flavonoids and Flavonolignans. *J. Agric. Food Chem.* **2020**, *68* (7), 1763–1779. <https://doi.org/10.1021/acs.jafc.9b00694>.
- 70 Sun, J.; Deng, Z.; Yan, A. Bacterial Multidrug Efflux Pumps: Mechanisms, Physiology and Pharmacological Exploitations. *Biochem. Biophys. Res. Commun.* **2014**, *453* (2), 254–267. <https://doi.org/10.1016/j.bbrc.2014.05.090>.
- 71 Patel, D.; Kosmidis, C.; Seo, S. M.; Kaatz, G. W. Ethidium Bromide MIC Screening for Enhanced Efflux Pump Gene Expression or Efflux Activity in *Staphylococcus aureus*. *Antimicrob. Agents Chemother.* **2010**, *54* (12), 5070–5073. <https://doi.org/10.1128/AAC.01058-10>.
- 72 Poole, K. Efflux Pumps as Antimicrobial Resistance Mechanisms. *Ann. Med.* **2007**, *39* (3), 162–176. <https://doi.org/10.1080/07853890701195262>.
- 73 Srivalli, K. M. R.; Lakshmi, P. K. Overview of P-Glycoprotein Inhibitors: A Rational Outlook. *Braz. J. Pharm. Sci.* **2012**, *48* (3), 353–367. <https://doi.org/10.1590/s1984-82502012000300002>.
- 74 Jorgensen, W. L. Efficient Drug Lead Discovery and Optimization. *Acc. Chem. Res.* **2009**, *42* (6), 724–733. <https://doi.org/10.1021/ar800236t>.
- 75 Cavasotto, C. N.; Adler, N. S.; Aucar, M. G. Quantum Chemical Approaches in Structure-Based Virtual Screening and Lead Optimization. *Front. Chem.* **2018**, *6*. <https://doi.org/10.3389/fchem.2018.00188>.
- 76 Leis, S.; Zacharias, M. ReFlexIn: A Flexible Receptor Protein-Ligand Docking Scheme Evaluated on HIV-1 Protease. *PLoS One* **2012**, *7* (10), e48008. <https://doi.org/10.1371/journal.pone.0048008>.

- 77 Huang, S.-Y.; Zou, X. Advances and Challenges in Protein-Ligand Docking. *Int. J. Mol. Sci.* **2010**, *11* (8), 3016–3034. <https://doi.org/10.3390/ijms11083016>.
- 78 Petrenko, R.; Meller, J. Molecular Dynamics. *eLS*. Wiley March 15, 2010. <https://doi.org/10.1002/9780470015902.a0003048.pub2>.
- 79 Bello, M.; Martínez-Archundia, M.; Correa-Basurto, J. Automated Docking for Novel Drug Discovery. *Expert Opin. Drug Discov.* **2013**, *8* (7), 821–834. <https://doi.org/10.1517/17460441.2013.794780>.
- 80 Morris, G. M.; Huey, R.; Lindstrom, W.; Sanner, M. F.; Belew, R. K.; Goodsell, D. S.; Olson, A. J. AutoDock4 and AutoDockTools4: Automated Docking with Selective Receptor Flexibility. *J. Comput. Chem.* **2009**, *30* (16), 2785–2791. <https://doi.org/10.1002/jcc.21256>.
- 81 Lang, P. T.; Brozell, S. R.; Mukherjee, S.; Pettersen, E. F.; Meng, E. C.; Thomas, V.; Rizzo, R. C.; Case, D. A.; James, T. L.; Kuntz, I. D. DOCK 6: Combining Techniques to Model RNA-Small Molecule Complexes. *RNA* **2009**, *15* (6), 1219–1230. <https://doi.org/10.1261/rna.1563609>.
- 82 Zavodszky, M. I.; Rohatgi, A.; Van Voorst, J. R.; Yan, H.; Kuhn, L. A. Scoring Ligand Similarity in Structure-Based Virtual Screening. *J. Mol. Recognit.* **2009**, *22* (4), 280–292. <https://doi.org/10.1002/jmr.942>.
- 83 Lemmon, G.; Meiler, J. Rosetta Ligand Docking with Flexible XML Protocols. *Methods Mol. Biol.* **2012**, *819*, 143–155. [https://doi.org/10.1007/978-1-61779-465-0\\_10](https://doi.org/10.1007/978-1-61779-465-0_10).
- 84 Tuccinardi, T.; Botta, M.; Giordano, A.; Martinelli, A. Protein Kinases: Docking and Homology Modeling Reliability. *J. Chem. Inf. Model.* **2010**, *50* (8), 1432–1441. <https://doi.org/10.1021/ci100161z>.
- 85 Ripphausen, P.; Nisius, B.; Wawer, M.; Bajorath, J. Rationalizing the Role of SAR Tolerance for Ligand-Based Virtual Screening. *J. Chem. Inf. Model.* **2011**, *51* (4), 837–842. <https://doi.org/10.1021/ci200064c>.
- 86 Davis, I. W.; Raha, K.; Head, M. S.; Baker, D. Blind Docking of Pharmaceutically Relevant Compounds Using RosettaLigand: Blind Docking with RosettaLigand. *Protein Sci.* **2009**, *18* (9), 1998–2002. <https://doi.org/10.1002/pro.192>.
- 87 Dias, R.; de Azevedo, W. F., Jr. Molecular Docking Algorithms. *Curr. Drug Targets* **2008**, *9* (12), 1040–1047. <https://doi.org/10.2174/138945008786949432>.
- 88 Timmers, L. F. S. M.; Caceres, R. A.; Vivan, A. L.; Gava, L. M.; Dias, R.; Ducati, R. G.; Basso, L. A.; Santos, D. S.; de Azevedo, W. F., Jr. Structural Studies of Human Purine Nucleoside Phosphorylase: Towards a New Specific Empirical Scoring Function. *Arch. Biochem. Biophys.* **2008**, *479* (1), 28–38. <https://doi.org/10.1016/j.abb.2008.08.015>.

- 89 Correa-Basurto, J.; Ramos-Morales, F. R.; Matus, M. H.; Rosales-Hernández, M. C.; Mancilla-Percino, T.; Trujillo-Ferrara, J.; Ilizaliturri-Flores, I. Docking and DFT Studies to Explore the Topoisomerase II ATP Pocket Employing 3-Substituted 2,6-Piperazindiones for Drug Design. *Mol. Simul.* **2012**, *38* (13), 1072–1084. <https://doi.org/10.1080/08927022.2012.690877>.
- 90 Trott, O.; Olson, A. J. AutoDock Vina: Improving the Speed and Accuracy of Docking with a New Scoring Function, Efficient Optimization, and Multithreading. *J. Comput. Chem.* **2010**, *31* (2), 455–461. <https://doi.org/10.1002/jcc.21334>.
- 91 Fu, D. Y.; Meiler, J. Predictive Power of Different Types of Experimental Restraints in Small Molecule Docking: A Review. *J. Chem. Inf. Model.* **2018**, *58* (2), 225–233. <https://doi.org/10.1021/acs.jcim.7b00418>.
- 92 Biesiada, J.; Porollo, A.; Meller, J. On Setting up and Assessing Docking Simulations for Virtual Screening. *Methods Mol. Biol.* **2012**, *928*, 1–16. [https://doi.org/10.1007/978-1-62703-008-3\\_1](https://doi.org/10.1007/978-1-62703-008-3_1).
- 93 Alkozi, H. A.; Sánchez Montero, J. M.; Doadrio, A. L.; Pintor, J. Docking Studies for Melatonin Receptors. *Expert Opin. Drug Discov.* **2018**, *13* (3), 241–248. <https://doi.org/10.1080/17460441.2018.1419184>.
- 94 Chinthala, Y.; Thakur, S.; Tirunagari, S.; Chinde, S.; Domatti, A. K.; Arigari, N. K.; K V N S, S.; Alam, S.; Jonnala, K. K.; Khan, F.; Tiwari, A.; Grover, P. Synthesis, Docking and ADMET Studies of Novel Chalcone Triazoles for Anti-Cancer and Anti-Diabetic Activity. *Eur. J. Med. Chem.* **2015**, *93*, 564–573. <https://doi.org/10.1016/j.ejmech.2015.02.027>.
- 95 Scotti, L.; Ishiki, H.; Mendonça Júnior, F. J. B.; Da Silva, M. S.; Scotti, M. T. In-Silico Analyses of Natural Products on Leishmania Enzyme Targets. *Mini Rev. Med. Chem.* **2015**, *15* (3), 253–269. <https://doi.org/10.2174/138955751503150312141854>.
- 96 Vaz, R. J.; Zamora, I.; Li, Y.; Reiling, S.; Shen, J.; Cruciani, G. The Challenges of in Silico Contributions to Drug Metabolism in Lead Optimization. *Expert Opin. Drug Metab. Toxicol.* **2010**, *6* (7), 851–861. <https://doi.org/10.1517/17425255.2010.499123>.
- 97 Scotti, L.; Mendonca Junior, F. J. B.; Ishiki, H. M.; Ribeiro, F. F.; Singla, R. K.; Barbosa Filho, J. M.; Da Silva, M. S.; Scotti, M. T. Docking Studies for Multi-Target Drugs. *Curr. Drug Targets* **2017**, *18* (5), 592–604. <https://doi.org/10.2174/1389450116666150825111818>.
- 98 Dantas, N.; de Aquino, T. M.; de Araújo-Júnior, J. X.; da Silva-Júnior, E.; Gomes, E. A.; Gomes, A. A. S.; Siqueira-Júnior, J. P.; Mendonça Junior, F. J. B. Aminoguanidine Hydrazones (AGH's) as Modulators of Norfloxacin Resistance in *Staphylococcus aureus* That Overexpress NorA Efflux Pump. *Chem. Biol. Interact.* **2018**, *280*, 8–14. <https://doi.org/10.1016/j.cbi.2017.12.009>.



- 99 Oliveira, M. M.; Santos, H. S.; Coutinho, H. D. M.; Bandeira, P. N.; da Silva, P. T.; Freitas, T. S.; Rocha, J. E.; Xavier, J. C.; Campina, F. F.; Barbosa, C. R. S.; Araújo Neto, J. B.; Pereira, R. L. S.; Silva, M. M. C.; Muniz, D. F.; Teixeira, A. M. R.; Frota, V. M.; Rodrigues, T. H. S.; Amado, A. M.; Marques, M. P. M.; Batista de Carvalho, L. A. E.; Nogueira, C. E. S. Spectroscopic Characterization and Efflux Pump Modulation of a Thiophene Curcumin Derivative. *J. Mol. Struct.* **2020**, *1215* (128291), 128291. <https://doi.org/10.1016/j.molstruc.2020.128291>.
- 100 Melo Lucio, F. N.; Da Silva, J. E.; Marinho, E. M.; Da Silva Mendes, F. R.; Marinho, M. M.; Marinho, E. S. Methylcytisine Alkaloid Potentially Active against Dengue Virus: A Molecular Docking Study and Electronic Structural Characterization. *Int. J. Res. Granthaalayah* **2020**, *8* (1), 221–236. <https://doi.org/10.29121/granthaalayah.v8.i1.2020.270>.
- 101 Milite, C.; Amendola, G.; Nocentini, A.; Bua, S.; Cipriano, A.; Barresi, E.; Feoli, A.; Novellino, E.; Da Settimo, F.; Supuran, C. T.; Castellano, S.; Cosconati, S.; Taliani, S. Novel 2-Substituted-Benzimidazole-6-Sulfonamides as Carbonic Anhydrase Inhibitors: Synthesis, Biological Evaluation against Isoforms I, II, IX and XII and Molecular Docking Studies. *J. Enzyme Inhib. Med. Chem.* **2019**, *34* (1), 1697–1710. <https://doi.org/10.1080/14756366.2019.1666836>.
- 102 Stewart, J. J. P. Optimization of Parameters for Semiempirical Methods VI: More Modifications to the NDDO Approximations and Re-Optimization of Parameters. *J. Mol. Model.* **2013**, *19* (1), 1–32. <https://doi.org/10.1007/s00894-012-1667-x>.
- 103 Almeida-Neto, F. W. Q.; da Silva, L. P.; Ferreira, M. K. A.; Mendes, F. R. S.; de Castro, K. K. A.; Bandeira, P. N.; de Menezes, J. E. S. A.; dos Santos, H. S.; Monteiro, N. K. V.; Marinho, E. S.; de Lima-Neto, P. Characterization of the Structural, Spectroscopic, Nonlinear Optical, Electronic Properties and Antioxidant Activity of the N-4'-[(E)-3-(Fluorophenyl)-1-(Phenyl)-Prop-2-En-1-One]-Acetamide. *J. Mol. Struct.* **2020**, *1220* (128765), 128765. <https://doi.org/10.1016/j.molstruc.2020.128765>.
- 104 Shityakov, S.; Förster, C. In Silico Predictive Model to Determine Vector-Mediated Transport Properties for the Blood-Brain Barrier Choline Transporter. *Adv. Appl. Bioinform. Chem.* **2014**, *7*, 23–36. <https://doi.org/10.2147/AABC.S63749>.
- 105 Yusuf, D.; Davis, A. M.; Kleywegt, G. J.; Schmitt, S. An Alternative Method for the Evaluation of Docking Performance: RSR vs RMSD. *J. Chem. Inf. Model.* **2008**, *48* (7), 1411–1422. <https://doi.org/10.1021/ci800084x>.
- 106 Hockney, R. W.; Goel, S. P.; Eastwood, J. W. Quiet High-Resolution Computer Models of a Plasma. *J. Comput. Phys.* **1974**, *14* (2), 148–158. [https://doi.org/10.1016/0021-9991\(74\)90010-2](https://doi.org/10.1016/0021-9991(74)90010-2).

- 107Pettersen, E. F.; Goddard, T. D.; Huang, C. C.; Couch, G. S.; Greenblatt, D. M.; Meng, E. C.; Ferrin, T. E. UCSF Chimera--a Visualization System for Exploratory Research and Analysis. *J. Comput. Chem.* **2004**, *25* (13), 1605–1612. <https://doi.org/10.1002/jcc.20084>.
- 108Csizmadia, P. MarvinSketch and MarvinView: Molecule Applets for the World Wide Web. In *Proceedings of The 3rd International Electronic Conference on Synthetic Organic Chemistry*; MDPI: Basel, Switzerland, 1999.
- 109Pires, D. E. V.; Blundell, T. L.; Ascher, D. B. PkCSM: Predicting Small-Molecule Pharmacokinetic and Toxicity Properties Using Graph-Based Signatures. *J. Med. Chem.* **2015**, *58* (9), 4066–4072. <https://doi.org/10.1021/acs.jmedchem.5b00104>.
- 110Hay, T.; Jones, R.; Beaumont, K.; Kemp, M. Modulation of the Partition Coefficient between Octanol and Buffer at PH 7.4 and PKa to Achieve the Optimum Balance of Blood Clearance and Volume of Distribution for a Series of Tetrahydropyran Histamine Type 3 Receptor Antagonists. *Drug Metab. Dispos.* **2009**, *37* (9), 1864 – 1870. <https://doi.org/10.1124/dmd.109.027888>.
- 111Perisic-Janjic, N.; Kaliszan, R.; Wiczling, P.; Milosevic, N.; Uscumlic, G.; Banjac, N. Reversed-Phase TLC and HPLC Retention Data in Correlation Studies with in Silico Molecular Descriptors and Druglikeness Properties of Newly Synthesized Anticonvulsant Succinimide Derivatives. *Mol. Pharm.* **2011**, *8* (2), 555–563. <https://doi.org/10.1021/mp100373d>.
- 112Lipinski, C. A. Lead- and Drug-like Compounds: The Rule-of-Five Revolution. *Drug Discov. Today Technol.* **2004**, *1* (4), 337–341. <https://doi.org/10.1016/j.ddtec.2004.11.007>.
- 113Veber, D. F.; Johnson, S. R.; Cheng, H.-Y.; Smith, B. R.; Ward, K. W.; Kopple, K. D. Molecular Properties That Influence the Oral Bioavailability of Drug Candidates. *J. Med. Chem.* **2002**, *45* (12), 2615–2623. <https://doi.org/10.1021/jm020017n>.
- 114de Lange, E. C. M.; Ravenstijn, P. G. M.; Groenendaal, D.; van Steeg, T. J. Toward the Prediction of CNS Drug-Effect Profiles in Physiological and Pathological Conditions Using Microdialysis and Mechanism-Based Pharmacokinetic-Pharmacodynamic Modeling. *AAPS J.* **2005**, *7* (3), E532-43. <https://doi.org/10.1208/aapsj070354>.
- 115Hudson, I. R. The Efficacy of Intranasal Mupirocin in the Prevention of Staphylococcal Infections: A Review of Recent Experience. *J. Hosp. Infect.* **1994**, *27* (2), 81–98. [https://doi.org/10.1016/0195-6701\(94\)90001-9](https://doi.org/10.1016/0195-6701(94)90001-9).
- 116Schimmel, P.; Tao, J.; Hill, J. Aminoacyl TRNA Synthetases as Targets for New Anti-Infectives. *FASEB J.* **1998**, *12* (15), 1599–1609. <https://doi.org/10.1096/fasebj.12.15.1599>.
- 117Qiu, X.; Janson, C. A.; Smith, W. W.; Green, S. M.; McDevitt, P.; Johanson, K.; Carter, P.; Hibbs, M.; Lewis, C.; Chalker, A.; Fosberry, A.; Lalonde, J.; Berge, J.; Brown, P.; Houge-Frydrych, C. S.; Jarvest, R. L. Crystal Structure of *Staphylococcus aureus* Tyrosyl-TRNA

- Synthetase in Complex with a Class of Potent and Specific Inhibitors. *Protein Sci.* **2001**, *10* (10), 2008–2016. <https://doi.org/10.1110/ps.18001>.
- 118 Berge, J. M.; Broom, N. J.; Houge-Frydrych, C. S.; Jarvest, R. L.; Mensah, L.; McNair, D. J.; O'Hanlon, P. J.; Pope, A. J.; Rittenhouse, S. Synthesis and Activity of Analogues of SB-219383: Novel Potent Inhibitors of Bacterial Tyrosyl TRNA Synthetase. *J. Antibiot. (Tokyo)* **2000**, *53* (11), 1282–1292. <https://doi.org/10.7164/antibiotics.53.1282>.
- 119 Huey, R.; Morris, G. M.; Olson, A. J.; Goodsell, D. S. A Semiempirical Free Energy Force Field with Charge-Based Desolvation. *J. Comput. Chem.* **2007**, *28* (6), 1145–1152. <https://doi.org/10.1002/jcc.20634>.
- 120 Imberty, A.; Hardman, K. D.; Carver, J. P.; Pérez, S. Molecular Modelling of Protein-Carbohydrate Interactions. Docking of Monosaccharides in the Binding Site of Concanavalin A. *Glycobiology* **1991**, *1* (6), 631–642. <https://doi.org/10.1093/glycob/1.6.631>.
- 121 Meunier, B.; de Visser, S. P.; Shaik, S. Mechanism of Oxidation Reactions Catalyzed by Cytochrome P450 Enzymes. *Chem. Rev.* **2004**, *104* (9), 3947–3980. <https://doi.org/10.1021/cr020443g>.
- 122 Louet, M.; Labbé, C. M.; Fagnen, C.; Aono, C. M.; Homem-de-Mello, P.; Villoutreix, B. O.; Miteva, M. A. Insights into Molecular Mechanisms of Drug Metabolism Dysfunction of Human CYP2C9\*30. *PLoS One* **2018**, *13* (5), e0197249. <https://doi.org/10.1371/journal.pone.0197249>.
- 123 Cho, Y.-A.; Choi, J.-S.; Burm, J.-P. Effects of the Antioxidant Baicalein on the Pharmacokinetics of Nimodipine in Rats: A Possible Role of P-Glycoprotein and CYP3A4 Inhibition by Baicalein. *Pharmacol. Rep.* **2011**, *63* (4), 1066–1073. [https://doi.org/10.1016/s1734-1140\(11\)70624-7](https://doi.org/10.1016/s1734-1140(11)70624-7).
- 124 Olivo, M.; Bhuvaneshwari, R.; Lucky, S. S.; Dendukuri, N.; Soo-Ping Thong, P. Targeted Therapy of Cancer Using Photodynamic Therapy in Combination with Multi-Faceted Anti-Tumor Modalities. *Pharmaceuticals (Basel)* **2010**, *3* (5), 1507–1529. <https://doi.org/10.3390/ph3051507>.
- 125 D'Eliseo, D.; Velotti, F. Omega-3 Fatty Acids and Cancer Cell Cytotoxicity: Implications for Multi-Targeted Cancer Therapy. *J. Clin. Med.* **2016**, *5* (2), 15. <https://doi.org/10.3390/jcm5020015>.

**Article 1** - Anxiolytic-like and anticonvulsant effect in adult zebrafish (*Danio rerio*) through GABAergic system and molecular docking study of chalcone derived from natural products

**Authors:** Jayze da Cunha Xavier<sup>a</sup>, Maria Kueirislene Amancio Ferreira<sup>b</sup>, Antônio Wlisses da Silva<sup>d</sup>, Jane Eire Silva Alencar de Menezes<sup>b</sup>, Paulo Nogueira Bandeira<sup>d</sup>, Alexandre Magno Rodrigues Teixeira<sup>a</sup>, Emanuelle Machado Marinho<sup>g</sup>, Emmanuel Silva Marinho<sup>e</sup>, Márcia M. Marinho<sup>f</sup>, Hécio Silva dos Santos<sup>a,b,d\*</sup>











Journal: Biointerface Research in Applied Chemistry

Situation: Published

### Resumo:

Benzodiazepínicos são usados para tratar distúrbios de ansiedade. O uso crônico dessas drogas pode causar tolerância ou efeitos adversos relevantes, exigindo a busca de novos compostos mais seguros e eficazes. Nesse contexto, o presente trabalho teve como objetivo investigar o potencial efeito ansiolítico de a chalcona sintetizada, bem como seu mecanismo de ação, peixe-zebra adulto (Zfa) como modelo animal. Os animais foram tratados com a nova chalcona (4,0; 20 e 40,0 mg/kg) no campo aberto de 96 h e teste de toxicidade. As concentrações que causaram alteração locomotora foram avaliados no teste ansiolítico claro e escuro, com o menor dose que está sendo usada para avaliar o mecanismo através do sistema GABAérgico. A chalcona provou ser segura em comparação com o modelo Zebrafish adulto até 96 h de análise e causou alteração locomotora de Zfa semelhante ao dos benzodiazepínicos. A chalcona apresentou efeito ansiolítico, que foi bloqueado pelo flumazenil, um antagonista do receptor GABAA, demonstrando que a chalcona deve, através do mecanismo do Sistema GAB. Nesta perspectiva, a chalcona tem potencial para ser utilizada como uma ferramenta farmacológica no tratamento de transtornos de ansiedade

## Anxiolytic-like and Anticonvulsant Effect in Adult Zebrafish (*Danio rerio*) through GABAergic System and Molecular Docking Study of Chalcone Derived from Natural Products

Jayze da Cunha Xavier <sup>1</sup> , Maria Kueirislene Amâncio Ferreira <sup>2</sup> , Antonio Wilsses da Silva <sup>4</sup> ,  
Jane Elre Silva Alencar de Menezes <sup>2</sup> , Alexandre Magno Rodrigues Teixeira <sup>1</sup> ,  
Paulo Nogueira Bandeira <sup>2</sup> , Emanuelle Machado Marinho <sup>7</sup> , Emmanuel Silva Marinho <sup>5</sup> ,  
Márcia Machado Marinho <sup>6</sup> , Hélcio Silva dos Santos <sup>1,2,3,\*</sup> 

**CHAPTER 5** - Anxiolytic-like and anticonvulsant effect in adult zebrafish (*Danio rerio*) through GABAergic system and molecular docking study of chalcone derived from natural products

**Abstract:** (1) Background: Anxiety and seizure are mental disorders commonly treated in the clinic with benzodiazepines (BZDs), However, long-term treatment with these drugs causes side effects such as decreased motor coordination, drowsiness, sedation and, when used for a long time, leads to dependence and withdrawal syndromes. The objective of this study was to evaluate the anxiolytic-like and anticonvulsant effect in adult zebrafish (*Danio rerio*) through GABAergic system of synthetic chalcone derived from cinnamaldehyde and a natural acetophenone isolated from *Croton anisodontus* and their mechanisms of action via the Gabaergic system, using adult zebrafish. (2) Methods: The animals were treated with chalcone (0.1 or 0.5 or 1.0 mg / kg; 20  $\mu$ L; *i.p.*) and subjected to the open field test. The chalcone caused locomotor alteration when evaluated in the light & dark anxiolytic test. The lowest effective dose was chosen to assess possible involvement in the GABA<sub>A</sub> receptor. (3) Results: The chalcone showed anxiolytic and anticonvulsant effects in all doses in both tests. (4) Conclusions: The chalcone presented anticonvulsant activity, being a possible inhibitor of Carbonic Anhydrase and an anxiolytic effect dependent on the GABAergic system, coupling it in a different region from the diazepam inhibitor.

**Keywords:** Cinnamaldehyde, chalcone, zebrafish, anxiety, seizures

---

### 1. Introduction

Zebrafish (*Danio rerio*) is a fish found in fresh water and has been used for pharmacological investigation of new bioactive compounds. The use of this animal as an experimental model is due to the fact that it is a small animal, with easy maintenance, good reproductive rate, besides presenting a sequenced genome with 70% homology to that of the human being and an anatomy of the central nervous system known. All of these advantages make using this model satisfactory in behavioral, toxicological and pharmacological studies with the aim of elucidate mechanisms of several human diseases [1]. Literature points out that Zebrafish comes being used for studies of anxiety [2], seizure [3], Alzheimer's [4],

inflammation [5], diabetes [6], cholesterol [7], fatty liver [8], cardiovascular disease [9, 10], oxidative stress [11] and antimicrobial and antifungal activities [12-14].

Anxiety and seizure are mental disorders commonly treated in the clinic with benzodiazepines (BZDs), these drugs were introduced into therapeutic practice more than 50 years ago due to their central nervous system depressing effects [15]. However, long-term treatment with these drugs causes side effects such as decreased motor coordination, drowsiness, sedation and, when used for a long time, leads to dependence and withdrawal syndromes, and in high doses they can be fatal. The anxiolytic-like effect showed by chalcones derivatives, make this class of compounds an important tool to help the discovery new agents with increased strength, low cost, superior pharmacokinetic properties, and minimum side effects [16]. Its structure comprises at least two aromatic rings connected by an unsaturated  $\alpha$ - $\beta$  bridge, probably the most responsible for its biological activities [17-20]. They can be obtained from natural sources or by synthesis, and are widely distributed in fruits, vegetables, and tea [21, 22]. This class of compound has arisen much interest due to the wide spectrum of pharmacological activities that they present, including: antinociceptive, anti-inflammatory, antitumor, antibacterial, Anxiolytic, antifungal, antileishmanial and antioxidant activity [23, 24].

The aim of this work *was to evaluate the* anxiolytic-like and anticonvulsant effect in adult zebrafish (*Danio rerio*) through GABAergic system of chalcone (2*E*, 4*E*)-1-(2-hydroxy-3,4,6-trimethoxyphenyl)-5-phenylpenta-2,4-dien-1-one derived from cinnamaldehyde and a natural acetophenone isolated from *Croton anisodontus*.

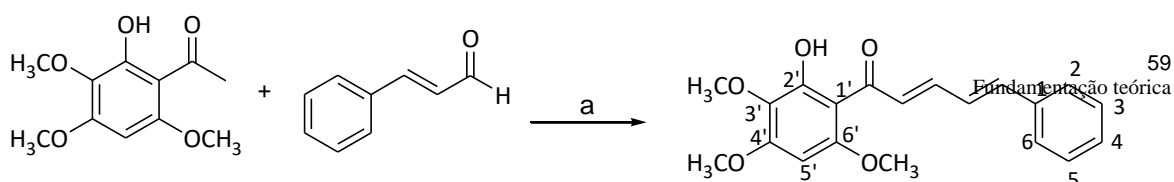
## 2. Materials and Methods

### 2.1 Drugs and reagents

Diazepam (Dzp, Neo Química®), Flumazenil (Fmz; Sandoz®), Dimethyl sulfoxide (3% DMSO; Dynamic®), Pentylentetrazole (PTZ, Sigma-Aldrich).

### 2.2 Synthesis and structural data

The compounds 2-hydroxy-3,4,6 trimethoxyacetophenone (2 mmol) and cinnamaldehyde (2 mmol) were placed in a volumetric flask (25 mL). Then 5 mL of ethanolic NaOH (50%) solution was added and mixed with stirring for 48 h at room temperature. The progress of the reaction was checked by TLC (n-hexane: ethylacetate, 2:1). After 48 h the reaction mixture was neutralized with dilute HCl (10%) and ice water added. The product was obtained as a yellow solid (yield: 35.4%, m.p. 144.8–145.2 °C) filtered under reduced pressure, washed with cold water, and recrystallized from ethanol (Scheme 1) [25].



**Scheme 1.** Preparation of chalcone. a) NaOH 50 % w v<sup>-1</sup>, ethanol, t.a., 48 h.

(2*E*, 4*E*)-1- (2-hydroxy-3,4,6-trimethoxyphenyl)-5-phenylpenta-2,4-dien-1-one (**1**)

Yellow solid (Yield: 35.4%), m.p. 144.8-145.2°C. IR (KBr,  $\nu_{\text{cm}^{-1}}$ ): 1634, 1600, 1588, 1575, 1480, 1167. <sup>1</sup>H NMR (CDCl<sub>3</sub>, ppm): 3.84 (s, MeO-X); 3.93 (s, MeO-Y); 3.95(s, MeO-Z); 6.99 (s, H-5'); 7.44 (m, H-4); 7.38 (d, H-3/5, J = 7,1 Hz,); 7.51 (d, H-2/6, J=7,2 Hz); 7.62 (d, H $\alpha$ , J=14,6 Hz); 7.64 (d, H $\beta$ , J=14,6 Hz); 7.40 (d, H $\alpha$ , J=14,6 Hz); 7.43 (d, H $\beta$ , J=14,6 Hz). <sup>13</sup>C NMR (CDCl<sub>3</sub>, ppm): 193.2 (C=O); 60.9 (MeO-3'); 56.1 (MeO-4'); 56.2 (MeO-6'); 107.0 (C-1'); 158.7 (C-2'); 131.0 (C-3'); 159.6 (C-4'); 87.2 (C-5'); 158.5 (C-6'); 136.5 (C-1); 127.7 (C-2/6); 129.1 (C-3/5); 131.0 (C-4); 129.2 (C $\alpha$ ); 143.5 (C $\beta$ ); 127.0 (C $\alpha$ ); 141.8 (C $\beta$ ). MS-EI  $m/z$  = 340).

### 2.3 Involvement of the GABAergic system in anxiety

To assess the involvement of the GABAergic system of anxiolytic activity, a group of animals (n = 6 / each) received the GABAA antagonist flumazenil (4.0 mg / kg; *i.p.*) 15 minutes before the chalcone cinamaldehyde or diazepam. After 30 min of the treatments, the animals were submitted to the light & dark test [16].

### 2.4 Pentylentetrazole-induced seizure (PTZ)

PTZ-induced seizure reversal was investigated (n = 6 / group) and the animals were treated with chalcone (0.1; 0.5 and 1 mg / mL; 20  $\mu$ L; *ip*), Diazepam (1.0 mg / mL; 20 $\mu$ L; *ip*), vehicle (3% DMSO; 20 $\mu$ L; *ip*). An untreated group (n = 6 / group) was included (Naive). After 30 min, the animals were exposed to PTZ at 7.5 mM, and the behavior similar to seizure in three stages was evaluated: stage I - dramatically increased swimming activity; stage II - swirling swimming behavior; stage III - clonus-like seizures, followed by loss of posture when the animal falls to one side and remains immobile for 1-3 s [26, 27]. At the end of the analysis of the 3 stages of the test, the animals were euthanized on the ice.

### 2.5 Docking of the anxiolytic effect on the GABAergic system

For the study of molecular docking involving anxiolytic activity, the GABA<sub>A</sub> receptor was selected. Its structure was obtained from the Protein Data Bank database (<https://www.rcsb.org/>), identified as “CryoEM structure of human full-length

alpha1beta3gamma2L GABA (A) R in complex with diazepam (Valium), GABA and megabody Mb38 (PDB 6HUP), deposited with a resolution of 3.58 Å, determined by electron microscopy, classified as membrane protein, *Homo sapiens* organism and *Homo sapiens* and *Escherichia coli* expression system. Computer simulations were performed using the AutoDock Vina code (version 1.1.2), using 3-way *multithreading*, *Lamarckian Genetic Algorithm* [28]. The grid box was defined with parameters of 126Åx100Åx126Å, centered on the entire protein with the dimensions (x, y, z) = (125,281, 139,534, 136,018). 50 independent simulations were carried out with 20 poses each, as a standard procedure. For the selection of simulations with better poses, the simulations that presented RMSD (Root Mean Square Deviation) value less than 2 Å [29] and free binding energy ( $\Delta G$ ) below -6.0 kcal / mol were used as criteria [30]. The Discovery Studio Visualizer [31] and UCSF Chimera codes were used to analyze the results and generate the two-dimensional chemical interaction maps [32].

## 2.6. Docking of the anticonvulsant effect

For the *in silico* study of the potential anticonvulsant effect of chalcone, the structure of the enzyme Carbonic Anhydrase II (AC II) (PDB 3F8E) was obtained from the Protein Data Bank database (<https://www.rcsb.org/>), identified as “Coumarins are a novel class of suicide carbonic anhydrase inhibitors”. The protein structure is deposited in the Protein Data Bank with the co-crystallized TE1 inhibitor (coumarin), with a resolution of 2.00 Å, determined by X-Ray Diffraction, classified as lyase and *Homo sapiens* organism. For docking simulations, the AutoDock Vina code (version 1.1.2) was used [28]. The grid box was defined with parameters of 94Åx96Åx106Å, centered on the whole protein with the dimensions (x, y, z) = (-8,086, -0,658, 17,136), being carried out 50 independent simulations with obtaining 20 poses each. For the selection of simulations with better poses, the simulations that presented RMSD (Root Mean Square Deviation) value less than 2 Å [29] and free binding energy ( $\Delta G$ ) below -6.0 kcal / mol were used as criteria [30]. The results were analyzed and visualized using the codes Discovery Studio Visualizer [31] and UCSF Chimera [32].

## 2.7 Statistical Analysis

The zebrafish results were expressed as mean  $\pm$  standard error of mean, for *in vivo* tests (n = 6 / group). After confirming the normality and homogeneity distribution of the data, differences between the groups were subjected to analysis of variance (one-way ANOVA), followed by the Tukey test, using the GraphPad Prism v software. 7.0. The level of statistical significance was considered to be 5% (p <0.05).



### 3. Results and Discussion

#### 3.1 Mechanism of anxiolytic action

Flumazenil reduced (###  $p < 0.001$ ) the anxiolytic effect of chalcone cinnamaldehyde (0.5 mg / mL; 20  $\mu$ L; *ip*) and Diazepam (1.0 mg / mL; 20  $\mu$ L; *ip*) (Figure 1). The anxiolytic activity of chalcone cinnamaldehyde performed by Xavier et al., (2020) arouse the interest in investigating the mechanism of anxiolytic action of chalcone. Thus, we performed a light & dark test using flumazenil, a GABAA receptor antagonist. Based on Fig. 1, pretreatment with flumazenil altered the effects of Chalcona (0.5 mg / mL; 20  $\mu$ L; *ip*) and Diazepam (1.0 mg / mL; 20  $\mu$ L; *ip*) in adult zebrafish, that is, it significantly reduced ( $p < 0.0001$  vs. Vehicle and Naive) the anxiolytic / sedative effect of the animals, indicating that the chalcone's anxiolytic activity is dependent on the GABAergic system.

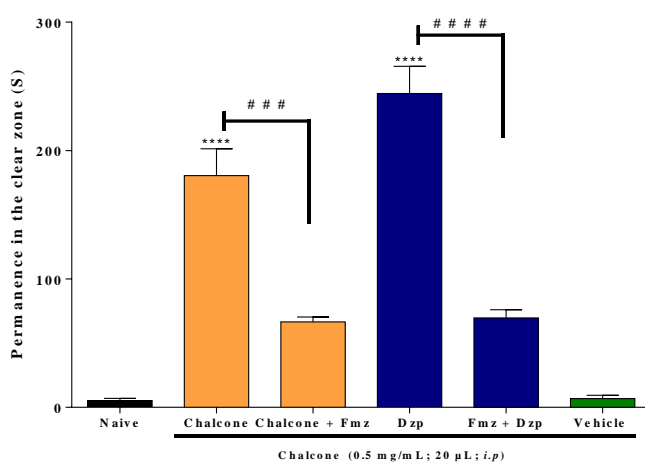


**Figure 1.** Effect of Flumazenil (Fmz) under the anxiolytic effect of the Chalcone - Cinnamaldehyde in the Light & Dark Test. Chalcone - Cinnamaldehyde (0.5 mg / mL; 20  $\mu$ L, *ip*). Dzp - Diazepam (1.0 mg / mL; 20  $\mu$ L, *ip*). Fmz - flumazenil (0.1 mg / mL; 20  $\mu$ L; *ip*). The values represent the mean  $\pm$  standard error of the mean (E.P.M.) for 6 animals / group. ANOVA followed by Tukey (\*\*\*\*  $p < 0.0001$  vs. Naive or vehicle; ####  $p < 0.0001$  vs. Fmz + Dzp or Fmz + Chalcone).

#### 3.2 Docking of the anxiolytic effect on the GABAergic system

The best conformation simulation presented an RMSD of 1,746 Å and a high affinity energy, in the order of -8.1 Kcal / mol, highlighting that the complex formed presented interactions varying between 1.98Å and 3.64Å (Table 1).

**Table 1.** Interactions between the GABA<sub>A</sub> receptor and the chalcone ligand.

Ligand	Receptor	Interaction	Distance (Å)
Chalcone	TYR753C	H-Bond	2.36 Å
	ASP887C	H-Bond	3.20 Å
	SER890C	H-Bond	2.24 Å
	LYS1191D	H-Bond	1.98 Å
	TYR753C	Hydrophobic	3.61 Å
	PHE772C	Hydrophobic	3.63 Å
	PHE772C	Hydrophobic	3.64 Å

In order to investigate the potential anxiolytic activity of chalcone in the GABAergic system, docking simulations were carried out with the GABA<sub>A</sub> receptor, one of the most important drug targets for presenting several allosteric sites, which allow the binding of compounds with anxiolytic properties, such as benzodiazepines, modulators typically positive [33]. Regarding the interactions (Figure 2), it was possible to identify the formation of four hydrogen bonds with the GABA<sub>A</sub> receptor, three of which were classified as strong [34] with the LYS1191D, TYR753C, SER890C residues and a moderate interaction with the ASP887C residue. The chalcone also presented three hydrophobic interactions with residues TYR753 and PHE772, coupling in a different region from the inhibitor Diazepam (Figure 3), a classic agonist of the GABA<sub>A</sub> receptor, thus being an indicator of potential candidate for studies on synergism.

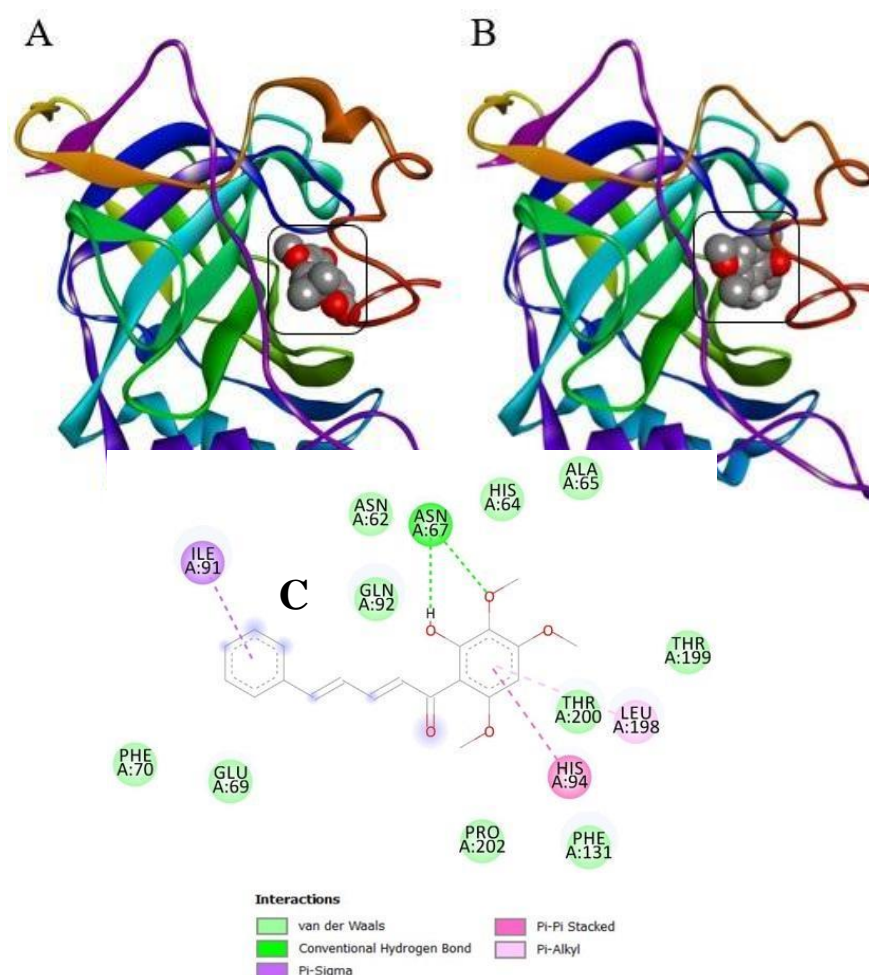


**Figure 2.** Interaction complex of inhibitor TE1 (A) and Chalcone (B) with the enzyme Carbonic Anhydrase II, and 2D map of interactions of the Carbonic Anhydrase II / chalcone complex (C).

### 3.3 Pentylentetrazole-induced seizure

The anticonvulsant effect of chalcone cinnamaldehyde was evaluated through seizures induced by PTZ in adult zebrafish. Chalcone (0.1; 0.5 and 1.0 mg / mL; 20  $\mu$ L; *ip*) as well as the positive control Dzp (1 mg / mL; 20  $\mu$ L; *ip*) increased latency time (\* p <0.1 , \*\* p <0.01, \*\*\* p <0.001, \*\*\*\* p <0.0001 vs. vehicle) for the onset of PTZ-induced crises in the three stages, suggesting an anticonvulsant action (Figure 2). Pentylenetetrazole is a chemoconvulsant that acts allosterically on the GABAA receptor [35] and is used in zebrafish to induce epileptic-like effects and to study seizures [36, 37]. We evaluated the anticonvulsant effect of chalcone and Dzp on PTZ-induced seizures in adult zebrafish. Both increased the latency time for the onset of PTZ-induced crises in the three stages, suggesting an anticonvulsant action (Figure 3). Antiepileptic drugs can have a sedative effect and the treated animals show slow movements or alter locomotion [26, 27] as was demonstrated in another study carried out with chalcone cinnamaldehyde [25], in our study the highest doses of chalcone caused motor impairment , which may justify its anticonvulsant action (Figure 3A).

Flumazenil is well known as an antagonist of GABAergic receptors in  $\alpha$   $\beta$   $\gamma$  subunits [1-3, 5], it antagonizes the sedative effects caused by benzodiazepine overdoses, and reverses these effects in addition to preventing respiratory depression by blocking GABA receptors [38, 39]. Thus, it is an excellent tool for the study of seizures in this receptor. We investigated the association of Diazepam and chalcone in the GABAA receptor in PTZ-induced seizures in zebrafish (Figure 1). Our data show that pretreatment with flumazenil blocked the anticonvulsant effect of chalcone and Dzp in adult zebrafish in the three stages of seizure (Figure 3).

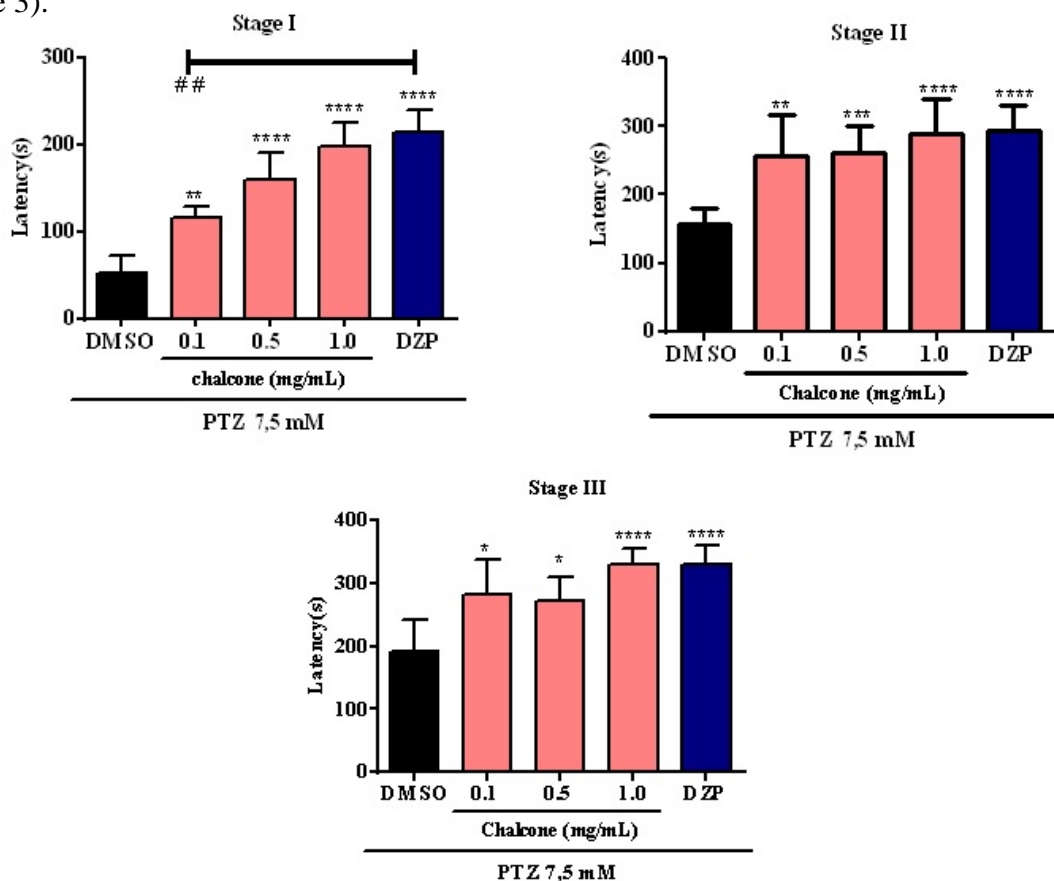


**Figure 3.** Effect of cinnamaldehyde chalcone on pentylenetetrazole induced seizure in adult zebrafish, stage I (A), stage II (B), stage III (C). Dzp-Diazepam (1.0 mg/mL; 20  $\mu$ L; *p.o.*); Vehicle – 3% DMSO (20  $\mu$ L; *p.o.*). The values represent the mean  $\pm$  standart error of the mean (E.P.M.) for 6 animals/group. ANOVA followed by *Tukey* (\*  $p < 0.05$ , \*\*  $p < 0.01$ , \*\*\*  $p < 0.001$ , \*\*\*\*  $p < 0.0001$  vs. Naive; ##  $p < 0.01$  vs. Dzp).

### 3.4 Docking of the anticonvulsant effect

The docking simulation between the chalcone ligand and the Carbonic Anhydrase II with better conformation, presented RMSD of 1.72 Å and affinity energy in the order of -5.9 Kcal / mol. The formed complex presented interactions varying between 2.38Å and 3.72Å (Table 2).

**Table 2.** Interactions between the enzyme Carbonic Anhydrase II and the chalcone ligand

Ligand	Receptor	Interaction	Distance (Å)
Chalcone	*ASN67A	H-Bond	2.46 Å
	*GLN92A	H-Bond	2.38 Å
	*ASN62A	H-Bond	3.47 Å
	*ILE91A	Hydrophobic	3.66 Å
	*ILE91A	Hydrophobic	3.69 Å
	*GLU69A	Hydrophobic	3.68 Å
	LEU198A	Hydrophobic	3.69 Å

\* Residues belonging to the catalytic site of the co-crystallized inhibitor

For the study of the anticonvulsant effect, the enzyme Carbonic Anhydrase II was selected. Although the mechanisms that trigger seizures are not yet specifically known, pH changes in the brain are one of the related factors. The CO<sub>2</sub> / HCO<sub>3</sub><sup>-</sup> buffer is the main responsible for the buffering of the intra and extracellular spaces, with the Carbonic Anhydrase enzyme responsible for the balance of the two buffer species [40]. Carbonic anhydrase inhibitors have been studied as anticonvulsant drugs in epilepsy since the 1950s [41].

The chalcone presenting two hydrogen bonds, classified as strong [34] with residues ASN67A, GLN92A and one of medium intensity with residue ASN62A, being said residues belonging to the catalytic site of the protein target. The AC II / chalcone complex also showed hydrophobic interactions with the ILE91A residue of the active site and with the GLU69A and LEU198A residues of the target protein (Figure 4). In this context, the chalcone ligand coupled in the same region as the active site of the co-crystallized inhibitor (Figure 4), demonstrating a potential inhibitory effect on the carbonic anhydrase enzyme.

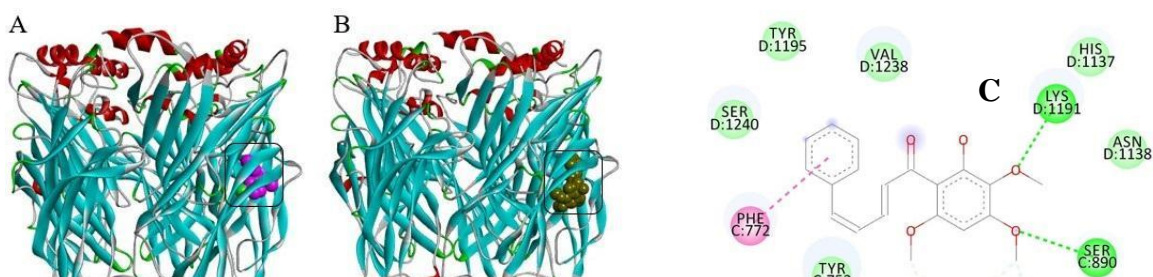


**Figure 4.** Diazepam (A) and Chalcone (B) interaction complex with the GABA<sub>A</sub> receptor, and 2D map of interactions of the GABA<sub>A</sub> / chalcone complex (C)

#### 4. Conclusions

The chalcone presented anticonvulsant activity, being a possible inhibitor of Carbonic Anhydrase and an anxiolytic effect dependent on the GABAergic system, coupling it in a different region from the diazepam inhibitor, thus being an indication of potential candidate for studies on synergism.

#### References

1. Silva, F.C.O.; de Menezes, J.E.S.A.; Ferreira, M.K.A.; da Silva, A.W.; Holanda, C.L.A.; dos Reis Lima, J.; Campos, A.R.; Evaristo, F.F.V.; Teixeira, E.H.; Magalhães, F.E.A.; Bandeira, P.N.; dos Santos, H.S. Antinociceptive activity of 3 $\beta$ -6 $\beta$ -16 $\beta$ -trihydroxylup-20 (29)-ene triterpene isolated from *Combretum leprosum* leaves in adult zebrafish (*Danio rerio*), *BBRC* **2020**, 533, 362-367, <https://doi.org/10.1016/j.bbrc.2020.07.107>.
2. Ferreira, M.K.A.; da Silva, A.W.; Silva, F.C.O.; Vieira Neto, A.E.; Campos, A.R.; Alves Rodrigues Santos, S.A.; Rodrigues Teixeira, A.M.; da Cunha Xavier, J.; Bandeira, P.N.; Sampaio Nogueira, C.E.; de Brito, D.H.A.; Rebouças, E.L.; Magalhães, F.E.A.; de Menezes, J.E.S.A.; dos Santos, H.S. Anxiolytic-like effect of chalcone N-{4'[(2E)-3-(3-nitrophenyl)-1-(phenyl)prop-2-en-1-one]} acetamide on adult zebrafish (*Danio rerio*): Involvement of the 5-HT system, *BBRC* **2020**, 526, 505-511, <https://doi.org/10.1016/j.bbrc.2020.03.129>.
3. Siebel, A.M.; Menezes, F.P.; Capiotti, K.M.; Kist, L.W.; Schaefer, I.d.C.; Frantz, J.Z.; Bogo, M.R.; Da Silva, R.S.; Bonan, C.D. Role of Adenosine Signaling on Pentylentetrazole-Induced Seizures in Zebrafish, *Zebrafish* **2015**, 12, 127-136, <https://doi.org/10.1089/zeb.2014.1004>.
4. Saleem, S.; Kannan, R.R. Zebrafish: an emerging real-time model system to study Alzheimer's disease and neurospecific drug discovery, *Cell Death Discov.* **2018**, 4, 45, <https://doi.org/10.1038/s41420-018-0109-7>.
5. Brugman, S. The zebrafish as a model to study intestinal inflammation, *Dev. Comp. Immunol.* **2016**, 64, 82-92, <https://doi.org/10.1016/j.dci.2016.02.020>.
6. Zang, L.; Maddison, L.A.; Chen, W. Zebrafish as a Model for Obesity and Diabetes, *Front. Cell Dev. Biol.* **2018**, 6, 91.

7. Yoon, Y.; Yoon, J.; Jang, M.-Y.; Na, Y.; Ko, Y.; Choi, J.-H.; Seok, S.H. High Cholesterol Diet Induces IL-1 $\beta$  Expression in Adult but Not Larval Zebrafish, *PLoS One* **2013**, 8, e66970, <https://doi.org/10.1371/journal.pone.0066970>.
8. Dai, W.; Wang, K.; Zheng, X.; Chen, X.; Zhang, W.; Zhang, Y.; Hou, J.; Liu, L. High fat plus high cholesterol diet lead to hepatic steatosis in zebrafish larvae: a novel model for screening anti-hepatic steatosis drugs, *Nutr. Metab. (Lond.)* **2015**, 12, 42, <https://doi.org/10.1186/s12986-015-0036-z>.
9. Nguyen, C.T.; Lu, Q.; Wang, Y.; Chen, J.-N. Zebrafish as a model for cardiovascular development and disease, *Drug Discov. Today Dis. Models* **2008**, 5, 135-140, <https://doi.org/10.1016/j.ddmod.2009.02.003>.
10. Giardoglou, P.; Beis, D. On Zebrafish Disease Models and Matters of the Heart, *Biomedicines* **2019**, 7, 15, <https://doi.org/10.3390/biomedicines7010015>.
11. Huang, X.; Li, Y.; Wang, T.; Liu, H.; Shi, J.; Zhang, X. Evaluation of the Oxidative Stress Status in Zebrafish (*Danio rerio*) Liver Induced by Three Typical Organic UV Filters (BP-4, PABA and PBSA), *Int. J. Env. Res. Public Health* **2020**, 17, 651, <https://doi.org/10.3390/ijerph17020651>.
12. Chang, C.T.; Doerr, K.M.; Whipps, C.M. Antibiotic treatment of zebrafish mycobacteriosis: tolerance and efficacy of treatments with tigecycline and clarithromycin, *J. Fish Dis.* **2017**, 40, 1473-1485, <https://doi.org/10.1111/jfd.12619>.
13. Gomes, M.C.; Mostowy, S. The Case for Modeling Human Infection in Zebrafish, *Trends Microbiol.* **2020**, 28, 10-18, <https://doi.org/10.1016/j.tim.2019.08.005>.
14. Kulatunga, D.C.M.; Dananjaya, S.H.S.; Nikapitiya, C.; Kim, C.-H.; Lee, J.; De Zoysa, M. *Candida albicans* Infection Model in Zebrafish (*Danio rerio*) for Screening Anticandidal Drugs, *Mycopathologia* **2019**, 184, 559-572, <https://doi.org/10.1007/s11046-019-00378-z>.
15. Kovačević, J.; Timić, T.; Tiruveedhula, V.V.; Batinić, B.; Namjoshi, O.A.; Milić, M.; Joksimović, S.; Cook, J.M.; Savić, M.M. Duration of treatment and activation of  $\alpha$ 1-containing GABAA receptors variably affect the level of anxiety and seizure susceptibility after diazepam withdrawal in rats, *Brain Res. Bull.* **2014**, 104, 1-6, <https://doi.org/10.1016/j.brainresbull.2014.03.002>.
16. Ferreira, M.K.A.; da Silva, A.W.; Silva, F.C.O.; Holanda, C.L.A.; Barroso, S.M.; Lima, J.d.R.; Vieira Neto, A.E.; Campos, A.R.; Bandeira, P.N.; dos Santos, H.S.; de Lemos, T.L.G.; Siqueira, S.M.C.; Magalhães, F.E.A.; de Menezes, J.E.S.A. Anxiolytic-like effect of chalcone N-{(4'-[(E)-3-(4-fluorophenyl)-1-(phenyl) prop-2-en-1-one])} acetamide on adult zebrafish (*Danio rerio*): Involvement of the GABAergic system, *Behav. Brain Res.* **2019**, 374, 111871, <https://doi.org/10.1016/j.bbr.2019.03.040>.
17. Almeida-Neto, F.W.Q.; da Silva, L.P.; Ferreira, M.K.A.; Mendes, F.R.S.; de Castro, K.K.A.; Bandeira, P.N.; de Menezes, J.E.S.A.; dos Santos, H.S.; Monteiro, N.K.V.; Marinho, E.S.; de Lima-Neto, P. Characterization of the structural, spectroscopic, nonlinear optical, electronic properties and antioxidant activity of the N-{4'-[(E)-3-(Fluorophenyl)-1-(phenyl)-prop-2-en-1-one]}-acetamide, *J. Mol. Struct.* **2020**, 1220, 128765, <https://doi.org/10.1016/j.molstruc.2020.128765>.
18. Silva, P.T.; Freitas, T.S.; Sena, D.M.; Bandeira, P.N.; Julião, M.S.; Marinho, E.S.; Alcanfor, A.A.; Marinho, E.M.; Lima-Neto, P.D.; Nogueira, C.E.; Coutinho, H.D.; Leal, A.L.; Barreto, H.M.; Martins, N.; Rodrigues Teixeira, A.M.; Santos, H.S. Structural, Vibrational and Electrochemical Analysis and Antibacterial Potential of Isomeric Chalcones Derived from Natural Acetophenone, *Applied Sciences* **2020**, 10, 4713, <https://doi.org/10.3390/app10144713>.
19. Silva, P.T.; Lopes, L.M.A.; Xavier, J.C.; Carvalho, M.C.S.; Moraes, M.O.; Pessoa, C.; Barros, F.W.A.; Bandeira, P.N.; Cavalcante, C.S.P.; Teixeira, A.M.R.; Fontenelle, R.O.S.; Santos, H.S. Atividade Citotóxica e Antifúngica de Chalconas Sintetizadas a partir de uma Acetofenona

- Natural Isolada de Croton anisodontus, *Rev. Virtual Quim.* **2020**, 12, 712-723, <https://doi.org/10.21577/1984-6835.20200057>.
20. Freitas, T.S.d.; Xavier, J.d.C.; Pereira, R.L.S.; Rocha, J.E.; Muniz, D.F.; da Silva, P.T.; da Hora, J.P.; dos Santos, H.S.; Bandeira, P.N.; Nogueira, C.E.S.; Teixeira, A.M.R.; Coutinho, H.D.M. Direct antibacterial and antibiotic resistance modulatory activity of chalcones synthesized from the natural product 2-hydroxy-3,4,6-trimethoxyacetophenone, *FEMS Microbiol. Lett.* **2020**, 367, fnaa124, <https://doi.org/10.1093/femsle/fnaa124>.
21. Ferraz, C.A.N.; Tintino, S.R.; Teixeira, A.M.R.; Bandeira, P.N.; Santos, H.S.; Cruz, B.G.; Nogueira, C.E.S.; Moura, T.F.; Pereira, R.L.S.; Sena, D.M.; Freitas, T.S.; Rocha, J.E.; Coutinho, H.D.M. Potentiation of antibiotic activity by chalcone (E)-1-(4'-aminophenyl)-3-(furan-2-yl)-prop-2-en-1-one against gram-positive and gram-negative MDR strains, *Microb. Pathog.* **2020**, 148, 104453, <https://doi.org/10.1016/j.micpath.2020.104453>.
22. da Silva, P.T.; da Cunha Xavier, J.; Freitas, T.S.; Oliveira, M.M.; Coutinho, H.D.M.; Leal, A.L.A.B.; Barreto, H.M.; Bandeira, P.N.; Nogueira, C.E.S.; Sena, D.M.; Almeida-Neto, F.W.Q.; Marinho, E.S.; Santos, H.S.; Teixeira, A.M.R. Synthesis, spectroscopic characterization and antibacterial evaluation by chalcones derived of acetophenone isolated from Croton anisodontus Müll.Arg, *J. Mol. Struct.* **2021**, 1226, 129403, <https://doi.org/10.1016/j.molstruc.2020.129403>.
23. Teixeira, A.M.R.; Santos, H.S.; Bandeira, P.N.; Julião, M.S.S.; Freire, P.T.C.; Lima, V.N.; Cruz, B.G.; da Silva, P.T.; Coutinho, H.D.M.; Sena, D.M. Structural, spectroscopic and microbiological characterization of the chalcone 2E-1-(2'-hydroxy-3',4',6'-trimethoxyphenyl)-3-(phenyl)-prop-2-en-1-one derived from the natural product 2-hydroxy-3,4,6-trimethoxyacetophenone, *J. Mol. Struct.* **2019**, 1179, 739-748, <https://doi.org/10.1016/j.molstruc.2018.11.075>.
24. Bandeira, P.N.; Fontenelle, R.O.S.; Costa, P.S.; Santos, H.S.; Lemos, T.L.G. Atividade Antifúngica In Vitro Contra Trychophyton Rubrum de P-Aminochalcones e 3'-Metoxi-4'-Hidroxi Chalcona, *Rev. Virtual Quim.* **2020**, 12, 703-711.
25. Xavier, J.d.C.; Almeida-Neto, F.W.Q.; da Silva, P.T.; Marinho, E.S.; Ferreira, M.K.A.; Magalhães, F.E.A.; Nogueira, C.E.S.; Bandeira, P.N.; de Menezes, J.E.S.A.; Teixeira, A.M.R.; Santos, H.S.d. Structural characterization, electronic properties, and anxiolytic-like effect in adult zebrafish (*Danio rerio*) of cinnamaldehyde chalcone, *J. Mol. Struct.* **2020**, 1222, 128954, <https://doi.org/10.1016/j.molstruc.2020.128954>.
26. Afrikanova, T.; Serruys, A.-S.K.; Buenafe, O.E.M.; Clinckers, R.; Smolders, I.; de Witte, P.A.M.; Crawford, A.D.; Esguerra, C.V. Validation of the Zebrafish Pentylentetrazol Seizure Model: Locomotor versus Electrographic Responses to Antiepileptic Drugs, *PLoS One* **2013**, 8, e54166, <https://doi.org/10.1371/journal.pone.0054166>.
27. Torres-Hernández, B.A.; Del Valle-Mojica, L.M.; Ortíz, J.G. Valerenic acid and Valeriana officinalis extracts delay onset of Pentylentetrazole (PTZ)-Induced seizures in adult *Danio rerio* (Zebrafish), *BMC Complement. Altern. Med.* **2015**, 15, 228, <https://doi.org/10.1186/s12906-015-0731-3>.
28. Trott, O.; Olson, A.J. AutoDock Vina: Improving the speed and accuracy of docking with a new scoring function, efficient optimization, and multithreading, *J. Comput. Chem.* **2010**, 31, 455-461, <https://doi.org/10.1002/jcc.21334>.
29. Yusuf, D.; Davis, A.M.; Kleywegt, G.J.; Schmitt, S. An Alternative Method for the Evaluation of Docking Performance: RSR vs RMSD, *J. Chem. Inf. Model.* **2008**, 48, 1411-1422, <https://doi.org/10.1021/ci800084x>.
30. Shityakov, S.; Förster, C. In silico predictive model to determine vector-mediated transport properties for the blood-brain barrier choline transporter, *Adv Appl Bioinform Chem.* **2014**, 7, 23-36, <https://doi.org/10.2147/AABC.S63749>.

31. Biovia, D.S. Discovery Studio Visualizer, Dassault Systemes, BIOVIA Corp., San Diego, CA, USA, 2017.
32. Pettersen, E.F.; Goddard, T.D.; Huang, C.C.; Couch, G.S.; Greenblatt, D.M.; Meng, E.C.; Ferrin, T.E. UCSF Chimera—A visualization system for exploratory research and analysis, *J. Comput. Chem.* **2004**, *25*, 1605-1612, <https://doi.org/10.1002/jcc.20084>.
33. Masiulis, S.; Desai, R.; Uchański, T.; Martin, I.S.; Laverty, D.; Karia, D.; Malinauskas, T.; Zivanov, J.; Pardon, E.; Kotecha, A.; Steyaert, J.; Miller, K.W.; Aricescu, A.R. Author Correction: GABAA receptor signalling mechanisms revealed by structural pharmacology, *Nature* **2019**, *566*, E8-E8, <https://doi.org/10.1038/s41586-019-0929-5>.
34. Imberty, A.; Hardman, K.D.; Carver, J.P.; Perez, S. Molecular modelling of protein-carbohydrate interactions. Docking of monosaccharides in the binding site of concanavalin A, *Glycobiology* **1991**, *1*, 631-642, <https://doi.org/10.1093/glycob/1.6.631>.
35. Shaikh, M.F.; Sancheti, J.; Sathaye, S. Effect of Eclipta alba on acute seizure models: A GABAA-mediated effect, *Indian J. Pharm. Sci.* **2013**, *75*, 380-384, <https://doi.org/10.4103/0250-474X.117432>.
36. Akbar, M.; Egli, M.; Cho, Y.-E.; Song, B.-J.; Noronha, A. Medications for alcohol use disorders: An overview, *Pharmacol. Ther.* **2018**, *185*, 64-85, <https://doi.org/10.1016/j.pharmthera.2017.11.007>.
37. Diniz, T.C.; de Oliveira Júnior, R.G.; Miranda Bezerra Medeiros, M.A.; Gama e Silva, M.; de Andrade Teles, R.B.; dos Passos Menezes, P.; de Sousa, B.M.H.; Abrahão Frank, L.; de Souza Araújo, A.A.; Russo Serafini, M.; Stanisçuaski Guterres, S.; Pereira Nunes, C.E.; Salvador, M.J.; da Silva Almeida, J.R.G. Anticonvulsant, sedative, anxiolytic and antidepressant activities of the essential oil of *Annona vepretorum* in mice: Involvement of GABAergic and serotonergic systems, *Biomed. Pharmacother.* **2019**, *111*, 1074-1087, <https://doi.org/10.1016/j.biopha.2018.12.114>.
38. Olsen, R.W.; Sieghart, W. GABAA receptors: Subtypes provide diversity of function and pharmacology, *Neuropharmacology* **2009**, *56*, 141-148, <https://doi.org/10.1016/j.neuropharm.2008.07.045>.
39. Penninga, E.I.; Graudal, N.; Ladekarl, M.B.; Jürgens, G. Adverse Events Associated with Flumazenil Treatment for the Management of Suspected Benzodiazepine Intoxication – A Systematic Review with Meta-Analyses of Randomised Trials, *Basic Clin. Pharmacol. Toxicol.* **2016**, *118*, 37-44, <https://doi.org/10.1111/bcpt.12434>.
40. Thiry, A.; Dogné, J.M.; Supuran, C.T.; Masereel, B. Carbonic Anhydrase Inhibitors as Anticonvulsant Agents, *Curr. Top. Med. Chem.* **2007**, *7*, 855-864, <http://dx.doi.org/10.2174/156802607780636726>.
41. Thiry, A.; Dogné, J.M.; Supuran, C.T.; Masereel, B., Drug Design of Carbonic Anhydrase Inhibitors as Anticonvulsant Agents, in: C.T.S.a.J.Y. Winum (Ed.) Drug Design of Zinc-Enzyme Inhibitors **2009**, <https://doi.org/10.1002/9780470508169.ch7>.



**Article 2**– Structural characterization, DFT calculations, ADMET studies, antibiotic potentiating activity, evaluation of efflux pump inhibition and molecular docking of chalcone (E)-1-(2-hydroxy-3, 4, 6-trimethoxyphenyl)-3-(4-methoxyphenyl) prop-2-en-1-one

Authors: da Cunha Xavier, J., de Queiroz Almeida-Neto, F. W., da Silva, P. T., de Sousa, A. P., Marinho, E. S., Marinho, M. M., ... & dos Santos, H. S.

Journal / link / Qualis *Journal of Molecular Structure* /  
<https://doi.org/10.1016/j.molstruc.2020.129692> / Qualis B2 in the biological sciences II. IF = 3.841

Situation: Published

### Resumo:

As chalconas são flavonóides de cadeia aberta caracterizadas por dois anéis aromáticos unidos por um sistema carbonil  $\alpha,\beta$ -insaturado de três carbonos. Ao longo dos últimos anos, as chalconas têm despertado o interesse de pesquisadores químicos e farmacológicos devido à sua estrutura química simples e atividades biológicas variadas. Aqui, realizamos as propriedades eletrônicas, da chalcona, (E)-1-(2-hidroxi-3,4,6-trimetoxifenil)-3-(4-metoxifenil)prop-2-en-1-ona sintetizada por Reação de condensação de Claisen-Schmidt. O método da teoria do funcional da densidade foi usado com o nível de teoria B3LYP/6-311++G (d,p) para calcular as propriedades estruturais, eletrônicas e de reatividade da chalcona. Além disso, testes microbiológicos foram realizados para investigar o potencial modulador e a inibição da bomba de efluxo em cepas multirresistentes de *Staphylococcus aureus*. As análises dos dados espectroscópicos permitiram determinar a estrutura molecular da chalcona sintetizada com posterior confirmação por meio de cálculos químicos quânticos. A adição de chalcona ao meio de crescimento causou efeito sinérgico ao reduzir os valores de concentração inibitória mínima (CIM) para a cepa de ciprofloxacina. Os resultados de encaixe mostraram que a chalcona se encaixa quase da mesma maneira que o antibiótico contra um modelo MepA. Critérios de Druglikeness baseados nas regras de Lipinski e Veber de que a chalcona tem as propriedades físico-químicas e farmacocinéticas ideais para ser uma boa candidata a fármaco por via oral. Os resultados confirmam a estrutura da chalcona sintetizada

e revelam que o composto pode ser utilizado como um possível inibidor da bomba de efluxo

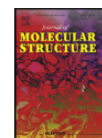
Journal of Molecular Structure 1227 (2021) 129692



Contents lists available at ScienceDirect

Journal of Molecular Structure

journal homepage: [www.elsevier.com/locate/molstr](http://www.elsevier.com/locate/molstr)



Structural characterization, DFT calculations, ADMET studies, antibiotic potentiating activity, evaluation of efflux pump inhibition and molecular docking of chalcone (*E*)-1-(2-hydroxy-3,4,6-trimethoxyphenyl)-3-(4-methoxyphenyl)prop-2-en-1-one



Jayze da Cunha Xavier<sup>a</sup>, Francisco Wagner de Queiroz Almeida-Neto<sup>b</sup>, Priscila Teixeira da Silva<sup>a</sup>, Amanda Pereira de Sousa<sup>f</sup>, Emmanuel Silva Marinho<sup>c</sup>, Márcia Machado Marinho<sup>g</sup>, Janaina Esmeraldo Rocha<sup>a</sup>, Priscila Ramos Freitas<sup>a</sup>, Ana Carolina Justino de Araújo<sup>a</sup>, Thiago Santiago Freitas<sup>a</sup>, Carlos Emídio Sampaio Nogueira<sup>a,e</sup>, Pedro de Lima-Neto<sup>b</sup>, Paulo Nogueira Bandeira<sup>f</sup>, Alexandre Magno Rodrigues Teixeira<sup>a</sup>, Henrique Douglas Melo Coutinho<sup>a</sup>, Hécio Silva dos Santos<sup>a,d,f,\*</sup>

Mep A.

**CHAPTER 6** - Structural characterization, DFT calculations, ADMET studies, antibiotic potentiating activity, evaluation of efflux pump inhibition and molecular docking of chalcone (*E*)-1-(2-hydroxy-3,4,6-trimethoxyphenyl)-3-(4-methoxyphenyl)prop-2-en-1-one

Jayze da Cunha Xavier<sup>a</sup>, Francisco Wagner Queiroz de Almeida-Neto<sup>b</sup>, Priscila Teixeira da Silva<sup>a</sup>, Amanda Pereira de Sousa<sup>f</sup>, Emmanuel Silva Marinho<sup>c</sup>, Márcia Machado Marinho<sup>g</sup>, Janaina Esmeraldo Rocha<sup>a</sup>, Priscila Ramos Freitas, Ana Carolina Justino de Araújo<sup>a</sup>, Thiago Santiago Freitas<sup>a</sup>, Carlos Emídio Sampaio Nogueira<sup>a,e</sup>, Pedro de Lima-Neto<sup>b</sup>, Paulo Nogueira Bandeira<sup>f</sup>, Alexandre Magno Rodrigues Teixeira<sup>a</sup>, Henrique Douglas Melo Coutinho<sup>a</sup>, Hécio Silva dos Santos<sup>a,d,f,\*</sup>

<sup>a</sup>Department of Biological Chemistry, Regional University of Cariri, Crato, CE, Brazil,

<sup>b</sup>Group of Theoretical Chemistry, Department of Analytical Chemistry and Physical Chemistry, Federal University of Ceará, Fortaleza, CE, Brazil

<sup>c</sup>Group of Theoretical Chemistry and Electrochemistry, State University of Ceará, Campus FAFIDAM, Limoeiro do Norte, CE, Brazil.

<sup>d</sup>Science and Technology Center, Postgraduate Program in Natural Sciences, State University of Ceará, Fortaleza, CE, Brazil

<sup>e</sup>Department of Physics, Regional University of Cariri, Juazeiro do Norte, CE, Brazil.

<sup>f</sup>Center for Exact Sciences and Technology - Chemistry Course, Vale do Acaraú University, Sobral, CE, Brazil

<sup>1\*</sup>Corresponding author. Postgraduate Program in Biological Chemistry, Department of Biological Chemistry, Regional University of Cariri, Campus Pimenta II, CEP: 63.100-000, Crato, CE, Brazil. E-mail addresses: [helciodossantos@gmail.com](mailto:helciodossantos@gmail.com)

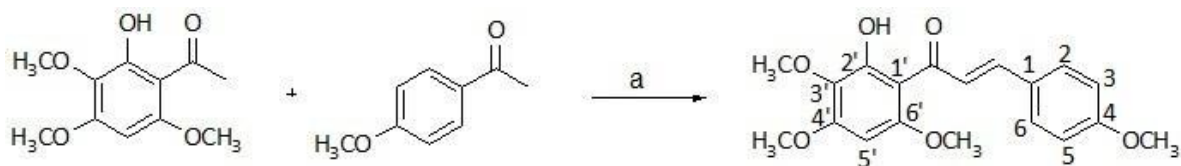
## Abstract

Chalcones are open-chain flavonoids characterized by two aromatic rings joined by a three-carbon  $\alpha,\beta$ -unsaturated carbonyl system. Over the last several years, chalcones have instigated the interest of chemical and pharmacological researchers due to their simple chemical structure and varied biological activities. Here, we performed the electronic properties, of the chalcone, (*E*)-1-(2-hydroxy-3,4,6-trimethoxyphenyl)-3-(4-methoxyphenyl) prop-2-en-1-one synthesized by Claisen-Schmidt condensation reaction. The density functional theory method was used with the B3LYP/6-311++G(d,p) level of theory to compute the structural, electronic, and reactivity properties of the chalcone. In addition, microbiological tests were performed to investigate the modulator potential and efflux pump inhibition on *Staphylococcus aureus* multi-resistant strains. The spectroscopic data analyses allowed drawing the molecular structure of the chalcone synthesized with subsequent confirmation using the quantum chemical calculations. The addition of chalcone to the growth medium caused a synergic effect by reduction of the minimum inhibitory concentration (MIC) values for ciprofloxacin strain. Docking results showed that the chalcone docks in almost the same way as the antibiotic against a MepA model. Druglikeness criteria based on the rules of Lipinski and Veber evaluated that the chalcone has the ideal physicochemical and pharmacokinetic properties to be a good candidate for drug orally. The results confirm the structure of the synthesized chalcone and revealing that the compound can be used as a possible inhibitor of the Mep A efflux pump.

**Keywords:** Chalcone, ATR-FTIR; UV-Vis; Fukui, efflux pump

## 1. Introduction

The search for new drugs is increasing due to the rapid growth of bacterial resistance that has become a medical concern today [1-3]. The bacterial resistance comes from factors such as selectivity (low plasma membrane permeability), adherence of the drug to the cell wall, its expulsion by efflux pumps, and the action of enzymes minimizing or inhibiting the antibiotic action [4, 5].



**Scheme 1.** Preparation of chalcone. a) NaOH 50% w v<sup>-1</sup>, ethanol, t.a., 48 h

Among bacterial pathogens, *S. aureus*, despite being present in the skin and nasal mucosa, is capable of causing many infections and diseases both in animals and in humans since skin infections [6], toxic shock syndrome [7], to sepsis [8]. These opportunists reach debilitated people in hospitals and are difficult to treat. Fighting these infections has become a difficult problem for health worldwide due to the growth of bacterial resistance to antibiotics [9]. In this sense, there are current interests in finding new antimicrobial agents [10].

Understanding the mechanism of action and metabolism of the biologically active molecules depends, to a large extent, on the analysis of its reactivity, which is determined by intermolecular forces, that is, lipophilic, polar, electrostatic, and stereo interactions, which depend on the characteristics of each molecule (electronic, Steric or conformational, energetic and thermodynamic) [11, 12]. It is precisely at this point that molecular modeling techniques can make their contribution to the study and development of active molecules because through it you can have a detailed description of the structure, intermolecular interactions, and, if applicable, chemical reactions between the ligand and biomacromolecules with chalcones [13-16].

Also, the electronic properties with respect to the frontier molecular orbitals, the quantum reactivity descriptors, the Fukui functions (electronic and condensed), and the molecular electrostatic potential were applied to characterize the reactive electrophilic and nucleophilic sites, which is extremely important because in previous studies the higher reactivity and electrophilicity of a synthetic chalcone, can be responsible for intermediated interactions with the bacterial cell wall and when combined with the gentamicin drug proved to be more efficient [17].

Previous studies showed that synthetic chalcones associated with antibiotics had obtained increasingly satisfactory results in containing resistant pathogen [18-24]. Chalcones are precursors to flavonoids and isoflavonoids [25, 26], but they can also be obtained by synthesis [23, 27]. This class of compound has arisen much interest due to the broad spectrum of pharmacological activities that they present, including antimicrobial [23, 28], antioxidant [29], antinociceptive [30, 31], antiparasitic [32], antitumor [33], and antiproliferative activities [34].

In this work, the chalcone (*E*)-1-(2-hydroxy-3,4,6-trimethoxyphenyl)-3-(4-methoxyphenyl) prop-2-en-1-one ( $C_{19}H_{20}O_6$ ) was synthesized by Claisen-Schmidt condensation reaction. The molecular structure was characterized by spectroscopy methods, and the Density Functional Theory was used to determine the electronic and reactivity properties. In addition, microbiological tests were performed to investigate the modulator potential and efflux pump inhibition on *S. aureus* multi-resistant strains.

## 2. Material and methods

### 2.1 Spectroscopic methods: NMR, FTIR, UV-vis

The chemical reagents were purchased from Sigma-Aldrich.  $^1\text{H}$  and  $^{13}\text{C}$  NMR spectra were obtained using a Bruker Spectrometer, model Avance DPX-500, operating at a frequency of 500 MHz for hydrogen and 125 MHz for carbon, respectively. The spectra were measured in  $\text{CDCl}_3$ , and chemical shifts are reported as  $\delta$  values in parts per million (ppm) relative to  $\text{CDCl}_3$ . The attenuated total reflectance Fourier transform infrared spectroscopy (ATR-FTIR) was performed using a Bruker vacuum infrared spectrometer VERTEX 70V. The measurements were recorded at room temperature in the range 400 to 4000  $\text{cm}^{-1}$ , with a resolution of 2  $\text{cm}^{-1}$  and accumulating 60 scans per spectrum. The UV-Visible absorption spectrum of the compound was obtained using a GENESYS 10S UV-Vis spectrophotometer (Thermo Scientific, Waltham, MA, USA) in the wavelength range of 210 to 430 nm with spectral resolution (1.8 nm). The samples were prepared at a concentration of 0.1  $\text{mmol L}^{-1}$  using ethanol as a solvent to perform the absorption measurements in the UV-Vis region. All absorption measurements were carried out at room temperature in quartz cells with 1 cm optical path.

### 2.2 Synthesis of the chalcone

The compounds 2-hydroxy-3,4,6-trimethoxyacetophenone (2 mmol) and anisaldehyde (2 mmol) were placed in a volumetric flask (25 mL). Then 5 mL of ethanolic NaOH (50%) solution was added and mixed with stirring for 48 h at room temperature. The progress of the reaction was checked by TLC (n-hexane: ethyl acetate, 2:1). After 48 h, the reaction mixture was neutralized with dilute HCl (10%) and ice water added. The product was obtained as a yellow solid filtered under reduced pressure, washed with cold water, and recrystallized from ethanol [27, 35] (Scheme 1).

### 2.3 Quantum chemical computational calculations

The quantum chemical calculations were used extensively to support the experimental data during the structural characterization of a newly synthesized molecule using the density functional theory (DFT) method. From a previous work from our group, three DFT methods were compared for the characterization of a chalcone acetamide derivative (PAAPFBA) [17], and all the methods used were accurate to describe the structural and electronic properties of a chalcone derivative molecule. Hence, due to the low computational cost, the title chalcone

was geometrically optimized using the exchange-correlation functional B3LYP at the 6-311++G(d,p) basis set [36, 37], which was the same method used in other work of our group to describe the structural and electronic properties of the chalcone derivative (2*E*,4*E*)-1-(2-hydroxy-3,4,6-trimethoxyphenyl)-5-phenylpenta-2,4-dien-1-one (cinnamaldehyde) [38]. The quantum chemical calculations were carried out using the Gaussian 09 [39] software and the Gauss View 5 [40] to draw the input molecule. The optimization was done with chloroform as an implicit solvent using the IEF-PCM solvation model [41-43] available in Gaussian 09. Conformational analysis was carried from the optimized structure to obtain the potential energy surface (PES). Next, the fundamental vibrational modes were computed at the same level of theory together with the thermodynamic properties at 298.15 K and 1 atm of pressure. The absence of negative frequencies implies that the simulated molecule can be used to describe the structural and electronic properties of the newly synthesized chalcone. The infrared spectrum was obtained from the optimized molecular geometry, and the theoretical wavenumbers were scaled by 0.983 for below 1700 cm<sup>-1</sup> and by 0.958 for above 1700 cm<sup>-1</sup> [44]. The theoretical assignments of the highlighted band from the experimental infrared spectrum were done using the potential energy distribution (PED) with the VEDA [45] software, and only the PED 10% were considered. Then, the <sup>1</sup>H and <sup>13</sup>C NMR spectra were calculated using the GIAO method [46-48] available in Gaussian 09 to obtain the theoretical isotropic shielding for the carbon ( $\sigma_C$ ) and hydrogen ( $\sigma_H$ ) atoms. Tetramethylsilane (TMS) was used as a reference compound to calculate the theoretical chemical shifts as follows:  $\delta_C = \sigma_{C(TMS)} - \sigma_C$  and  $\delta_H = \sigma_{H(TMS)} - \sigma_C$ . The frontier molecular orbitals (FMO) were calculated from the optimization calculation to understand the electronic density distribution over the entire molecule and the energy values of those molecular orbitals were used to compute the global quantum reactivity descriptors: the HOMO-LUMO energy gap ( $\Delta E_{GAP}$ , equation 1) [49]; From the Koopmans' theorem [50], the ionization potential ( $I$ , equation 2) and the electron affinity ( $A$ , equation 3); According to the works of Chermette [51] and Iczkowski and Margrave [52], the electronegativity ( $\chi$ , equation 4); From the Pearson's Hard and Soft Acid and Base (HSAB) theory [53] and according to the Janak theorem [54], and the work of Szentpály [55], the global hardness ( $\eta$ , equation 5) and the global softness ( $S$ , equation 6) introduced in the work of Yang and Parr [56]; the electrophilicity index ( $\omega$ , equation 7) according to the work of Parr and Szentpály [57]; the nucleophilicity index ( $\varepsilon$ , equation 8) from the work of Chattaraj [58]. The trial version of the ChemCraft [59] software was used to render the frontier molecular orbitals.

$$\Delta E_{GAP} = E_{LUMO} - E_{HOMO} \quad (1)$$

$$I = - E_{HOMO} \quad (2)$$

$$A = - E_{LUMO} \quad (3)$$

$$\chi = \frac{I + A}{2} \quad (4)$$

To complete the understanding of the reactivity of chalcone, the following Fukui functions are applied: Electronic [60] (equations 9 – 12) and condensed [61] (equations 13 – 15) to the nucleophilic ( and ), electrophilic ( and ), and radical ( and ) attack; and the local quantum descriptors: the dual descriptor [62] ( $\Delta f$ , equation 16) and the multiphilic index [63] ( $\Delta\omega$ , equation 17) to characterize the nucleophilic and electrophilic sites of the molecule. The electronic Fukui functions were obtained using the Multiwfn [64] software, and the isosurfaces were rendered using the VESTA [65] software. The molecular electrostatic potential (MEP) was computed at B3LYP/6-311++G(d,p) computational level to complete the local analysis of the chemical reactivity of the chalcone. The Gabedit program [66] was used to compute the MEP.

$$f^+ \approx \nu_{\text{LUMO}} \quad (10)$$

$$f^- \approx \nu_{\text{HOMO}} \quad (11)$$

$$f^0 \approx \frac{\nu_{\text{LUMO}} + \nu_{\text{HOMO}}}{2} \quad (12)$$

$$f_k^+ = q_k(N+1) - q_k(N) \quad (13)$$

$$f_k^- = q_k(N) - q_k(N-1) \quad (14)$$

$$f_k^0 = \frac{q_k(N+1) - q_k(N-1)}{2} \quad (15)$$

$$\Delta f = f_k^+ - f_k^- \quad (16)$$

$$\Delta\omega = \omega \cdot \Delta f \quad (17)$$

Where the  $q_k(N+1)$ ,  $q_k(N)$ , and  $q_k(N-1)$  are the Hirshfeld charge population [67] on the atom  $k$  of the anionic, neutral, and cationic species.

Finally, the UV-Vis spectrum was calculated using the Time-Dependent Density Functional Theory (TD-DFT) using the CAM-B3LYP [51] at 6-311++G(d,p) level of theory

in ethanol as an implicit solvent and the electronic transition was assignment using the GaussSum 3.0.1 [68, 69].

#### *2.4 Assays for modulation of the antibiotic resistance and evaluation of efflux pump inhibition by MIC reduction*

Antimicrobial activity of the chalcone was evaluated against *S. aureus* K2068, which is resistant to ciprofloxacin due to overexpression of the MepA genes encoding the MepA efflux pumps. The SA-K2068 strains were provided by Dr. Glenn W. Kaatz, John Dingell VA Medical Center, Detroit, MI, USA. Evaluation of the modulatory effect on the resistance to antibiotics was performed according to previously described [70]. Briefly, 150  $\mu$ L of each suspended bacterial inoculum in saline solution, corresponding to 0.5 of the McFarland scale, were added to microtubes (2mL) together with 1350  $\mu$ L of Brain heart infusion (BHI) as a control. In tests, 150  $\mu$ L of each suspended bacterial inoculum in saline solution, corresponding to 0.5 of the McFarland scale, were added together with EPIs (MIC/8) and completed with brain heart infusion. These were then transferred to 96-well microtiter plates, and 100  $\mu$ L of the antimicrobial drug and ethidium bromide serial dilutions were performed (1:1). The plates were incubated at 37 °C for 24 h, and bacterial growth was assessed by using resazurin. MIC was defined with antibiotics and ethidium bromide concentrations ranging from 0.5 to 512  $\mu$ g/mL. The MIC of controls was assessed using the antibiotics and ethidium bromide alone [71].

#### *2.5 Docking procedure*

The MepA model was generated by retrieving the protein sequence for the NCTC 8325 strain from the Uniprot database. Then, the SWISS-MODEL [72] service was used to build the homology model. Of all the 50 templates generated, the one with the best Global Model Quality Estimation score was based on the structure of the multidrug and toxic compound extrusion transporter of the *Bacillus halodurans* (PDB-ID: 5C6N). For the docking procedure, which was carried out using the Autodock Vina [73] software, the grid box was defined as a 126Åx126Åx126Å box around the geometrical center of the model, with spacing = 0.431 e exhaustiveness = 8. Partial Gasteiger charges were added to ligand atoms, non-polar hydrogen atoms were mixed while all other parameters were kept at their default values. The best results were chosen based on the binding score.

#### *2.6 Evaluation of physicochemical properties and drug-likeness criteria*

Calculations of physical and chemical properties, which include acid dissociation constant (pKa), molecular weight (MW), consensus partition coefficient (Clog P), hydrogen



bond donor (HBD) and acceptor (HBA) count, distribution coefficient at pH 7.4 ( $\log D_{\text{pH}7.4}$ ), solubility coefficient at pH 7.4 ( $\log S_{\text{pH}7.4}$ ), topological polar surface area (TPSA), number of rotatable bonds (Nrot) were performed using the plugins provided in the MarvinSketch® code [74]. To validate the “drug-likeness” criteria [75], the bioavailability radar was used, generated on the SwissADME web-server [76], which uses an algorithm based on a filter that combines the descriptors of the “rule of five” of Lipinski et al. [75] ( $\text{MW} \leq 500$ ,  $\log P \leq 5$ , H-bond donor  $\leq 5$  and H-bond acceptors  $\leq 10$ ) and the rule by Veber et al., (2002)<sup>7</sup> ( $\text{TPSA} \leq 140$  and rotatable bonds  $\leq 10$ ), establishing the parameters of lipophilicity ( $-0.7 < \log P < 5.0$ ), size ( $150 \text{ g/mol} < \text{MW} < 500 \text{ g/mol}$ ), polarity ( $20 \text{ \AA}^2 < \text{TPSA} < 130 \text{ \AA}^2$ ), insolubility ( $-6 < \log S < 0$ ), unsaturation ( $0.25 < \text{Fraction Csp}^3 < 1$ ) and flexibility ( $0 < \text{Num. Rotatable bonds} < 9$ ) as a determining spatial spectrum for good oral bioavailability.

### 2.7 Virtual screening of pharmacokinetics properties

Molecular descriptors of structure-activity relationship (QSAR) of the properties of absorption, distribution, metabolism, and excretion (ADME) were used to evaluate the pharmacokinetic behavior of chalcone. Through the MW, log P, and TPSA descriptors, statistical evaluation was made for the models of human intestinal absorption (HIA) [77], human adenocarcinoma colon cells permeability (Caco-2) [78], blood-brain barrier penetration (BBB) [79] and P-glycoprotein substrate (Pgp) [80].

### 2.8 Evaluation of the multi-target bioactivity

To evaluate bioactivity, the code SMILES [COc2ccc(C=CC(=O)c1c(O)c(OC)c(OC)cc1OC)cc2] was generated, using the plug-in JSME molecular editor [81], deployed on the web-server Molinspiration (<https://molinspiration.com/>) and submitted to interaction simulation with main human biological targets: G-protein coupled receptor (GPCR), ion channel modulator, a kinase inhibitor, nuclear receptor ligand, protease inhibitor, and enzyme inhibitor. The simulation is based on the test of similarity of the “drug-likeness” properties of known compounds deposited in the server database, and the results are available in scores, where values above 0.5 indicate strong interaction with the specified target, between 0.2 and 0.5 moderate interactions and for values less than 0.2 low interaction potential.

### 2.9 Acute oral toxicity prediction model

For the prediction of Acute oral toxicity, the LabMol web-server LabMol (<http://stoptox.labmol.com.br>) was used, which has its algorithm based on the structure-activity relationship (QSAR) of the acute oral toxicity model in bees, meeting the guidelines

of the Organization for Economic Cooperation and Development (OECD) and the Registration, Evaluation, Authorization, and restriction of chemical substances (REACH). For this test, results with a confidence index of 70% have closer proximity to the acute toxicity indexes in bees and are expressed in a contribution map by the toxic fragments, where the green-colored region is the positive contribution and the region colored red the negative contributions to this class of toxicity.

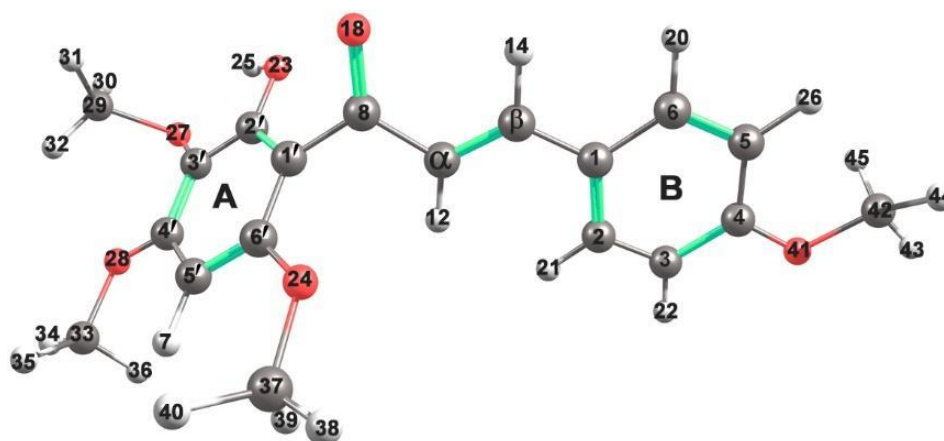


**Fig. 1.** Optimized geometry of the title chalcone obtained at B3LYP/6-311++G(d,p) level of theory.

## 2.10 Statistical Analysis

All bacteriological tests were performed in triplicates. Data were analyzed using a two-way ANOVA followed by Bonferroni's post-hoc test (where  $p < 0.05$  was considered significant). The geometric mean of the triplicates was used as the central data  $\pm$  standard error of the mean. The GraphPad Prism 5.0 statistical program was used for the analysis.

## 3. Results and discussion

### 3.1 Conformational analysis

The molecular structure and atom numbering scheme of the title chalcone is shown in Figure 1. Chalcones may exist in two isomeric forms, *E* (*trans*) or *Z* (*cis*). The *E*-isomer is the thermodynamically most stable form in most cases [82]. The title chalcone possesses the *trans* form. The relaxed PES scan of the title chalcone calculated at the B3LYP/6-311++G (d,p) level for the dihedral angle  $\phi$  (C6-C1-C $\alpha$ -C $\beta$ ) with step variation of  $15^\circ$  is shown in Figure 2a. The dashed red line in the plot in this figure corresponds the zero energy. The potential energy curve shows three minimum energy structures, two global minima at  $-179.87^\circ$  and  $179.87^\circ$ , and a local minimum at  $0.13^\circ$ .

The conformations at  $-179.87^\circ$  and  $179.87^\circ$  are equivalent and correspond to the conformer I (Figure 2b), while the conformation at  $0.13^\circ$  corresponds to the conformer II (Figure 2c). According to our calculation, the conformer I is more stable than the conformer II by  $0.26 \text{ kcal}\cdot\text{mol}^{-1}$ . It is also noted that the conformers I and II present the isomeric form *E* (*trans*). Figures 2b and 2c show the conformers I and II, respectively, with the blue planes containing the A ring, and the red planes containing the B ring. Therefore, the conformers I and II are fully nonplanar. The A and B rings in the conformer I are twisted by  $54.23^\circ$ , while they are twisted by  $53.61^\circ$  in the conformer II. Furthermore, the conformers I and II differ by the orientation of the ethoxy group in the B-ring. It is clearly known that there are differences in the structural conformations of chalcones, especially between some of their dihedral angles [83, 84].

### 3.2 NMR data

The  $^1\text{H}$  NMR spectrum (Figure 2) of this chalcone showed signals at  $\delta_{\text{H}}$  3.78 - 3.91 ppm relative to the hydrogens of methoxy groups. These signals can also be observed in the

$^{13}\text{C}$  NMR spectrum at  $\delta_{\text{C}}$  55.5 to 60.9 ppm. The signals at  $\delta_{\text{H}}$  7.24 and 7.75 ppm ( $J = 14.6 \text{ Hz}$ ) were attributed to doublets referring to  $\alpha,\beta$ -unsaturated hydrogens, whose coupling constant ( $J$ ) confirms the stereochemistry *E*, in the  $^{13}\text{C}$  NMR, these signals are observed at  $\delta_{\text{C}}$  142.9 ( $\text{C}\beta$ ) and 128.4 ( $\text{C}\alpha$ ) being related to olefinic carbons  $\alpha$  and  $\beta$ , respectively.

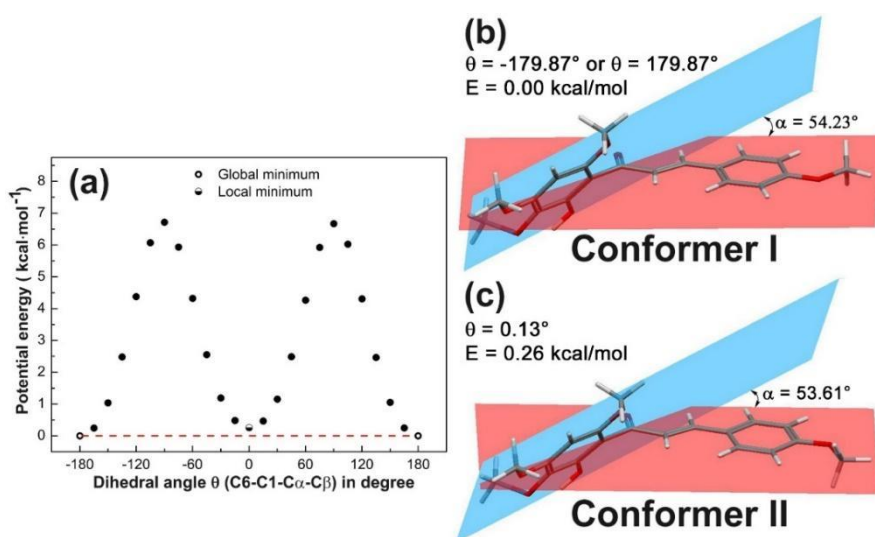


Fig. 2. (a) Potential energy profiles of the title chalcone calculated at the B3LYP/6-311++G(d,p) level of theory for rotation around C6-C1-C $\beta$ -C $\alpha$  dihedral angle. The global and local minima for the optimized structures are indicated by means of open circle, and half open circle. In (b) and (c) are shown the conformers I and II,

respectively, with their respective dihedral angle ( $\theta$ ), and potential energies (E), and with the blue planes containing the A ring, and the red planes containing the B ring

The singlet observed at  $\delta_{\text{H}}$  5.93 ppm refers to hydrogen attached to the carbon 5' whose signal is observed at  $\delta_{\text{C}}$  87.3 ppm in the  $^{13}\text{C}$  NMR spectrum. The signal at  $\delta_{\text{C}}$  193.3 ppm concerns to  $\alpha,\beta$ -unsaturated carbonyl group. The ketone absorbs 203.8 ppm, however, the presence of  $\alpha, \beta$  unsaturation, causes a displacement to the high field, and the probable cause is the delocalization of charge by the benzene ring or by the double bond that makes carbonyl carbon less electron deficient. In addition, the signs at  $\delta_{\text{C}}$  159.5 (C-4'), 158.7 (C-2'), 158.6 (C-6'), 130.3 (C-3'), and 107.1 (C-1') refer to the non-hydrogenated carbons present in ring A of the chalcone. The signals at  $\delta_{\text{H}}$  7.53 (d,  $J = 8.4$  Hz, H-2/6) and 7.89 ppm (d,  $J = 8.4$  Hz, H-3/5) are related to the signs at 125.2 (C-2/6) and 130.3 (C-3/5) in the  $^{13}\text{C}$  NMR spectrum (Figure S2), and the signs at  $\delta_{\text{C}}$  131.0 (C-4) and 130.7 ppm (C-1) refer to the non-hydrogenated carbons present in ring B (Table 1).

This chalcone has two aromatic rings linked by a three-carbon  $\alpha,\beta$ -unsaturated carbonyl system. The ring A is formed by the atoms C1', C2', C3', C4', C5' and C6', and the ring B is formed by the atoms C1, C2, C3, C4, C5, and C6. The molecule was drawn according to this experimental result, and the geometrical optimization calculation carried out using the B3LYP/6-311++G(d,p) computational level in chloroform as an implicit solvent. The optimized structure for the chalcone is shown in Figure 1. The  $^1\text{H}$  and  $^{13}\text{NMR}$  were theoretically calculated at the same level of theory as the optimization. The theoretical results for the calculated chemical shift were displaced in Table 1. To understand the correlation between the experimental and theoretical data, the linear fitting was made using the experimental and calculated chemical shifts for the  $^1\text{H}$  and  $^{13}\text{C}$  NMR (Figure S3). The linear correlation was computed with the coefficient of determination ( $R^2$ ) of 0.98669 with the linear equation of  $y = 0.94812x + 0.77857$ . This result shows an excellent agreement between the experimental and theoretical data; hence the chalcone had its molecular structure confirmed to be the same as in Figure 1.

The molecular structure of the chalcone was described to the in the global minimum of energy due to the absence of any imaginary frequency in the vibrational spectrum; hence the simulated molecule describes the real molecule of the chalcone. The molecule is not planar: the ring A is about  $54.16^\circ$  out of the plane delimited by the  $\alpha,\beta$ -unsaturated carbonyl. The O18, C8, C $\alpha$ , and C $\beta$  structure ( $\alpha,\beta$ -unsaturated carbonyl) is almost planar with a little deviation of  $-1.081^\circ$ .

**Table 1.** <sup>1</sup>H and <sup>13</sup>C NMR data of the experimental and theoretical of title chalcone in CDCl<sub>3</sub>. Chemical shifts in δC and δH are in ppm.

Chalcone				
C	δC	δH	δc (calc)	δH (calc)
1'	107.1		119.62645	
2'	158.7		158.73965	
3'	130.3		136.06635	
4'	159.5		162.63845	
5'	87.3	5.93 (s)	89.05915	5.9333417
6'	158.6		163.82965	
MeO	60.9	3.78 (s)	57.79455	3.7992417
MeO	56.2	3.86 (s)	57.34895	3.7871417
MeO	55.8	3.90 (s)	57.44635	3.8286417
MeO	55.5	3.91 (s)	62.94755	3.8801417
C=O	193.3		198.28065	
1	130.7		134.79935	
2/6	125.2	7.53 (d, <i>J</i> = 8.4 Hz)	133.55165	7.7428417
3/5	130.3	7.89 (d, <i>J</i> = 8.4 Hz)	143.30375	7.2150417
4	131.0		124.87655	
Cα	128.4	7.24 (d, <i>J</i> = 14.6 Hz)	114.79385	7.3393417
Cβ	142.9	7.75 (d, <i>J</i> = 14.6 Hz)	171.32305	8.0473417

The ring B is in the same plane as the structure previously describes with an angle of only 0.11°. The four methoxy groups showed bond length for the carbon (ring)-oxygen sigma bond of 1.38 Å (C3'-O27), 1.36 Å (C4'-O28), 1.36 Å (C6'-O24), and 1.36 Å (C4-O41). The hydroxyl group showed a bond length of 1.36 Å (C2'-O23), and the carbonyl group value of 1.23 Å (C8-O10). The π-bond between the carbon atoms Cα and Cβ demonstrate the bond length of 1.35 Å, and the bonds Cα-H12 and Cβ-H14 the values respectively of 1.08 Å and 1.09 Å. The bonds C8-C1', C8-Cα, and Cβ-C1 have a bond length of 1.50 Å, 1.48 Å, and 1.46 Å, respectively. For the methyl groups, the bond lengths are 1.44 Å (O27-C29), 1.09 Å (C29-H31), 1.09 Å (C29-H30), and 1.09 Å (C29-H32); 1.43 Å (O28-C33), 1.09 Å (C33-H34), 1.09 Å (C33-H35), and 1.093 Å (C33-H36); 1.43 Å (O24-C37), 1.09 Å (C37-H38), 1.09 Å (C33-H39), and 1.093 Å (C37-H40); 1.43 Å (O41-C42), 1.09 Å (C42-H43), 1.09 Å (C42-H44), and 1.09 Å (C42-H45). For the ring A, the unique C-H bond showed a bond length of 1.08 Å. For the ring B, the four C-H bonds have the bond length of 1.08 Å (C2-H21), 1.08 Å (C3-H22), 1.08 Å (C5-H25), and 1.08 Å (C6-H20). Finally, the carbon-carbon bonds in the rings A and B are described by the following bond lengths: for the 1.40 Å (C1'-C2'), 1.40 Å (C2'-C3'), 1.40 Å (C3'-C4'), 1.40 Å (C4'-C5), 1.40 Å (C5'-C6'), and 1.41 Å (C6'-C1') respectively in the ring A; for the 1.41 Å (C1-C2), 1.38 Å (C2-C3), 1.40 Å (C3-C4), 1.40 Å (C4-C5), 1.39 Å (C5-C6), and 1.40 Å (C6-C1) respectively for ring B.

**Table 2.** ATR-FTIR experimental frequencies (ATR-FTIR, in cm<sup>-1</sup>), calculated scaled vibrational wavenumbers (scal in cm<sup>-1</sup>) by the dual scale factor 0.983 (below 1700 cm<sup>-1</sup>) and 0.958 (above 1700 cm<sup>-1</sup>) and assignment for some of the vibrational modes for title chalcone (C<sub>19</sub>H<sub>20</sub>O<sub>6</sub>) associated with the bands of the infrared absorbance spectrum show in Figure 4.

EXP ATR-FTIR (cm <sup>-1</sup> )	DFT scal (cm <sup>-1</sup> )	Assignment for some absorbance bands for title chalcone (C <sub>19</sub> H <sub>20</sub> O <sub>6</sub> )
3119	3012.795	v (CβH14) (97)
2933	2950.918	as(C37H39) (48) + as(C37H40) (51)
2832	2889.462	s(C37H40) (44) + s(C37H39) (46)
1619	1629.596	v (CαCβ) (24) + v (C8O18) (17)
1547	1564.356	v (CαCβ) (12) + v (C4C5) (21)
1507	1512.355	β (H21C2C3) (14) + β (H20C6C5) (14) + β (H22C3C4) (14) + β (H26C5C6) (15)
1468	1462.183	β (H39C37H38) (16) + β (H34C33H36) (22) + β (H35C33H34) (29) + β (H38C37H40) (30)
1415	1415.884	v (C3'C2') (16) + v (C2'C1') (16) + v (O23C2') (18)
1333	1318.36	β (H21C2C3) (10) + β (H12CαCβ) (11) + v (CβCα) (11) + β (H14CβCα) (15)
1290	1290.679	β (H21C2C3) (11) + v (CβC1') (14) + β (H14CβCα) (18)
1210	1234.353	β (H7C5'C4') (14) + v (O27C3') (26)
1151	1136.358	v (O28C33) (11) + v (O28C4') (17)
1117	1114.958	v (O24C37) (16) + v (O23C2') (20)
992	1002.139	β (C4C5C6) (12) + β (C2C3C4) (21) + v (O27C29) (23)
828	829.4751	γ (O41C3C5C4) (10) + τ (H22C3C4C5) (10) + τ (H21C2C3C4) (13)
678	703.887	γ (O28C5'C3'C4') (13) + γ (O24C5'C1'C6') (14)
588	557.7345	τ (H25O23C2'C3') (82)
425	411.6313	β (C33O28C4') (13) + β (C6C1Cβ) (15)

Nomenclature: τ = torsion; γ = deformation out of plane; δ = deformation; v = stretching; vas = asymmetric stretching; vs = symmetric stretching.

Finally, the thermodynamics properties were computed at 298.15 K and 1 atm of pressure to complete the structural description of the chalcone using B3LYP/6-311++G(d,p) computational level in chloroform as an implicit solvent. The calculated values of the thermodynamic properties Internal Energy (U), the Heat Capacity at constant volume (C<sub>v</sub>), Enthalpy (H), Entropy (S), and Gibbs Free Energy (G) were respectively 239.64 kcal.mol<sup>-1</sup>, 0.09 kcal.mol<sup>-1</sup>.K<sup>-1</sup>, 703.77 kcal.mol<sup>-1</sup>, 0.18 kcal.mol<sup>-1</sup>.K<sup>-1</sup>, and 651.58 kcal.mol<sup>-1</sup>. The Zero-Point Energy (ZPE) was 223.90 kcal.mol<sup>-1</sup>. For comparison, the thermodynamics properties Internal Energy, Enthalpy, Entropy, and Gibbs Free Energy for the chalcones previously studied [17, 38] are respectively 181.23 kcal.mol<sup>-1</sup>, 532.47 kcal.mol<sup>-1</sup>, 0.15 kcal.mol<sup>-1</sup>.K<sup>-1</sup>, and 488.07 kcal.mol<sup>-1</sup> for the PAAPFBA chalcone [17]; 239.84 kcal.mol<sup>-1</sup>, 704.87 kcal.mol<sup>-1</sup>, 0.17 kcal.mol<sup>-1</sup>.K<sup>-1</sup>, and 653.22 kcal.mol<sup>-1</sup> for the cinnamaldehyde chalcone [38]. The molecular structure of the chalcone is more similar to the cinnamaldehyde chalcone; hence the values for

the thermodynamics properties are similar. However, the PAAPFBA chalcone has a fluorine atom bonded in ring B and an acetamide group bonded in ring A and the values for the same properties are different from the values obtained to the title and cinnamaldehyde chalcone, which shows how the ligands in both phenyls ring A and B can change the properties of the entire molecule.

**Fig. 3.** Experimental ATR-IR and theoretical Infrared spectrum obtained at B3LYP/6-311++G(d,p) level of theory.

### 3.3 Infrared analyses

The ATR-IR absorption spectrum of the title compound is shown in Figure 3. The experimental and theoretical infrared spectra are compared. The experimental spectrum shows several absorption bands, with the most prominent ones at 3119, 2933, 2832, 1619, 1547, 1507, 1466, 1415, 1333, 1290, 1210, 1151, 1117, 992, 828, 789, 678, 588, and 425 cm<sup>-1</sup>.

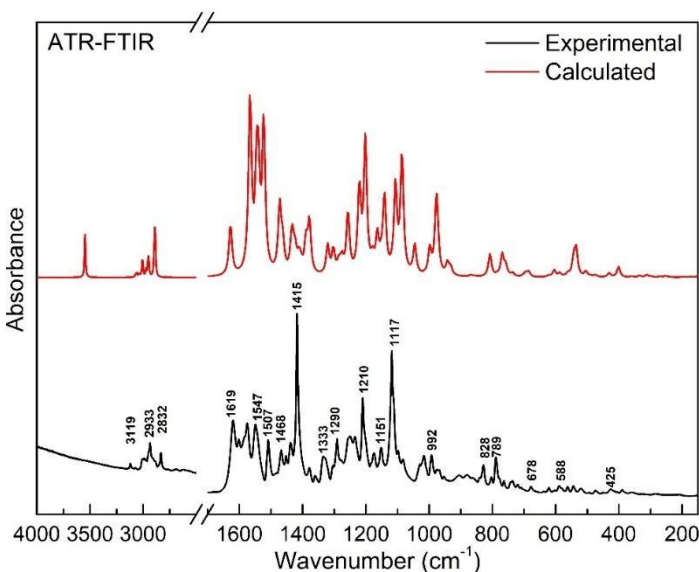


Figure 3. We compared the experimental ATR-FTIR spectrum of the title compound with the theoretical infrared spectrum obtained at B3LYP/6-311++G(d,p) level of theory. The experimental spectrum shows several absorption bands, with the most prominent ones at 3119, 2933, 2832, 1619, 1547, 1507, 1466, 1415, 1333, 1290, 1210, 1151, 1117, 992, 828, 789, 678, 588, and 425 cm<sup>-1</sup>.

The bands of wavenumbers at 3119 cm<sup>-1</sup>, 2933 cm<sup>-1</sup>, and 2832 cm<sup>-1</sup> in the experimental infrared spectrum of the title chalcone are associated with stretching modes of the groups, CβH14 (97%), asymmetrical stretching in the methyl group C37H39 (48%) and C37H40 (51%), and symmetrical stretching of the methyl group C37H39 (46%) and C37H40 (44%),

The bands of wavenumbers at 1619 cm<sup>-1</sup>, 1547 cm<sup>-1</sup>, 1507 cm<sup>-1</sup>, 1466 cm<sup>-1</sup>, 1415 cm<sup>-1</sup>, 1333 cm<sup>-1</sup>, 1290 cm<sup>-1</sup>, 1210 cm<sup>-1</sup>, 1151 cm<sup>-1</sup>, 1117 cm<sup>-1</sup>, 992 cm<sup>-1</sup>, 828 cm<sup>-1</sup>, 789 cm<sup>-1</sup>, 678 cm<sup>-1</sup>, 588 cm<sup>-1</sup>, and 425 cm<sup>-1</sup> in the experimental infrared spectrum of the title chalcone are associated with bending modes of the groups, CβH14 (97%), asymmetrical stretching in the methyl group C37H39 (48%) and C37H40 (51%), and symmetrical stretching of the methyl group C37H39 (46%) and C37H40 (44%),

respectively, whereas the infrared band at  $1619\text{ cm}^{-1}$  is associated with the mixture of carbonyl stretching mode (C8=O18) with  $C\alpha$ - $C\beta$  stretching mode. The C-C stretching modes of the ring B are observed in the infrared spectrum at  $1547\text{ cm}^{-1}$  with the movement of the atoms C4-C5 mainly (PED = 21%) and the  $C\alpha$  $C\beta$  stretching (PED = 12%).

The ATR-IR absorbance bands observed at  $1507\text{ cm}^{-1}$  corresponds to a combination of the bending modes of the H21C2C3 (14%), H20C6C5 (14%), H22C3C4 (14%), and H26C5C6 (15%), whereas the infrared band at  $1468\text{ cm}^{-1}$  corresponds to the bending modes of the H39C37H38 (16%), H34C33H36 (22%), H35C33H34 (29%), H38C37H40 (30%). The more intense infrared band located at  $1415\text{ cm}^{-1}$  is associated with the stretching modes of the C3'C2' (16%), C2'C1' (16%), O23C2' (18%) in ring A. At  $1333\text{ cm}^{-1}$  and  $1290\text{ cm}^{-1}$ , there are mixed vibrational modes for the bending and stretching of the following group of atoms respectively: H21C2C3 (10%), H12C $\alpha$ C $\beta$  (11%), H14C $\beta$ C $\alpha$  (15%), and C $\beta$ C $\alpha$  (11%) at  $1333\text{ cm}^{-1}$ ; H21C2C3 (11%), H14C $\beta$ C $\alpha$  (18%), and C $\beta$ C1' (14%) at  $1290\text{ cm}^{-1}$ . The band at  $1210\text{ cm}^{-1}$  is associated with the bending and stretching modes of the groups H7C5'C4' (14%) and O27C3' (26%), respectively. Stretching modes of the carbon-oxygen bonds O28C33 (11%) and O28C4' (17%) are observed in the band at  $1151\text{ cm}^{-1}$ . A strong infrared band, which is associated with the stretching of the methoxy group O24C37 (16%), O23C2' (20%), is observed at  $1117\text{ cm}^{-1}$ . Stretching and bending modes of the O27C29 (23%), C4C5C6 (12%), and C2C3C4 (21%) are observed at  $992\text{ cm}^{-1}$ .

At  $828\text{ cm}^{-1}$  it was observed mixed modes between the out of plane deformations and two torsions respectively in the ring B for the group of atoms O41C3C5C4 (10%), H22C3C4C5 (10%), and H21C2C3C4 (13%). Out of plane deformation and torsion of the ring A respectively are observed in the wavenumbers 678 (O28C5'C3'C4' with PED = 13% and O24C5'C1'C6' with PED = 14%) and  $588\text{ cm}^{-1}$  (H25O23C2'C3' with PED = 82%), whereas the mode at  $425\text{ cm}^{-1}$  has low intensity and corresponds to bending modes of the C33O28C4' (13%) and C6C1C $\beta$  (15%). Therefore, the vibrational analysis allowed us to obtain information on the main infrared bands of the chalcone.

### 3.4 Electronic Properties analysis

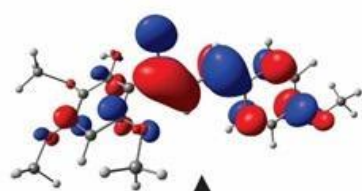
The Frontier Molecular Orbitals (FMO) for the title chalcone were calculated using the B3LYP/6-311++G(d,p) computational level, and they are shown in Figure 4. The Highest Occupied Molecular Orbital (HOMO) is related to the molecule's ability to donate electronic density (nucleophilic character), while the Lowest Unoccupied



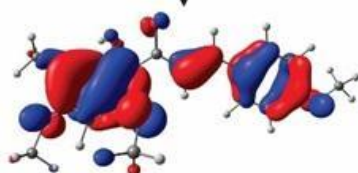
Molecular Orbital (LUMO) is related to the molecule's ability to accept electronic density (electrophilic character). The HOMO is mainly spread over the phenyl group of the ring A due to the  $\pi$ -bonds, also is spread over the oxygen atoms of the methoxy groups (O24, O27, and O28), in the  $\pi$ -bond between the carbon atoms  $C\alpha C\beta$ , in the oxygen atom (O18) of the carbonyl group, in the  $\pi$ -bonds of the phenyl group in the ring B, and in the oxygen atom (O41) of the methoxy group. Besides, the LUMO is mainly spread over the  $\pi^*$  antibonding positions of the phenyl group in the ring B, the bond between the  $C\alpha C\beta$ , and the oxygen atom (O18) of the carbonyl group. There is a little contribution of the  $\pi^*$  antibonding for the ring A. Hence, the region of the molecule responsible for donating electronic density is the ring A, the ring B, and the olefin group ( $C\alpha C\beta$ ), while the region responsible for accepting electronic density is the ring B and the  $\alpha,\beta$ -unsaturated carbonyl group. The electronic transition between the HOMO and the LUMO is  $\pi \rightarrow \pi^*$ .

To understand the chemical behavior of the chalcone, the quantum reactivity descriptors were computed at the same level of theory from the energies values of the HOMO and the LUMO, and they are shown in Table 3. The values of the quantum descriptors show that the title chalcone has an electrophilic character due to the higher values of the electronegativity and the electrophilicity index.

$$E_{\text{LUMO}} = - 2.1908 \text{ eV}$$



$$\Delta E_{\text{gap}} = 3.7752 \text{ eV}$$



$$E_{\text{HOMO}} = - 5.9660 \text{ eV}$$

**Fig. 4.** Frontier Molecular Orbitals (HOMO and LUMO) calculated for title chalcone at B3LYP/6-311++G(d,p) level of theory

The LUMO as a spread over the entire molecule, the extra negative charge. Besides, the molecule has a high ionization potential, which means it is difficult to donate electronic density. This result is confirmed by the low value of the nucleophilicity index. The molecule can be classified as a hard molecule due to the high value of the global hardness in comparison with the global softness and the high value of the energy gap, which agrees with the difficulty of electronic-donation of this molecule. Therefore, the chalcone should interact better with substrates that have a good electronic donation character. Also, in Table 3 is shown the comparison of the quantum reactivity descriptors computed for the chalcone and the PAAPFBA [17] and cinnamaldehyde [38] chalcones. The chalcone should be more reactive than the PAAPFBA and should be less reactive than the cinnamaldehyde chalcone due to the values of the HOMO-LUMO energy gap. The chalcone has a lower value of electronegativity; hence this molecule also has the lower electrophilic character, consequently the higher nucleophilic character, which is proved by the higher value of the energy value for the HOMO when compared to the others chalcones.

**Table 3.** Calculated quantum reactivity descriptors for title chalcone computed at B3LYP/6-311++G(d,p) level of theory.

Quantum reactivity descriptor	Chalcone (In this work)	PAAPFBA (Ref. [17])	Cinnamaldehyde (Ref. [38])
HOMO energy (EHOMO/ eV)	-5.96603	-6.58330	-6.06057
LUMO energy (ELUMO/ eV)	-2.19084	-2.68007	-2.69721
Energy Gap ( $\Delta$ EGAP/ eV)	3.775189	3.903232	3.363354
Ionization Potential (I / eV)	5.966034	6.583302	6.060568
Electron Affinity (A / eV)	2.190845	2.68007	2.697214
Electronegativity ( $\chi$ / eV)	4.078439	4.631686	4.378891
Global Hardness ( $\eta$ / eV)	1.887595	1.951616	1.681677
Global Softness (S / eV <sup>-1</sup> )	0.529775	0.512396	0.594645
Electrophilicity Index ( $\omega$ / eV)	4.406049	5.496091	5.701061
Nucleophilicity Index ( $\varepsilon$ / eV <sup>-1</sup> )	0.226961	0.181947	0.175406

### 3.5 Fukui functions and local reactivity descriptors analysis

The Fukui functions (Electronic and Condensed) are used to understand how each atom behaves during a chemical reaction. The quantum reactivity descriptors give an overview of the molecule's reactivity; however, the Fukui functions together with the dual descriptor ( $\Delta f$ ) and the multiphilic index ( $\Delta\omega$ ), a more selective analysis can be made on each atom.

The Electronic Fukui functions for the nucleophilic attack ( $f^+$ ), electrophilic attack ( $f^-$ ), and radical attack ( $f^0$ ) obtained with isodensity value 0.00072736 of the chalcone are shown in Figure 5. The green and the blue colored represent the positive and the negative signs of the Fukui functions, respectively. The higher the value of the Fukui function, the higher the propensity for the determined attack (nucleophilic, electrophilic, or radical). For the nucleophilic attack, the most susceptible atoms are  $C\alpha$ ,  $C\beta$ , O18, C2, C4, C6, and O41. In this case, the molecule behaves like an electrophilic site; hence the function is related to the LUMO. These atoms have mainly the LUMO spread over them; hence they are most prone to accept electronic density. For the electrophilic attack, the most susceptible atoms are C1, C2, C3, C4, C5, C6, C8, O41,  $C\alpha$ ,  $C\beta$ , O18, C1', C3', O24, and O28. The function is related to the HOMO because the molecule behaves as a nucleophilic site. Despite a larger number of atoms that are susceptible to donate electronic density, this molecule has a low energy level for the HOMO and higher ionization potential due to the more delocalization of the electronic density within the molecule. For the radical attack ( $f^0$ ), the most susceptible atoms are C1, C2, C3, C4, C5, C6, O41,  $C\alpha$ ,  $C\beta$ , O18, C1', C2', C3', and the hydrogen atoms. The carbon and oxygen atoms can stabilize the radical due to the resonance effect, and the hydrogen atoms are lost during the reaction between a radical species.

The results from the calculations of the Condensed Fukui functions, dual descriptor, and multiphilic index are shown in Table 4. The Condensed Fukui functions were computed from the Hirshfeld charge analysis [67] for the anionic (N+1), neutral (N), and cationic (N-1) species of the title chalcone. According to the results, for a nucleophilic attack, the most susceptible atoms are C2', C5', C1, C2, C3, C4, C5, C6, O24, O27, C33, and C37. For the electrophilic attack, the most propensity atoms are C1', C2', C4', C5', C6', C8, C2, O27, C29, C37, and C42. For the radical attack, the most susceptible atoms are C1', C2', C4', C5', C6', C1, C3, C5, O24, O27, O28, C29, C33, C37, and C42. The relation between the Condensed Fukui functions and the local reactivity descriptors (the dual descriptor and the multiphilic index) lies in the following fact: if both  $\Delta f$  and  $\Delta\omega$  are positive, the reactive site has an electrophilic character, and if  $\Delta f$  and  $\Delta\omega$  are negative, the reactive site has nucleophilic character. The values in Table 4 show that the electrophilic sites are in atoms C1', C2', C3',

C4', C5', C6', C1, C3, C5, O24, O27, O28, C29, C33, C37, O41, and C42. The nucleophilic sites are in the atoms C8, C $\alpha$ , C $\beta$ , O18, C2, C4, and C6.

The negative values for the condensed Fukui functions confirm the analysis made by the Electronic Fukui Functions that the HOMO is not too available to donate electronic density since the electronic density is spread over the entire molecule due to the resonance effect, hence due to the higher nucleophilic character of the chalcone when compared to the PAAPFBA [17] and cinnamaldehyde [38], the title chalcone can use the inner molecular orbitals (HOMO-1, HOMO-2, etc.) to donate electronic density during a nucleophilic attack [86, 87].

When the electronic density is reduced in the HOMO due to the electron donation process for the title chalcone, the nodal surfaces of the HOMO does not reduce as expected, hence since the inner occupied molecular orbitals have different nodal surfaces proved by the Wintner's theorem [88], these molecular orbitals are less shielded from the nuclei and the orbital relaxation occurs [86, 87].

The contract of the inner molecular orbitals causes the increase of the electronic density which is greater than the reduced electronic density of the HOMO, therefore it is expected that the condensed Fukui function ( $f^+$ ) to be negative since the Hirshfeld charge of the atom after the oxidation process is larger than the neutral chalcone.

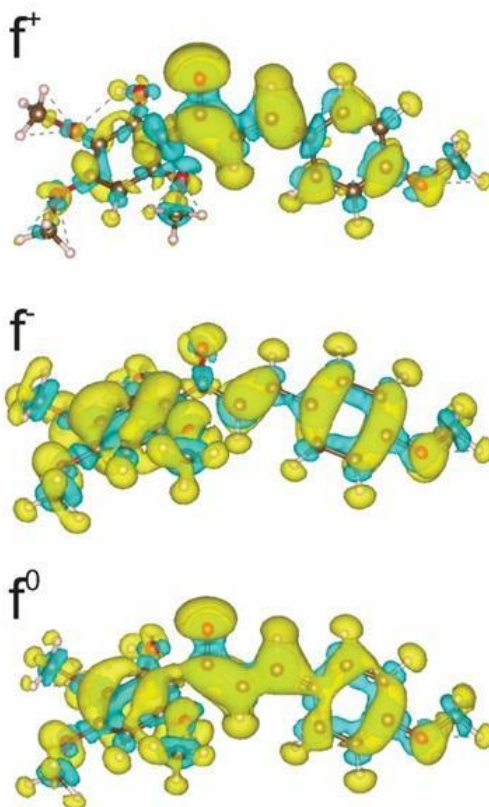


**Fig. 5.** The Electronic Fukui functions for the nucleophilic attack ( $f^+$ ), electrophilic attack ( $f^-$ ), and radical attack ( $f^0$ ) obtained with isodensity value 0.00072736 of the title chalcone.

**Table 4.** Condensed Fukui functions, the dual descriptor ( $\Delta f$ ), and the multiphilic index ( $\Delta\omega$ ) calculated from the Hirshfeld charge analysis for the anionic, neutral, and cationic species of the title chalcone.

Atom				$\Delta f$	$\Delta\omega$
C3'	-0.01171	-0.05893	-0.03532	0.047228	0.208089
C4'	-0.02256	-0.0352	-0.02888	0.012637	0.055679
C2'	-0.01691	-0.01906	-0.01798	0.002149	0.009469
C1'	-0.00571	-0.04048	-0.02309	0.034768	0.15319
C6'	-0.01533	-0.03728	-0.02631	0.021951	0.096717
C5'	-0.01372	-0.02216	-0.01794	0.008435	0.037165
H7	-0.00959	-0.01433	-0.01196	0.004739	0.02088
C8	-0.09686	-0.01172	-0.05429	-0.08514	-0.37515
C $\alpha$	-0.0644	-0.04803	-0.05621	-0.01638	-0.07215
O18	-0.118	-0.03586	-0.07693	-0.08214	-0.3619
C $\beta$	-0.10464	-0.03139	-0.06801	-0.07325	-0.32276
H12	-0.03088	-0.01429	-0.02258	-0.01659	-0.07311
C1	-0.02126	-0.03813	-0.0297	0.016873	0.074343
H14	-0.04153	-0.01647	-0.029	-0.02506	-0.11041
C2	-0.03923	-0.02333	-0.03128	-0.0159	-0.07004
C6	-0.04183	-0.03197	-0.0369	-0.00986	-0.04344
C3	-0.02646	-0.03012	-0.02829	0.003664	0.016144
C5	-0.02567	-0.03105	-0.02836	0.005373	0.023674
C4	-0.04719	-0.03945	-0.04332	-0.00774	-0.03412
H20	-0.02091	-0.01694	-0.01893	-0.00398	-0.01752
H21	-0.0201	-0.0124	-0.01625	-0.00771	-0.03395
H22	-0.01822	-0.01705	-0.01764	-0.00118	-0.00518
H23	-0.0106	-0.02066	-0.01563	0.010062	0.044334
O24	-0.00508	-0.04054	-0.02281	0.035455	0.156216
H25	-0.00997	-0.01183	-0.0109	0.001851	0.008156
H26	-0.01631	-0.01629	-0.0163	-1.7E-05	-7.5E-05
O27	-0.0065	-0.02923	-0.01786	0.022737	0.10018
O28	-0.01272	-0.03242	-0.02257	0.019705	0.086821
C29	-0.0045	-0.01307	-0.00878	0.008572	0.037769
H30	-0.00529	-0.01215	-0.00872	0.006858	0.030217
H31	-0.003	-0.01044	-0.00672	0.007445	0.032803
H32	-0.00383	-0.00845	-0.00614	0.004617	0.020343
C33	-0.00546	-0.0115	-0.00848	0.006042	0.026621
H34	-0.00609	-0.01078	-0.00844	0.004689	0.02066
H35	-0.00481	-0.01043	-0.00762	0.005614	0.024736
H36	-0.00457	-0.01011	-0.00734	0.005534	0.024383
C37	-0.00699	-0.01325	-0.01012	0.006255	0.02756
H38	-0.00554	-0.01103	-0.00829	0.005494	0.024207
H39	-0.00631	-0.01248	-0.0094	0.006171	0.02719
H40	-0.00823	-0.01425	-0.01124	0.006018	0.026516
O41	-0.02538	-0.04163	-0.0335	0.016248	0.071589
C42	-0.00946	-0.01156	-0.01051	0.002094	0.009226
H43	-0.00939	-0.01035	-0.00987	0.00096	0.00423
H44	-0.00841	-0.0109	-0.00966	0.002487	0.010958
H45	-0.00839	-0.01093	-0.00966	0.002533	0.011161

Echegaray et al. [87] proposed that molecular with very small HOMO-LUMO energy gap can be shown negative values for the condensed Fukui functions, hence this work and the work of the PAAPFBA chalcone [17] showed that despite the HOMO-LUMO energy gap to be around 3.80 eV, this class of molecules can show negative values for the condensed Fukui functions due to its molecular structure.

### 3.6 Molecule Electrostatic Potential (MEP)

The Molecular Electrostatic Potential (MEP) was computed at B3LYP/6-311++G(d,p) level of theory (Figure 6). The MEP has the following color scheme: the red-colored is related to a negatively charged region, the yellow-colored to a partially negative charge region, the green-colored to a neutral region, the light blue color to a partially positive region, and the blue-colored to a positively charged region.

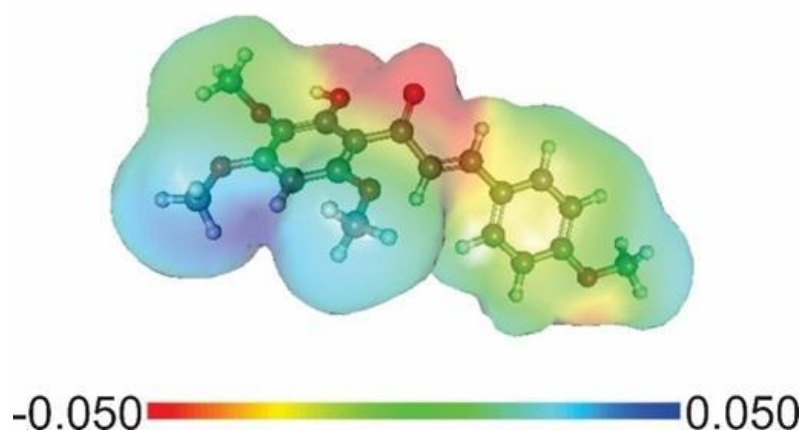


**Fig. 6.** Calculated Molecular Electrostatic Potential (MEP) for title chalcone at B3LYP/6-311++G(d,p) level of theory

The nucleophilic sites of the molecule are displayed as red to yellow colored regions due to higher concentration of electronic density. The electrophilic sites are displayed as light blue to blue colored regions due to the electron deficient. The oxygen atoms from the carbonyl, methoxy, and hydroxyl groups, the  $\pi$  electrons from the phenyl rings, and the  $\pi$  electrons from the  $C\alpha C\beta$  bond are most susceptible to interact with positive regions of a substrate. The hydrogen atoms with a partially positive charge are most susceptible to interact with negative regions from other molecules. These results are directly related to the Fukui functions and the FMO analysis.

### 3.7 UV-Vis spectrum analysis

In addition, the spectrum of UV-Vis absorption of chalcone is presented in Figure 7. Analyzing this spectrum, it is possible to observe the maximum wavelength,  $\lambda_{\max}$ , at 365.51 nm, which corresponds to an energy value of 3.39 eV. For the theoretical characterization, the UV-Vis absorption spectrum was computed using the Time-Dependent Density Functional Theory (TD-DFT) at CAM-B3LYP/6-311++G(d,p) level of theory in ethanol media.

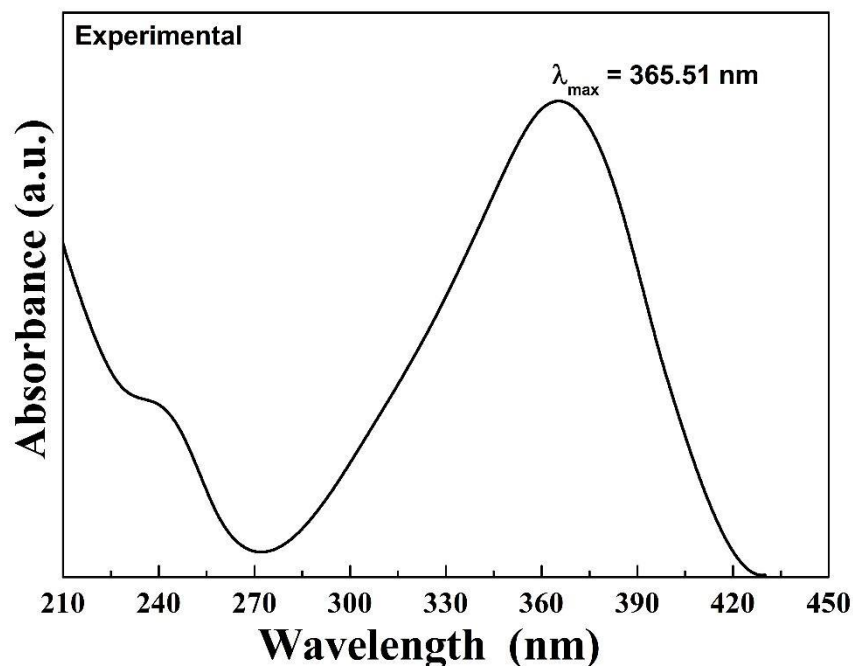


**Fig. 7.** Experimental UV-Vis spectrum of the title chalcone.

The calculated UV-Vis spectrum is shown in Figure 8. The maximum value for the absorption wavelength was found at 333.10 nm, which correspondent energy of 3.7221 eV with an oscillator strength of 0.5846. The electronic transitions which are responsible for this transition are the HOMO-2→LUMO (6%), the HOMO-4→LUMO (29%), and the HOMO→LUMO (56%). Hence, the absorption band in the experimental UV-Vis spectrum of the chalcone is described mainly for the  $\pi \rightarrow \pi^*$  transition between the HOMO and the LUMO, and the difference between the experimental and theoretical maximum wavelength is 32.41 nm, which corresponds to a percentual error of 8.87 %.

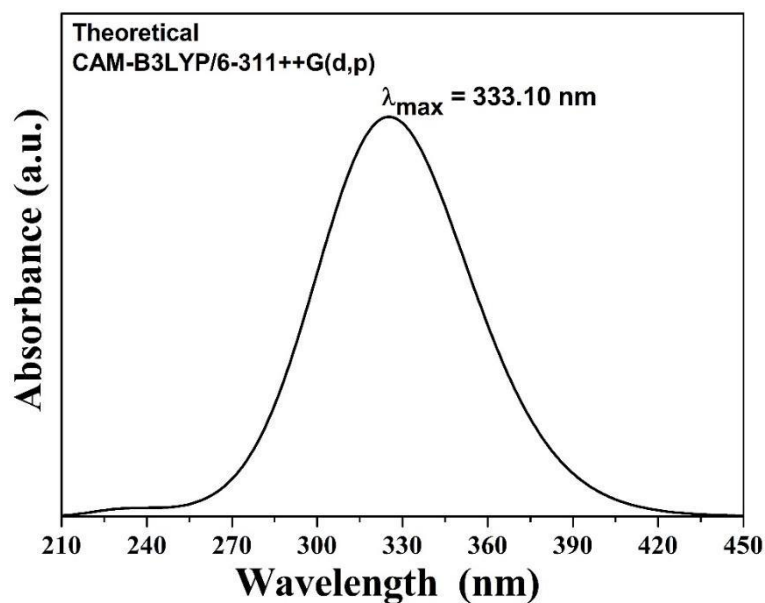


**Fig. 8.** Theoretical UV–Vis spectrum of the title chalcone using the TD-DFT method with the CAM-B3LYP/6-311++G(d,p) level of theory and ethanol as an implicit solven

### 3.8 Evaluation of the major microspecies

By analyzing the calculated pKa value of chalcone in the order of 7.76, it is possible to observe the chemical balance between the microspecies of the molecular system of the substance. The graph expressed in Figure 9 shows the distribution of chalcone microspecies as a function of pH variation, where it is worth noting that the loaded species is formed close to the physiological pH levels (approximately 7.4), since the blue curve shows a trend decreasing the concentration of the neutral species of the compound, while the concentration of the ionic species shown by the orange curve tends to 100%. Considering the relations established by the Henderson–Hasselbalch equation and the calculated value compatible with experimental data from other phenolic hydroxyls, at the time when  $\text{pH} > \text{pKa}$ , the chemical equilibrium shifts towards the formation of the ionic species as the most abundant in the system, since such behavior occurs only at high basic pH levels. Thus, it was possible to identify a concentration of 69.49% associated with neutral species as the major microspecies at pH 7.4 (Figure 9).



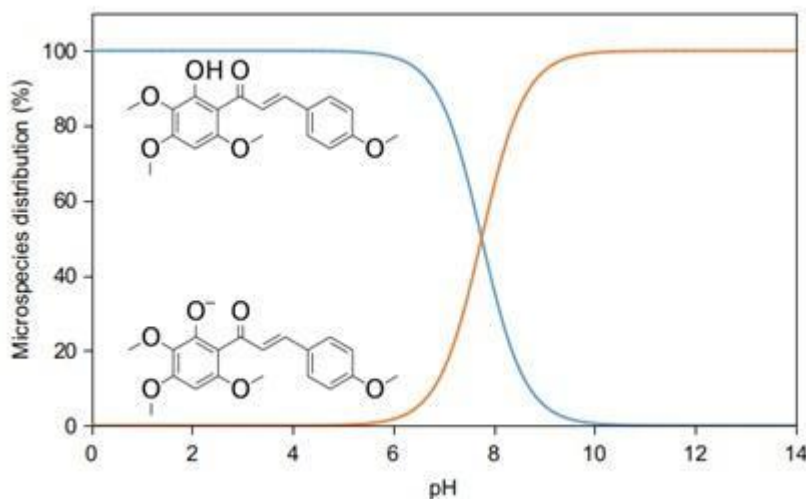


**Fig. 9.** Graph of the distribution of chalcone micro species as a function of pH variation through the acid dissociation constant (pKa).

### 3.9 Evaluation of the physicochemical properties

Chalcones are often mentioned in studies that relate to structure-activity (QSAR). The predicted and observed antimycobacterial, antibacterial, antituberculosis, and anticancer biological activities show a linear trend of fidelity between theoretical molecular descriptors and the bioactivity performed by these small molecules [75, 89-91]. Directly associated with lipophilicity and permeability, important descriptors of rational drug planning such as partition coefficient between n-octanol and water ( $\log P_{o/w}$ ) e topological polar surface area (TPSA) and topological polar surface area (TPSA) can provide information on the pharmacokinetic behavior of a given substance, as well as its oral bioavailability. As a rule, most of the experimental findings involving these two properties in theoretical screens suggest that compounds with positive values of  $\log P$  are associated with compounds with hydrophobic behavior and  $TPSA \leq 140 \text{ \AA}^2$  values with compounds capable of penetrating diverse biological membranes [76, 90, 91]. Thus, the calculated value of  $\text{Clog } P$  in the order of 3.61 indicates that chalcone is predominantly lipophilic, while its TPSA value of  $74.22 \text{ \AA}^2$  indicates a good capacity for cell permeability (Table 5).

In the filter that combines the drug-likeness criteria of Lipinski's "rule of five" ( $MW \leq 500$ ,  $\log P \leq 5$ , H-bond donors  $\leq 5$  and H-bond acceptors  $\leq 10$ ) [75] and Veber's parameters ( $TPSA \leq 140$  and rotatable bonds  $\leq 10$ ) [91], the bioavailability radar shown in Figure 10 shows the ideal physicochemical properties that refine chalcone as a good candidate for an oral drug [76]. It is verifiable that, despite the violation in the unsaturation score (INSATU) of type  $Fsp3 < 0.25$ , the compound does not violate any criteria of the rules of Lipinski and Veber, satisfying the conditions within the ideal spectrum that combines

lipophilicity properties (LIPO), size molecular (SIZE), polarity (POLAR), flexibility (FLEX) and insolubility (INSOLU) (Figure 10).

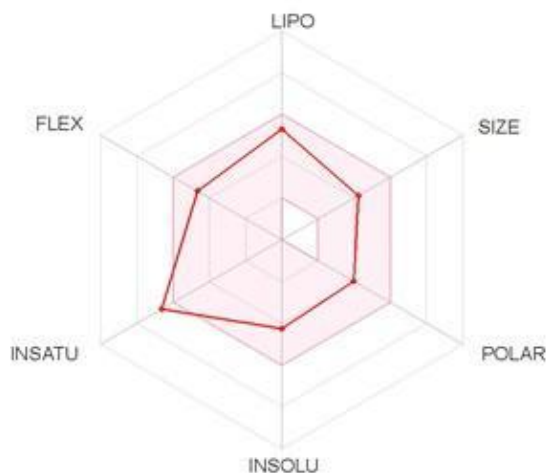


**Fig. 10.** Bioavailability radar of the title chalcone L by the druglikeness criteria (Lipophilicity ( $-0.7 < \log P < 5.0$ ), size ( $150 \text{ g/mol} < \text{MW} < 500 \text{ g/mol}$ ), polarity ( $20 \text{ \AA}^2 < \text{TPSA} < 130 \text{ \AA}^2$ ), insolubility ( $-6 < \log S < 0$ ), insaturação ( $0.25 < \text{Fraction Csp}^3 < 1$ ) and flexibility ( $0 < \text{Num. Rotatable bonds} < 9$ )

### 3.10 Virtual screening of pharmacokinetics properties

In a systematic statistical analysis that relates structure to permeability, some descriptors make it possible to predict intestinal absorption of small molecules, such as the distribution coefficient ( $\log D$ ), which, directly related to lipophilicity ( $\log P$ ), indicates the absorption potential in specific pH. In these conditions, the lipophilicity indexes incorporated into the  $\log D$  values between 0 and 3 are associated with compounds with good intestinal absorption. In addition, the model is used to identify anticancer compounds by permeability in Caco-2 model cells, associated with compounds with  $\log P$  between 1 and 10 [77, 92].

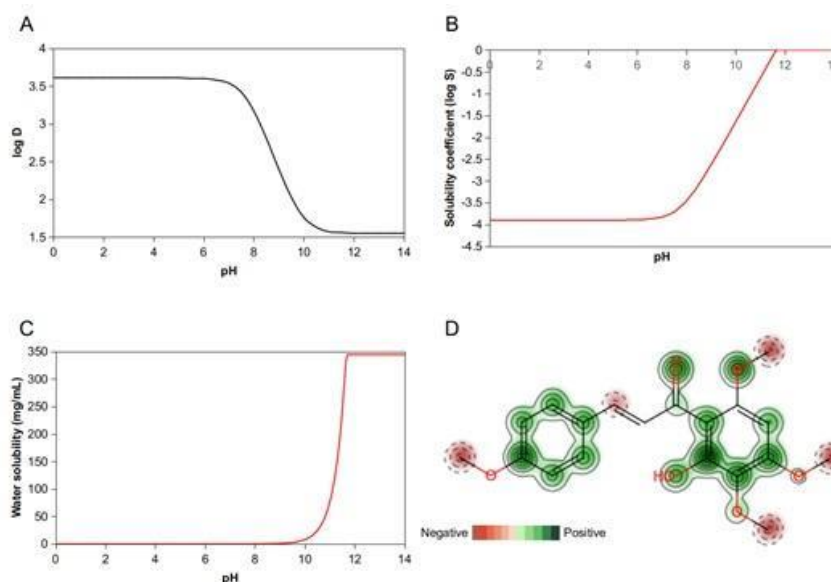


**Fig. 11.** Models of structure-activity relationship (QSAR) of chalcone: A - absorption represented by the log D and pH values, B - solubility class represented by the log S and pH values, C - water solubility represented by the concentration in mg/mL and pH values and D - Molecular fragments of the acute oral toxicity model.

The calculated log value  $D_{pH7.4}$  3.45 indicates that chalcone has a high intestinal absorption (Figure 11A), while the model indicates that the compound has moderate permeability potential in Caco-2 cells, which can vary from 20 - 70 %. In addition, it is possible to observe that the decrease in the values of log D as a function of the increase in pH implies in the reduction of the potential for absorption of the compound, behavior related to ionic species resulting from the chemical balance between the microspecies in physiological pH, at the same time in there is an increase in the solubility coefficient evaluated in log S - 3.74 at pH 7.4 (Figure 11B) with a moderate concentration of approximately 0.06 mg / mL, reaching high concentrations that can reach up to 344.36 mg/mL at high pH levels (Figure 11C).

As activity in the drug distribution stage, the transport of substances in the central nervous system (CNS) is an analysis of great importance in pharmacokinetic studies, since only 15 % of compounds that penetrate the blood-brain barrier (BBB) perform efflux by plasma proteins, such as P-glycoprotein (Pgp) [93]. In experimental observations made by Kelder et al. (1999) [78], compounds with TPSA values  $TPSA < 60-70 \text{ \AA}^2$  are more likely to be active in the CNS by penetrating the BBB in phase II clinical tests, while the statistical observations refine compounds as substrates of Pgp those with  $\log P > 0$  and MW between 200 and 400 g/mol [79].

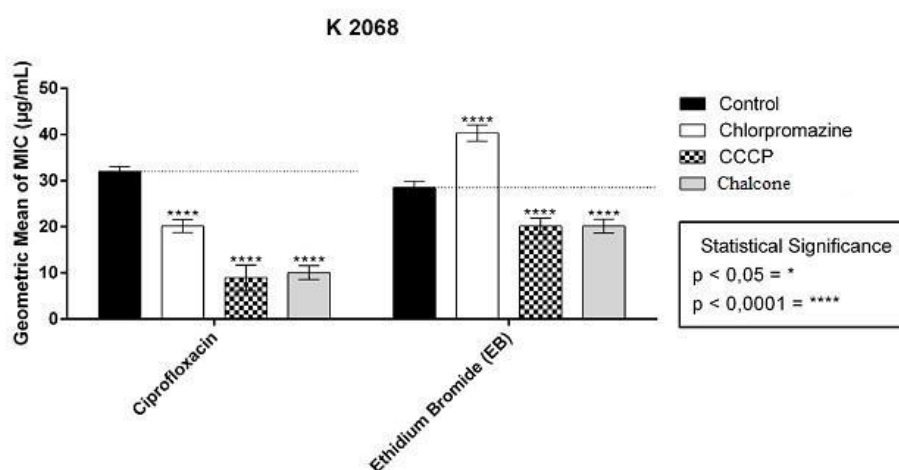
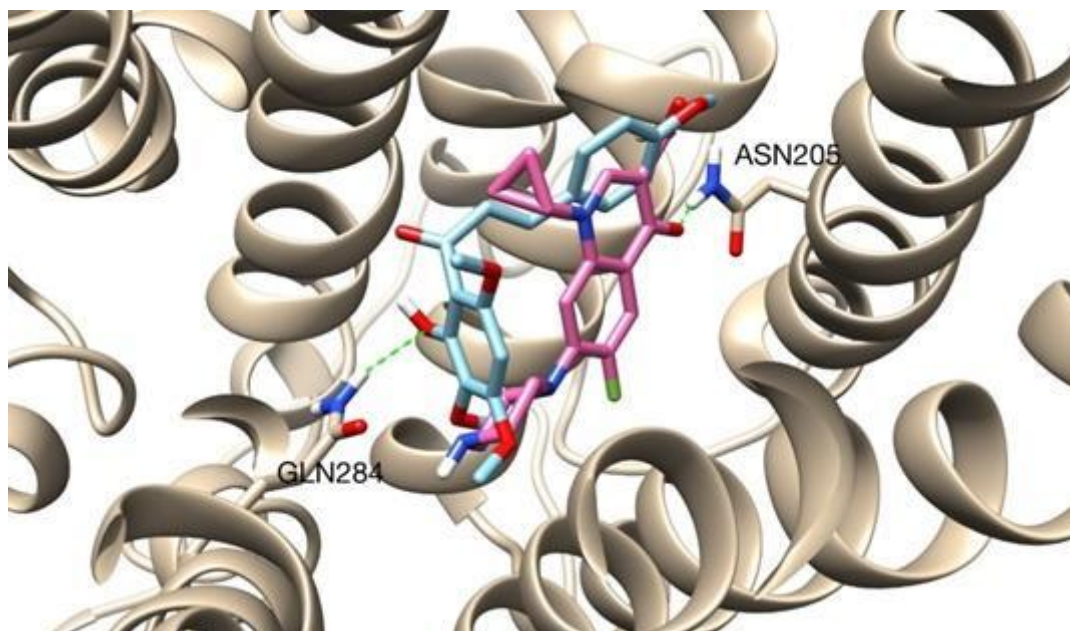


Fig. 12. MICs of the Ciprofloxacin (Cip) and Ethidium Bromide (EB) in the absence or presence of binary mixture acetophenone (59.14%) and title chalcone (40.86%), as well as Chlorpromazine (CPZ) and carbonylcyanide m-chlorophenyl hydrazone (CCCP) against K2068 (MepA)

Through the filter that combines the two observations to describe the behavior of chalcone in the CNS, it can be observed that, despite the ellipse formed between the values of

MW and Clog P showing chalcone as a substrate for Pgp, the substance has a high probability of being inactive in the CNS because it does not permeate from the BBB (Table 5).



**Fig. 13.** The best pose of chalcone (pink) and the best pose of ciprofloxacin (blue) on the binding site of the MepA mode

**Table 5.** Physicochemical and pharmacokinetics properties by the ADMET parameters for title chalcone

Physicochemical		ADMET		
Properties	Value	Properties	Value	
MW	344.36 g/mol	Absorption	HIA	High
Clog P	3.61		Caco-2	Moderately
log $D_{pH7.4}$	3.45	Distribution	BBB	No
log $S_{pH7.4}$	-3.74		Pgp	Yes
Wsol	0.06	Metabolism	GPCR	-0.10
HBD	1		Ion CM	-0.08
HBA	6		Kinase	-0.18
TPSA	74.22 Å <sup>2</sup>		Nuclear	-0.03
Nrot	7		Protease	-0.20
Fsp3	0.21		Enzyme	0.02
Nvio	0	Toxicity	Acute	Non-toxic
			oral	

legend: MW (molecular weight (g/mol)), Clog P (consensus partition coefficient), log  $D_{pH7.4}$  (distribution coefficient at pH 7.4), log  $S_{pH7.4}$  (solubility coefficient at pH 7.4), Wsol (water solubility (mg/mL)), HBD (hydrogen bond donor count), HBA (hydrogen bond acceptor count), TPSA (topological polar surface area (Å<sup>2</sup>)),

Nrot (number of rotatable bonds), Fsp3 (fraction Csp3), Nvio (number of violations by the Lipinski and Veber druglikeness criteria), HIA (human intestinal absorption), Caco-2 (human adenocarcinoma colon cells), BBB (blood-brain barrier penetration), Pgp (P-glycoprotein substrate), bioactivity by the GPCR (G-protein coupled receptor), ion CM (ion channel modulator), kinase inhibitor, nuclear receptor ligand, protease inhibitor and enzyme inhibitor models and toxicity by the acute oral model.

### *3.11 Evaluation of the multi-target bioactivity*

The prediction of toxicological effects is gaining more and more prominence in pharmacokinetic studies, especially in the identification of toxic fragments that intercalate between the cyclic structures of DNA molecules in an intracellular environment, resulting in tumorigenicity. The so-called mutagens are precursors of mutagenicity that involves the DNA structures of a host in the development of tumorigenic activity in human cells. In this context, the virtual screening by the interaction with the different human biological targets allows to identify the carcinogenic activity of a certain chemical species [79, 94-97]. Thus, the score of interaction with the target of G-protein coupled receptor (GPCR) in the order of -0.10 associated with a low index of chalcone interaction with this target, located in the membranes of human cells, indicating minimal toxicological risk due to modification of intracellular gene pool (Table 5).

Considered one of the main ion channel modulators, the human Ether-to-go-go-Related Gene (hERG) ion transporter is associated with the electrical conduction of the system that surrounds the human heart and in the modulation of cells in the nervous system, and its inhibition results in complications such as cardiac arrhythmia and cancer events such as leukemia [98-102], where the inhibition score of -0.08 for chalcone indicates low cardiotoxic risk (Table 5).

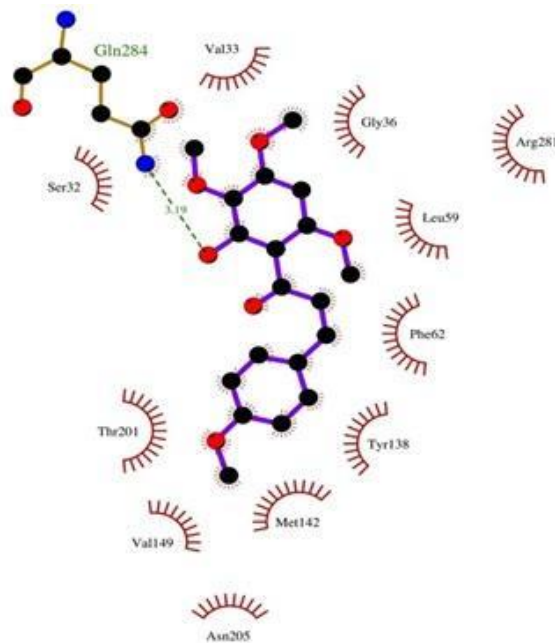
In the stage of phase I metabolism, the cytochrome P450 (CYP450) isoenzymes, in particular the CYP3A4 and CYP2C9 enzymes, play a fundamental role in the biotransformation of drugs through O- type oxidation reactions [103]. Physico-chemical properties such as  $\log D_{pH7.4}$  and  $\log P$  are related to CYP450 substrates since the sites of interaction with these enzymes are predominantly lipophilic [104]. The positive values of  $\log D_{pH7.4}$  and  $\log P$  suggest that chalcone interacts as a substrate of the main CYP450 isoenzymes, while the inhibition score of them evaluated at 0.02 indicates the low probability of inhibitory actions of these isoenzymes, indicating that the compound is subject to drug modifications by oxidation of the phenolic hydroxyl (Table 5).

Figure 11D shows the contributions of the structure-activity relationship (QSAR) to the chalcone acute oral toxicity model. In this model, the green-colored area represents the positive contributions to the toxicity model, showing the non-toxic molecular fragments, while the red-colored region indicates the negative contributions. Thus, the toxicity model of

the test indicates, with a 70% reliability index, that the minimum oral dose administered does not result in toxicity.

### 3.12 Potential Antibacterial Activity and Evaluation of Efflux Pump Inhibition

The modulating effect of the chalcone on the resistance of the SA-K2068 strain to ciprofloxacin can be seen in Figure 12.



**Fig. 14.** 2D ligand-protein interaction diagram of the title chalcone and the MepA model. Contact distances are shown in green

It can be seen that the addition of chalcone in subinhibitory concentrations to the growth medium caused a reduction of the MIC values for ciprofloxacin strain. The synergic effect presented by the chalcone was the same as the modulating effect observed for CCCP, which is cited in the literature as an inhibitor of the MepA efflux pump [71]. This effect against the MepA efflux pump is due to the inhibition of the efflux pump mechanism, which can be proven by similar behavior observed examining the association of this chalcone with ethidium bromide (Figure 12). Previous studies showed a similar effect when the DB Thiophene chalcone was tested for the SA-K2068 strain. DB Thiophene showed a better inhibition potential for CCCP-sensitive efflux pumps than the standard inhibitor, also acting as a strong inhibitor of efflux pumps in the Ciprofloxacin test [71].

### 3.13 Docking Results

In order to better understand the MepA inhibition mechanism displayed by the chalcone, a docking essay was carried out. Both the chalcone and ciprofloxacin were individually docked against a MepA model. Figure 13 shows the best poses of both molecules docked on the binding site of the MepA mode; as can be clearly seen from the figure, the chalcone docks to the model in almost the same way as the antibiotic. It also interacts with essentially the same residues. Figure 14 shows the two-dimensional map of the interactions between the title chalcone and the MepA model. Despite of the HOMO is mainly spread over the ring A, the ring B makes a  $\pi$  interaction with the amino acids methionine (MET 142) and phenylalanine (PHE 62) since this chalcone has electronic density to donate, and the LUMO is mainly spread over the ring B; hence this chalcone can also receive electronic density from the amino acids.

The binding energy of the best pose of chalcone was  $-6.80 \text{ kcal.mol}^{-1}$ . Although the binding energy is essentially a ranking system for the poses of the ligand, one could use it to compare affinities to the model, provided the ligands being compared have similar molecular weights. With that caveat in mind, the binding energy of the ciprofloxacin antibiotic was  $-7.60 \text{ kcal.mol}^{-1}$ . The slightly higher affinity of ciprofloxacin could be attributed to the hydrogen bond between the antibiotic and the Asn205 residue, which is shorter than the hydrogen bond between chalcone and Gln284. Also, these binding energies are not only close to each other, but also on par with those reported on the literature for MepA and NorA models. Rezende-Júnior et al. [105] have reported that the binding energies of chalcones to a NorA model are approximately  $-7.00 \text{ kcal.mol}^{-1}$ .

#### 4. Conclusion

The analyses allowed drawing the molecular structure of the chalcone synthesized with subsequent confirmation using the quantum chemical calculations with an excellent linear correlation between the experimental and theoretical chemical shifts. The spectroscopic analysis allowed obtaining information of the main infrared bands of chalcone, and together with the theoretical assignments of the vibrational modes of those band, the Infrared spectroscopic analysis contributed to confirm the molecular structure of chalcone, and the electronic characterization identified the regions of the molecule that are responsible to donate (nucleophilic) and to accept (electrophilic) electronic density. The drug-likeness criteria based on the rules of Lipinski and Veber evaluated that the compound has the ideal physicochemical properties for the realization of its active ingredient as an oral drug, and the low interaction with plasma proteins indicates a molecular fraction of the bioavailable substance for interactions with specific biological targets in docking tests and molecular dynamics. The

molecular size and lipophilicity models suggest that the substance has a high probability of being an inactive drug in the CNS, and its transport by Pgp indicates that there is no risk of toxicity due to residual drug accumulation in the blood. The structure-activity relationship (QSAR) of chalcone and the low rates of interaction with the targets GPCR and Ion CM suggest that the minimum oral dose administered does not present a toxic risk to the nervous system and the respiratory system, constituting a good candidate for drug orally. In addition, the microbiological tests show that the chalcone can be used as a possible inhibitor of the Mep A efflux pump, also revealing that chalcone can be used as a base for the design of substances with antibiotic modifying activity.

## References

- [1] D.E. Payne, B.R. Boles, Emerging interactions between matrix components during biofilm development, *Curr. Genet.*, 62 (2016) 137-141. <https://doi.org/10.1007/s00294-015-0527-5>
- [2] M. Jamal, W. Ahmad, S. Andleeb, F. Jalil, M. Imran, M.A. Nawaz, T. Hussain, M. Ali, M. Rafiq, M.A. Kamil, Bacterial biofilm and associated infections, *J. Chin. Med. Assoc.*, 81 (2018) 7-11. <https://doi.org/10.1016/j.jcma.2017.07.012>.
- [3] S.J. Dancer, The effect of antibiotics on methicillin-resistant *Staphylococcus aureus*, *J. Antimicrob. Chemother.*, 61 (2008) 246-253. <https://doi.org/10.1093/jac/dkm465>.
- [4] F. Aqil, I. Ahmad, M. Owais, Evaluation of anti-methicillin-resistant *Staphylococcus aureus* (MRSA) activity and synergy of some bioactive plant extracts, *Biotechnol. J.*, 1 (2006) 1093-1102. <https://doi.org/10.1002/biot.200600130>.
- [5] H.D.M. Coutinho, J.G.M. Costa, E.O. Lima, V.S. Falcao-Silva, J.P. Siqueira, Jr., Enhancement of the antibiotic activity against a multiresistant *Escherichia coli* by *Mentha arvensis* L. and chlorpromazine, *Chemotherapy*, 54 (2008) 328-330. <https://doi.org/10.1159/000151267>.
- [6] S. Krishna, L.S. Miller, Host-pathogen interactions between the skin and *Staphylococcus aureus*, *Curr. Opin. Microbiol.*, 15 (2012) 28-35. <http://dx.doi.org/10.1016/j.mib.2011.11.003>.
- [7] P.M. Dugourd, A. Dupont, T. Hubiche, C. Chiaverini, A. Alkhalifa, L. Roudiere, A. Tristan, C.A. Gustave, P. Del Giudice, Staphylococcal toxic shock syndrome should be considered in the event of diffuse erythema with fever and shock, *Ann. Dermatol. Venereol.*, 146 (2019) 287-291. <https://doi.org/10.1016/j.annder.2018.12.002>.
- [8] S.P. Bergin, T.L. Holland, V.G. Fowler, S.Y.C. Tong, Bacteremia, Sepsis, and Infective Endocarditis Associated with *Staphylococcus aureus*, in: F. Bagnoli, R. Rappuoli, G. Grandi (Eds.) *Staphylococcus aureus: Microbiology, Pathology, Immunology, Therapy and Prophylaxis*, Springer International Publishing, Cham, 2017, pp. 263-296.
- [9] P.M. Wright, I.B. Seiple, A.G. Myers, The Evolving Role of Chemical Synthesis in Antibacterial Drug Discovery, *Angewandte Chemie-International Edition*, 53 (2014) 8840-8869. <https://doi.org/10.1002/anie.201310843>.
- [10] M.T.A. Oliveira, A.M.R. Teixeira, H.D.M. Coutinho, I.R.A. Menezes, D.M. Sena, H.S. Santos, B.M. de Mesquita, M.R.J.R. Albuquerque, P.N. Bandeira, R. Braz-Filho, Identification and Modulatory Activity Assessment of 2-Hydroxy-3,4,6-trimethoxyacetophenone Isolated from Croton



anisodontus Mull. Arg.(Euphorbiaceae), Nat. Prod. Commun., 9 (2014) 1934578X1400900520. <http://dx.doi.org/10.1177/1934578X1400900520>.

[11] P.H.M. Torres, A.C.R. Sodero, P. Jofily, F.P. Silva-Jr, Key Topics in Molecular Docking for Drug Design, Int. J. Mol. Sci., 20 (2019). <https://doi.org/10.3390/ijms20184574>.

[12] S. Saikia, M. Bordoloi, Molecular Docking: Challenges, Advances and its Use in Drug Discovery Perspective, Curr. Drug Targets, 20 (2019) 501-521. <https://doi.org/10.2174/1389450119666181022153016>.

[13] D.G. do Rego, B.G. de Oliveira, Um Estudo Químico-quântico da Covalência Intermolecular em Sistemas Estabilizados por Ligações de Hidrogênio  $\pi\cdots H$  e  $N\cdots H$ : Cálculos DFT, ChelpG, NBO e QTAIM, Orbital: Electron. J. Chem., 1 (2016) 1-11.

[14] S. Burmaoglu, S. Ozcan, S. Balcioglu, M. Gencel, S.A.A. Noma, S. Essiz, B. Ates, O. Algul, Synthesis, biological evaluation and molecular docking studies of bis-chalcone derivatives as xanthine oxidase inhibitors and anticancer agents, Bioorg. Chem., 91 (2019) 103149. <https://doi.org/10.1016/j.bioorg.2019.103149>.

[15] S. Burmaoglu, E.A. Kazancioglu, R. Kaya, M. Kazancioglu, M. Karaman, O. Algul, I. Gulcin, Synthesis of novel organohalogen chalcone derivatives and screening of their molecular docking study and some enzymes inhibition effects, J. Mol. Struct., 1208 (2020) 127868. <https://doi.org/10.1016/j.molstruc.2020.127868>.

[16] P. Yadav, J.K. Yadav, A. Agarwal, S.K. Awasthi, Insights into the interaction of potent antimicrobial chalcone triazole analogs with human serum albumin: spectroscopy and molecular docking approaches, RSC Advances, 9 (2019) 31969-31978. <https://doi.org/10.1039/C9RA04192C>.

[17] F.W.Q. Almeida-Neto, L.P. da Silva, M.K.A. Ferreira, F.R.S. Mendes, K.K.A. de Castro, P.N. Bandeira, J.E.S.A. de Menezes, H.S. dos Santos, N.K.V. Monteiro, E.S. Marinho, P. de Lima-Neto, Characterization of the structural, spectroscopic, nonlinear optical, electronic properties and antioxidant activity of the N-{4'-[(E)-3-(Fluorophenyl)-1-(phenyl)-prop-2-en-1-one]}-acetamide, J. Mol. Struct., 1220 (2020) 128765. <https://doi.org/10.1016/j.molstruc.2020.128765>.

[18] P.T. Silva, L.L.M. A., J.C. Xavier, M.C.S. Carvalho, M.O. Moraes, C. Pessoa, F.W.A. Barros, P.N. Bandeira, C.S.P. Cavalcante, A.M.R. Teixeira, R.O.S. Fontenelle, H.S. Santos, Atividade Citotóxica e Antifúngica de Chalconas Sintetizadas a partir de uma Acetofenona Natural Isolada de Croton anisodontus, Rev. Virtual Quím., 12 (2020) 712-723. <https://doi.org/10.21577/1984-6835.20200057>.

[19] P.T. Silva, T.S. Freitas, D.M. Sena, Jr., P.N. Bandeira, M.S.S. Julião, E.S. Marinho, A.A.C. Alcanfor, E.M. Marinho, P. Lima-Neto, C.E.S. Nogueira, H.D.M. Coutinho, A.L.A.B. Leal, H.M. Barreto, N. Martins, Rodrigues Teixeira, A. M., H.S. Santos, Structural, Vibrational and Electrochemical Analysis and Antibacterial Potential of Isomeric Chalcones Derived from Natural Acetophenone, Applied Sciences, 10 (2020) 4713. <http://dx.doi.org/10.3390/app10144713>.

[20] T.S.d. Freitas, J.d.C. Xavier, R.L.S. Pereira, J.E. Rocha, D.F. Muniz, P.T. da Silva, J.P. da Hora, H.S. dos Santos, P.N. Bandeira, C.E.S. Nogueira, A.M.R. Teixeira, H.D.M. Coutinho, Direct antibacterial and antibiotic resistance modulatory activity of chalcones synthesized from the natural product 2-hydroxy-3,4,6-trimethoxyacetophenone, FEMS Microbiol. Lett., 367 (2020). <http://dx.doi.org/10.1093/femsle/fnaa124>.

[21] C.A.N. Ferraz, S.R. Tintino, A.M.R. Teixeira, P.N. Bandeira, H.S. Santos, B.G. Cruz, C.E.S. Nogueira, T.F. Moura, R.L.S. Pereira, D.M. Sena, T.S. Freitas, J.E. Rocha, H.D.M. Coutinho, Potentiation of antibiotic activity by chalcone (E)-1-(4'-aminophenyl)-3-(furan-2-yl)-prop-2-en-1-one against gram-positive and gram-negative MDR strains, Microb. Pathog., 148 (2020) 104453. <https://doi.org/10.1016/j.micpath.2020.104453>.

- [22] P.T. da Silva, J.d.C. Xavier, T.S. Freitas, M.M. Oliveira, H.D.M. Coutinho, A.L.A.B. Leal, H.M. Barreto, P.N. Bandeira, C.E.S. Nogueira, D.M. Sena, F.W.Q. Almeida-Neto, E.S. Marinho, H.S. Santos, A.M.R. Teixeira, Synthesis, spectroscopic characterization and antibacterial evaluation by chalcones derived of acetophenone isolated from *Croton anisodontus* Müll.Arg, *JMoSt*, DOI [https://doi.org/10.1016/j.molstruc.2020.129403\(2021\)129403](https://doi.org/10.1016/j.molstruc.2020.129403(2021)129403).  
<https://doi.org/10.1016/j.molstruc.2020.129403>.
- [23] A.M.R. Teixeira, H.S. Santos, P.N. Bandeira, M.S.S. Juliao, P.T.C. Freire, V.N. Lima, B.G. Cruz, P.T. da Silva, H.D.M. Coutinho, D.M. Sena, Structural, spectroscopic and microbiological characterization of the chalcone 2E-1-(2'-hydroxy-3',4',6'-trimethoxyphenyl)-3-(phenyl)-prop-2-en-1-one derived from the natural product 2-hydroxy-3,4,6-trimethoxyacetophenone, *J. Mol. Struct.*, 1179 (2019) 739-748. <https://doi.org/10.1016/j.molstruc.2018.11.075>.
- [24] P.N. Bandeira, R.O.S. Fontenelle, P.S. Costa, H.S. Santos, T.L.G. Lemos, Atividade Antifúngica In Vitro Contra *Trychophyton Rubrum* de P-Aminochalcones e 3'-Metoxi-4'-Hidroxi Chalcona, *Rev. Virtual Quím.*, 12 (2020) 703-711. <https://doi.org/10.21577/1984-6835.20200056>.
- [25] Z. Rozmer, P. Perjési, Naturally occurring chalcones and their biological activities, *Phytochem. Rev.*, 15 (2016) 87-120. <https://doi.org/10.1007/s11101-014-9387-8>.
- [26] C.L. Zhuang, W. Zhang, C.Q. Sheng, W.N. Zhang, C.G. Xing, Z.Y. Miao, Chalcone: A Privileged Structure in Medicinal Chemistry, *Chem. Rev.*, 117 (2017) 7762-7810. <http://dx.doi.org/10.1021/acs.chemrev.7b00020>.
- [27] P.N. Bandeira, T.L.G. Lemos, H. S. Santos, M.C.S. de Carvalho, D.P. Pinheiro, M.O. de Moraes Filho, C. Pessoa, F.W.A. Barros-Nepomuceno, T.H.S. Rodrigues, P.R.V. Ribeiro, H.S. Magalhães, A.M.R. Teixeira, Synthesis, structural characterization, and cytotoxic evaluation of chalcone derivatives, *Med. Chem. Res.*, DOI [https://doi.org/10.1007/s00044-019-02434-1\(2019\)](https://doi.org/10.1007/s00044-019-02434-1(2019)).  
<https://doi.org/10.1007/s00044-019-02434-1>.
- [28] T.R. Garcia, T.S. de Freitas, H.S. dos Santos, P.N. Bandeira, M.S.S. Julião, J.E. Rocha, C.E.S. Nogueira, R.L.S. Pereira, A.C.H. Barreto, P.T.C. Freire, H.D.M. Coutinho, A.M.R. Teixeira, Structural, vibrational and electrochemical analysis and antibiotic activity study of chalcone (2E)-1-(3',-methoxy-4',-hydroxyphenyl)-3-(3-nitrophenyl)prop-2-en-1-one, *J. Mol. Struct.*, 1216 (2020) 128358. <https://doi.org/10.1016/j.molstruc.2020.128358>.
- [29] T.O. Ajiboye, M.T. Yakubu, A.T. Oladiji, Electrophilic and Reactive Oxygen Species Detoxification Potentials of Chalcone Dimers is Mediated by Redox Transcription Factor Nrf-2, *J. Biochem. Mol. Toxicol.*, 28 (2014) 11-22. <https://doi.org/10.1002/jbt.21517>.
- [30] M.K.A. Ferreira, A.W. da Silva, F.C.O. Silva, C.L.A. Holanda, S.M. Barroso, J.d.R. Lima, A.E. Vieira Neto, A.R. Campos, P.N. Bandeira, H.S. dos Santos, T.L.G. de Lemos, S.M.C. Siqueira, F.E.A. Magalhães, J.E.S.A. de Menezes, Anxiolytic-like effect of chalcone N-{(4'-[(E)-3-(4-fluorophenyl)-1-(phenyl) prop-2-en-1-one]} acetamide on adult zebrafish (*Danio rerio*): Involvement of the GABAergic system, *Behav. Brain Res.*, 374 (2019) 111871. <https://doi.org/10.1016/j.bbr.2019.03.040>.
- [31] M.K.A. Ferreira, A.W. da Silva, F.C.O. Silva, A.E. Vieira Neto, A.R. Campos, S.A. Alves Rodrigues Santos, A.M. Rodrigues Teixeira, J. da Cunha Xavier, P.N. Bandeira, C.E. Sampaio Nogueira, D.H.A. de Brito, E.L. Rebouças, F.E.A. Magalhães, J. de Menezes, H.S. Dos Santos, Anxiolytic-like effect of chalcone N-4'[(2E)-3-(3-nitrophenyl)-1-(phenyl)prop-2-en-1-one]} acetamide on adult zebrafish (*Danio rerio*): Involvement of the 5-HT system, *Biochem. Biophys. Res. Commun.*, 526 (2020) 505-511. <https://doi.org/10.1016/j.bbrc.2020.03.129>.
- [32] E.O. Ajaiyeoba, O.O. Ogbole, O.O. Abiodun, J.S. Ashidi, P.J. Houghton, C.W. Wright, Cajachalcone: An antimalarial compound from *Cajanus cajan* leaf extract, *J. Parasitol. Res.*, 2013 (2013). <https://doi.org/10.1155/2013/703781>.

- [33] X.W. Fang, B.Q. Yang, Z. Cheng, M.P. Yang, N. Su, L.Z. Zhou, J. Zhou, Synthesis and Antitumor Activity of Novel Nitrogen Mustard-Linked Chalcones, *Arch. Pharm.*, 346 (2013) 292-299. <https://doi.org/10.1002/ardp.201200443>.
- [34] H. Wei, X. Zhang, G. Wu, X. Yang, S. Pan, Y. Wang, J. Ruan, Chalcone derivatives from the fern *Cyclosorus parasiticus* and their anti-proliferative activity, *Food Chem. Toxicol.*, 60 (2013) 147-152. <https://doi.org/10.1016/j.fct.2013.07.045>.
- [35] C.E.S. Nogueira, M.M. de Oliveira, A.M.R. Teixeira, P.N. Bandeira, H.S. dos Santos, A.P. Ayala, B.P. Bezerra, A.C.H. Barreto, P.T.C. Freire, Crystal structure, FT-Raman and FTIR spectra and DFT calculations of chalcone (2E)-1-(4-aminophenyl)-3-(furan-2-yl)prop-2-en-1-one monohydrate, *J. Mol. Struct.*, 1212 (2020) 128141. <https://doi.org/10.1016/j.molstruc.2020.128141>.
- [36] A.D. Becke, Density-Functional Thermochemistry .1. The Effect of The Exchange-Only Gradient Correction, *J. Chem. Phys.*, 96 (1992) 2155-2160. <http://dx.doi.org/10.1063/1.462066>.
- [37] C. Lee, W. Yang, R.G. Parr, Development of the Colle-Salvetti correlation-energy formula into a functional of the electron density, *PhRvB*, 37 (1988) 785-789. <https://doi.org/10.1103/PhysRevB.37.785>.
- [38] J.d.C. Xavier, F.W.Q. Almeida-Neto, P.T. da Silva, E.S. Marinho, M.K.A. Ferreira, F.E.A. Magalhães, C.E.S. Nogueira, P.N. Bandeira, J.E.S.A. de Menezes, A.M.R. Teixeira, H.S.d. Santos, Structural characterization, electronic properties, and anxiolytic-like effect in adult zebrafish (*Danio rerio*) of cinnamaldehyde chalcone, *J. Mol. Struct.*, 1222 (2020) 128954. <https://doi.org/10.1016/j.molstruc.2020.128954>.
- [39] M.J. Frisch, G.W. Trucks, H.B. Schlegel, G.E. Scuseria, M.A. Robb, J.R. Cheeseman, G. Scalmani, V. Barone, B. Mennucci, G.A. Petersson, H. Nakatsuji, M. Caricato, X. Li, H.P. Hratchian, A.F. Izmaylov, J. Bloino, G. Zheng, J.L. Sonnenberg, M. Hada, M. Ehara, K. Toyota, R. Cammi, C. Pomelli, J.W. Ochterski, R.L. Martin, K. Morokuma, V.G. Zakrzewski, G.A. Voth, P. Salvador, J.J. Dannenberg, S. Dapprich, A.D. Daniels, Ö. Farkas, J.B. Foresman, J.V. Ortiz, J. Cioslowski, D.J. Fox, Gaussian 09, Gaussian, Inc., Wallingford, CT, USA, 2009.
- [40] R. Dennington, T. Keith, J. Millam, GaussView, Version 5, 2009.
- [41] R. Cammi, J. Tomasi, Remarks on the use of the apparent surface charges (ASC) methods in solvation problems: Iterative versus matrix-inversion procedures and the renormalization of the apparent charges, *J. Comput. Chem.*, 16 (1995) 1449-1458. <https://doi.org/10.1002/jcc.540161202>.
- [42] B. Mennucci, E. Cancès, J. Tomasi, Evaluation of Solvent Effects in Isotropic and Anisotropic Dielectrics and in Ionic Solutions with a Unified Integral Equation Method: Theoretical Bases, Computational Implementation, and Numerical Applications, *J. Phys. Chem. B*, 101 (1997) 10506-10517. <https://doi.org/10.1021/jp971959k>.
- [43] E. Cancès, B. Mennucci, J. Tomasi, A new integral equation formalism for the polarizable continuum model: Theoretical background and applications to isotropic and anisotropic dielectrics, *J. Chem. Phys.*, 107 (1997) 3032-3041. <https://doi.org/10.1063/1.474659>.
- [44] S. Kaya, H. Gokce, T. Arslan, G. Alpaslan, Synthesis, spectroscopic characterization, DFT computations, nonlinear optical profile and molecular docking study of a novel chalcone derivative, *J. Mol. Struct.*, 1202 (2020) 11. <https://doi.org/10.1016/j.molstruc.2019.127270>.
- [45] M.H. Jamroz, Vibrational energy distribution analysis (VEDA): Scopes and limitations, *Spectrochimica Acta Part a-Molecular and Biomolecular Spectroscopy*, 114 (2013) 220-230. <https://doi.org/10.1016/j.saa.2013.05.096>.
- [46] R. McWeeny, Perturbation Theory for the Fock-Dirac Density Matrix, *Phys. Rev.*, 126 (1962) 1028-1034. <http://dx.doi.org/10.1103/PhysRev.126.1028>.

- [47] R. Ditchfield, Self-consistent perturbation-theory of diamagnetism .1. Gauge-invariant LCAO method for NMR chemical-shifts, *Mol. Phys.*, 27 (1974) 789-807. <https://doi.org/10.1080/00268977400100711>.
- [48] K. Wolinski, J.F. Hinton, P. Pulay, Efficient implementation of the gauge-independent atomic orbital method for NMR chemical shift calculations, *JACS*, 112 (1990) 8251-8260. <http://dx.doi.org/10.1021/ja00179a005>.
- [49] R.G. Pearson, Hard and soft acids and bases, *JACS*, 85 (1963) 3533-&. <http://dx.doi.org/10.1021/ja00905a001>.
- [50] T. Koopmans, Über die Zuordnung von Wellenfunktionen und Eigenwerten zu den Einzelnen Elektronen Eines Atoms, *Phy*, 1 (1934) 104-113. [https://doi.org/10.1016/S0031-8914\(34\)90011-2](https://doi.org/10.1016/S0031-8914(34)90011-2).
- [51] H. Chermette, Chemical reactivity indexes in density functional theory, *J. Comput. Chem.*, 20 (1999) 129-154. [http://dx.doi.org/10.1002/\(SICI\)1096-987X\(19990115\)20:1<129::AID-JCC13>3.0.CO;2-A](http://dx.doi.org/10.1002/(SICI)1096-987X(19990115)20:1<129::AID-JCC13>3.0.CO;2-A).
- [52] R.P. Iczkowski, J.L. Margrave, Electronegativity, *JACS*, 83 (1961) 3547-3551. <https://doi.org/10.1021/ja01478a001>.
- [53] R.G. Pearson, Recent advances in the concept of hard and soft acids and bases, *J. Chem. Educ.*, 64 (1987) 561. <https://doi.org/10.1021/ed064p561>.
- [54] J.F. Janak, Proof that  $\partial E/\partial n_i = \epsilon_i$  in density-functional theory, *PhRvB*, 18 (1978) 7165-7168. <https://doi.org/10.1103/PhysRevB.18.7165>.
- [55] L. Von Szentpály, Studies on electronegativity equalization: Part 1. Consistent diatomic partial charges, *J. Mol. Struct.-THEOCHEM*, 233 (1991) 71-81. [https://doi.org/10.1016/0166-1280\(91\)85055-C](https://doi.org/10.1016/0166-1280(91)85055-C).
- [56] W.T. Yang, R.G. Parr, Hardness, softness, and the Fukui function in the electronic theory of metals and catalysis, *Proc. Natl. Acad. Sci. U.S.A.*, 82 (1985) 6723-6726. <https://doi.org/10.1073/pnas.82.20.6723>.
- [57] R.G. Parr, L.v. Szentpály, S. Liu, Electrophilicity Index, *JACS*, 121 (1999) 1922-1924. <https://doi.org/10.1021/ja983494x>.
- [58] P.K. Chattaraj, S. Giri, S. Duley, Update 2 of: Electrophilicity Index, *Chem. Rev.*, 111 (2011) PR43-PR75. <https://doi.org/10.1021/cr100149p>.
- [59] Chemcraft - graphical software for visualization of quantum chemistry computations, 2006.
- [60] K. Fukui, Role of frontier orbitals in chemical-reactions, *Science*, 218 (1982) 747-754. <https://doi.org/10.1126/science.218.4574.747>.
- [61] I.B. Obot, D.D. Macdonald, Z.M. Gasem, Density functional theory (DFT) as a powerful tool for designing new organic corrosion inhibitors. Part 1: An overview, *Corros. Sci.*, 99 (2015) 1-30. <https://doi.org/10.1016/j.corsci.2015.01.037>.
- [62] C. Morell, A. Grand, A. Toro-Labbé, New Dual Descriptor for Chemical Reactivity, *J. Phys. Chem. A*, 109 (2005) 205-212. <https://doi.org/10.1021/jp046577a>.
- [63] J. Padmanabhan, R. Parthasarathi, M. Elango, V. Subramanian, B.S. Krishnamoorthy, S. Gutierrez-Oliva, A. Toro-Labbé, D.R. Roy, P.K. Chattaraj, Multiphlic Descriptor for Chemical Reactivity and Selectivity, *J. Phys. Chem. A*, 111 (2007) 9130-9138. <https://doi.org/10.1021/jp0718909>.

- [64] T. Lu, F. Chen, Multiwfn: A multifunctional wavefunction analyzer, *J. Comput. Chem.*, 33 (2012) 580-592. <https://doi.org/10.1002/jcc.22885>.
- [65] K. Momma, F. Izumi, VESTA 3 for three-dimensional visualization of crystal, volumetric and morphology data, *J. Appl. Crystallogr.*, 44 (2011) 1272-1276. <https://doi.org/10.1107/s0021889811038970>.
- [66] A.-R. Allouche, Gabedit—A graphical user interface for computational chemistry softwares, *J. Comput. Chem.*, 32 (2011) 174-182. <https://doi.org/10.1002/jcc.21600>.
- [67] F.L. Hirshfeld, Bonded-atom fragments for describing molecular charge densities, *Theor. Chim. Acta*, 44 (1977) 129-138. <https://doi.org/10.1007/BF00549096>.
- [68] N.M. O'Boyle, A.L. Tenderholt, K.M. Langner, cclib: A library for package-independent computational chemistry algorithms, *J. Comput. Chem.*, 29 (2008) 839-845. <http://dx.doi.org/10.1002/jcc.20823>.
- [69] T. Yanai, D.P. Tew, N.C. Handy, A new hybrid exchange-correlation functional using the Coulomb-attenuating method (CAM-B3LYP), *Chem. Phys. Lett.*, 393 (2004) 51-57. <https://doi.org/10.1016/j.cplett.2004.06.011>.
- [70] A.L. Alves Borges Leal, A.J.T. Machado, C.F. Bezerra, C.E. Serra Inácio, J.E. Rocha, D.L. Sales, T.S. de Freitas, W. de Oliveira Almeida, W.d. Amaral, L. Everson da Silva, A.P. Ferriani, B.H.L. de Noronha Sales Maia, M.F. Bezerra Morais-Braga, H.M. Barreto, H.D.M. Coutinho, Chemical identification and antimicrobial potential of essential oil of *Piper rivinoides kunth* (BETIS-WHITE), *Food Chem. Toxicol.*, 131 (2019) 110559. <https://doi.org/10.1016/j.fct.2019.06.006>.
- [71] M.M. Oliveira, H.S. Santos, H.D.M. Coutinho, P.N. Bandeira, P.T. da Silva, T.S. Freitas, J.E. Rocha, J.C. Xavier, F.F. Campina, Batista de Carvalho, C.E.S. Nogueira, Spectroscopic characterization and efflux pump modulation of a thiophene curcumin derivative, *J. Mol. Struct.*, 1215 (2020) 128291. <https://doi.org/10.1016/j.molstruc.2020.128291>.
- [72] A. Waterhouse, M. Bertoni, S. Bienert, G. Studer, G. Tauriello, R. Gumienny, F.T. Heer, T.A.P. de Beer, C. Rempfer, L. Bordoli, R. Lepore, T. Schwede, SWISS-MODEL: homology modelling of protein structures and complexes, *Nucleic Acids Res.*, 46 (2018) W296-W303. <https://doi.org/10.1093/nar/gky427>.
- [73] O. Trott, A.J. Olson, AutoDock Vina: Improving the speed and accuracy of docking with a new scoring function, efficient optimization, and multithreading, *J. Comput. Chem.*, 31 (2010) 455-461. <https://doi.org/10.1002/jcc.21334>.
- [74] Marvin Sketch, V. 20.15, Calculation Module Developed by ChemAxon, 2020.
- [75] C.A. Lipinski, F. Lombardo, B.W. Dominy, P.J. Feeney, Experimental and computational approaches to estimate solubility and permeability in drug discovery and development settings, *Adv. Drug Del. Rev.*, 23 (1997) 3-25. [https://doi.org/10.1016/S0169-409X\(96\)00423-1](https://doi.org/10.1016/S0169-409X(96)00423-1).
- [76] A. Daina, O. Michielin, V. Zoete, SwissADME: a free web tool to evaluate pharmacokinetics, drug-likeness and medicinal chemistry friendliness of small molecules, *Sci. Rep.*, 7 (2017) 42717. <https://doi.org/10.1038/srep42717>.
- [77] S. Yee, In Vitro Permeability Across Caco-2 Cells (Colonic) Can Predict In Vivo (Small Intestinal) Absorption in Man—Fact or Myth, *Pharm. Res.*, 14 (1997) 763-766. <https://doi.org/10.1023/A:1012102522787>.
- [78] J. Kelder, P.D. Grootenhuis, D.M. Bayada, L.P. Delbressine, J.P. Ploemen, Polar molecular surface as a dominating determinant for oral absorption and brain penetration of drugs, *Pharm. Res.*, 16 (1999) 1514-1519. <https://doi.org/10.1023/a:1015040217741>.

- [79] V. Prachayasittikul, P. Mandi, S. Prachayasittikul, V. Prachayasittikul, C. Nantasenamat, Exploring the Chemical Space of P-Glycoprotein Interacting Compounds, *Mini Rev. Med. Chem.*, 17 (2017) 1332-1345. <https://doi.org/10.2174/1389557516666160121120344>.
- [80] B. Bienfait, P. Ertl, JSME: a free molecule editor in JavaScript, *J. Cheminform.*, 5 (2013) 24. <https://doi.org/10.1186/1758-2946-5-24>.
- [81] R.C. Braga, V.M. Alves, M.F. Silva, E. Muratov, D. Fourches, A. Tropsha, C.H. Andrade, Tuning HERG out: antitarget QSAR models for drug development, *Curr. Top. Med. Chem.*, 14 (2014) 1399-1415. <https://doi.org/10.2174/1568026614666140506124442>.
- [82] B.E. KSOZ, R. ERTAN, Chemical and Structural Properties of Chalcones I, *Fabad J. Pharm. Sci.*, 36 (2011) 232-242.
- [83] I.K.C. Lima, F.D. de Sousa, A.J.d.M. Bento, B.G. Cruz, P.T. da Silva, P.N. Bandeira, H.S. dos Santos, G.D. Saraiva, A.C.H. Barreto, P.d.T.C. Freire, A.M.R. Teixeira, Structural and spectroscopic investigation of the chalcones (E)-1-(4-aminophenyl)-3-(4'-ethoxyphenyl)-prop-2-en-1-one and (E)-1-(aminophenyl)-3-(4'-methoxyphenyl)-prop-2-en-1-one, *Vib. Spectrosc.*, 110 (2020) 103118. <https://doi.org/10.1016/j.vibspec.2020.103118>.
- [84] Y. Xue, X. Gong, The conformational, electronic and spectral properties of chalcones: A density functional theory study, *J. Mol. Struct.-THEOCHEM*, 901 (2009) 226-231. <https://doi.org/10.1016/j.theochem.2009.01.034>.
- [85] C. Parlak, P. Ramasami, Theoretical and experimental study of infrared spectral data of 2-bromo-4-chlorobenzaldehyde, *SN Applied Sciences*, 2 (2020) 1148. <http://dx.doi.org/10.1007/s42452-020-2935-5>.
- [86] E. Echegaray, C. Cárdenas, S. Rabi, N. Rabi, S. Lee, F.H. Zadeh, A. Toro-Labbe, J.S.M. Anderson, P.W. Ayers, In pursuit of negative Fukui functions: examples where the highest occupied molecular orbital fails to dominate the chemical reactivity, *J. Mol. Model.*, 19 (2013) 2779-2783. <https://doi.org/10.1007/s00894-012-1637-3>.
- [87] E. Echegaray, S. Rabi, C. Cárdenas, F.H. Zadeh, N. Rabi, S. Lee, J.S.M. Anderson, A. Toro-Labbe, P.W. Ayers, In pursuit of negative Fukui functions: molecules with very small band gaps, *J. Mol. Model.*, 20 (2014) 2162. <https://doi.org/10.1007/s00894-014-2162-3>.
- [88] A. Wintner, On the Counting of Nodal Curves and Surfaces, *J. Chem. Phys.*, 16 (1948) 405-406. <https://doi.org/10.1063/1.1746903>.
- [89] U.M. Hanumegowda, G. Wenke, A. Regueiro-Ren, R. Yordanova, J.P. Corradi, S.P. Adams, Phospholipidosis as a Function of Basicity, Lipophilicity, and Volume of Distribution of Compounds, *Chem. Res. Toxicol.*, 23 (2010) 749-755. <https://doi.org/10.1021/tx9003825>.
- [90] P. Ertl, B. Rohde, P. Selzer, Fast Calculation of Molecular Polar Surface Area as a Sum of Fragment-Based Contributions and Its Application to the Prediction of Drug Transport Properties, *J. Med. Chem.*, 43 (2000) 3714-3717. <https://doi.org/10.1021/jm000942e>.
- [91] D.F. Veber, S.R. Johnson, H.Y. Cheng, B.R. Smith, K.W. Ward, K.D. Kopple, Molecular properties that influence the oral bioavailability of drug candidates, *J. Med. Chem.*, 45 (2002) 2615-2623. <https://doi.org/10.1021/jm020017n>.
- [92] T. Fichert, M. Yazdanian, J.R. Proudfoot, A structure-Permeability study of small drug-like molecules, *Biorg. Med. Chem. Lett.*, 13 (2003) 719-722. [https://doi.org/10.1016/S0960-894X\(02\)01035-1](https://doi.org/10.1016/S0960-894X(02)01035-1).
- [93] W.M. Pardridge, Blood-brain barrier genomics and the use of endogenous transporters to cause drug penetration into the brain, *Curr. Opin. Drug Discov. Devel.*, 6 (2003) 683-691.

- [94] M. Olivo, R. Bhuvanewari, S.S. Lucky, N. Dendukuri, P. Soo-Ping Thong, Targeted Therapy of Cancer Using Photodynamic Therapy in Combination with Multi-faceted Anti-Tumor Modalities, *Pharmaceuticals (Basel)*, 3 (2010) 1507-1529. <https://doi.org/10.3390/ph3051507>.
- [95] D. D'Eliseo, F. Velotti, Omega-3 Fatty Acids and Cancer Cell Cytotoxicity: Implications for Multi-Targeted Cancer Therapy, *J. Clin. Med.*, 5 (2016). <https://doi.org/10.3390/jcm5020015>.
- [96] N. Takebe, P.J. Harris, R.Q. Warren, S.P. Ivy, Targeting cancer stem cells by inhibiting Wnt, Notch, and Hedgehog pathways, *Nat. Rev. Clin. Oncol.*, 8 (2011) 97-106. <https://doi.org/10.1038/nrclinonc.2010.196>.
- [97] B.N. Ames, K. Hooper, Does carcinogenic potency correlate with mutagenic potency in the Ames assay?, *Nature*, 274 (1978) 19-20. <https://doi.org/10.1038/274019a0>.
- [98] J.M. Kratz, U. Grienke, O. Scheel, S.A. Mann, J.M. Rollinger, Natural products modulating the hERG channel: heartaches and hope, *Nat. Prod. Rep.*, 34 (2017) 957-980. <https://doi.org/10.1039/c7np00014f>.
- [99] N. Chiesa, B. Rosati, A. Arcangeli, M. Olivotto, E. Wanke, A novel role for HERG K<sup>+</sup> channels: spike-frequency adaptation, *J. Physiol.*, 501 ( Pt 2) (1997) 313-318. <https://doi.org/10.1111/j.1469-7793.1997.313bn.x>.
- [100] J.L. Overholt, E. Ficker, T. Yang, H. Shams, G.R. Bright, N.R. Prabhakar, HERG-Like potassium current regulates the resting membrane potential in glomus cells of the rabbit carotid body, *J. Neurophysiol.*, 83 (2000) 1150-1157. <https://doi.org/10.1152/jn.2000.83.3.1150>.
- [101] M.C. Sanguinetti, M. Tristani-Firouzi, hERG potassium channels and cardiac arrhythmia, *Nature*, 440 (2006) 463-469. <https://doi.org/10.1038/nature04710>.
- [102] A. Arcangeli, Expression and role of hERG channels in cancer cells, *Novartis Found. Symp.*, 266 (2005) 225-232; discussion 232-224.
- [103] B. Meunier, S.P. de Visser, S. Shaik, Mechanism of Oxidation Reactions Catalyzed by Cytochrome P450 Enzymes, *Chem. Rev.*, 104 (2004) 3947-3980. <https://doi.org/10.1021/cr020443g>.
- [104] D. Korolev, K.V. Balakin, Y. Nikolsky, E. Kirillov, Y.A. Ivanenkov, N.P. Savchuk, A.A. Ivashchenko, T. Nikolskaya, Modeling of Human Cytochrome P450-Mediated Drug Metabolism Using Unsupervised Machine Learning Approach, *J. Med. Chem.*, 46 (2003) 3631-3643. <https://doi.org/10.1021/jm030102a>.
- [105] L.M. Rezende-Junior, L.M. de Sousa Andrade, A.L. Alves Borges Leal, A.B. de Souza Mesquita, A.L. Portela de Araujo dos Santos, J.d.S. Lima Neto, J.P. Siqueira-Junior, C.E. Sampaio Nogueira, G.W. Kaatz, H.D. Melo Coutinho, N. Martins, C.Q. Rocha, H.M. Barreto, Chalcones Isolated from Arrabidaea brachypoda Flowers as Inhibitors of NorA and MepA Multidrug Efflux pumps of *Staphylococcus aureus*, *Antibiotics-Basel*, 9 (2020). <https://doi.org/10.3390/antibiotics9060351>.

**Article 3** – Structural characterization, electronic properties, and anxiolytic-like effect in adult zebrafish (*Danio rerio*) of cinnamaldehyde chalcone.2020)

Authors: da Cunha Xavier, J., Almeida-Neto, F. W. Q., da Silva, P. T., Marinho, E. S., Ferreira, M. K. A., Magalhães, F. E. A., ... & dos Santos, H. S. (

Journal / link / Qualis *Journal of Molecular Structure* /

<https://doi.org/10.1016/j.molstruc.2020.128954> / Biological Sciences II, Qualis

B2. IF = 3.841

Situation: Published

### **Resumo**

Zebrafish é um animal modelo que é usado para estudos neurocomportamentais. É um excelente organismo modelo para estudos farmacológicos e/ou pesquisa de segurança em um estágio inicial de desenvolvimento de medicamentos. Neste trabalho, a chalcona (2E, 4E)-1-(2-hidroxi-3,4,6-trimetoxifenil)-5-fenilpenta-2,4-dien-1-ona, foi sintetizada pela condensação de Claisen-Schmidt a partir de dois produtos naturais: 2-hidroxi-3,4,6-trimetoxiacetofenona e cinamaldeído. A estrutura molecular deste composto foi confirmada por métodos espectroscópicos como NMR, infravermelho, UV-vis e cálculos químicos quânticos. Além disso, foi avaliado o efeito ansiolítico da chalcona cinamaldeído em peixe-zebra adulto (*Danio*



erio). Os resultados mostraram que a chalcona causou uma redução de aproximadamente 80% na atividade locomotora do peixe-zebra e induziu a permanência máxima do peixe-zebra na zona clara (61,16%) na dose de 0,5 mg kg<sup>-1</sup>. Os dados sugerem que a chalcona cinnamaldeído tem ação ansiolítica.

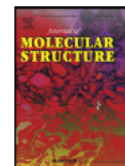
Journal of Molecular Structure 1222 (2020) 128954



Contents lists available at ScienceDirect

Journal of Molecular Structure

journal homepage: [www.elsevier.com/locate/molstr](http://www.elsevier.com/locate/molstr)



## Structural characterization, electronic properties, and anxiolytic-like effect in adult zebrafish (*Danio rerio*) of cinnamaldehyde chalcone



Jayze da Cunha Xavier<sup>a</sup>, Francisco Wagner Queiroz Almeida-Neto<sup>b</sup>, Priscila Teixeira da Silva<sup>a</sup>, Emmanuel Silva Marinho<sup>c</sup>, Maria Kueirislene Amâncio Ferreira<sup>d</sup>, Francisco Ernani Alves Magalhães<sup>d,g</sup>, Carlos Emídio Sampaio Nogueira<sup>a,e</sup>, Paulo Nogueira Bandeira<sup>f</sup>, Jane Eire Silva Alencar de Menezes<sup>d</sup>, Alexandre Magno Rodrigues Teixeira<sup>a,e</sup>, Hércio Silva dos Santos<sup>a,d,f,\*</sup>

## CHAPTER 7- Structural characterization, electronic properties, and anxiolytic-like effect in adult zebrafish (*Danio rerio*) of cinnamaldehyde chalcone

Jayze da Cunha Xavier<sup>a</sup>, Francisco Wagner Queiroz Almeida-Neto<sup>b</sup>, Priscila Teixeira da Silva<sup>a</sup>, Emmanuel Silva Marinho<sup>c</sup>, Maria Kueirislene Amâncio Ferreira<sup>d</sup>, Francisco Ernani Alves Magalhães<sup>d,g</sup>, Carlos Emídio Sampaio Nogueira<sup>a,e</sup>, Paulo Nogueira Bandeira<sup>f</sup>, Jane Eire Silva Alencar de Menezes<sup>d</sup>, Alexandre Magno Rodrigues Teixeira<sup>a</sup>, Hércio Silva dos Santos<sup>a,d,f,2\*</sup>

<sup>a</sup> Department of Biological Chemistry, Regional University of Cariri, Crato-CE, Brazil, <sup>b</sup>Group of Theoretical Chemistry, Department of Analytical Chemistry and Physical Chemistry, Federal University of Ceará, Fortaleza, CE, Brazil, <sup>c</sup>Group of Theoretical Chemistry and Electrochemistry, State University of Ceará, Campus FAFIDAM, Limoeiro do Norte, CE, Brazil. <sup>d</sup>Science and Technology Center, Postgraduate Program in Natural Sciences, State University of Ceará, Fortaleza, CE, Brazil, <sup>e</sup>Department of Physics, Regional University of Cariri, Juazeiro do Norte-CE, Brazil. <sup>f</sup>Center for Exact Sciences and Technology - Chemistry Course, Vale do Acaraú University, Sobral, CE, Brazil, <sup>g</sup>State

## Abstract

Zebrafish is a model animal that is used for neurobehavioral studies. It is an excellent model organism for pharmacological studies and/or safety research at an early stage of drug development. In this work, the chalcone (2*E*, 4*E*)-1-(2-hydroxy-3,4,6-trimethoxyphenyl)-5-phenylpenta-2,4-dien-1-one, was synthesized by the Claisen-Schmidt condensation from two natural products: 2-hydroxy-3,4,6-trimethoxyacetophenone and cinnamaldehyde. The molecular structure of this compound was confirmed by spectroscopic methods such as NMR, Infrared, UV-vis, and quantum chemical calculations. In addition, the anxiolytic-like effect of the cinnamaldehyde chalcone in adult zebrafish (*Danio rerio*) was evaluated. The results showed that chalcone caused an approximately 80% reduction in zebrafish locomotor activity and induced maximum permanence of zebrafish in the clear zone (61.16%) at a dose of 0.5 mg kg<sup>-1</sup>. The data suggest that the cinnamaldehyde chalcone has anxiolytic activity.

**Keywords:** NMR, IR, Fukui functions, anxiolytic-like effect, zebrafish, cinnamaldehyde chalcone

## 1. Introduction

Zebrafish (*Danio rerio*) (Figure 1) are used in behavioral neuroscience, including research involving the brain and psychopharmacology [1]. This fish is a suitable model to study the central nervous system because its genotype has 70% homology with mammalian neurotransmitter receptors [2]. Because of the side effects associated with allopathic drugs, there is a growing interest in the development of alternative therapies to treat psychiatric disorders [3]. Natural products were selected over the years with the needed efficiency and selectivity to reach cellular targets, and would be a molecular inspiration for medicinal chemists or the source of drugs with high complex chemical structures. Previous studies demonstrated the anxiolytic action of several phytochemical groups such as polyphenols and chalcones [4–6].

The genus *Croton*, which belongs to the Euphorbiaceae family, is the second largest genus of a large and diverse group of plants rich in tropical species. Around 712 species of *Croton* are recognized [7] [8], and they generally have important pharmacological properties, which were already reported in literature [9]. The substance 2-hydroxy-3,4,6-trimethoxyacetophenone (Figure 1b) was isolated from *Croton anisodontus* (Figure 1a) [10]. This structure can basically be used to synthesize new chalcones from reactions between acetophenones and aromatic aldehydes.

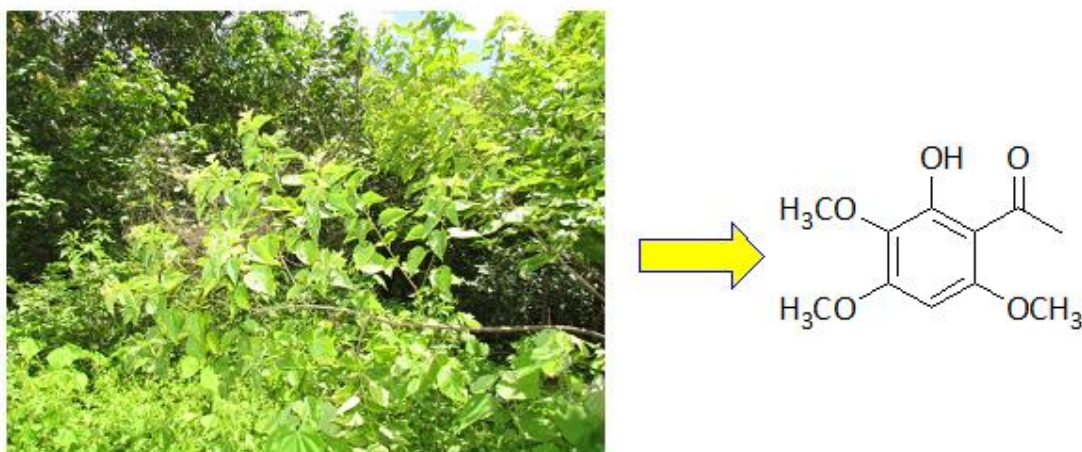


**Fig. 1.** Aerial parts of *C. Anisodontus* (a) 2-hydroxy-3,4,6-trimethoxyacetophenone (b)

Chalcones have at least two aromatic rings linked together by a three-carbon unsaturated  $\alpha,\beta$ -bond (Figure 2). Natural chalcones are precursors of flavonoids and isoflavonoids [11]. They can also be obtained by organic synthesis. This compound class attracted much interest because of the wide spectrum of pharmacological activities that they represent, including antimicrobial [12], antioxidant [13], antinociceptive [14], antiparasitic [15], antitumor [16], and antiproliferative activities [17].

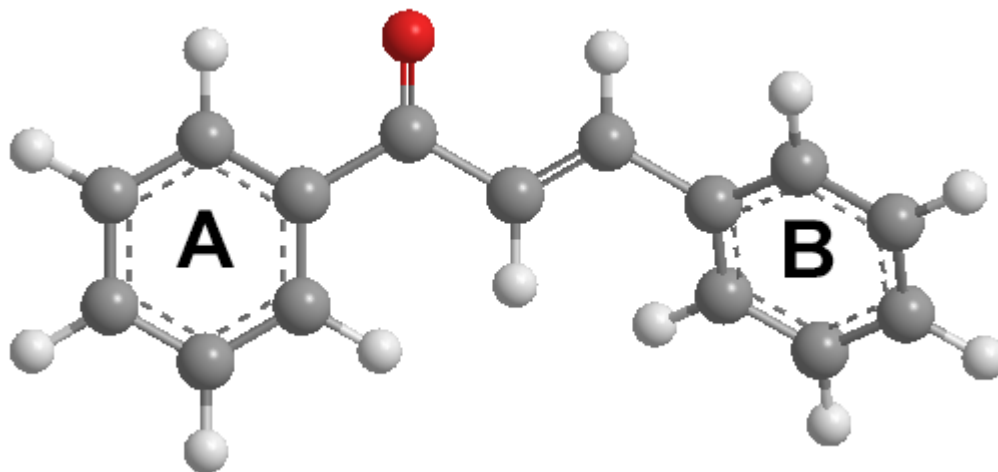


**Fig. 2.** Fundamental structure of chalcone

To obtain a complete structural characterization of the chalcone, quantum chemical calculations were carried out using density functional theory (DFT) with B3LYP/6-311++G(d,p) level of theory to compute the geometry optimization, and infrared, UV-vis, and <sup>1</sup>H and <sup>13</sup>C NMR spectra compared to experimental results generated by the same techniques. Also, the electronic properties with respect to the frontier molecular orbitals, the quantum reactivity descriptors, the Fukui functions (electronic and condensed), and the molecular

electrostatic potential were applied to characterize the reactive electrophilic and nucleophilic sites.

In this work, the chalcone (*2E, 4E*)-1-(2-hydroxy-3,4,6-trimethoxyphenyl)-5-phenylpenta-2,4-dien-1-one was synthesized by the Claisen-Schmidt condensation using the natural products 2-hydroxy-3,4,6-trimethoxyacetophenone and cinnamaldehyde. In addition, the anxiolytic-like effect of the prepared cinnamaldehyde chalcone was evaluated using adult zebrafish (*Danio rerio*).

## 2. Material and methods

### 2.1 Spectroscopic methods: NMR, FTIR, UV-vis and MS-EI

The chemical reagents were purchased from Sigma-Aldrich.  $^1\text{H}$  and  $^{13}\text{C}$  NMR spectra were obtained using a Bruker Spectrometer, model Avance DPX-500, operating at a frequency of 500 MHz for hydrogen, and 125 MHz for carbon, respectively. The spectra were measured in  $\text{CDCl}_3$ , and chemical shifts are reported as  $\delta$  values in parts per million (ppm) relative to  $\text{CDCl}_3$ . The attenuated total reflectance Fourier transform infrared spectroscopy (ATR-FTIR) was performed using a Bruker vacuum infrared spectrometer VERTEX 70V. The measurements were recorded at room temperature in the range 400 to 4000  $\text{cm}^{-1}$ , with a resolution of 2  $\text{cm}^{-1}$  and accumulating 60 scans per spectrum. The UV-vis absorption spectrum was obtained with a GENESYS<sup>TM</sup> 10S spectrophotometer in the wavelength range from 190 to 800 nm. The samples were prepared at a concentration of 0.1  $\text{mmol L}^{-1}$  using ethanol as a solvent to perform the absorption. All absorption measurements were carried out at room temperature in quartz cells with 1 cm optical path. The GCMS analyses were conducted on an Agilent instrument model GC-7890B/MSD-5977A with a quadrupole mass analyzer of electron impact at 70 eV and a RTX5-MS (30 m  $\times$  0.25 mm  $\times$  0.25  $\mu\text{m}$ ) capillary column. The mass spectrometer was adjusted for acquisition in the range of 40–660  $m/z$ . The injector temperature was kept constant at 230  $^\circ\text{C}$  with a helium flow rate of 1.00  $\text{mL min}^{-1}$  (carrier gas). The temperatures of the source and transfer lines were set at 230  $^\circ\text{C}$  and 280  $^\circ\text{C}$ , respectively. The following program was used in the chromatographic oven: initial temperature of 40  $^\circ\text{C}$ , with a heating ramp from 3  $^\circ\text{C min}^{-1}$  to 280  $^\circ\text{C}$  for 5 min at the end of the run.

### 2.2 Adult zebrafish (*D. rerio*) (aZF)

Wild adult zebrafish (60 to 90 days old;  $0.4 \pm 0.1$  g,  $3.5 \pm 0.5$  cm) of both genders were obtained from a commercial supplier (Fortaleza, CE). Groups of animals ( $n = 72$ ) were acclimatized for 24 h at 25  $^\circ\text{C}$  and pH 7.0 in a 10 L glass tank (30  $\times$  15  $\times$  20 cm) containing

dechlorinated tap water (ProtecPlus<sup>®</sup>), a submersible filter, and an air pump, under a circadian cycle of 14:10 h (light/dark). Animals received *ad libitum* feed 24 h prior to the experiments. After the experiments, the animals were euthanized by immersion in ice water (2–4 °C) for 10 min until the loss of opercular movements occurred. All experimental procedures were approved by the Animal Research Ethics Committee of the State University of Ceará (CEUA-UECE # 7210149/2016).

### 2.3 Evaluation of locomotor activity

The open field test was used to evaluate whether there was alteration of the motor coordination. The animals aZF (n=6/group) were treated intraperitoneally (*i.p.*) with chalcone (0.1, 0.5 and 1.0 mg kg<sup>-1</sup>; 20 µL; 6 fishes for each concentration), vehicle (DMSO 3%; 20 µL; 6 fishes) or diazepam (DZP 1mg mL<sup>-1</sup>; 20 µL; 6 fishes). Thirty minutes after the treatments, the animals were added to Petri dishes containing the same water of the aquarium, marked with four quadrants and the locomotor activity was analyzed by counting the number of line crossings, during 5 minutes. Animals (6 fishes) that did not receive treatments (Naïve) were considered as baseline (100% locomotor activity) [19].

### 2.4 Light & dark test

The anxiolytic-like effect of chalcone was investigated through the light & dark test [19]. The animals aZF (n=6/group) were treated intraperitoneally with chalcone (0.1, 0.5 and 1.0 mg kg<sup>-1</sup>; 20 µL; 6 fishes for each concentration), vehicle (control, 3% DMSO, 20 µL; 6 fishes) or diazepam (Dzp; 1mg mL<sup>-1</sup>; 20 µL; 6 fishes). An untreated group (Naïve; 6 fishes) was included. The animals were added to the light zone of the glass aquarium (30 × 15 × 20 cm) 30 min after the treatments, which was divided into light and dark zones, and contained pre-treated water with anti-chlorine. The anxiolytic-like effect was characterized by the presence of the animals in the light zone, during 5 min of analysis.

### 2.5 Chalcone synthesis

The compounds 2-hydroxy-3,4,6 trimethoxyacetophenone (2 mmol) and cinnamaldehyde (2 mmol) were placed in a volumetric flask (25 mL). Then 5 mL of ethanolic NaOH (50%) solution was added and mixed with stirring for 48 h at room temperature. The progress of the reaction was checked by TLC (n-hexane: ethylacetate, 2:1). After 48 h the reaction mixture was neutralized with dilute HCl (10%) and ice water added. The product was

obtained as a yellow solid (yield: 35.4%, m.p. 144.8–145.2 °C) filtered under reduced pressure, washed with cold water, and recrystallized from ethanol (Scheme 1) [11].

## 2.6 Quantum chemical calculations

The quantum chemical calculations were used extensively to support the experimental data during the structural characterization of a newly synthesized molecule. Therefore, the chalcone was geometrically optimized using the density functional theory (DFT) method with the exchange-correlation functional B3LYP [20,21] at the 6-311++G(d,p) basis set. The calculations were carried out using the Gaussian 09 [22] software and the Gauss View 5 [23] to draw the input molecule. The cinnamaldehyde molecule was optimized to obtain the global minimum structure which allows the calculation of the structural and electronic properties. The optimization was done with chloroform as an implicit solvent using the IEF-PCM solvation model [24–26] available in Gaussian 09. Next, the fundamental vibrational modes were computed at the same level of theory together with the thermodynamic properties at 298.15 K and 1 atm of pressure. The absence of negative frequencies implies that the molecule achieves the global minimum of energy and the properties calculated are related to the ground state structure. The infrared spectrum was obtained from this calculation and the theoretical wavenumbers were scaled by 0.983 for below 1700  $\text{cm}^{-1}$  and by 0.958 for above 1700  $\text{cm}^{-1}$  [27]. The theoretical assignments of the highlighted band from the experimental infrared spectrum were done using the potential energy distribution (PED) with the VEDA [28] software and only the PED  $\geq 10\%$  were considered. Then, the  $^1\text{H}$  and  $^{13}\text{C}$  NMR spectra were calculated using the GIAO method [29 – 32] available in Gaussian 09 to obtain the theoretical isotropic shielding for the carbon ( $\sigma_C$ ) and hydrogen ( $\sigma_H$ ) atoms. Tetramethylsilane was used as a reference compound to calculate the theoretical chemical shifts as follows:  $\delta_C = \sigma_{C(TMS)} - \sigma_C$  and  $\delta_H = \sigma_{H(TMS)} - \sigma_H$ . The frontier molecular orbitals (FMO) were calculated from the optimization calculation to understand the electronic density distribution over the entire molecule and the energy values of those molecular orbitals were used to compute the global quantum reactivity descriptors: the energy gap ( $\Delta E_{GAP}$ , equation 1) [33], the ionization potential (I, equation 2) [34], the electron affinity (A, equation 3) [34], the electronegativity ( $\chi$ , equation 4) [35,36], the global hardness ( $\eta$ , equation 5) [37–39], the global softness (S, equation 6) [40], the electrophilicity index ( $\omega$ , equation 7) [41], and the nucleophilicity index ( $\varepsilon$ , equation 8) [42]. The trial version of the ChemCraft [43] software was used to render the frontier molecular orbitals.

$$\Delta E_{GAP} = E_{LUMO} - E_{HOMO} \quad (1)$$

$$I = -E_{HOMO} \quad (2)$$

$$A = -E_{LUMO} \quad (3)$$

$$\chi = \frac{I + A}{2} \quad (4)$$

$$\eta = \frac{I - A}{2} \quad (5)$$

$$S = \frac{1}{\eta} \quad (6)$$

$$\omega = \frac{\chi^2}{2\eta} \quad (7)$$

$$\varepsilon = \frac{1}{\omega} \quad (8)$$

To complete the understanding of the reactivity of cinnamaldehyde chalcone, the following Fukui functions are applied: Electronic [44] (equations 9 – 12) and condensed [45] (equations 13 – 15) to the nucleophilic ( $f^+$  and  $f_k^+$ ), electrophilic ( $f^-$  and  $f_k^-$ ), and radical ( $f^-$  and  $f_k^0$ ) attack; and the local quantum descriptors: the dual descriptor [46] ( $\Delta f$ , equation 16) and the multiphilic index [47] ( $\Delta\omega$ , equation 17) to characterize the nucleophilic and electrophilic sites of the molecule. The electronic Fukui functions were obtained using the Multiwfn [48] software and the isosurfaces were rendered using the VESTA [49] software. The molecular electrostatic potential (MEP) was computed to complete the local analysis of the chemical reactivity of the chalcone. The Gabedit program [50] was used to compute the MEP.

$$f = \left( \frac{\partial \rho(r)}{\partial N} \right)_{v(r)} \quad (9)$$

$$f^+ \approx v_{LUMO} \quad (10)$$

$$f^- \approx v_{HOMO} \quad (11)$$

$$f^0 \approx \frac{v_{LUMO} + v_{HOMO}}{2} \quad (12)$$

$$f_k^+ = q_k(N + 1) - q_k(N) \quad (13)$$

$$f_k^- = q_k(N) - q_k(N - 1) \quad (14)$$

$$f_k^0 = \frac{q_k(N + 1) - q_k(N - 1)}{2} \quad (15)$$

$$\Delta f = f_k^+ - f_k^- \quad (16)$$

$$\Delta\omega = \omega \cdot \Delta f \quad (17)$$

Where the  $q_k(N + 1)$ ,  $q_k(N)$ , and  $q_k(N - 1)$  are the Hirshfeld charge population on the atom  $k$  of the anionic, neutral, and cationic species.

**Table 1.**  $^1\text{H}$  and  $^{13}\text{C}$  NMR data of chalcone in  $\text{CDCl}_3$ . Experimental and theoretical chemical shifts in  $\delta_{\text{C}}$  and  $\delta_{\text{H}}$  are in ppm.

Chalcone				
C	$\delta_{\text{C}}$	$\delta_{\text{H}}$	$\delta_{\text{C}}(\text{calc})$	$\delta_{\text{H}}(\text{calc})$
1'	107.0		113.45	
2'	158.7		170.57	

3'	131.0		137.40	
4'	159.6		167.65	
5'	87.2	6.07 (s)	88.35	5.76
6'	158.5		167.42	
MeO-3'	60.9	3.84 (s)	62.28	3.85/3.93/3.50
MeO-4'	56.1	3.93 (s)	57.85	4.22/3.82/3.77
MeO-6'	56.2	3.95 (s)	57.20	4.36/3.83/3.80
C=O	193.2		198.84	
1	136.5		144.03	
2/6	127.7	7.51 (d, $J = 7.2$ Hz)	139.50/131.0	7.63/8.26
			5	
3/5	129.1	7.38 (d, $J = 7.1$ Hz)	136.34/135.8	7.65/7.70
			4	
4	131.0	7.44 (m)	137	7.59
C $_{\alpha}$	129.2	7.62 (d, $J = 14.6$ Hz)	136.65	8.02
C $_{\beta}$	143.5	7.64 (d, $J = 14.6$ Hz)	153.81	8.27
C $_{\alpha}$	127.0	7.40 (d, $J = 14.6$ Hz)	134.06	7.62
C $_{\beta}$	141.8	7.43 (d, $J = 14.6$ Hz)	152.20	7.39

The UV-vis spectrum was obtained using the time-dependent density functional theory (TD-DFT) method using the CAM-B3LYP/6-311++G(d,p) [51] computational level in chloroform as an implicit solvent. To assign the electronic transitions the GaussSum 3.0.1 [52] software was used to complete the structural characterization of the newly synthesized chalcone.

### 2.7 Statistical analysis

Results were expressed as mean  $\pm$  standard deviation of the mean for *in vitro* tests (n=3) as well as mean  $\pm$  standard error of the mean for *in vivo* tests (n=6/group). After confirming the distribution of normality and homogeneity of data, differences between the groups were submitted to analysis of variance (one-way ANOVA), followed by the Tukey test, using the software GraphPad Prism v. 7.0. The level of statistical significance was considered at 5% ( $p < 0.05$ ).

## 3. Results and discussion

### 3.1 Structural data

The  $^1\text{H}$  NMR spectrum of the synthesized chalcone showed three signals at  $\delta_{\text{H}}$  3.84 (MeO-3'), 3.93 (MeO-4'), and 3.95 ppm (MeO-6') relative to the hydrogens of the methoxy groups. The signals at  $\delta_{\text{H}}$  7.62 (H $_{\alpha}$ ) and 7.64 (H $_{\beta}$ ) ppm (d,  $J = 14.6$  Hz), and 7.40 (H $_{\alpha}$ ) and



7.43 (H $\beta$ ) ppm were attributed to doublets referring to  $\alpha,\beta$ -unsaturated hydrogens, whose coupling constant ( $J$ ) confirms the stereochemistry  $E$ . The singlet observed at  $\delta_{\text{H}}$  6.07 ppm refers to hydrogen attached to the carbon 5'-carbon of ring A. In addition, the signals at  $\delta_{\text{H}}$  7.51 (d,  $J = 7.2$  Hz, H2/6), 7.38 (d,  $J = 7.1$  Hz, H3/5), and 7.44 (m, H4) complete the assignment of hydrogen atoms relative to ring B.

The  $^{13}\text{C}$  NMR spectrum showed a peak at  $\delta_{\text{C}}$  193.3 ppm corresponding to an  $\alpha,\beta$ -unsaturated carbonyl. The ketone carbonyl absorbs at 203.8 ppm, however, the presence of  $\alpha,\beta$ -unsaturation causes displacement to the high field, and the probable cause is the delocalization of charge by the benzene ring or by the double bond that makes the carbonyl carbon less electron deficient. The olefinic carbons  $\alpha$  and  $\beta$  are observed at  $\delta_{\text{C}}$  122.5 (C $\alpha$ ) and 129.5 (C $\beta$ ). In addition, the signals at  $\delta_{\text{C}}$  140.2 (C-1'), 130.9 (C-2'/C6'), 112.7 (C3'/C5'), 153.9 (C-4') are the signals referring to the carbons present in ring A. The signals at  $\delta_{\text{C}}$  131.0 (C-4), 136.5 (C-1), 129.1 (C-3/5), and 153.9 (C-2/6) refer to ring B carbons. In addition, the signals at  $\delta_{\text{C}}$  60.9 (MeO-3'), 56.1 (MeO-4'), and 56.2 ppm (MeO-6') are attributed to the carbons of the methoxy groups (Table 1). After spectroscopic data analysis, the structure was confirmed to be chalcone ( $2E, 4E$ )-1-(2-hydroxy-3,4,6-trimethoxyphenyl)-5-phenylpenta-2,4-dien-1-one (C<sub>20</sub>H<sub>20</sub>O<sub>5</sub>, MS-EI  $m/z = 340$ ). C1' (140.20 ppm); C2'/C6' (130.86 ppm); C3'/C5' (112.77 ppm) C4' (153.89 ppm) C $\alpha$  (122.46 ppm); C $\beta$  (129.47 ppm) C1 (139.0 ppm); C2 (124.27 ppm); C3 (139.46 ppm); C4 (124.85 ppm); C5 (129.47 ppm); C6 (121.16 ppm); C7 (123.58 ppm); C8 (139.31 ppm)

To confirm the experimental spectroscopic data analysis, the molecule was optimized using the B3LYP/6-311++G(d,p) level of theory in chloroform as an implicit solvent. The optimized geometry is shown in Figure 3. The structure corresponds to the ground state of chalcone (global minimum energy) due to the absence of imaginary frequencies in the vibrational spectrum. The  $\alpha,\beta$ -unsaturated carbonyl group (O26-C25-C $\alpha$ 1-C $\beta$ 1-C $\alpha$ 2-C $\beta$ 2) exhibited a certain angulation: the O26-C25- C $\alpha$ 1-C $\beta$ 1 torsion angle is about 7.028° due to the possibility to create a hydrogen bond between the atoms O26 and H9, which are at a distance of about 1.55 Å, providing an extra stabilization to the entire structure. The olefin skeleton is in the same plane with a torsion angle (C $\alpha$ 1-C $\beta$ 1-C $\alpha$ 2-C $\beta$ 2) of about 0.685°, the torsion angle C25-C $\alpha$ 1-C $\beta$ 1-C $\alpha$ 2 is about 1.306°, and it is in the same plane as ring B with a torsion angle (C $\alpha$ 2-C $\beta$ 2-C1-C6) of 0.008°; the ring A shows a torsion angle of about (C6'-C1'-C25-C $\alpha$ 1) 14.211°, hence this ring A is not in the same plane delimited by the  $\alpha,\beta$ -unsaturated carbonyl. The calculated bond lengths at B3LYP/6-311++G(d,p) are shown in Table 2.

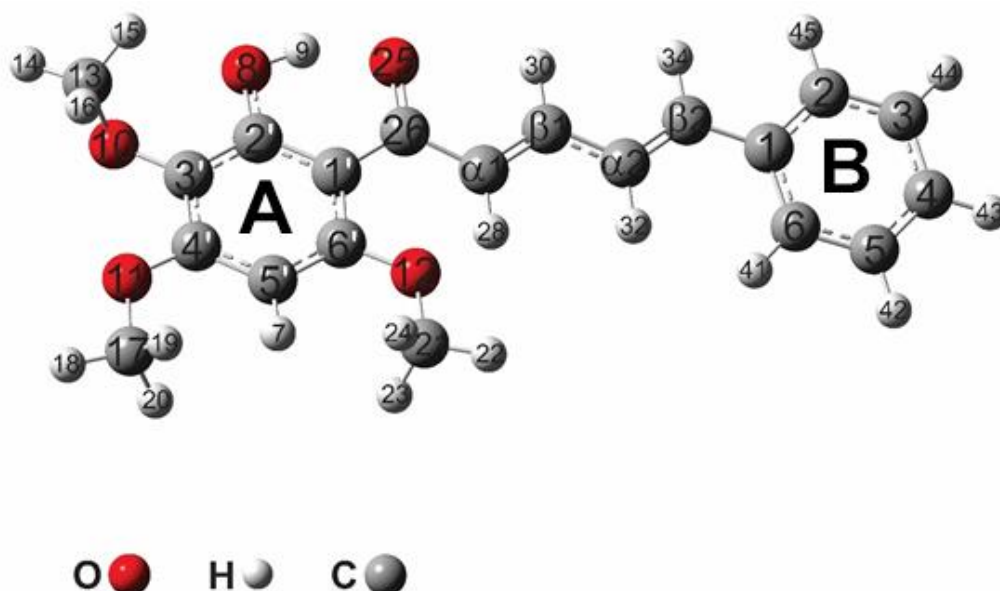


**Fig. 3.** Optimized geometry of the chalcone obtained at B3LYP/6-311++G(d,p) level of theory

To complete the structural characterization, the thermodynamic properties were computed at 298.15 K and 1 atm of pressure at B3LYP/6-311++G(d,p) computational level. The calculated values for the electronic energy ( $E_0$ ), the zero-point energy ( $E_{ZPE}$ ), the internal energy (U), the heat capacity at constant volume ( $C_v$ ), the enthalpy (H), the entropy (S), and the Gibbs free energy (G) are  $-1150.561203$  Hartree,  $224.60$  kcal mol $^{-1}$ ,  $239.84$  kcal mol $^{-1}$ ,  $90.03$  cal mol $^{-1}$ K $^{-1}$ ,  $704.87$  kcal mol $^{-1}$ ,  $173.234$  cal mol $^{-1}$ K $^{-1}$ , and  $653.22$  kcal mol $^{-1}$ , respectively.

**Table 2** Calculated bond lengths for the title chalcone at B3LYP/6-311++G(d,p) level of theory.

Bond assignment	Calculated bond length (Å)
C1'-C25	1.47
C25-O26	1.26
C25- C $\alpha$ 1	1.47
C $\alpha$ 1-C $\beta$ 1	1.35
C $\beta$ 1- C $\alpha$ 2	1.44
C $\alpha$ 2-C $\beta$ 2	1.35
C $\beta$ 2-C1	1.46
C $\alpha$ 1-H28	1.08
C $\beta$ 1-H30	1.09
C $\alpha$ 2-H32	1.09
C $\beta$ 2-H34	1.09
C2'-O8	1.34
C3'-O10	1.37
O10-C13	1.44
C4'-O11	1.35
O11-C17	1.43
C6'-O12	1.36
O12-C21	1.43
O8-H9	1.00
C31-H14	1.09
C13-H15	1.09
C13-H16	1.09

C17-H18	1.09
C17-H19	1.09
C17-H20	1.09
C21-H22	1.09
C21-H23	1.09
C21-H24	1.09
C1' - C2'	1.44
C2' - C3'	1.40
C3' - C4'	1.40
C4' - C5'	1.40
C5' - C6'	1.39
C6' - C1'	1.43
C5' - H7	1.08
C1 - C2	1.41
C2 - C3	1.39
C3 - C4	1.39
C4 - C5	1.40
C5 - C6	1.39
C6 - C1	1.41
C2-H45	1.08
C3-H44	1.08
C4-H43	1.08
C5-H42	1.08
C6-H41	1.08

---

The  $^1\text{H}$  and  $^{13}\text{C}$  NMR spectra were computed at the same level of theory as the optimization calculation using the gauge-independent atomic orbital (GIAO) method. The calculated chemical shifts for the carbon and hydrogen atoms are shown in Table 1. The linear fitting (Figure 4) was made using the experimental and theoretical chemical shifts to understand how these values are related. The coefficient of determination ( $R^2$ ) for this linear fitting was 0.9938 with a linear equation of  $y = 0.94644x + 0.34504$ . This result shows an excellent agreement between the experimental and the calculated chemical shifts. Therefore, the structure of the synthesized chalcone was elucidated by the experimental and theoretical  $^1\text{H}$  and  $^{13}\text{C}$  NMR spectroscopic data analysis, and it was structurally characterized by the computational chemical calculations.

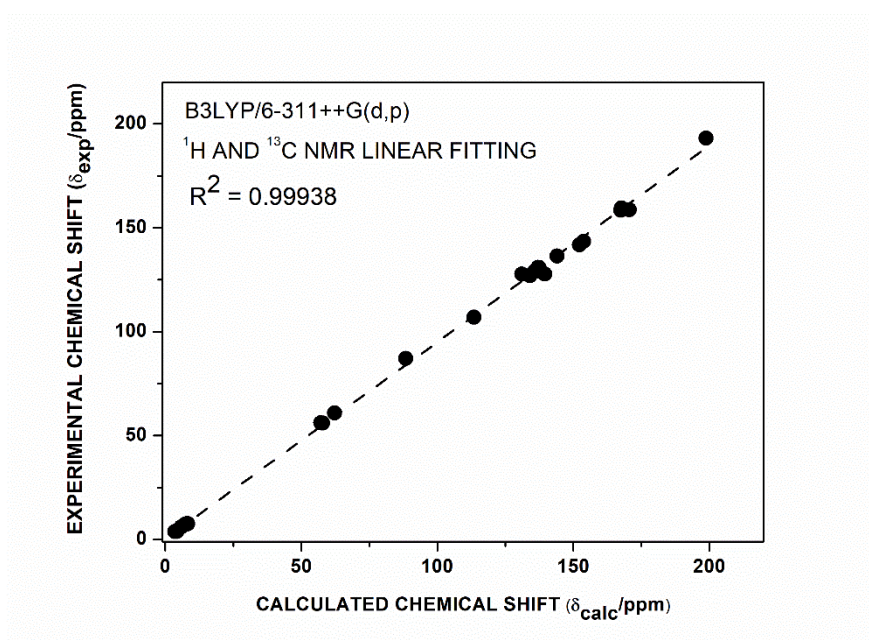


**Fig. 4.** Linear fitting of the experimental and theoretical chemical shifts for the structural characterization of the chalcone

### 3.2 Vibrational spectral analysis

The ATR-IR absorbance and calculated infrared spectrum of the chalcone is presented in Figure 5. The linear fitting (Figure 6) was also conducted to understand the relation between the experimental and theoretical wavenumbers. The coefficient of determination ( $R^2$ )

was 0.99945 with the linear equation  $y = 0.9958x + 6.94487$ . This result shows an excellent agreement between the experimental spectroscopic data and the calculated wavenumbers; hence these vibrational modes can describe the fundamental vibrational modes of the chalcone. The theoretical assignment is shown in Table 3.

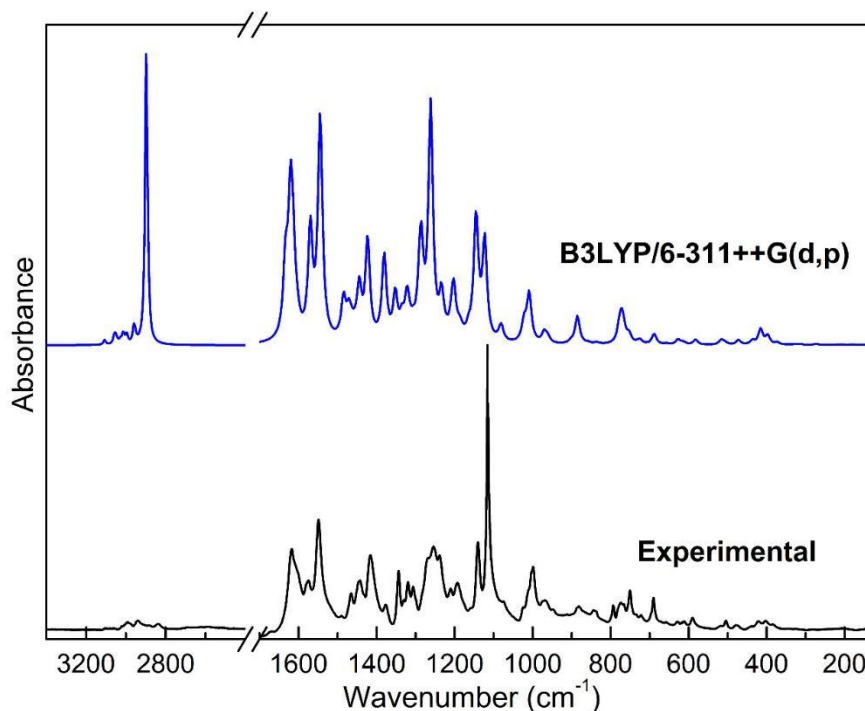


**Fig. 5.** Experimental ATR-IR and theoretical Infrared spectrum obtained at B3LYP/6- 311++G(d,p) level of theory.

**Table 3** ATR-FTIR experimental frequencies ( $\tilde{\nu}_{\text{ATR-FTIR}}$ , in  $\text{cm}^{-1}$ ), calculated vibrational wavenumbers ( $\tilde{\nu}_{\text{IR}}$ , in  $\text{cm}^{-1}$ ), and scaled vibrational wavenumbers ( $\tilde{\nu}_{\text{scal}}$ , in  $\text{cm}^{-1}$ ) by the dual scale factor 0.983 (below  $1700 \text{ cm}^{-1}$ ) and 0.958 (above  $1700 \text{ cm}^{-1}$ ) and assignment for some of the vibrational modes for the chalcone.

$\tilde{\nu}_{\text{ATR-FTIR}}$	$\tilde{\nu}_{\text{IR}}$	$\tilde{\nu}_{\text{scal}}$	Theoretical vibrational assignment
2992	3090.2	2960.412	$\nu_{as}(\text{C17H19}) (40) + \nu_{as}(\text{C21H23}) (41) + \nu_{as}(\text{C21H24}) (41) + \nu_{as}(\text{C17H20}) (42)$
2937	3025.65	2898.573	$\nu(\text{H9O8}) (95)$
2837	3015.92	2889.251	$\nu_s(\text{C13H14}) (13) + \nu_s(\text{C13H15}) (33) + \nu_s(\text{C13H16}) (52)$
1608	1641.92	1614.007	$\nu(\text{Ca2C}\beta 2) (17) + \nu(\text{Ca1C}\beta 1) (33)$
1549	1571.35	1544.637	$\beta(\text{H7C5'C6'}) (11) + \nu(\text{C4'C5'}) (14) + \nu(\text{C25O26}) (17)$
1416	1447.63	1423.02	$\nu(\text{C3'C4'}) (10) + \nu(\text{C2'C3'}) (10) + \nu(\text{C2'O8}) (15) + \beta(\text{H9O8C2'}) (27)$
1344	1375.55	1352.166	$\beta(\text{H28Ca1C}\beta 1) (13) + \beta(\text{H34C}\beta 2\text{C1}) (24)$
1254	1283.25	1261.435	$\nu(\text{C1'C25}) (15) + \beta(\text{H32Ca2C}\beta 2) (18)$
1115	1142.31	1122.891	$\nu(\text{C6'O12}) (12) + \nu(\text{C5'O8}) (20) + \nu(\text{C21O12}) (22)$
1101	1102.64	1083.895	$\nu(\text{C5C6}) (10) + \beta(\text{H43C4C3}) (11) + \nu(\text{C2C3}) (16)$
881	900.63	885.3193	$\tau(\text{H9O8C2'C1'}) (85)$
751	765.87	752.8502	$\tau(\text{C1C2C3C4}) (10) + \tau(\text{H42C5C4C3}) (10) + \gamma(\text{O8C1'C2'C3'}) (11) + \tau(\text{H44C3C2C1}) (13)$

691	700.53	688.621	$\gamma$ (C $\beta$ 2C1C2C6) (14) + $\tau$ (C3C4C5C6) (15) + $\tau$ (C1C2C3C4) (21) + $\tau$ (H43C4C3C2) (24)
590	625.33	614.6994	$\gamma$ (O11C3'C4'C5') (14) + $\gamma$ (O8C1'C2'C3') (22)
505	516.09	507.3165	$\gamma$ (C1C2C5C6) (23)
402	403.97	397.1025	$\beta$ (O8C2'C3') (12) + $\beta$ (C17O11C4') (19)
202	207.35	203.8251	$\gamma$ (O10C3'C2'C4') (13) + $\tau$ (C2'C3'C4'C5') (13)

Nomenclature:  $\square\square$ =torsion;  $\square$  = deformation out of plane;  $\square$  = deformation;  $\square$  = stretching;  $\square_{as}$  = asymmetric stretching;  $\square_s$  = symmetric stretching.

The bands at 2992 cm<sup>-1</sup>, 2937 cm<sup>-1</sup>, and 2837 cm<sup>-1</sup>, respectively, are related to the asymmetrical stretching of the methyl groups C17H19 (40%) and C17H20 (42%), and C21H23 (41%) and C21H24 (41%); the stretching of the hydroxy group H9O8 (95%); the symmetrical stretching of the methyl group C13H14 (13%), C13H15 (33%), and C13H16 (52%). The band at 1608 cm<sup>-1</sup> corresponds to the stretching of the olefin  $\pi$ -bonds between the C $\alpha$ 2C $\beta$ 2 (17%) and C $\alpha$ 1C $\beta$ 1 (33%). The band at 1549 cm<sup>-1</sup> is related to the mixed vibrational modes of the bending H7C5'C6' (11%) in ring A, the stretching C4'C5' (14%) in ring A, and the well-known carbonyl stretching C25O26 (17%). The band at 1416 cm<sup>-1</sup> is related to the mixed modes present in the ring A, including the stretching of the bonds C3'C4' (10%), C2'C3' (10%), and C2'O8 (15%), and the bending of the hydroxyl group with the carbon atom in the ring A (H9O8C2' with PED = 27%). At 1344 cm<sup>-1</sup>, the vibrational modes associated with this band are the bending of the carbon-hydrogen atoms present in the olefin skeleton (H28C $\alpha$ 1C $\beta$ 1 with PED = 13% and H34C $\beta$ 2C1 with PED = 24%). At 1254 cm<sup>-1</sup>, the bending mode of the carbon-hydrogen of the olefin skeleton (H32C $\alpha$ 2C $\beta$ 2 with PED = 18%), the stretching of the carbon in the carbonyl group, and the carbon C1' in the ring A (C1'C25 with PED = 15%) was observed. At 1115 cm<sup>-1</sup>, the stretching modes of the carbon-oxygen atoms present in the methoxy groups: C6'O12 (12%), C5'O8 (20%), and C21O12 (22%) were noticed. At 1101 cm<sup>-1</sup>, the present vibrations are associated to the modes in the ring B:

the stretching of the C5C6 (10%) and C2C3 (16%), and the bending of the H43C4C3 (11%).

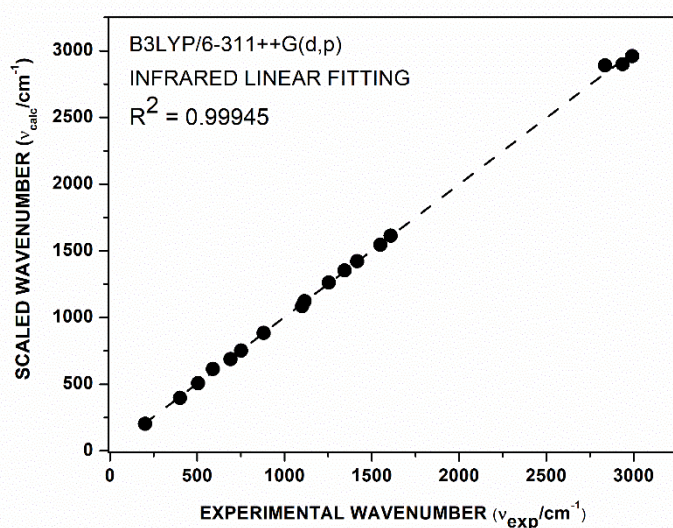


**Fig. 6.** Linear fitting using the experimental and calculated wavenumbers.

The bands below  $1000\text{ cm}^{-1}$  are mainly associated to the torsion and out of plane bending modes: at  $881\text{ cm}^{-1}$  the torsion of the hydroxyl group in ring A (H9O8C2'C1' with PED = 85%); at  $751\text{ cm}^{-1}$  the torsions C1C2C3C4 (10%), H42C5C4C3 (10%), and H44C3C2C1 (13%) and the out of plane bending of the hydroxyl group and the carbon atoms in ring A (O8C1'C2'C3' with PED = 11%); at  $691\text{ cm}^{-1}$  the out of plane bending of the C $\beta$ 2C1C2C6 (14%) and the torsions in ring B: C3C4C5C6 (15%), C1C2C3C4 (21%), and H43C4C3C2 (24%); at  $590\text{ cm}^{-1}$  the out of plane bending of the O11C3'C4'C5' (14%) and O8C1'C2'C3' (22%) in ring A; at  $505\text{ cm}^{-1}$  the out of plane bending of C1C2C5C6 (23%) in ring B; at  $402\text{ cm}^{-1}$  the bending modes of O8C2'C3' (12%) and C17O11C4' (19%) in ring A; at  $202\text{ cm}^{-1}$  the out of plane bending of O10C3'C2'C4' (13%) and the torsion C2'C3'C4'C5' (13%).

### 3.3 Frontier molecular orbitals and quantum reactivity descriptor analysis

The highest occupied molecular orbital (HOMO) and the lowest occupied molecular orbital (LUMO), frequently denominated frontier molecular orbitals (FMO), are important, characterizing the chemical behavior (nucleophilic or electrophilic) of a molecule. The nucleophilic character is related to the HOMO because this is the electron density available to donate and the electrophilic character is associated with the LUMO because this empty molecular orbital can accept electron density due to its lower energy compared to the others empty molecular orbitals. For the chalcone, the HOMO is mainly spread over ring A: the carbon atoms C1', C2', C3', C4', C5', and C6'; the oxygen atoms in the hydroxyl group (O8), and in the methoxy groups (O10, O11, and O12). Also, there are contributions of the  $\pi$ -bonds of the C $\alpha$ 1C $\beta$ 1, C $\alpha$ 2C $\beta$ 2, the carbon atoms C1, C2, C4, and C6. The LUMO is mainly spread over the  $\pi$ -bonds of the C $\alpha$ 1C $\beta$ 1 and C $\alpha$ 2C $\beta$ 2, the oxygen atom of the carbonyl group (O26), the carbon atoms C2, C4, and C6 in ring B, the carbon atoms C2', C4', and C6' in-ring A, and the oxygen atoms O8 and O11. Hence, ring A is most susceptible to donate electron density; the ring B and the olefin skeleton are most susceptible to accept electron density.

To understand how the chalcone can behave during a chemical reaction, the quantum reactivity descriptors (Table 4) were computed from the energy values of the HOMO ( $E_{HOMO}$

= -6.0607 eV) and LUMO ( $E_{LUMO} = -2.6972$  eV) (Figure 7). The energy gap ( $\Delta E_{GAP}$ ) is more used to compute the reactivity, because the higher the value of the energy gap, the lower is the chemical reactivity. The chalcone exhibited the energy gap of 3.3635 eV. This value is directly related to the ionization potential ( $I = 6.0607$  eV) and the electron affinity ( $A = 2.6972$  eV) which means the chalcone is more susceptible to accept electron density than donate due to its higher ionization potential.

**Table 4** Calculated Quantum Reactivity Descriptors at B3LYP/6-311++G(d,p) level of theory

HOMO energy ( $E_{HOMO}/\text{eV}$ )	-6.0607
LUMO energy ( $E_{LUMO}/\text{eV}$ )	-2.6972
Energy Gap ( $\Delta E_{GAP}/\text{eV}$ )	3.363504
Ionization Potential ( $I/\text{eV}$ )	6.060704
Electron Affinity ( $A/\text{eV}$ )	2.6972
Electronegativity ( $\chi/\text{eV}$ )	4.378952
Global Hardness ( $\eta/\text{eV}$ )	1.681752
Global Softness ( $S/\text{eV}^{-1}$ )	0.594618
Electrophilicity Index ( $\omega/\text{eV}$ )	5.700965
Nucleophilicity Index ( $\varepsilon/\text{eV}^{-1}$ )	0.175409

The electron density spread over the HOMO is tightly bonded due to the delocalization mainly over ring A. This chalcone can accept electron density and mainly spreads the extra negative charge over the olefin skeleton and ring B, which means a greater electrophilic than nucleophilic character. The large value for the electronegativity ( $\chi = 4.378952$  eV) is related to the tendency of the chalcone to receive electron density. Then, the global hardness ( $\eta = 1.681752$  eV) is greater than the global softness ( $S = 0.594618$  eV<sup>-1</sup>), which means that this chalcone would interact better with other hard species than soft ones. Finally, the electrophilic character of the title chalcone is confirmed due to its higher value of





**Fig. 8.** Isosurface for the Electronic Fukui functions for the nucleophilic attack ( $f^+$ ), electrophilic attack ( $f^-$ ), and radical attack ( $f^0$ ).

These atoms are the same that the LUMO is spread over. For the electrophilic attack ( $f^-$ ), the molecule behaves as a nucleophilic site, the most susceptible atoms are  $C\alpha 1$ ,  $C\beta 1$ ,  $C\alpha 2$ ,  $C\beta 2$ ,  $C 2$ ,  $C 4$ ,  $C 6$ ,  $C 1'$ ,  $C 3'$ ,  $C 5'$ ,  $C 6'$ ,  $O 11$ , and  $O 12$ . These atoms are related to the delocalization of the HOMO which means that they can interact by electron density donation. For the radical attack ( $f^0$ ), the most susceptible atoms are  $C\alpha 1$ ,  $C\beta 1$ ,  $C\alpha 2$ ,  $C\beta 2$ ,  $C 2$ ,  $C 4$ ,  $C 6$ ,  $C 2'$ ,  $C 3'$ ,  $C 5'$ ,  $C 6'$ ,  $O 9$ ,  $O 11$ ,  $O 12$ , and  $O 26$ . These atoms are susceptible to this type of reaction due to the possibility of electron density delocalization of the radical formed, which implies stability for the radical.

To continue the characterization of the electronic properties, the condensed Fukui functions were computed by the Hirshfeld charge analysis and the results are listed in Table 5.

**Table 5** Calculated values for the Condensed Fukui functions for the nucleophilic attack ( $f^+$ ), electrophilic attack ( $f^-$ ), and radical attack ( $f^0$ ) using the Hirshfeld charge analysis, the dual descriptor ( $\Delta f$ ), and the multiphilic index ( $\Delta\omega$ )

Atom	$f^+$	$f^-$	$f^0$	$\Delta f$	$\Delta\omega$
C4'	-0.02832	-0.03471	-0.03152	0.006392	0.036441
C5'	-0.01604	-0.02256	-0.0193	0.006514	0.037136
C6'	-0.02161	-0.03769	-0.02965	0.016082	0.091683
C1'	-0.00987	-0.03743	-0.02365	0.027557	0.157101
C2'	-0.02176	-0.0203	-0.02103	-0.00146	-0.0083
C3'	-0.01299	-0.06665	-0.03982	0.053659	0.305908
H7	-0.00995	-0.01398	-0.01197	0.004028	0.022963
O8	-0.02633	-0.02439	-0.02536	-0.00194	-0.01104
H9	-0.01381	-0.01079	-0.0123	-0.00302	-0.01723
O10	-0.00775	-0.03174	-0.01975	0.023991	0.136772
O11	-0.01726	-0.03535	-0.02631	0.018094	0.103153

O12	-0.00689	-0.03349	-0.02019	0.026607	0.151686
C13	-0.00471	-0.01431	-0.00951	0.009605	0.054758
H14	-0.00599	-0.01292	-0.00945	0.006924	0.039473
H15	-0.00288	-0.00926	-0.00607	0.006374	0.036338
H16	-0.0041	-0.0102	-0.00715	0.006097	0.034759
C17	-0.00661	-0.01216	-0.00938	0.005558	0.031686
H18	-0.00694	-0.01104	-0.00899	0.004103	0.023391
H19	-0.00576	-0.01075	-0.00826	0.004992	0.028459
H20	-0.00577	-0.01076	-0.00826	0.004988	0.028436
C21	-0.00666	-0.01182	-0.00924	0.005168	0.029463
H22	-0.00541	-0.01003	-0.00772	0.00462	0.026338
H23	-0.00659	-0.01154	-0.00906	0.004952	0.028231
H24	-0.00721	-0.01224	-0.00972	0.005028	0.028664
C25	-0.07879	-0.0128	-0.0458	-0.06599	-0.37621
O26	-0.07704	-0.02352	-0.05028	-0.05351	-0.30508
C $\alpha$ 1	-0.05715	-0.04981	-0.05348	-0.00734	-0.04185
H28	-0.02407	-0.01487	-0.01947	-0.00921	-0.05248
C $\beta$ 1	-0.07518	-0.0299	-0.05254	-0.04529	-0.25818
H30	-0.02975	-0.01509	-0.02242	-0.01466	-0.08357
C $\alpha$ 2	-0.03722	-0.0436	-0.04041	0.006383	0.036389
H32	-0.01942	-0.0154	-0.01741	-0.00402	-0.0229
C $\beta$ 2	-0.07686	-0.04955	-0.0632	-0.0273	-0.15566
H34	-0.02703	-0.01868	-0.02285	-0.00835	-0.04761
C6	-0.02911	-0.02447	-0.02679	-0.00464	-0.02648
C5	-0.02061	-0.01913	-0.01987	-0.00147	-0.0084
C4	-0.04345	-0.04178	-0.04262	-0.00167	-0.0095
C3	-0.02199	-0.02048	-0.02123	-0.00151	-0.0086
C2	-0.02927	-0.02743	-0.02835	-0.00184	-0.01049
C1	-0.01498	-0.02059	-0.01779	0.005607	0.031965
H41	-0.01375	-0.01067	-0.01221	-0.00308	-0.01754
H42	-0.01347	-0.01228	-0.01287	-0.00119	-0.0068
H43	-0.0206	-0.01751	-0.01905	-0.0031	-0.01764
H44	-0.01415	-0.01297	-0.01356	-0.00118	-0.0067
H45	-0.01457	-0.0132	-0.01388	-0.00137	-0.00783

According to the results, the most susceptible atoms to a nucleophilic attack ( $f^+$ ) are C1', C2', C3', C4', C5', C6', O8, O10, O11, O12, C13, C17, C21, C1, C2, C3, C5, and C6. For the electrophilic attack ( $f^-$ ) the most susceptible atoms are C2', C3', C6', O8, C13, C17, C21, C25, O26, C $\beta$ 1, C1, C2, C3, C5, and C6. For the radical attack ( $f^0$ ) the most susceptible atoms are C5', C13, C17, C21, C5, C1. These descriptors are used to compute the local reactivity descriptors: the dual descriptor ( $\Delta f$ ) and the multiphilic index ( $\Delta\omega$ ).

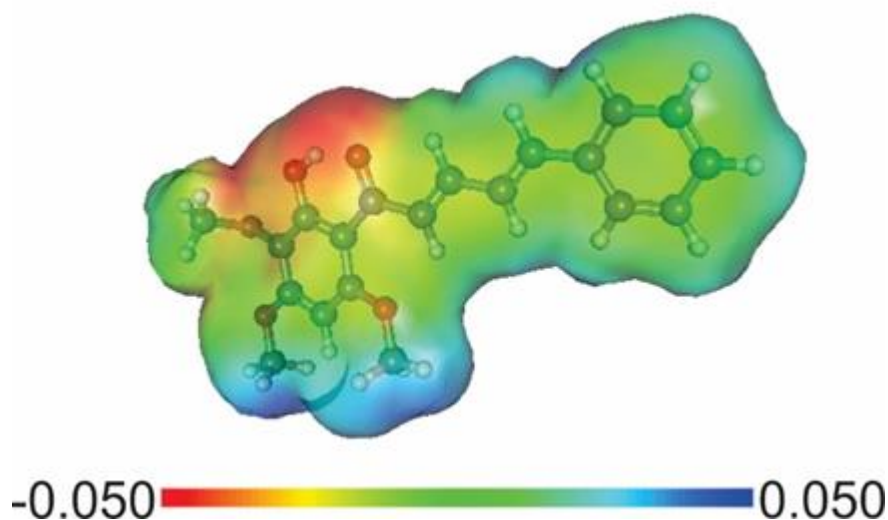


**Fig. 9.** Calculated Molecular Electrostatic Potential (MEP).

If both  $\Delta f$  and  $\Delta\omega$  are positive, the reactive site has an electrophilic character, and if both  $\Delta f$  and  $\Delta\omega$  are negative, the reactive site has a nucleophilic character. According to the results in Table 5, the most susceptible atoms to behave as an electrophilic site are C1', C3', C4', C5', C6', C13, C17, C21, C $\alpha$ 2, and C1. The most susceptible atoms to behave as a nucleophilic site are C2', O8, C25, O26, C $\alpha$ 1, C $\beta$ 1, C $\beta$ 2, C2, C3, C4, C5, and C6. This fact is related to the higher value of the function  $f^+$  for the electrophilic site when compared to the function  $f^-$  for the nucleophilic site. Therefore, the electrophilic and nucleophilic regions of the chalcone were determined and characterized.

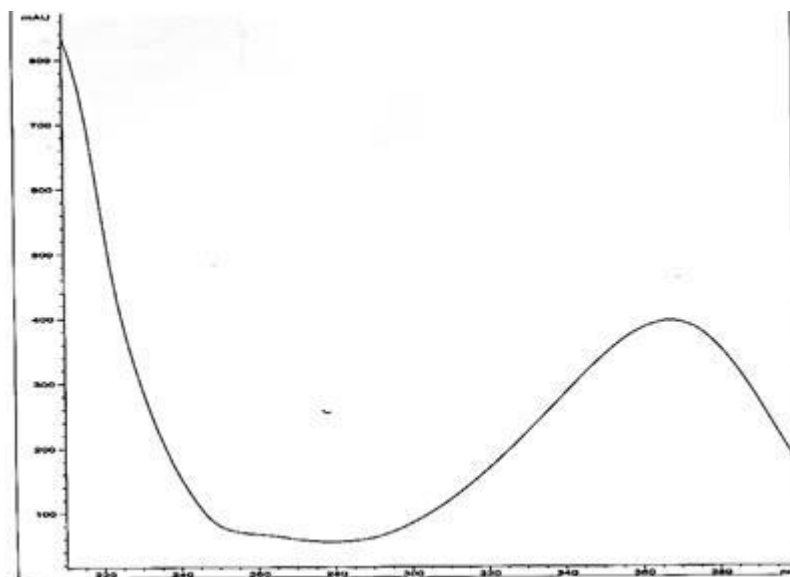


**Fig. 10.** Experimental UV-Vis spectrum

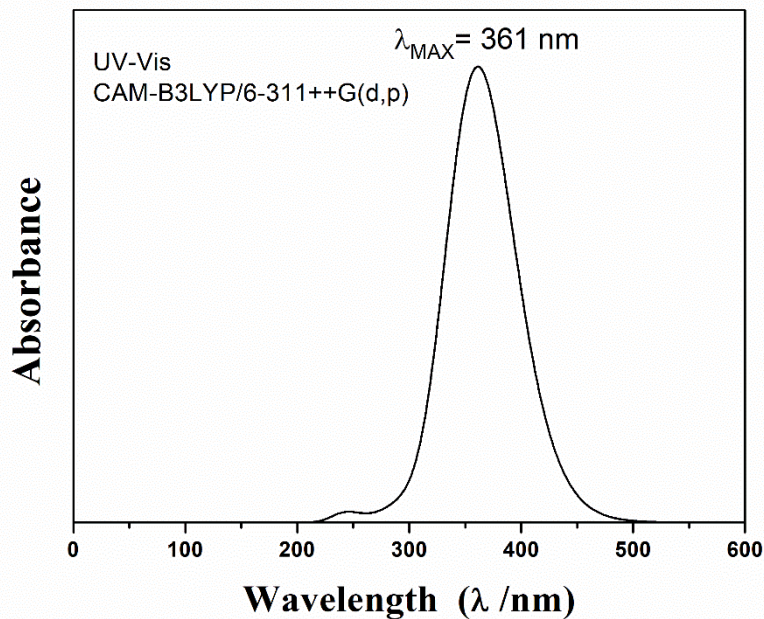
### 3.5 Molecular electrostatic potential (MEP)

Figure 9 shows the calculated molecular electrostatic potential (MEP) for the chalcone obtained at B3LYP/6-311++G(d,p) computational level. In this electrostatic map, the blue colors correspond to the positively charged regions, the light blue colors are related to the regions with partially positive charge, the green colors to the neutral regions, the yellow to

orange is associated to the partially negative charged regions, and the red colors to the negatively charged region. The electrophilic interaction will occur with the regions in blue and light blue due to the positive charge. The nucleophilic interaction will occur with the regions in red and yellow-to-orange because the negative charge is spread over these regions. The hydrogen atoms are most susceptible to an electrophilic interaction due to their partially positive charge, and the oxygen atoms of the hydroxyl and the carbonyl group are most susceptible to a nucleophilic interaction because of their partially negative charge available for donation. Therefore, the electrostatic interaction will mainly occur with ring A of the chalcone.

### 3.6 UV-vis spectroscopic analysis

The UV-vis absorption spectrum of chalcone is presented in Figure 10. The theoretical UV-vis spectrum (Figure 11) was also calculated using the time-dependent density functional theory (TD-DFT) with CAM-B3LYP/6-311++G(d,p) level of theory in chloroform as implicit solvent. The theoretical spectrum showed two absorption bands: the higher intensity absorption exhibited a wavelength of about 361 nm, which corresponds to the electronic transition for the HOMO→LUMO (91%), HOMO-1→LUMO (3%), and HOMO-2→LUMO+1 (2%); the lower intensity band showed an absorption wavelength of 246 nm, which correspond to the electronic transitions of HOMO→LUMO+1 (70%), HOMO-5→LUMO (8%), HOMO-3→LUMO (6%), and HOMO-1→LUMO+1 (4%). According to Figure 11, the experimental absorption band had a wavelength of about 370 nm. Therefore, the experimental and theoretical values for the absorption wavelength are in agreement, corresponding to the HOMO → LUMO electronic transition.



**Fig. 11.** Theoretical UV–Vis spectrum.

### 3.7 Anxiolytic-like effect

Zebrafish is a model animal that is used for neurobehavioral studies. It is an excellent model organism for pharmacological studies and/or safety research at an early stage of drug development [53]. The open field test was used to evaluate the effect of chalcone on the locomotor system of adult zebrafish. The locomotor activity analysis by open field tests generates a model that can assess hyperactivity, which is an indicator of anxiety [54]. We use the animal in the adult phase because the zebrafish has certain limitations for neurobehavioral research in the larval phase, being less complex in morphological terms [60].

It was observed that chalcone caused a locomotor impairment in the open field test, and induced maximum locomotor activity reduction at a dose of  $0.5 \text{ mg kg}^{-1}$  ( $p < 0.0001$  vs naive) (Figure 12). The treatment of zebrafish with anxiolytic drugs can increase their exploratory activity in the open field [55], induce a sedative effect, and decrease their locomotor activity [56]. Therefore, the anxiolytic activity of chalcone was evaluated by the light and dark test.

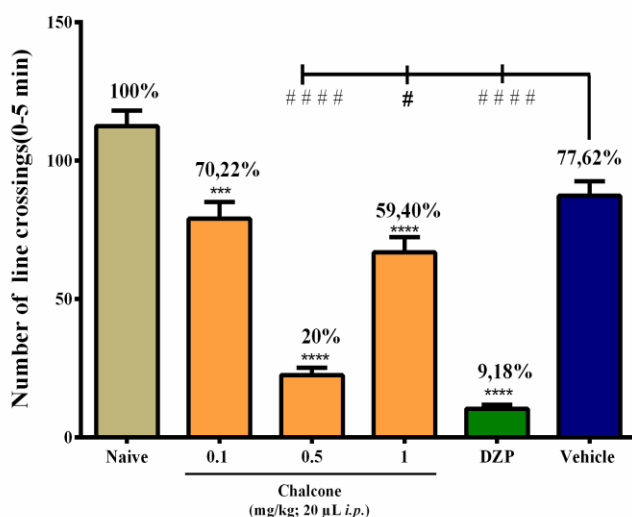


**Fig. 12.** Effect of chalcone under the locomotor behavior of zebrafish (*Danio rerio*) adult in the Open Field Test (0–5 min). Dzp – Diazepam (1.0 mg/mL, i.p.); Vehicle– Control (DMSO 3%; 20  $\mu$ L; i.p.). Values represent the mean  $\pm$  standard error of the mean for 6 animals/group; ANOVA followed by Tukey \*\*\*\*p

The light and dark test is generally applied to assess the anxiolytic effect of various substances on rodents. It has been recently adapted and validated for use in zebrafish models. Anxiety-like behavior is induced in zebrafish and rodents in response to similar environmental stimuli. Both animals prefer dark environments to light ones [57]. The intraperitoneal (*ip*) administration of chalcone, at doses of 0.1, 0.5 and 1.0 mg kg<sup>-1</sup>, and diazepam at a dose of 1.0 mg kg<sup>-1</sup>, increased ( $p < 0.0001$  vs. vehicle) the time spent by the zebrafish in the clear zone of the aquarium, suggesting an anxiolytic effect. It was observed that chalcone caused an anxiolytic effect in the light and dark test, and induced a maximum permanence in the clear zone at a dose of 0.5 mg kg<sup>-1</sup> ( $p < 0.0001$  vs. naive) (Figure 13).

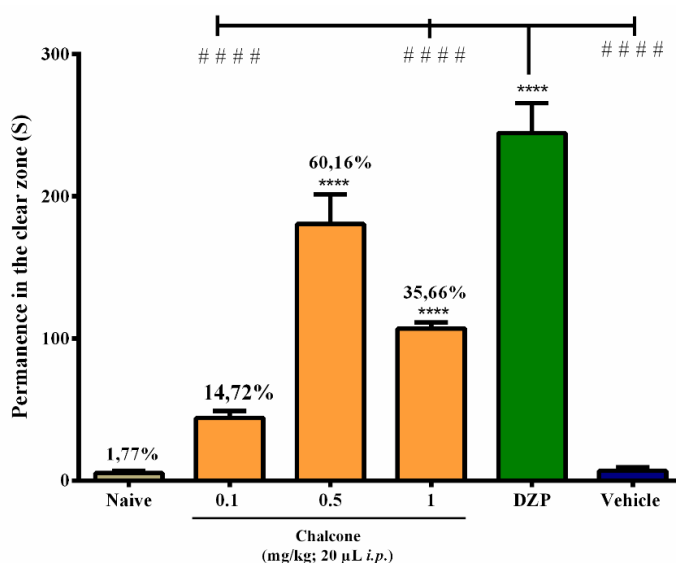
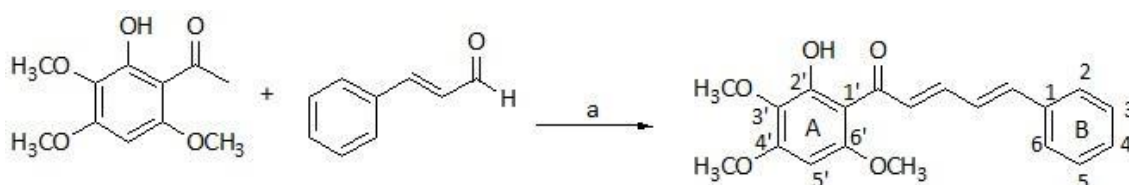


**Fig. 13.** Effect of chalcone on adult zebrafish in the Light & Dark Test (0–5 min). The numbers above each column indicate percentage of permanence in the light zone. Naïve – group without treatment; Vehicle – Control (DMSO 3%; 20  $\mu$ L; i.p.); Dzp – Diazepam (1.0 mg/mL; i.p.). Values represent the mean  $\pm$  standard error of the mean for 6 animals/group; ANOVA followed by Tukey. \*\*\*\*p

Recently, it was demonstrated that 5'-methyl-2'-hydroxichalcone has an anxiolytic effect in mice, as evaluated by the elevated plus-maze assay. This class of compounds holds promise for the development of novel anxiolytic agents because of their neuroprotective properties, which are applied to treat pathological conditions, including anxiety and stress [58]. Generally, chalcones with specific chemical groups such as hydroxyl, methoxy, methyl, dimethylamine, halogens, and nitro substituents show anxiolytic effects [59].

#### 4. Conclusion

NMR, infrared, UV-vis spectroscopic analysis, and quantum chemical calculations confirmed the molecular structure of chalcone (*2E*, *4E*)-1-(2-hydroxy-3,4,6-trimethoxyphenyl)-5-phenylpenta-2,4-dien-1-one synthesized from two natural products. The theoretical calculations together with the experimental NMR and infrared spectroscopic analyses elucidated the molecular structure and provided an excellent agreement between experimental and calculated (chemical shift and wavenumber, respectively) results. The electronic properties were used to identify the nucleophilic and electrophilic regions of the chalcone. The molecular structure of the chalcone was verified and evidence established that the evaluated compound has anxiolytic effects on adult zebrafish used as model. Thus, this study adds new evidence and highlights that chalcone can potentially be used to develop compounds with anxiolytic properties.



**Scheme 1.** Preparation of chalcone. a) NaOH 50% w v – 1, ethanol, t.a., 48 h.

#### Declaration of competing interests

The authors declare that they have no known competing financial interests or personal relationships that could have appeared to influence the work reported in this paper.

#### Acknowledgments

The authors thank FUNCAP, CAPES and CNPq for financial support and scholarship. CENAUREMN - Northeastern Center for the Application and Use of Nuclear Magnetic Resonance by obtaining the spectral data and to Robert W. Owen and Maria Teresa



Salles Trevisan by obtaining the mass spectra. The Department of Physics of the Federal University of Ceará for the technical support in the measurements ATR-FTIR. A.M.R. Teixeira acknowledges the financial support from the CNPq (Grant#: 305719/2018-1). The authors also thank Centro Nacional de Processamento de Alto Desempenho (CENAPAD) of the Federal University of Ceará (UFC) for providing computational resources.

## REFERENCES

- [1] J. Harro, Animals, anxiety, and anxiety disorders: How to measure anxiety in rodents and why, *Behav Brain Res.* 352 (2018) 81–93. <https://doi.org/10.1016/j.bbr.2017.10.016>
- [2] Y.C. Chen, M. Priyadarshini, P. Panula, Complementary developmental expression of the two tyrosine hydroxylase transcripts in zebrafish, *Histochem Cell Biol.* 132 (2009) 375–381. <https://doi.org/10.1007/s00418-009-0619-8>
- [3] M.P. Venuprasad, H. Kumar Kandikattu, S. Razack, F. Khanum, Phytochemical analysis of *Ocimum gratissimum* by LC-ESI-MS/MS and its antioxidant and anxiolytic effects. *S Afr J Bot.* 92 (2014) 151–158. <https://doi.org/10.1016/j.sajb.2014.02.010>
- [4] S.P. Fernandez, M. Nguyen, T.T. Yow, C. Chu, G.A.R. Johnston, J.R. Hanrahan, M. Chebib, The flavonoid glycosides, myricitrin, gossypin and naringin exert anxiolytic action in mice. *Neurochem Res.* 34 (2009) 1867–1875. <https://doi.org/10.1007/s11064-009-9969-9>
- [5] M.K.A. Ferreira, A.W. da Silva, F.C.O. Silva, C.L.A. Holanda, S.M. Barroso, J.Lima, A.E. dos R. Vieira Neto, A.R. Campos, P.N. Bandeira, H.S.dos Santos, T.L.G. Lemos, S.M.C. Siqueira, F.E.A. Magalhães, J.E.S.A de Menezes, Anxiolytic-like effect of chalcone N- $\{4'-(E)-3-(4\text{-fluorophenyl})-1\text{-}(phenyl) prop-2-en-1-one\}$  acetamide on adult zebrafish (*Danio rerio*): Involvement of the GABAergic system. *Behav. Brain Res.* 374 (2019) 3–8. <https://doi.org/10.1016/j.bbr.2019.03.040>
- [6] M.K.A. Ferreira, A.W. Da Silva, F.C.O. Silva, A.E.V. Neto, A.R. Campos, S. A.A.R. Santos, A.M.R. Teixeira, J.C. Xavier, P.N. Bandeira, C.E.S. Nogueira, D.H.A. Brito, E.L. Rebouças, F.E.A. Magalhães, J.E.S.A. De Menezes, H.S. Santos, Anxiolytic-like effect of chalcone N- $\{4[(2E)-3-(3\text{-nitrophenyl})-1\text{-}(phenyl)prop-2-en-1-one]\}$  acetamide on adult zebrafish (*Danio rerio*): Involvement of the 5-HT system. *Biochem Biophys Res Commun.* 526 (2020) 505-511. <https://doi.org/10.1016/j.bbrc.2020.03.129>
- [7] W.V.E. Benjamin, R. Riina, P.E. Berry, A revised infrageneric classification and molecular phylogeny of New World *Croton* (Euphorbiaceae). *Taxon.* 60 (2011) 791-823. <https://doi.org/10.1002/tax.603013>
- [8] C.S. de Heluani, C.A.N. Catalan, L.R. Hernandez, E. Burgueno-Tapia, P. Joseph-Nathan, Three new diterpenoids based on the novel sarcopetalane skeleton from *Croton sarcopetalus*. *J. Nat. Prod.* 63 (2000) 222-225. <https://doi.org/10.1021/np990292l>

- [9] A. Salatino, M.L.F. Salatino, G. Negri, Traditional uses, chemistry and pharmacology of Croton species (Euphorbiaceae), *J. Braz. Chem. Soc.* 18 (2007) 11-33. <https://doi.org/10.1590/S0103-50532007000100002>
- [10] M.T.A. Oliveira, A.M.R. Teixeira, H.D.M. Coutinho, I.R.A. Menezes, D.M. Sena Jr., H.S. Santos, B.M. de Mesquita, M.R.J.R. Albuquerque, P.N. Bandeira, R. Braz Filho, Identification and Modulatory Activity Assessment of 2-Hydroxy-3,4,6-trimethoxyacetophenone Isolated from *Croton anisodontus* Mull. Arg.(Euphorbiaceae). *Nat. Prod. Commun.* 9 (2014) 665-668. <https://doi.org/10.1177/1934578X1400900520>
- [11] N.B. Paulo, L.G.L. Telma, S.S. Hélcio, C.S.C. Mylena, P.P. Daniel, O.M.F. Manoel, P. Cláudia, W.A.B.N. Francisco, H.S.R. Tigressa, R.V.R. Paulo, S. M. Herbert, M.R.T. Alexandre, Synthesis, structural characterization, and cytotoxic evaluation of chalcone derivatives. *Med Chem Res.* 28 (2019) 2037-2049. <https://doi.org/10.1007/s00044-019-02434-1>
- [12] Y-H. Chen, W-H. Wang, Y-H. Wang, Z-Y. Lin, C-C. Wen, C-Y. Chern, Evaluation of the Anti-Inflammatory Effect of Chalcone and Chalcone Analogues in a Zebrafish Model. *Molecules* 18 (2013) 2052-2060. <https://doi.org/10.3390/molecules18022052>
- [13] T.O. Ajiboye, M.T. Yakubu, A.T. Oladiji, Electrophilic and Reactive Oxygen Species Detoxification Potentials of Chalcone Dimers is Mediated by Redox Transcription Factor Nrf-2. *J. Biochem. Mol. Toxicol.* 28 (2014) 11-22. <https://doi.org/10.1002/jbt.21517>
- [14] A. Mahamoud, J. S. Chevalier, W.V. Alibert-Franco, J.M. Kern, Antibiotic efflux pumps in Gram-negative bacteria: the inhibitor response strategy. *J. Antimicrob. Chemother.* 59 (2007) 1223-1229. <https://doi.org/10.1093/jac/dkl493>
- [15] Ajaiyeoba, E.O. Ogbale, O.O. Abiodun, O.O. Ashidi, J.S. Houghton, P.J. Wright, C.W. Cajachalcone: An antimalarial compound from *Cajanus cajan* leaf extract. *J. Parasitol. Res.* 2013 (2013) 1-9. <https://doi.org/10.1155/2013/703781>
- [16] X.W. Fang, B.Q. Yang, Z. Cheng, M.P. Su, Yang, N. Zhou, L.Z. Zhou, J. Synthesis and Antitumor Activity of Novel Nitrogen Mustard-Linked Chalcones. *Arch. Pharm.* 346 (2013) 292-299. <https://doi.org/10.1002/ardp.201200443>
- [17] H. Wei, X.N. Zhang, G.H. Wu, X. Yang, S.W. Pan, Y.Y. Wang, J.L. Ruan, Chalcone derivatives from the fern *Cyclosorus parasiticus* and their anti-proliferative activity. *Food Chem. Toxicol.* 60 (2013) 147-152. <https://doi.org/10.1016/j.fct.2013.07.045>
- [18] A.M.R. Teixeira, H.S. Santos, P.N. Bandeira, M.S.S. Julião, P.T.C. Freire, V.N. Lima, B.G. Cruz, P.T. da Silva, H.D.M. Coutinho, D.M. Sena Jr., Structural, spectroscopic and microbiological characterization of the chalcone 2E-1-(2'-hydroxy-3',4',6'-trimethoxyphenyl)-3-(phenyl)-prop-2-en-1-one derived from the natural product 2-hydroxy-3,4,6-trimethoxyacetophenone. *J. Mol. Struct.* 1179 (2019) 739-748. <https://doi.org/10.1016/j.molstruc.2018.11.075>
- [19] F.E.A. Magalhães, C.Á.P.B. de Sousa, S.A.A.R. Santos, R.B. Menezes, F.L.A. Batista, Â.O. Abreu, M.V. de Oliveira, L.F.W.G. Moura, R.S. Raposo, A.R. Campos, Adult Zebrafish (*Danio rerio*): An Alternative Behavioral Model of Formalin-Induced Nociception. *Zebrafish* 14 (2017) zeb.2017.1436. <https://doi.org/10.1089/zeb.2017.1436>
- [20] A.D. Becke, Density functional thermochemistry. I. The effect of the exchange only gradient correction. *J. Chem. Phys.* 96 (1992) 2155-2160. <https://doi.org/10.1063/1.462066>

- [21] C. Lee, W. Yang, R.G. Parr, Development of the Colle-Salvetti correlation-energy formula into a functional of the electron density. *Phys. Rev. B* 37 (1988) 785–789. <https://doi.org/10.1103/PhysRevB.37.785>
- [22] M.J. Frisch, G.W. Trucks, H.B. Schlegel, G.E. Scuseria, M.A. Robb, J.R. Cheeseman, G. Scalmani, V. Barone, G.A. Petersson, H. Nakatsuji, Gaussian 09, Revision A.02 2009.
- [23] R. Dennington, T. Keith, J. Millam, GaussView, Version 5 2009.
- [24] J. Tomasi, R. Cammi, Remarks on the Use of the Apparent Surface Charges (ASC) Methods in Solvation Problems: Iterative versus Matrix-Inversion Procedures and Renormalization of the Apparent Charges. *J. Comput. Chem.* 16 (1995) 1449–1458. <https://doi.org/10.1002/jcc.540161202>
- [25] B. Mennucci, E. Cancès, J. Tomasi, Evaluation of solvent effects in isotropic and anisotropic dielectrics and in ionic solutions with a unified integral equation method: Theoretical bases, computational implementation, and numerical applications. *J. Phys. Chem. B* 101(1997) 10506–10517. <https://doi.org/10.1021/jp971959k>
- [26] E. Cancès, B. Mennucci, J. Tomasi, A new integral equation formalism for the polarizable continuum model: Theoretical background and applications to Isotropic and anisotropic dielectrics. *J. Chem. Phys.* 107 (1997) 3032–3041. <https://doi.org/10.1063/1.474659>
- [27] S. Kaya, H. Gökce, T. Arslan, G. Alpaslan, Synthesis, spectroscopic characterization, DFT computations, nonlinear optical profile and molecular docking study of a novel chalcone derivative. *J. Mol. Struct.* 1202 (2020) 1–11. <https://doi.org/10.1016/j.molstruc.2019.127270>
- [28] H.M. Jamroz, Vibrational Energy Distribution Analysis VEDA 4 2010.
- [29] R. McWeeny, Perturbation Theory for the Fock-Dirac Density Matrix. *Phys. Rev.* 126 (1962) 1028–1034. <https://doi.org/10.1103/PhysRev.126.1028>
- [30] R. Ditchfield, Self-consistent perturbation theory of diamagnetism I. A gauge-invariant LCAO method for N.M.R. Chemical shifts. *Mol. Phys.* 27 (1974) 789–807. <https://doi.org/10.1080/00268977400100711>
- [31] K. Wolinski, J.F. Hinton, P. Pulay, Efficient Implementation of the Gauge-Independent Atomic Orbital Method for NMR Chemical Shift Calculations. *J. Am. Chem. Soc.* 112 (1990) 8251–8260. <https://doi.org/10.1021/ja00179a005>
- [32] J.R. Cheeseman, A comparison of models for calculating nuclear magnetic resonance shielding tensors. *J. Chem. Phys.* 104 (1996) 5497–5509. <https://doi.org/10.1063/1.471789>
- [33] R.G. Pearson, Hard and Soft Acids and Bases. *J. Am. Chem. Soc.* 85 (1963) 3533–3539. <https://doi.org/10.1021/ja00905a001>
- [34] T. Koopmans, Über die Zuordnung von Wellenfunktionen und Eigenwerten zu den Einzelnen Elektronen Eines Atoms. *Physica* 1 (1934) 104–113. [https://doi.org/10.1016/S0031-8914\(34\)90011-2](https://doi.org/10.1016/S0031-8914(34)90011-2)
- [35] H. Chermette, Chemical reactivity indexes in density functional theory. *J. Comput. Chem.* 20 (1999) 129–154. [https://doi.org/10.1002/\(SICI\)1096-987X\(19990115\)20:1<129::AID-JCC13>3.0.CO;2-A](https://doi.org/10.1002/(SICI)1096-987X(19990115)20:1<129::AID-JCC13>3.0.CO;2-A)

- [36] R.P. Iczkowski, J.L. Margrave, Electronegativity. *J. Am. Chem. Soc.* 83 (1961) 3547–3551. <https://doi.org/10.1021/ja01478a001>
- [37] R.G. Pearson, Recent advances in the concept of hard and soft acids and bases. *J. Chem. Educ.* 64 (1987) 561–567. <https://doi.org/10.1021/ed064p561>
- [38] J.F. Janak, Proof that  $\partial E/\partial n_i = \epsilon_i$  in density-functional theory. *Phys. Rev. B* 18 (1978) 7165–7168. <https://doi.org/10.1103/PhysRevB.18.7165>
- [39] L.Von Szentpály, Studies on electronegativity equalization. Part 1. Consistent diatomic partial charges. *J. Mol. Struct. THEOCHEM* 233 (1991) 71–81. [https://doi.org/10.1016/0166-1280\(91\)85055-C](https://doi.org/10.1016/0166-1280(91)85055-C)
- [40] W. Yang, R.G. Parr, Hardness, softness, and the fukui function in the electronic theory of metals and catalysis. *Proc. Natl. Acad. Sci. U. S. A.* 82 (1985) 6723–6726. <https://doi.org/10.1073/pnas.82.20.6723>
- [41] R.G. Parr, L.V. Szentpály, S. Liu, Electrophilicity index. *J. Am. Chem. Soc.* 121 (1999) 1922–1924. <https://doi.org/10.1021/ja983494x>
- [42] Chattaraj, P.K. S. Giri, S. Duley, Update 2 of: Electrophilicity index. *Chem. Rev.* 111 (2011). <https://doi.org/10.1021/cr100149p>
- [43] Chemcraft - graphical software for visualization of quantum chemistry computations. 2004.
- [44] K. Fukui, Role of frontier orbitals in chemical reactions. *Science.* 218 (1982) 747–754. <https://doi.org/10.1126/science.218.4574.747>
- [45] I.B. Obot, D.D. Macdonald, Z.M. Gasem, Density functional theory (DFT) as a powerful tool for designing new organic corrosion inhibitors: Part 1: An overview. *Corros. Sci.* 99 (2015) 1–30. <https://doi.org/10.1016/j.corsci.2015.01.037>
- [46] C. Morell, A. Toro-labbe, New Dual Descriptor for Chemical Reactivity. *J. Phys. Chem. A* 2005, 205–212. <https://doi.org/10.1021/jp046577a>
- [47] J. Padmanabhan, R. Parthasarathi, M. Elango, V. Subramanian, B.S. Krishnamoorthy, D.R. Roy, P.K. Chattaraj, Multiphilic descriptor for chemical reactivity and selectivity. *J. Phys. Chem. A* 37 (2007) 9130–9138. <https://doi.org/10.1021/jp0718909>
- [48] T. Lu, F. Chen, Multiwfn : A Multifunctional Wavefunction Analyzer. *J. Comput. Chem* 33 (2011) 580-592. <https://doi.org/10.1002/jcc.22885>
- [49] K. Momma, F. Izumi, VESTA 3 for three-dimensional visualization of crystal, volumetric and morphology data. *J. Appl. Cryst.* 44 (2011) 1272–1276. <https://doi.org/10.1107/S0021889811038970>
- [50] A.R. Allouche, Gabedit - A graphical user interface for computational chemistry softwares. *J. Comput. Chem.* 32 (2010) 174–18. <https://doi.org/10.1002/jcc.21600>
- [51] T. Yanai, D.P. Tew, N.C. Handy, A new hybrid exchange-correlation functional using the Coulomb-attenuating method (CAM-B3LYP). *Chem. Phys. Lett.* 393 (2004) 51–57. <https://doi.org/10.1016/j.cplett.2004.06.011>

- [52] N.M. O’Boyle, A.L. Tenderholt, K.M. Langner, cclib: A Library for Package-Independent Computational Chemistry Algorithms. *J. Comput. Chem.* 29 (2008) 839–845. <https://doi.org/10.1002/jcc.20823>
- [53] P. Gupta, S. Khobragade, S. Rajaram, V. Shingatgeri, Assessment of locomotion behavior in adult Zebrafish after acute exposure to different pharmacological reference compounds. *Drug Dev. Ther.* 5 (2014)127. <https://doi.org/10.4103/2394-2002.139626>
- [54] R. R Resende, C.R. Soccol, *Biotecnologia aplicada à saúde: fundamentos e aplicações*, 1st ed. Capítulo 1: zebrafish como modelo para estudos comportamentais (2015).
- [55] J. Cachat, A. Stewart, E. Utterback, P. Hart, S. Gaikwad, K. Wong, E. Kyzar, N. Wu, A. V. Kalueff,. Three-dimensional neurophenotyping of adult zebrafish behavior. *PLoS One* 6 (2011). <https://doi.org/10.1371/journal.pone.0017597>
- [56] C.K. Benneh, R.P. Biney, P.K. Mante, A.Tandoh, D.W. Adongo, E. Woode, *Maerua angolensis* stem bark extract reverses anxiety and related behaviours in zebrafish—Involvement of GABAergic and 5-HT systems. *J. Ethnopharmacol.* 207 (2017) 129–145. <https://doi.org/10.1016/j.jep.2017.06.012>
- [57] A. Stewart, S. Gaikwad, E. Kyzar, J. Green, A. Roth, A.V. Kalueff, Neuropharmacology Modeling anxiety using adult zebra fish: A conceptual review. *Neuropharmacology* 62 (2012) 135–143. <https://doi.org/10.1016/j.neuropharm.2011.07.037>
- [58] Ben-Azu, B. Nwoke, E.E. Aderibigbe, A.O. Omogbiya, I.A. Ajayi, A.M. Olonode, E.T. Umukoro, S. Iwalewa, E.O. Possible neuroprotective mechanisms of action involved in the neurobehavioral property of naringin in mice. *Biomed. Pharmacother.* 109 (2019) 536–546. <https://doi.org/10.1016/j.biopha.2018.10.055>
- [59] J. Higgs, C.Wasowski, A. Marcos, M. Jukič, C.H. Paván, S. Gobec, F. de Tezanos Pinto, N. Colettis, M. Marder,. Chalcone derivatives: synthesis, in vitro and in vivo evaluation of their anti-anxiety, anti-depression and analgesic effects. *Heliyon* 5 (2019) e01376. <https://doi.org/10.1016/j.heliyon.2019.e01376>
- [60] A. Stewart, N. Wu, J. Cachat, P. Hart, S. Gaikwad, K.Wong, E. Utterback, T. Gilder, E. Kyzar, A. Newman. Pharmacological modulation of anxiety-like phenotypes in adult zebrafish behavioral models. *Prog Neuropsychopharmacol Biol Psychiatry* 35 (2011) 1421-1431. <https://doi.org/10.1016/j.pnpbp.2010.11.035>

**Article 4** – Antibacterial activity against multidrug-resistant *Staphylococcus aureus* and in the silica evaluation of the MepA efflux pump by cinnamaldehyde chalcone.,

Authors: da Cunha Xavier, J., de Freitas, T. S., da Silva, P. T., Coutinho, H. D. M., Teixeira, A. M. R., Rodrigues, L. G., ... & dos Santos, H. S. (2022). A












Journal / link / Qualis J Microbiology journal / <http://doi.org/10.33263/BRIAC126.75237531> /  
Qualis B2 in the biological sciences II.

Situation: Published

**Resumo:**

Estudos fitoquímicos em espécies de *Croton* identificaram a presença de metabólitos responsáveis por uma ampla variedade de atividades farmacológicas, entre elas atividade. A pesquisa de novas substâncias com atividade antimicrobiana derivada de produtos naturais pode dar uma grande contribuição para a saúde humana em todo o mundo ao encontrar fórmulas mais eficientes e menos tóxicas em a corrida contra a resistência dos microrganismos patogênicos. Entre os patógenos bacterianos, *Staphylococcus aureus*, apesar de estar presente na pele e mucosa nasal, pode causar muitas infecções e doenças. Esses oportunistas atingem pessoas debilitadas em hospitais e são difíceis de tratar. Aqui nós realizamos a caracterização estrutural, determinação da atividade antibiótica e potencial de inibição da bomba de efluxo MepA contra *S. aureus* da chalcona (2E, 4E) -1-(2-hidroxi-3,4,6-trimetoxifenil)-5-fenilpenta-2,4-dien-1-ona, derivado de produtos naturais 2-hidroxi-3,4,6-trimetoxiacetofenona isolada de *Croton anisodontus* e cinamaldeído. A chalcona foi sintetizado pela condensação de Claisen-Schmidt. Além disso, foram realizados testes microbiológicos para investigar a atividade antibacteriana, potencial modulador e inibição da bomba de efluxo contra o *S. aureus* multirresistentes. Os valores de CIM obtidos para chalcona não foram clinicamente relevantes (CIM  $\geq 1024$   $\mu\text{g/mL}$ ). No entanto, a chalcona dificulta a ligação do antibiótico ao sítio de ligação da bomba de efluxo do MepA. Atua como um inibidor competitivo, sendo expelido da bactéria no lugar do antibiótico e potencializando a ação da ciprofloxacina contra cepas bacterianas multirresistentes de K2068. Portanto, chalcona pode ser usada como base para o projeto de substâncias com atividade modificadora de antibióticos.

## Antibacterial Activity Against Multidrug-Resistant *Staphylococcus aureus* and *in Silico* Evaluation of MepA Efflux Pump by Cinnamaldehyde Chalcone

Jayze da Cunha Xavier <sup>1</sup> , Thiago Sampaio de Freitas <sup>1</sup> , Priscila Teixeira da Silva <sup>1</sup> , Henrique Douglas Melo Coutinho <sup>1</sup> , Alexandre Magno Rodrigues Teixeira <sup>1</sup> , Leilane Gomes Rodrigues <sup>2</sup> , Paulo Nogueira Bandeira <sup>2</sup> , Carlos Emídio Sampaio Nogueira <sup>3</sup> , Larissa Santos Oliveira <sup>4</sup> , Emmanuel Silva Marinho <sup>4</sup> , Hécio Silva dos Santos <sup>1,2,4,\*</sup> 

### CHAPTER 8 Antibacterial Activity Against Multidrug-Resistant *Staphylococcus aureus* and *in Silico* Evaluation of MepA Efflux Pump by Cinnamaldehyde Chalcone

Jayze da Cunha Xavier <sup>1</sup>, Thiago Sampaio de Freitas <sup>1</sup>, Priscila Teixeira da Silva <sup>1</sup>, Henrique Douglas Melo Coutinho <sup>1</sup>, Alexandre Magno Rodrigues Teixeira <sup>1</sup>, Leilane Gomes Rodrigues <sup>2</sup>, Paulo Nogueira Bandeira <sup>2</sup>, Carlos Emídio Sampaio Nogueira <sup>3</sup>, Larissa Santos Oliveira <sup>4</sup>, Emmanuel Silva Marinho <sup>4</sup>, Hécio Silva dos Santos <sup>1,2,4,\*</sup>

<sup>1</sup> Department of Biological Chemistry, Regional University of Cariri, Crato, CE, Brazil; [jayzecx@gmail.com](mailto:jayzecx@gmail.com) (J.C.X.); [thiagocrato@hotmail.com](mailto:thiagocrato@hotmail.com) (T.S.F.); [pi.teixeiradasilva@gmail.com](mailto:pi.teixeiradasilva@gmail.com) (P.T.S.); [carlosemidio@ymail.com](mailto:carlosemidio@ymail.com) (C.E.S.N.); [hdmcoutinho@gmail.com](mailto:hdmcoutinho@gmail.com) (H.D.M.C.); [alexandre.teixeira@urca.br](mailto:alexandre.teixeira@urca.br) (A.M.R.T.);

<sup>2</sup> Science and Technology Centre - Chemistry Course, State University Vale do Acaraú, Sobral, CE, Brazil; [bandeirapn@yahoo.com.br](mailto:bandeirapn@yahoo.com.br) (P.N.B.); [leilane16@gmail.com](mailto:leilane16@gmail.com) (L.G.R.);

<sup>3</sup> Department of Physics, Regional University of Cariri, Juazeiro do Norte-CE, Brazil

<sup>4</sup> Science and Technology Center, Postgraduate Program in Natural Sciences, State University of Ceará, Fortaleza, CE, Brazil; [larissa\\_as10@hotmail.com](mailto:larissa_as10@hotmail.com) (L.S.O.); [emmanuel.marinho@uece.br](mailto:emmanuel.marinho@uece.br) (E.S.M.);

\* Correspondence: [helciodossantos@gmail.com](mailto:helciodossantos@gmail.com) (H.S.S.)

**Abstract:** Phytochemical studies on *Croton* species have identified the presence of secondary metabolites responsible for a wide variety of pharmacological activities, among them antimicrobial activity. Research for new substances with antimicrobial activity derived from natural products can give a major contribution to human health worldwide by finding more efficient and fewer toxic formulas in the race against pathogenic microorganisms resistance. Among bacterial pathogens, *Staphylococcus aureus* species, despite being present in the skin and nasal mucosa, can cause many infections and diseases. These opportunists reach debilitated people in hospitals and are challenging to treat. Here, we performed the structural characterization, determination of antibiotic activity, and MepA efflux pump inhibition potential against *S. aureus* of the chalcone (2E, 4E) -1- (2-hydroxy-3,4,6-trimethoxyphenyl)-5-phenylpenta-2,4-dien-1-one, derived from natural products 2-hydroxy-3,4,6-trimethoxyacetophenone isolated from *Croton anisodontus* and cinnamaldehyde. The

chalcone was synthesized by the Claisen-Schmidt condensation. In addition, microbiological tests were performed to investigate the antibacterial activity, modulator potential, and efflux pump inhibition against the *S. aureus* multi-resistant strains. MIC values obtained to chalcone were not clinically relevant ( $\text{MIC} \geq 1024 \mu\text{g/mL}$ ). However, chalcone hampers the binding of the antibiotic to the binding site of the MepA efflux pump. It acts as a competitive inhibitor, being expelled from the bacteria in place of the antibiotic and potentiating ciprofloxacin's action against multidrug-resistant bacterial strains of K2068. Therefore, chalcone can be used as a base for substance design with antibiotic modifying activity.

**Keywords** Chalcone, cinnamaldehyde, *Staphylococcus aureus*, efflux pump.

## 1. Introduction

Over the years, natural products have been selected with the efficiency and selectivity needed to reach cellular targets and avoid resistance naturally, characteristics that many pure synthetic molecules do not possess. Cinnamaldehyde, is a natural  $\alpha,\beta$ -unsaturated aromatic aldehyde found in *cinnamon bark* oil. It has been reported to have antimicrobial and antibiofilm activities against a wide range of Gram-positive and Gram-negative bacterial pathogens, including *Pseudomonas aeruginosa*, *Escherichia coli*, *Staphylococcus aureus*, *Staphylococcus epidermidis*, and *Streptococcus mutans*, and *Enterococcus faecalis* [1-13]. The antimicrobial and modulatory activity of the natural 2-hydroxy-3,4,6-trimethoxyacetophenone isolated from *Croton anisodontus* (Figure 1) towards *Escherichia coli*, *Pseudomonas aeruginosa*, and *Staphylococcus aureus* strains have been reported [14]. The results indicated that acetophenone isolated from *C. anisodontus* might be a starting compound for the synthesis of chalcones with antimicrobial activity [15-23].



**Figure 1.** (a) Aerial parts of *C. Anisodontus*; (b) 2-hydroxy-3,4,6-trimethoxyacetophenone.

Chalcones have an open chain flavonoid structure in which the two aromatic rings are joined by a three-carbon  $\alpha,\beta$ -unsaturated carbonyl linker [24]. They can be obtained from natural sources or by synthesis and are widely distributed in fruits, vegetables, and tea. This class of compound has aroused much interest due to the broad spectrum of pharmacological activities that they present, including anticancer [25,26], anti-inflammatory [27], and antioxidant [28] properties towards human diseases.

This work aimed to evaluate the antibacterial activity and efflux pump inhibition against *S. aureus* of the chalcone (2*E*, 4*E*)-1-(2-hydroxy-3,4,6-trimethoxyphenyl)-5-phenylpenta-2,4-dien-1-one synthesized by natural products cinnamaldehyde and 2-hydroxy-3,4,6-trimethoxy acetophenone.



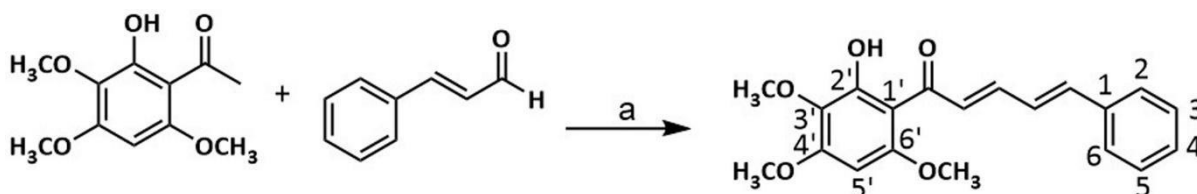
## 2. Materials and Methods

### 2.1. General procedures.

Cinnamaldehyde was purchased from Sigma-Aldrich.  $^1\text{H}$  and  $^{13}\text{C}$  NMR were recorded on a Bruker Avance DRX-500 (500 MHz for  $^1\text{H}$  and 125 MHz for  $^{13}\text{C}$ ); chemical shifts were given in ppm ( $\delta_{\text{C}}$  and  $\delta_{\text{H}}$ ), relative to residual  $\text{CHCl}_3$  (7.24 and 77.0 ppm). The infrared spectrum of the chalcone was measured at room temperature by Attenuated Total Reflectance Fourier Transform Infrared spectroscopy (ATR-FTIR) using a Bruker vacuum infrared spectrometer (FTIR) VERTEX 70V at room temperature in the range of 130 to 4000  $\text{cm}^{-1}$ , with a resolution of 2  $\text{cm}^{-1}$ .

### 2.2. Synthesis of the chalcone.

The description of the procedure of the synthesis of the chalcone is shown in Scheme 1. The chalcone was synthesized by a Claisen–Schmidt condensation reaction in a basic medium [19]. At ethanol solution of 2-hydroxy-3,4,6 trimethoxyacetophenone (2 mmol) was added to a benzaldehyde solution and the derivatives (2 mmol), followed by the addition of ten drops of 50% w/v aq. NaOH with stirring for 48 h. The solid that formed was filtered under reduced pressure, washed with cold water, and analyzed by TLC.



**Scheme 1.** Preparation of chalcone. a) NaOH 50 % w v<sup>-1</sup>, ethanol, t.a., 48 h.

(2E,4E)-1-(2-hydroxy-3,4,6-trimethoxyphenyl)-5-phenylpenta-2,4-dien-1-one: Yellow solid (Yield: 35.4%), m.p. 144.8-145.2°C. IR (KBr,  $\nu_{\text{cm}^{-1}}$ ): 1634, 1600, 1588, 1575, 1480, 1167.  $^1\text{H}$  RMN ( $\text{CDCl}_3$ , ppm): 3.84 (s, MeO); 3.93 (s, MeO); 3.95 (s, MeO); 6.99 (s, H-5'); 7.44 (m, H-4); 7.38 (d, H-3/5,  $J = 7,1$  Hz); 7.51 (d, H-2/6,  $J = 7,2$  Hz); 7.62 (d, H $\alpha$ ,  $J = 14,6$  Hz); 7.64 (d, H $\beta$ ,  $J = 14,6$  Hz); 7.40 (d, H $\alpha$ ,  $J = 14,6$  Hz); 7.43 (d, H $\beta$ ,  $J = 14,6$  Hz).  $^{13}\text{C}$  RMN ( $\text{CDCl}_3$ , ppm): 193.2 (C=O); 60.9 (MeO-3'); 56.1 (MeO-4'); 56.2 (MeO-6'); 107.0 (C-1'); 158.7 (C-2'); 131.0 (C-3'); 159.6 (C-4'); 87.2 (C-5'); 158.5 (C-6'); 136.5 (C-1); 127.7 (C-2/6); 129.1 (C-3/5); 131.0 (C-4); 129.2 (C $\alpha$ ); 143.5 (C $\beta$ ); 127.0 (C $\alpha$ ); 141.8 (C $\beta$ ). MS-EI  $m/z = 340$ .

### 2.3. Bacterial strains.

Multidrug-resistant *S. aureus* strains 1199B and K2068 were used in both direct and modulatory antibacterial activity assays. The 1199B strain carries the NorA gene that expresses a protein responsible for the efflux of quinolones, and the K2068 strain is related to the MepA gene, another class of bacterial efflux pumps. Both strains were obtained from cultures grown at the Laboratory of Microbiology and Molecular Biology (LMBM) of the Regional University of Cariri (URCA), Brazil.

### 2.4. Drugs.

The drugs chlorpromazine (CPZ), carbonyl cyanide m-chlorophenylhydrazone (CCCP), and ethidium bromide (EB) were obtained from Sigma Aldrich Co. Ltd. The antibiotics were dissolved in dimethyl sulfoxide (DMSO) and after in sterile water (concentration of 1024 µg/mL). Norfloxacin (NorA) and ciprofloxacin (Cip) were the antibiotics used. CPZ and EB solutions were dissolved in distilled, sterile water, stored at -20°C, and kept protected from light (concentration of 1024 µg/mL). The CCCP was dissolved in methanol/water (1:1, v/v) and stored at -20°C (concentration of 1024 µg/mL).

#### *2.5 .Antibacterial activity test by Minimum Inhibitory Concentration (MIC).*

The MIC was determined by microdilution assay using 100 µL of each suspended bacterial inoculum in saline solution, corresponding to 0.5 of the McFarland scale, followed by the addition of 900 µL of brain heart infusion (BHI) in microtubes (2mL). These were then transferred to 96-well microtiter plates, and serial dilutions of each substance were performed with concentrations ranging from 0.5 to 512 µg/mL (1:1). The plates were incubated at 37 °C for 24 h, and bacterial growth was assessed by using resazurin. The MIC was defined as the lowest concentration in which no growth can be observed [18]. The antibacterial assays were performed in triplicates, and results were expressed as an average of replicates.

#### *2.6. Evaluation of efflux pump inhibition by MIC reduction.*

Briefly, 150 µL of each suspended bacterial inoculum in saline solution, corresponding to 0.5 of the McFarland scale, were added to microtubes (2mL) together with 1350 µL of BHI as a control. In tests, 150 µL of each suspended bacterial inoculum in saline solution, corresponding to 0.5 of the McFarland scale, were added together with EPIs (MIC/8) and completed with BHI. These were then transferred to 96-well microtiter plates, and 100 µL of the antimicrobial drug and EB serial dilutions were performed (1:1). The plates were incubated at 37 °C for 24 h, and bacterial growth was assessed by using resazurin. MIC was defined with antibiotics and EB concentrations ranging from 0.5 to 512 µg/mL. The MIC of controls was assessed using antibiotics and EB alone [18].

#### *2.7. Statistical analysis.*

All bacteriological tests were performed in triplicates. Data were analyzed using a two-way ANOVA followed by Bonferroni's post hoc test (where  $p < 0.05$  was considered significant). The geometric mean of the triplicates was used as the central data  $\pm$  standard error of the mean. The GraphPad Prism 5.0 statistical program was used for the analysis.

#### *2.8. Docking procedure.*

The MepA model was generated by retrieving the protein sequence for the NCTC 8325 strain from the Uniprot database. Then, the SWISS-MODEL [29] service was used to build the homology model. A total of 50 templates were generated, and the template with the best Global Model Quality Estimation score was based on the structure of the multidrug and toxic compound extrusion transporter of the *Bacillus halodurans* (PDB-ID: 5C6N). For the docking procedure, which was carried out using the Autodock Vina [30] software, the grid

box was defined as an 80 Å x 80 Å x 80 Å box around the geometrical center of the model. Partial Gasteiger charges were added to ligand atoms, non-polar hydrogen atoms were mixed, while all other parameters were kept at their default values. The best results were chosen based on the binding score.

### 3. Results and Discussion

#### 3.1. Antibacterial activity and potential antibacterial activity.

Minimum Inhibitory Concentration (MIC) of chalcone were  $\geq 1024 \mu\text{g}/\text{mL}$ , and it does not display antibacterial activity against either of the strains compared to the antibacterial effects of the efflux pump inhibitors CCCP (MIC  $32 \mu\text{g} / \text{mL}$ ) and CPZ (MIC =  $812 \mu\text{g} / \text{mL}$ ) against the K2068 strain. The CCCP modifies the electrochemical gradient of the membrane inhibiting the efflux pumps that need this source of energy. The chlorpromazine (CPZ), by providing an energetic collapse in NorA, consequently impedes the outflow of toxins, antibiotics, and biocides [31]. The CCCP, nevertheless, possesses toxicity to prokaryotes and eukaryotic cells [32]; for this reason, it is important to research new pump inhibitors that do not have this potential.

The decrease in the MIC proves the inhibition of the MepA pump. The results showed that the chalcone did not present chlorpromazine sensitive pump for the bromide, but it shows sensitivity to CCCP. The data also showed that although chlorpromazine did not inhibit the pump, the chalcone inhibited as much as the CCCP. Due to the reversal of the bacterial resistance promoted by the inhibition of efflux pumps, there was a relative reduction in the MIC of the two antibiotics in the K 2068 strain, including synergism with the significance of  $p < 0.001$ . The K 2068 strain possesses a pump for ciprofloxacin sensitive to chlorpromazine and the CCCP. A K 2068 possesses efflux pump for ciprofloxacin sensitive to chlorpromazine and CCCP (Figure 2).

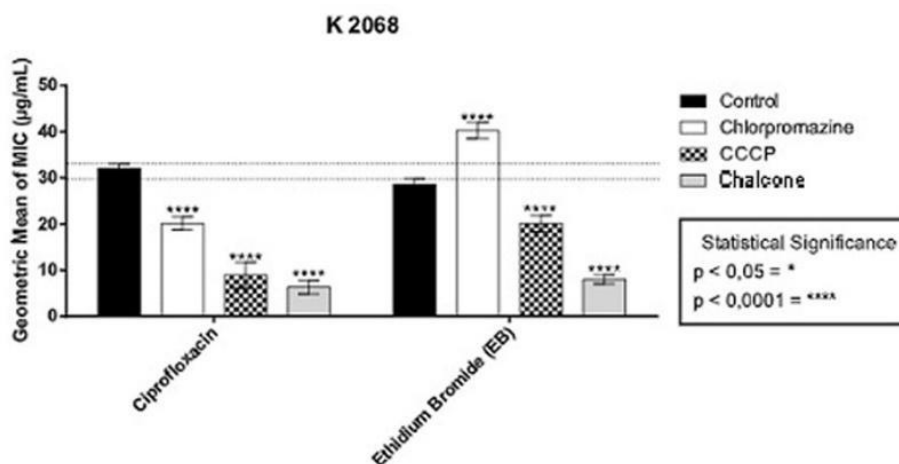


**Figure 2.** MICs of the Ciprofloxacin (Cip) and Ethidium Bromide (EB) in the absence or presence of the cinnamaldehyde chalcone, as well as Chlorpromazine (CPZ) and carbonylcyanide m-chlorophenyl hydrazone (CCCP) against K2068 (MepA).

The K 2068 possesses efflux pump for ciprofloxacin sensitive to chlorpromazine and CCCP (Figure 2). N-methylation and N-acetylation provide an increase of approximately twice in the concentration necessary to achieve 50% inhibition of the pump causing a negative

effect for NorA and MepA. In addition, phenyl ether is important for inhibition of efflux in the Mep A but not in the Nor A [33].

Previous studies showed a similar effect when the DB Thiophene chalcone was tested for the K2068 strain. DB Thiophene showed a better inhibition potential for CCCP-sensitive efflux pumps than the standard inhibitor, also acting as a strong inhibitor of efflux pumps in the Ciprofloxacin test. The inhibition mechanism was investigated by molecular docking, with the likely mechanism being an interaction with the pump, acting as a competitive inhibitor [34].

In the ethidium bromide test with strain 1199b (Figure 3), the chalcone showed the same inhibitory activities as chlorpromazine and was better than CCCP in pump inhibition. This is possibly due to the modification of the characteristic membrane of the NorA. In the 1199B strain, a chlorpromazine-sensitive pump guarantees the existence of an efflux pump since this is the only mechanism for expelling the bromide. In a previous study [35], inhibitory activities from 117 chalcones on NorA strains and their capacity to potentiate the activity of ciprofloxacin against ethidium bromide efflux mediated by the NorA on SA1199B strains were reported. From these, only twenty chalcones inhibited the pump of the tested efflux pumps, and only three of them showed synergism. Another chalcone isolated from the plant reduced by 16 times the MIC against NCTC 8325-4 strain, which is specific to NorA [36,37]. Structural differences regarding the ligands used and their positions in the aromatic rings between the chalcones of the tests mentioned and chalcone may have been responsible for the differences found.

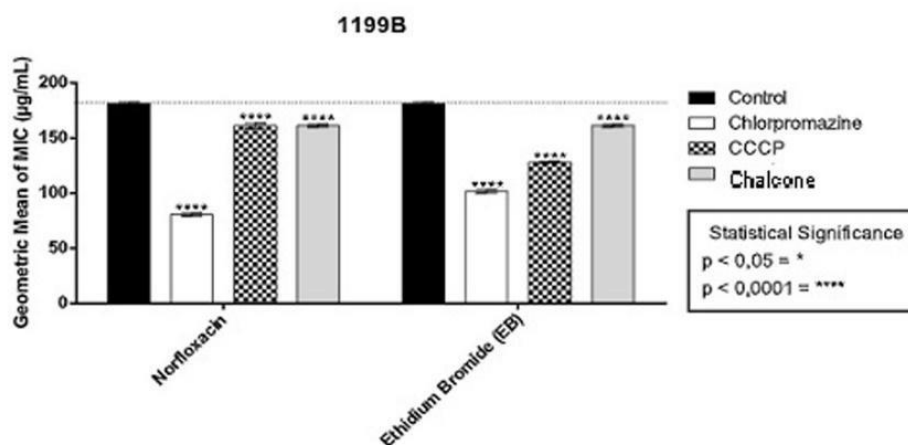


**Figure 3.** MICs of the Norfloxacin (NorA) and Ethidium Bromide (EtBr) in the absence or presence of the cinnamaldehyde chalcone, as well as, Chlorpromazine (CPZ) and Carbonylcyanide m-chlorophenyl hydrazone (CCCP) against SA1199-B (NorA).

### 3.2. Docking results.

To better understand the MepA inhibition mechanism of the chalcone, a docking essay was carried out using a MepA model. Figure 4 shows the best pose on the binding site of the MepA model. There are short contacts with residues Met142, Thr201, Phe153, Phe62, Tyr138, Leu59, and Phe280, as well as a hydrogen bond with Asn205. To verify if the chalcone could be a competitive inhibitor of the efflux pump, the ciprofloxacin molecule was docked against the same MepA model. The superposition of the best poses of ciprofloxacin and is shown in Figure 5. As can be seen from this figure, not only does the molecule bind to the same region of the binding site, it makes a hydrogen bond with the same residue as ciprofloxacin (Asn205). Ciprofloxacin also interacts with roughly the same residues as, in

particular, Tyr138 and Met 142. As such, the chalcone could surely function as a competitive inhibitor of the MepA efflux pump.

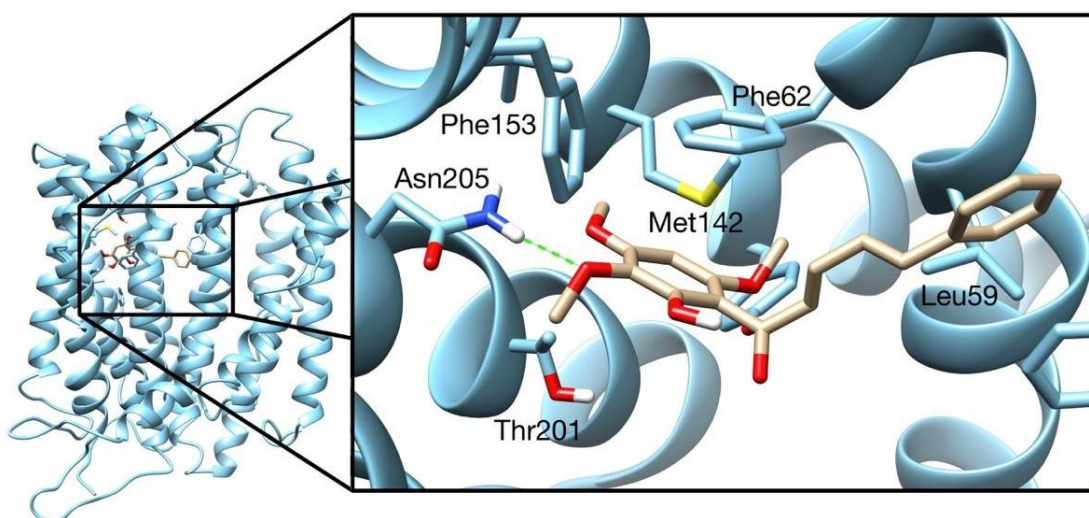


**Figure 4.** Best pose of the chalcone docked on the binding site of the MepA model. Hydrogen bonds are depicted in green.

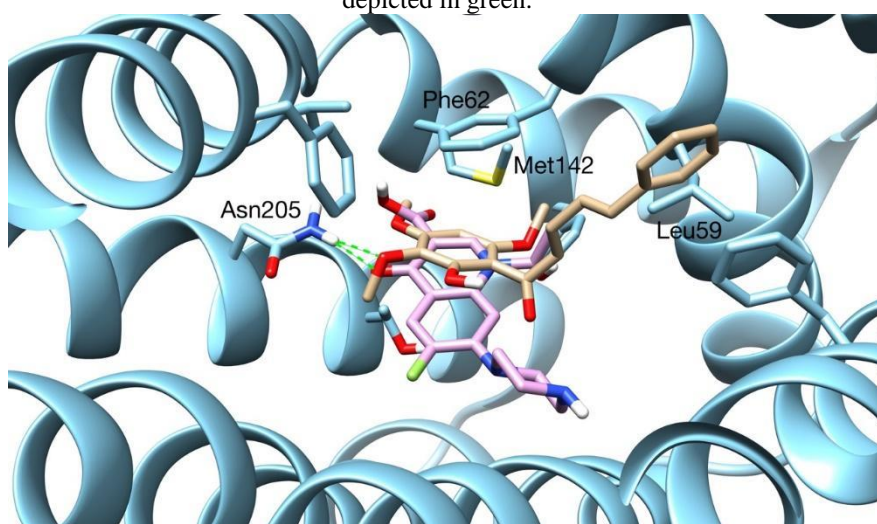


**Figure 5.** Superposition of the best poses of the chalcone (gold) and ciprofloxacin (pink).

#### 4. Conclusions

The NMR and infrared spectroscopic data contributed to the confirmation of the molecular structure of the chalcone derived from natural product 2-hydroxy-3,4,6 trimethoxy acetophenone isolated from *C. anisodontus*. The results of the microbiological tests showed that the chalcone could be used as a possible inhibitor of the Mep A efflux pump, also revealing that chalcone can be used as a base for the design of substances with antibiotic modifying activity. Although when associated with 1199B, it was able to potentiate the action of Cip against MDRS of K2068. The combined action of EPI and antibiotics as their substrates can keep a higher percentage of drugs within the cell, making existing *anti-staphylococcal* agents more effective.

#### References

1. Islam, A. A. A.; Jukka, P.M.; Celine, M.L.; Prasanna, N. *Trans*-Cinnamaldehyde Attenuates *Enterococcus faecalis* Virulence and Inhibits Biofilm Formation. *Antibiotics* **2021**, *10*, 702, <https://doi.org/10.3390/antibiotics10060702>.
2. Amalaradjou, M.A.; Narayanan, A.; Baskaran, S.A.; Venkitanarayanan, K. Antibiofilm Effect of *Trans*-cinnamaldehyde on Uropathogenic *Escherichia coli*. *J. Urol.* **2010**, *184*, 358–363, <https://doi.org/10.1016/j.juro.2010.03.006>.
3. Yuan, W.; Yuk, H.G. Effects of Sublethal Thymol, Carvacrol, and *Trans*-cinnamaldehyde Adaptation on Virulence Properties of *Escherichia coli* O157:H7. *Appl. Environ. Microbiol.* **2019**, *85*, e00271-19, <https://doi.org/10.1128/AEM.00271-19>.
4. Jia, P.; Xue, Y.J.; Duan, X.J.; Shao, S.H. Effect of Cinnamaldehyde on Biofilm Formation and *sarA* Expression by Methicillin-resistant *Staphylococcus aureus*. *Lett. Appl. Microbiol.* **2011**, *53*, 409–416, <https://doi.org/10.1111/j.1472-765X.2011.03122.x>.
5. Kot, B.; Sytykiewicz, H.; Sprawka, I.; Witeska, M. Effect of *Trans*-cinnamaldehyde on Methicillin-resistant *Staphylococcus aureus* Biofilm Formation: Metabolic Activity Assessment and Analysis of the Biofilm-associated Genes Expression. *Int. J. Mol. Sci.* **2019**, *21*, 102, <https://dx.doi.org/10.3390%2Fijms21010102>.
6. Albano, M.; Crulhas, B.P.; Alves, F.C.B.; Pereira, A.F.M.; Andrade, B.; Barbosa, L.N.; Furlanetto, A.; Lyra, L.; Rall, V.L.M.; Júnior, A.F. Antibacterial and Anti-biofilm Activities of Cinnamaldehyde against *S. epidermidis*. *Microb. Pathog.* **2019**, *126*, 231–238, <https://doi.org/10.1016/j.micpath.2018.11.009>.
7. He, Z.; Huang, Z.; Jiang, W.; Zhou, W. Antimicrobial Activity of Cinnamaldehyde on *Streptococcus mutans* Biofilms. *Front. Microbiol.* **2019**, *10*, 2241, <https://doi.org/10.3389/fmicb.2019.02241>.
8. Chang, S.T.; Chen, P.F.; Chang, S.C. Antibacterial Activity of Leaf Essential Oils and Their Constituents from *Cinnamomum osmophloeum*. *J. Ethnopharmacol.* **2001**, *77*, 123–127, [https://doi.org/10.1016/S0378-8741\(01\)00273-2](https://doi.org/10.1016/S0378-8741(01)00273-2).
9. Ferro, T.A.; Araújo, J.M.; Dos Santos Pinto, B.L.; Dos Santos, J.S.; Souza, E.B.; da Silva, B.L.; Colares, V.L.; Novais, T.M.; Filho, C.M.; Struve, C.; et al. Cinnamaldehyde Inhibits *Staphylococcus aureus* Virulence Factors and Protects against Infection in a *Galleria mellonella* Model. *Front. Microbiol.* **2016**, *7*, 2052, <https://doi.org/10.3389/fmicb.2016.02052>.
10. Ali, I.A.A.; Cheung, B.P.K.; Matinlinna, J.; Lévesque, C.M.; Neelakantan, P. *Trans*-cinnamaldehyde Potently Kills *Enterococcus faecalis* Biofilm Cells and Prevents Biofilm Recovery. *Microb. Pathog.* **2020**, *149*, 104482, <https://doi.org/10.1016/j.micpath.2020.104482>.
11. Kim, Y.G.; Lee, J.H.; Kim, S.I.; Baek, K.H.; Lee, J. Cinnamon Bark Oil and Its Components Inhibit Biofilm Formation and Toxin Production. *Int. J. Food Microbiol.* **2015**, *195*, 30–39, <https://doi.org/10.1016/j.ijfoodmicro.2014.11.028>.
12. Topa, S.H.; Subramoni, S.; Palombo, E.A.; Kingshott, P.; Rice, S.A.; Blackall, L.L. Cinnamaldehyde Disrupts Biofilm Formation and Swarming Motility of *Pseudomonas aeruginosa*. *Microbiology* **2018**, *164*, 1087–1097, <https://doi.org/10.1099/mic.0.000692>.
13. Ferro, T.A.F.; Souza, E.B.; Suarez, M.A.M.; Rodrigues, J.F.S.; Pereira, D.M.S.; Mendes, S.J.F.; Gonzaga, L.F.; Machado, M.; Bomfim, M.R.Q.; Calixto, J.B.; et al. Topical Application of Cinnamaldehyde Promotes Faster Healing of Skin Wounds Infected with *Pseudomonas aeruginosa*. *Molecules* **2019**, *24*, 1627, <https://doi.org/10.3390/molecules24081627>.
14. Maria, T.A.O.; Alexandre, M.R.T.; Henrique, D.M.C.; Irwin, R.A.M.; Diniz, M.S.; Helcio, S.S.; Bruna, .M.M.; Maria, R.J.R. A.; Paulo, N.B.; Raimundo, B.F. Identification And Modulatory Activity Assessment Of 2-Hydroxy-3,4,6-Trimethoxyacetophenone Isolated From *Croton Anisodontus* Mull. Arg.(Euphorbiaceae), *Nat. Prod. Commun.* **2014**, *9*, 665-668. <https://doi.org/10.1177/1934578X1400900520>.
15. Priscila, T.S.; Jayze, C.X.; Tiago, S.F.; Mauro, M.O.; Henrique, D.M.C.; Antonio, L.A.B.L.; Humberto, B.M.; Paulo, N.B.; Carlos, E.S.N.; Diniz, M.S.; Francisco, W.Q. A.N.; Emmanuel, S.M.; Hécio, S.S.; Alexandre, M.R T. Synthesis, Spectroscopic characterization and antibacterial evaluation by chalcones derived of acetophenone isolated from *Croton Anisodontus* Müll.Arg.. *J. Mol. Struct.* **2021**, *1226*, 129403, <https://doi.org/10.1016/j.molstruc.2020.129403>.
16. Marina, M.R.S.; Paulo, T.C.F.; Beatriz, G.C.; Thiago, S.F.; Paulo, N.B.; Hécio, S.S.; Carlos, E.S.N.; Alexandre, M.R.T.; Raimundo, L.S.P.; Jayze, C.X.; Fábía, F.C.; Cristina, R.S.B.; José, B.A.N.; Maria, M.C.S.; José, P.S.J.; Henrique, D.M.C. Aminophenyl chalcones potentiating antibiotic activity and inhibiting bacterial efflux pump. *Eur J Pharm Sci.* **2021**, *158*, 105695, <https://doi.org/10.1016/j.ejps.2020.105695>.

17. Jayze, C.X.; Francisco, W.Q.A.N.; Janaína, E.R.; Thiago, S.F.; Priscila, R.F.; Ana, C.J. A.; Priscila, T.S.; Carlos, E.S.N.; Paulo, N.B.; Márcia, M.M.; Emmanuel, S.M.; Nitin, K.; Antônio, C.H.B.; Henrique, D.M.C.; Murilo, S.S.J.; Hélcio, S.S.; Alexandre, M.R.T. Spectroscopic Analysis By NMR, Ft-Raman, ATR-FTIR, And UV-Vis, Evaluation of antimicrobial activity, and in silico studies of chalcones derived From 2-Hydroxyacetophenone. *J. Mol. Struct* **2021**, *1241*, 130647, <https://doi.org/10.1016/j.molstruc.2021.130647>.
18. Antonio, L.A.B.L.; Priscila, T.S.; Matheus, N.R.; Emanuelle, M.M.; Emmanuel, S.M.; Márcia, M.M.; Paulo, N. B.; Carlos, E.S.N.; Humberto, M.B.; Alexandre, M.R.T.; Hélcio, S.S. Potentiating activity of Norfloxacin by synthetic chalcones against NorA overproducing *Staphylococcus aureus*. *Microb. Pathog*, **2021**, *155*, 104894, <https://doi.org/10.1016/j.micpath.2021.104894>.
19. Javier, A.I.H.; Rodolfo, G.B.; Didier, N.R.; José, G.G.E.; David, A. M.J.; Alejandro, M.Z.; Tonatiuh, A.C.S.; Nelly, T.B.; Ricardo, A.L.M. Novel Compounds Based on Chalcone- and Pyrazoline-DIM Hybrids as Inhibitors of *Staphylococcus aureus*, Synthesis, DFT Studies, Biological Evaluation and Docking Studies *J. Mol. Struct* **2022**, *1249*, 131499, <https://doi.org/10.1016/j.molstruc.2021.131499>.
20. Magaly, G.A.; Raoni, S.B.G.; Camilo, H.S.L.; Fernanda, L.A.M.; Sérgio, P. M.; Laudicéa, N.O.; Talis, U.S.; Solange, M.S.V.W. Crystal structures, DFT calculations and Hirshfeld surface analysis of two (*E*)-3-(aryl)-1-(naphthalen-1-yl)prop-2-en-1-one chalcone derivatives, potential *Mycobacterium tuberculosis* Enoyl ACP reductase (InhA) inhibitors and optical materials: conformational differences within the prop-2-en-1-one unit. *J. Mol. Struct* **2021**, *146*, 131091, <https://doi.org/10.1016/j.molstruc.2020.128652>.
21. Poonam, R.; Singh, R.N.; Alok, R.; Anshu, G.; Sweta, T.; Mukesh, K. Study of antimicrobial and antioxidant activities of pyrrole-chalcones. *J. Mol. Struct* **2021**, *1228*, 129483, <https://doi.org/10.1016/j.molstruc.2020.129483>.
22. Rizwan, A.; Manish, R.; Shama, Y.; Amaduddin.; Shahzad, K.; Mohammad, A.; Khan, M.S.; Rahisuddin. Facile synthesis of chalcone derivatives as antibacterial agents: Synthesis, DNA binding, molecular docking, DFT and antioxidant studies. *J. Mol. Struct* **2020**, *1208*, 127905, <https://doi.org/10.1016/j.molstruc.2020.127905>.
23. Elecia, J.H.; Susan, J.B.; Pauline, G.; Michel, C.; Jonh, P.C. Ferrocenyl chalcone derivatives as possible antimicrobial agents, *J. Antibiot.* **2020**, *73*, 299–308, <https://doi.org/10.1038/s41429-020-0280-y>.
24. Twinkle, A.R.; Leenaraj, D.R.; Zoran, R.; Arunsasi, B.S.; Bright, K.C.; Reshma. R. Ferrocenyl chalcone derivative (E)-3-(2-methylpyrimidin-5-yl)-1-ferroceynprop-2-en-1-one: Synthesis, Structural analysis, Docking study and their Antibacterial evaluation. *J. Mol. Struct* **2020**, *1210*, 128049, <https://doi.org/10.1016/j.molstruc.2020.128049>.
25. Marwa, N.N.; Tarek, A.F.; Saleh, A.; Mohammed, M.E.; Doaa, F.D.; Fathy, H. Multi-sensing response, molecular docking, and anticancer activity of donor–acceptor chalcone containing phenanthrene and thiophene moieties. *J. Mol. Struct* **2021**, *1240*, 130581, <https://doi.org/10.1016/j.molstruc.2021.130581>.
26. Nirmala, G.; Kumar, E. P.; Prashanth, K.K.; Shravani, P.; Sree, K.S.; Subhashini, N.J.P. Synthesis, biological evaluation and molecular docking studies of novel 1,2,3-triazole tethered chalcone hybrids as potential anticancer agents. *J. Mol. Struct* **2020**, *1217*, 128356, <https://doi.org/10.1016/j.molstruc.2020.128356>.
27. Chen, Yau-Hung.; Wei-Hua, Wang.; Yun-Hsin, Wang.; Zi-Yu, Lin.; Chi-Chung, Wen.; Ching-Yuh, Chern. Evaluation of the anti-inflammatory effect of chalcone and chalcone analogues in a zebrafish model. *Molecules* **2013**, *18*, 2052-2060, <https://doi.org/10.3390/molecules18022052>.
28. Taofeek, O.A.; Musa, T.Y.; Adenike, T.O.; Electrophilic And Reactive Oxygen Species Detoxification Potentials Of Chalcone Dimers Is Mediated By Redox Transcription Factor Nrf-2, *J. Biochem. Mol. Toxicol.* **2014**, *28*, 11-22, <https://doi.org/10.1002/jbt.21517>.
29. Waterhouse, A.; Bertoni, M.; Bienert, S.; Studer, G.; Tauriello, G.; Gumienny, R.; Heer, F.T.; de Beer, T.A.P.; Rempfer, C.; Bordoli, L.; Lepore, R.; Schwede, T. () SWISS-MODEL: homology modelling of protein structures and complexes. *Nucleic Acids Res.* **2018**, *46*, 296-303, <https://doi.org/10.1093/nar/gky427>.
30. Trott, O.; Olson, A.J. AutoDock Vina: Improving the speed and accuracy of docking with a new scoring function, efficient optimization, and multithreading. *J Comput Chem* **2010**, *31*, 455-461, <https://doi.org/10.1002/jcc.21334>.
31. Kaatz, G.W.; Moudgal, V.V.; Seo, S.M.; Kristiansen, J.E. Phenothiazines and Thioxanthenes Inhibit Multidrug Efflux Pump Activity in *Staphylococcus aureus*. *Antimicrob. Agents Chemother.* **2003**, *47*, 719, <https://doi.org/10.1128/AAC.47.2.719-726.2003>.

32. Lima, W.G.; Ramos-Alves, M.C.; Soares, A.C. Dos distúrbios psiquiátricos à antibioticoterapia: reposicionamento da clorpromazina como agente antibacteriano. *Rev. Colomb. Cienc. Quím. Farm.*, **2019**, *48*, 5-28. <https://doi.org/10.15446/rcciquifa.v48n1.80062>.
33. Francoise, V.B.; Jean-Marie, P.; Ving, J.L. Inhibitors of Bacterial Efflux Pumps as Adjuvants in Antibiotic Treatments and Diagnostic Tools for Detection of Resistance by Efflux. *Recent Pat Antiinfect Drug Discov.* **2006**, *1*, 157-175. <https://doi.org/10.2174/15748910677452692>.
22. Wei, P.; Kaatz, G.W.; Kerns, R.J. Structural differences between paroxetine and femoxetine responsible for differential inhibition of *Staphylococcus aureus* efflux pumps. *Bioorg Med Chem Lett* **2004**, *14*, 3093-3097. <https://doi.org/10.1016/j.bmcl.2004.04.018>.
34. Wei, H.; Zhang, X.; Wu, G.; Yang, X.; Pan, S.; Wang, Y.; Ruan, J. Chalcone derivatives from the fern *Cyclosorus parasiticus* and their anti-proliferative activity. *Food Chem. Toxicol.* **2013**, *60*, 147-152. <https://doi.org/10.1016/j.fct.2013.07.045>.
35. Holler, J.G.; Slotved, H-C.; Mølgaard, P.; Olsen, C.E.; Christensen, S.B. Chalcone inhibitors of the NorA efflux pump in *Staphylococcus aureus* whole cells and enriched everted membrane vesicles. *Bioorg. Med. Chem.* **2012**, *20*, 4514-4521. <https://doi.org/10.1016/j.bmc.2012.05.025>.
36. Belofsky, G.; Percivill, D.; Lewis, K.; Tegos, G.P.; Ekart, J. Phenolic Metabolites of *Dalea versicolor* that Enhance Antibiotic Activity against Model Pathogenic Bacteria. *J. Nat. Prod.* **2004**, *67*, 481-484. <https://doi.org/10.1021/np030409c>.
37. Rezende-Júnior, L.M.; Andrade, L.M.d.S.; Leal, A.L.A.B.; Mesquita, A.B.d.S.; Santos, A.L.P.d.A.d.; Neto, J.d.S.L.; Siqueira-Júnior, J.P.; Nogueira, C.E.S.; Kaatz, G.W.; Coutinho, H.D.M.; Martins, N.; da Rocha, C.Q.; Barreto, H.M. Chalcones Isolated from *Arrabidaea brachypoda* Flowers as Inhibitors of NorA and MepA Multidrug Efflux Pumps of *Staphylococcus aureus*. *Antibiotics* **2020**, *9*, 351. <https://doi.org/10.3390/antibiotics9060351>.

**Article 5** Spectroscopic analysis by NMR, FT-Raman, ATR-FTIR, and UV-Vis, evaluation of antimicrobial activity, and *in silico* studies of chalcones derived from 2-hydroxyacetophenone.

Authors: Jayze da Cunha Xavier<sup>a</sup> Francisco W.Q.de Almeida-Neto<sup>b</sup> Janaína e Rocha<sup>a</sup> Thiago S. Freitas<sup>a</sup> Priscila R. Freitas<sup>a</sup> Ana C.J. de Araújo<sup>a</sup> Priscila T. da Silva<sup>a</sup> Carlos E.S. Nogueira<sup>ac</sup> Paulo N. Bandeira<sup>d</sup> Márcia M. Marinho<sup>e</sup> Emmanuel S. Marinho<sup>f</sup> Nitin Kumar<sup>g</sup> Antônio C.H. Barreto<sup>h</sup> Henrique D.M.Coutinho<sup>a</sup> Murilo S.S.Julião<sup>b</sup> Hécio S. dos Santos<sup>ad</sup> Alexandre M.R. Teixeira<sup>ac</sup>

Journal / link / Qualis *Journal of Molecular Structure*, /

<https://doi.org/10.1016/j.molstruc.2021.130647> / Qualis B2 in the biological sciences II. IF = 3.841

Situation: Published

## Resumo:

Seis 2'-hidroxichalconas foram sintetizadas e caracterizadas por RMN, FT-Raman, ATR-FTIR e UV-Vis. Essas chalconas isoladas e em combinação com antibióticos ciprofloxacina, penicilina e eritromicina foram testadas contra cepas multirresistentes de *Staphylococcus aureus*. Também foi verificado por estudos *in vitro* e *in silico* a capacidade dessas chalconas em inibir a bomba de efluxo NorA. Os valores de MICs da ciprofloxacina foram reduzidos na presença de todas as chalconas testadas. Para o antibiótico norfloxacina, as chalconas A1, A4, A5 e A6 promoveram a redução nos valores de CIM. A chalcona A2 foi a única a reduzir os valores de CIM quando associada à penicilina. Nenhuma chalcona foi capaz de reduzir os valores de CIM quando associada à eritromicina. Esses resultados indicam que os efeitos sinérgicos demonstrados para as chalconas sintetizadas foram influenciados pela introdução de um anel furânico (A1), um átomo de cloro e um grupo metoxi na posição C4 (A2 e A4), uma segunda ligação dupla (A5), e um átomo de flúor na posição C2 (A6). A análise do



ADMET prevê que as chalconas A2, A3, A5 e A6 apresentam maior permeabilidade celular. A região nucleofílica torna a chalcona A5 capaz de se ligar covalentemente às proteínas plasmáticas, e a presença de substituições aromáticas oxigenadas torna as chalconas A1 e A4 mais solúveis em água e, conseqüentemente, mais fáceis de excretar. Por outro lado, a substituição do grupo metoxi da chalcona A4 a torna mais suscetível a reações de O-desmetilação pela isoenzima CYP3A4. A ancoragem molecular revelou que todas as seis chalconas podem dificultar a ligação da norfloxacin a bomba de efluxo NorA.

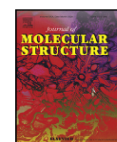
Journal of Molecular Structure 1241 (2021) 130647



Contents lists available at ScienceDirect

Journal of Molecular Structure

journal homepage: [www.elsevier.com/locate/molstr](http://www.elsevier.com/locate/molstr)



Spectroscopic analysis by NMR, FT-Raman, ATR-FTIR, and UV-Vis, evaluation of antimicrobial activity, and *in silico* studies of chalcones derived from 2-hydroxyacetophenone



Jayze da Cunha Xavier<sup>a</sup>, Francisco W.Q. de Almeida-Neto<sup>b</sup>, Janaína E. Rocha<sup>a</sup>, Thiago S. Freitas<sup>a</sup>, Priscila R. Freitas<sup>a</sup>, Ana C.J. de Araújo<sup>a</sup>, Priscila T. da Silva<sup>a</sup>, Carlos E.S. Nogueira<sup>a,c</sup>, Paulo N. Bandeira<sup>d</sup>, Márcia M. Marinho<sup>e</sup>, Emmanuel S. Marinho<sup>f</sup>, Nitin Kumar<sup>g</sup>, Antônio C.H. Barreto<sup>h</sup>, Henrique D.M. Coutinho<sup>a</sup>, Murilo S.S. Julião<sup>b</sup>, Hércio S. dos Santos<sup>a,d</sup>, Alexandre M.R. Teixeira<sup>a,c,\*</sup>

## CHAPTER 9 - Spectroscopic analysis by NMR, FT-Raman, ATR-FTIR, and UV-Vis, evaluation of antimicrobial activity, and *in silico* studies of chalcones derived from 2-hydroxyacetophenone

Jayze da Cunha Xavier<sup>a</sup>, Francisco W.Q. de Almeida-Neto<sup>h</sup>, Janaina E. Rocha<sup>a</sup>, Thiago S. Freitas<sup>a</sup>, Priscila R. Freitas<sup>a</sup>, Ana C.J. de Araújo<sup>a</sup>, Priscila.T. da Silva<sup>b</sup>, Carlos E.S. Nogueira<sup>a,d</sup>, Paulo N. Bandeira<sup>b</sup>, Marcia M. Marinho<sup>e</sup>, Emmanuel S. Marinho<sup>f</sup>, Nitin Kumar<sup>c</sup>, Antonio C.H. Barreto<sup>g</sup>, Henrique D.M. Coutinho<sup>a</sup>, Murilo S.S. Julião<sup>b</sup>, Hércio S. dos Santos<sup>a,b</sup>, Alexandre M.R. Teixeira<sup>a,d3\*</sup>

<sup>a</sup> Department of Biological Chemistry, Regional University of Cariri, CE, Brazil.

<sup>b</sup> Center for Exact Sciences and Technology, Chemistry Course, Vale do Acaraú University, Sobral, CE, Brazil.

<sup>c</sup> KR Mangalan University, Sohna Road, Gurugram, India

<sup>d</sup> Department of Physics, Regional University of Cariri, Juazeiro do Norte, CE, Brazil

<sup>e</sup> State University of Ceará, Faculty of Education, Science and Letters of Iguatu Iguatu, CE, Brazil.

<sup>f</sup> State University of Ceará, Faculty of Philosophy Dom Aureliano Matos, Limoeiro do Norte, CE, Brazil

<sup>g</sup> Department of Physics, Federal University of Ceará, Fortaleza, CE, Brazil.

<sup>h</sup> Department of Analytical Chemistry and Physical Chemistry, Federal University of Ceará, Fortaleza, CE, Brazil

**Abstract**

Six 2'-hydroxychalcones were synthesized, and characterized by NMR, FT-Raman, ATR-FTIR, and UV-Vis. These chalcones alone and in combination with the ciprofloxacin, penicillin, and erythromycin antibiotics were tested against multiresistant strains of *Staphylococcus aureus*. It was also verified, *in vitro* and *in silico* their capacity to inhibit the NorA efflux pump. The MICs values of ciprofloxacin were reduced in the presence of all tested chalcones. For norfloxacin antibiotic the chalcones A1, A4, A5 and A6 promoted the reduced in the MIC values. The A2 chalcone was the only one to reduce the MIC values when associated with penicillin. Any chalcones were not able to reduce MIC values when associated with erythromycin. These results indicate that the modulating effect demonstrated by synthesized chalcones were influenced by introduction of a furanic ring (A1), chlorine atom and methoxy group at C4 position (A2 and A4), a second double bond (A5), and a fluorine atom at C2 position (A6). The ADMET analysis predicts that the chalcones A2, A3, A5 and A6 have easier cell permeation. The nucleophilic region makes the A5 chalcone capable of covalently bonding with plasma proteins, and the presence of oxygenated aromatic substitutions makes the A1 and A4 more water-soluble and consequently easier to excretion. On the other hand, the substitution of the methoxy group of A4 chalcone makes it more susceptible to O-demethylation reactions by the CYP3A4 isoenzyme. The molecular docking revealed that all six chalcones could hinder the binding of norfloxacin to the NorA efflux pump.

**Keywords:** Chalcones; Spectroscopy; ADMET; Antimicrobial activity; Efflux pump.

## 1. Introduction

The prevalence of bacteria resistant to antibiotics has increased dramatically in recent years. The infections caused by multidrug-resistant bacteria are estimated to cause approximately 700,000 deaths per year, and they will rise to ten million lives annually by 2050 [1]. Due to the emergence and spread of multidrug-resistant strains, the treatment of *staphylococcal* infections with traditionally used antibiotics, such as penicillin and cephalosporin, has become ineffective [2]. Despite the effectiveness of vancomycin against multidrug-resistant strains of *S. aureus*, this antibiotic has some limitations, such as toxicity and poor absorption [3]. Fluoroquinolones such as norfloxacin and ciprofloxacin have been used as a therapeutic alternative against multidrug-resistant *S. aureus*, however, resistance to these antibiotics has been reported frequently [4, 5]. This unbridled growth of bacterial resistance has become a serious problem of current medicine, which triggered the search for new therapeutic agents [6].

Resistance mediated by efflux pumps is one of the most prevalent mechanisms in multi-resistant bacteria, which has aroused the interest of several researchers in the search for possible efflux pump inhibitors [7, 8]. In view of the aforementioned considerations, it is important that new strategies, such as the synthesis of new compounds, which can be made available as a viable strategy in antimicrobial therapy.

Chalcones are group of naturally occurring compound, precursors of flavonoids and important constituents of natural product such as fruits, vegetables, spices, and tea. Chemically chalcones have two aromatic rings linked by highly electrophilic three-carbon  $\alpha,\beta$ -unsaturated carbonyl system. The conjugated double bonds and a completely delocated  $\pi$ -electron system present in chalcones showed relatively low redox potentials and a greater probability of undergoing electron transfer reactions. Recently, studies have shown different pharmacological activities for chalcones, such as antimicrobial, antioxidant, antinociceptive, antiparasitic, antitumor, analgesic, antidepressant, antiviral, anticonvulsant, antidiabetic, anti-inflammatory, neuroprotective, and anxiolytic activities [7, 8].

Finding novel substances able to reverse the antimicrobial resistance mechanisms is a challenge. It is known that chalcones derived from 2-hydroxyacetophenone had already presented potential antimicrobial [9-12], and like inhibitors of efflux pumps [13-15]. Considering that this compound class can contribute to the control of bacterial resistance, we carried out the synthesis of six 2'-hydroxychalcones. They were chosen by presenting similarity structural to understand how these molecules can modify their structural, vibrational, and electronic properties, as well as, the substitution of heteroatoms, in-ring B alter the potential antimicrobial and the efflux pump mechanism of them.

## 2. Materials and methods

### 2.1 General

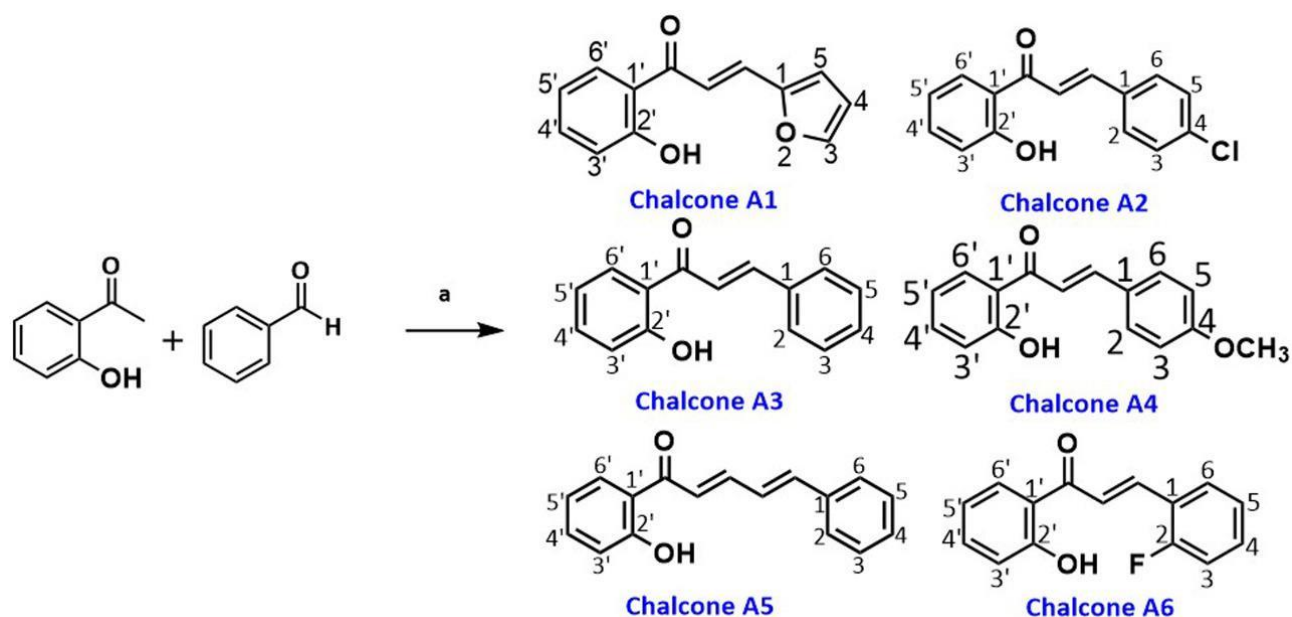
All the chemicals used were of analytical grade and purchased from Sigma-Aldrich. The chlorpromazine (CPZ), carbonyl cyanide *m*-chlorophenylhydrazone (CCCP), ethidium bromide (EB), ciprofloxacin (CIP), norfloxacin (NOR), penicillin (PEN), erythromycin (ERI) were obtained from Sigma Aldrich Co. Ltd.  $^1\text{H}$  and  $^{13}\text{C}$  NMR spectra were obtained using Bruker DRX 500 MHz, operating at a frequency of 500 MHz for hydrogen, and 125 MHz for carbon, respectively. The spectra were measured in  $\text{CDCl}_3$  solvent, and chemical shifts are reported as  $\delta$  values in parts per million (ppm). FT-Raman spectra were taken using a Bruker RFS100/S FTR system and a D418-T detector, with the sample excited by means of the 1064 nm line of a Nd: YAG laser. The infrared spectra were measured by Attenuated Total Reflectance Fourier Transform Infrared spectroscopy (ATR-FTIR) using a Bruker vacuum spectrometer, model VERTEX 70V with a HeNe laser source with 633 nm wavelength. The UV-Visible (UV-Vis) absorption spectrum of the compound was obtained using a GENESYS 10S UV-Vis spectrophotometer (Thermo Scientific, Waltham, MA, USA) in the wavelength range of 190 to 500 nm.

Density Functional Theory (DFT) calculations using the Gaussian 09 software [16] with the hybrid density functional B3LYP method with 6-311++ G(d,p) basis set were carried out to obtain the vibrational wavenumbers to help interpret the experimental vibrational spectra, and also to obtain the frontier molecular orbitals [lowest unoccupied molecular orbital (LUMO) and highest occupied molecular orbital (HOMO)], to determinate the quantum chemical parameters of the chalcones A1-A6. Time-Dependent-DFT method was used to compute the electronic transition and the UV-Vis spectrum at the same level of theory with ethanol as implicit solvent.

### 2.2 Synthesis of chalcones

The procedure description of the synthesis chalcones chalcone is shown in Scheme 1. These chalcones were synthesized by Claisen-Schmidt condensation reaction. Equimolar quantities of 2-hydroxycetophenone (2 mmoles) and the appropriate benzaldehyde and the derivatives (2 mmoles) were dissolved in ethanol (15 mL). To this mixture, ten drops of 50% w/v aq. NaOH was added with stirring dropwise, and the reaction mixture was left for 48 h at room temperature. Later it resulted in the precipitation of chalcones (A1-A6). These chalcones were then filtered under reduced pressure, washed with cold water, dried, and recrystallized from ethanol, and then purity is checked by single spot on TLC. The structural data of the six 2'-hydroxychalcones which were synthesized in this work are given below. As seen, these chalcones possess the trans form. Chalcones may exist in two isomeric forms, E (trans) or Z (cis). The E-isomer is the

thermodynamically most stable form in most cases [17]. It is clearly known that there are differences in the structural conformations of chalcones, especially between some of their dihedral



Scheme 1. Scheme of the synthesis of the chalcones (A1–A6)

### 2.2.1 (*E*)-3-(furan-2-yl)-1-(2-hydroxyphenyl)prop-2-en-1-one (A1)

Yield 88%; m.p. 186–188°C; IR (KBr,  $\text{cm}^{-1}$ ): 1638 (C=O str.), 1581 (C=C str. of Ar), 1554 (CH=CH), 3129 (Ar C-H str.), 1214 (O-H bend), 1337 (C-O str. Phenol), 1258 (C-O str., furfuryl);  $^1\text{H}$  NMR (500 MHz,  $\text{CDCl}_3$ , ppm): 7.56 (1H, d,  $J=14$  Hz, -CO-CH=), 8.00 (1H, d,  $J=15.6$  Hz, =CH-furyl), 7.54–7.79 (4H, m, Ar-H), 7.10 (1H, d,  $J=8.4$  Hz, -CH=), 7.02 (1H, t,  $J=7.5$  Hz, -CH=), 8.00 (1H, d,  $J=11.2$  Hz, -CH=), 6.85 (1H, d,  $J=3.4$  Hz, -CH=, furyl), 6.62 (1H, dd,  $J=8.3, 2.6$  Hz, -CH=, furyl), 5.35 (1H, s, -OH);  $^{13}\text{C}$  NMR (100 MHz,  $\text{CDCl}_3$ , ppm): 151.6 (C-1 and C-2), 112.9 (C-3), 117.1 (C-4), 145.4 (C-5), 120.1 (C-1'), 163.6 (C-2'), 117.6 (C-3'), 131.2 (C-4'), 118.8 (C-5'), 129.6 (C-6'), 193.4 (C=O), 118.5 ( $\text{C}_\alpha$ ), 136.1 ( $\text{C}_\beta$ ).

### 2.2.2 (*E*)-3-(4-chlorophenyl)-1-(2-hydroxyphenyl)prop-2-en-1-one (A2)

Yield 85%; m.p. 237–239°C; IR (KBr,  $\text{cm}^{-1}$ ): 1691 (C=O str.), 1563 (C=C str. of Ar), 1511 (CH=CH), 3059 (Ar C-H str.), 1203 (O-H bend., phenol), 1366 (C-O str. Phenol), 1619 (C=C str., alkene) 756 (C-Cl str., p-chlorophenyl);  $^1\text{H}$  NMR (500 MHz,  $\text{CDCl}_3$ , ppm): 7.59 (1H, d,  $J=15.5$  Hz, -CO-CH=), 7.95 (1H, d,  $J=15.5$  Hz, =CH-phenyl), 7.66–7.73 (4H, m, Ar-H), 7.12 (1H, d,  $J=8.3$  Hz, -CH=), 7.03 (1H, t,  $J=7.5$  Hz, -CH=), 8.00 (1H, d,  $J=11.2$  Hz, -CH=), 7.49 (1H, d,  $J=8.5$  Hz, -CH=, C-2 of chlorophenyl), 7.58 (1H, d,  $J=8.5$  Hz, -CH=, C-3 of chlorophenyl), 5.36 (1H, s, -OH);  $^{13}\text{C}$  NMR (125 MHz,  $\text{CDCl}_3$ , ppm): 133.2 (C-1), 129.4 (C-2 and C-6), 129.8

(C-3 and C-5), 136.9 (C-4), 120.6 (C-1'), 163.6 (C-2'), 119.9 (C-3'), 136.5 (C-4'), 118.7 (C-5'), 129.6 (C-6'), 193.5 (C=O), 118.9 (C<sub>α</sub>), 143.9 (C<sub>β</sub>).

### 2.2. 3 (*E*)-1-(2-hydroxyphenyl)-3-phenylprop-2-en-1-one (A3)

Yield 78%; m.p. 195–197°C; IR (KBr, cm<sup>-1</sup>): 1689 (C=O str.), 1570 (C=C str. of Ar), 1485 (CH=CH), 3060 (C-Hstr., Ar), 1201 (O-H bend., phenol), 1338 (C-O str. Phenol), 1636 (C=C str., alkene); <sup>1</sup>H NMR (500 MHz, CDCl<sub>3</sub>, ppm): 7.60 (1H, d, J= 15.5 Hz, -CO-CH=), 8.02 (1H, d, J= 15.6 Hz, =CH-phenyl), 7.72–7.78 (2H, m, Ar-H), 7.59–7.61 (2H, m, Ar-H), 7.02 (1H, t, J= 7.6 Hz, -CH=), 8.02 (1H, d, J= 8.2 Hz, -CH=), 7.53 (1H, m, -CH=, phenyl), 7.12 (1H, m, Ar-H), 7.13 (1H, m, Ar-H), 5.35 (1H, s, -OH); <sup>13</sup>C NMR (125 MHz, CDCl<sub>3</sub>, ppm): 134.7 (C-1), 129.0 (C-2 and C-6), 129.7 (C-3 and C-5), 136.4 (C-4), 120.2 (C-1'), 163.6 (C-2'), 120.0 (C-3'), 136.2 (C-4'), 118.7 (C-5'), 130.9 (C-6'), 193.8 (C=O), 118.9 (C<sub>α</sub>), 145.4 (C<sub>β</sub>).

### 2.2. 4 (*E*)-1-(2-hydroxyphenyl)-3-(4-methoxyphenyl)prop-2-en-1-one (A4)

Yield 75%; m.p. 240–242°C; IR (KBr, cm<sup>-1</sup>): 1683 (C=O str.), 1555 (C=C str. of Ar), 1488 (CH=CH), 3020 (C-Hstr., Ar), 2989 (C-H str., OCH<sub>3</sub>), 1198 (O-H bend., phenol), 1340 (C-O str. Phenol), 1630 (C=C str., alkene); <sup>1</sup>H NMR (500 MHz, CDCl<sub>3</sub>, ppm): 7.54 (1H, d, J= 15.5 Hz, -CO-CH=), 7.91 (1H, d, J= 15.6 Hz, =CH-phenyl), 3.87 (3H, s, OCH<sub>3</sub>), 6.94–7.04 (1H, m, Ar-H), 7.49–7.57 (1H, m, Ar-H), 7.88–7.93 (1H, m, Ar-H), 7.02 (1H, d, J= 8.3 Hz, -CH=, Ar-H), 7.64 (2H, d, J= 8.7 Hz, -CH=, phenyl), 6.92 (1H, d, -CH=, phenyl), 5.38 (1H, s, -OH); <sup>13</sup>C NMR (125 MHz, CDCl<sub>3</sub>, ppm): 129.7 (C-1), 127.5 (C-2 and C-6), 114.7 (C-3 and C-5), 162.2 (C-4), 120.3 (C-1'), 163.7 (C-2'), 117.8 (C-3'), 136.3 (C-4'), 118.7 (C-5'), 130.7 (C-6'), 193.8 (C=O), 118.9 (C<sub>α</sub>), 145.5 (C<sub>β</sub>).

### 2.2. 5 (2*E*, 4*E*)-1-(2-hydroxyphenyl)-5-phenylpenta-2,4-dien-1-one (A5)

Yield 82%; m.p. 212–214°C; IR (KBr, cm<sup>-1</sup>): 1674 (C=O str.), 1562 (C=C str. of Ar), 1488 (CH=CH), 3052 (C-Hstr., Ar), 1228 (O-H bend., phenol), 1370 (C-O str. Phenol), 1633 (C=C str., alkene); <sup>1</sup>H NMR (500 MHz, CDCl<sub>3</sub>, ppm): 7.70 (1H, d, J= 14.7 Hz, -CO-CH=), 7.72 (1H, d, J= 14.1 Hz, =CH-), 7.37 (1H, d, J= 15.6 Hz, -CH=), 7.40 (1H, d, J= 14.8 Hz, =CH-phenyl), 7.03 (1H, d, J= 8.5 Hz, Ar-H), 7.46–7.51 (1H, m, Ar-H), 6.93 (1H, t, J= 8.1 Hz, Ar-H), 7.83–7.86 (1H, m, Ar-H), 7.52 (2H, d, J= 7.5 Hz, -CH=, Ar-H), 7.38 (2H, d, J= 7.4 Hz, -CH=), 7.43 (1H, m, -CH=, phenyl), 5.31 (1H, s, -OH); <sup>13</sup>C NMR (125 MHz, CDCl<sub>3</sub>, ppm): 136.4 (C-1), 127.6 (C-2 and C-6), 129.6 (C-3 and C-5), 129.7 (C-4), 120.2 (C-1'), 163.7 (C-2'), 118.7 (C-3'), 136.1 (C-4'), 118.9 (C-5'), 129.6 (C-6'), 193.9 (C=O), 127.3 (C<sub>α</sub>), 145.7 (C<sub>β</sub>), 127.0 (C<sub>α</sub>), 143.1 (C<sub>β</sub>).

## 2.2. 6 (*E*)-3-(2-fluorophenyl)-1-(2-hydroxyphenyl)prop-2-en-1-one (A6)

Yield 91%; m.p. 237–239°C; IR (KBr,  $\text{cm}^{-1}$ ): 1692 (C=O str.), 1564 (C=C str. of Ar), 1484 (CH=CH), 3042 (C-Hstr., Ar), 1203 (O-H bend., phenol), 1365 (C-O str. Phenol), 1639 (C=C str., alkene), 1296 (C-F str., fluorophenyl);  $^1\text{H}$  NMR (500 MHz,  $\text{CDCl}_3$ , ppm): 7.77 (1H, d,  $J=15.6$  Hz, -CO-CH=), 8.00 (1H, d,  $J=15.6$  Hz, =CH-phenyl), 7.03 (1H, d,  $J=8.4$  Hz, Ar-H), 7.49 (1H, t,  $J=7.1$  Hz, Ar-H), 6.96 (1H, t,  $J=8.0$  Hz, Ar-H), 7.91 (1H, d,  $J=8.0$  Hz, Ar-H), 7.62-7.68 (1H, m, -CH=, Ar-H), 7.39-7.42 (1H, m, Ar-H), 7.21-7.24 (1H, m, Ar-H), 7.15-7.18 (1H, m, Ar-H), 5.30 (1H, s, -OH);  $^{13}\text{C}$  NMR (125 MHz,  $\text{CDCl}_3$ , ppm): 123.0 (C-1), 160.3 (C-2), 116.4 (C-3), 130.3 (C-4), 124.7 (C-5), 120.3 (C-6), 120.1 (C-1'), 163.8 (C-2'), 118.8 (C-3'), 136.7 (C-4'), 119.1 (C-5'), 129.9 (C-6'), 193.9 (C=O), 124.8 ( $\text{C}_\alpha$ ), 138.4 ( $\text{C}_\beta$ ).

## 2.3. Antimicrobial Activity

Multi-resistant and standard *S. aureus* strains RN4220, K4414, 1199B, and K2068 were used in both the direct and modulatory antibacterial activity assays. The antibiotics Eritromicin, Penicillin, Norfloxacin, and Ciprofloxacin, were used. The antibiotics were first dissolved in dimethyl sulfoxide (DMSO), and then further dilution was carried in sterile water (concentration of 1024  $\mu\text{g}/\text{mL}$ ). CPZ and ethidium bromide (EB) solutions were dissolved in distilled, sterile water, stored at  $-20^\circ\text{C}$ , and kept protected from light (concentration of 1024  $\mu\text{g}/\text{mL}$ ). The CCCP was dissolved in methanol/water (1:1, v/v) and stored at  $-20^\circ\text{C}$  (concentration of 1024  $\mu\text{g}/\text{mL}$ ). All the strains were obtained from cultures grown at the Laboratory of Microbiology and Molecular Biology (LMBM) of the Regional University of Cariri (URCA).

### 2.3.1 Antibacterial Activity Test by Minimum Inhibitory Concentration (MIC)

The MIC of the efflux pump inhibitors, ethidium bromide, was determined in a microdilution assay utilizing 100  $\mu\text{L}$  of each suspended bacterial inoculum in saline solution, corresponding to 0.5 of the McFarland scale, followed by the addition of 900  $\mu\text{L}$  of brain heart infusion (BHI) in eppendorfs. Then they were transferred to 96-well microliter plates, and serial dilutions of each substance were performed with concentrations ranging from 0.5 to 512  $\mu\text{g}/\text{mL}$  (1:1). The plates were incubated at  $37^\circ\text{C}$  for 24 h, and bacterial growth was assessed by the use of resazurin. The MIC was defined as the lowest concentration in which no growth can be observed, according to CLSI [19]. The antibacterial assays were performed in triplicates, and results were expressed as an average of replicates.

### 2.3.2. Evaluation of Efflux Pump Inhibition by MIC Reduction

The inhibition of the efflux pump was tested using a sub-inhibitory concentration of EPIs (MIC/8). 150 $\mu$ L of each suspended bacterial inoculum in saline solution, corresponding to 0.5 of the McFarland scale, were added to eppendorfs together with 1350 $\mu$ L of brain heart infusion (BHI) as a control. In tests, 150  $\mu$ L of each suspended bacterial inoculum in saline solution, corresponding to 0.5 of the McFarland scale, were added together with EPIs (efflux pump inhibitors) (MIC/8) and completed with brain heart infusion (BHI). These were then transferred to 96-well microtiter plates, and 100  $\mu$ L of the antimicrobial drug and EB serial dilutions were performed (1:1). The plates were incubated at 37°C for 24 h, and bacterial growth was assessed by the use of resazurin. MIC was defined with the concentrations of antibiotics and EB ranging between 0.5 to 512  $\mu$ g/mL. The MIC of controls were assessed using the antibiotics and EB alone [20].

### 2.4. Evaluation of the predicted pharmacokinetic properties

The physical properties-clusters of ionization coefficient (pKa), partition coefficient (log P) and distribution (log D) and topological polar surface area (TPSA) of Chalcones A1-6 were calculated using MarvinSketch® software version 20.15 [21], used as descriptors that determine the bioavailability of the compounds. The pharmacokinetic behavior of substances was predicted through the absorption, distribution, metabolism, excretion and toxicity (ADMET) models of the pkCSM web-server (<http://biosig.unimelb.edu.au/pkcsm/prediction>) [22], as human intestinal absorption (HIA), blood-brain barrier permeability (BBB), interactions with cytochrome P450 metabolizing isoenzymes (CYP450) and AMES toxicity [23]. In addition, the prediction of bioactivity was made by interactions with the classes of multi biological human targets on the Molinspiration web-server (<https://molinspiration.com/cgi-bin/properties>), through the scores of GPCR ligand, Ion channel modulator, Kinase inhibitor, Nuclear receptor ligand, Protease inhibitor and Enzyme inhibitor, where values less than 0.02 indicate low activity and values greater than 0.05 indicate high activity.

### 2.5. Docking Procedure

The NorA sequence of *S. aureus* 1199 strain (Entry Q03325) was retrieved from the Universal Protein Resource database (Uniprot), and the web-based SWISS-MODEL [24] service was used to create a homology model of the NorA protein as described in ref [25]. Partial Gasteiger charges were used for both the ligands and the target protein. Non-polar hydrogen atoms were mixed, and the rotational freedom of each ligand was taken into account. The docking region was defined as a square 80Åx80Åx80Å box centered on the protein. Docking studies were carried out using the Autodock Vina [26] software with all parameters at their respective default values.



## 2.6 Statistical Analysis

All bacteriological tests were performed in triplicates. Data were analyzed using a two-way ANOVA followed by Bonferroni's post hoc test (where  $p < 0.05$  was considered significant). The geometric mean of the triplicates was used as the central data  $\pm$  standard error of the mean. The GraphPad Prism 5.0 statistical program was used for the analysis.

## 3. Results and Discussion

### 3.1. NMR study

#### 3.1.1 (*E*)-3-(furan-2-yl)-1-(2-hydroxyphenyl)prop-2-en-1-one (A1)

In the  $^1\text{H}$  NMR spectrum (Figure S1, supplementary material), the signals at  $\delta_{\text{H}}$  7.56 ( $J = 14.0$  Hz) and 8.00 ( $J = 15.6$  Hz) can be seen in two doublets referring to the hydrogens  $\alpha$  and  $\beta$ , whose coupling constant ( $J$ ) confirms the stereochemistry *E* of the double bond. The signals at  $\delta_{\text{H}}$  8.00 (d,  $J = 11.2$  Hz, H6'), 7.10 (d,  $J = 8.4$  Hz, H3'), 7.54-7.79 (m, H4'), and 7.01 (t,  $J = 7.5$  Hz, H5') refer to aromatic hydrogens in ring A. The three signals observed at  $\delta_{\text{H}}$  7.54-7.79 (m, H5), 6.85 (d,  $J = 3.4$  Hz, H3), and 6.62 (dd,  $J = 8.3; 2.6$  Hz, H4) are characteristic to the hydrogens of the furanic ring. In the  $^{13}\text{C}$  NMR spectrum (Figure S2, supplementary material) we have the signal referring to carbonyl  $\alpha$ ,  $\beta$  unsaturated at  $\delta_{\text{C}}$  193.4. The ketone carbonyl absorbs at  $\delta_{\text{C}}$  203.8, however, the presence of  $\alpha$ ,  $\beta$  unsaturation causes a displacement to high field and the probable cause is the displacement of charge by the benzene ring or by the double bond that makes carbonyl carbon less electron deficient. The olefinic carbons are observed at  $\delta_{\text{C}}$  136.1 (C $\beta$ ), and 118.5 (C $\alpha$ ). The signals referring to the carbons present in ring A can be observed at  $\delta_{\text{C}}$  163.6 (C-2'), 131.2 (C-4'), 129.6 (C-6'), 120.1 (C-1'), 118.8 (C-5') and 117.6 (C-3'), and the signals at  $\delta_{\text{C}}$  151.6 (C-1), 145.4 (C-5), 117.1 (C-4) and 112.9 (C-3) refer to the furan ring carbons.

#### 3.1.2 (*E*)-3-(4-chlorophenyl)-1-(2-hydroxyphenyl)prop-2-en-1-one (A2)

In the spectrum of  $^1\text{H}$  NMR (Figure S3, supplementary material) the doublets observed at  $\delta_{\text{H}}$  7.59 (d,  $J = 15.5$  Hz) and 7.95 (d,  $J = 15.6$  Hz) can be unequivocally attributed to the olefinic hydrogen  $\alpha$ , and  $\beta$ , the stereochemistry *E* of the double bond was confirmed by the value of the coupling constant. The signals related to aromatic hydrogens in ring A can be observed at  $\delta_{\text{H}}$  8.00 (d,  $J = 11.2$  Hz, H6'), 7.12 (d,  $J = 8.4$  Hz, H3'), 7.66-7.73 (m, H4'), and 7.03 (t,  $J = 7.5$  Hz, H5'). The presence of the chlorine atom in carbon C4 of ring B makes the hydrogens H3/5, and H2/6 equivalent, they can be observed as doublets at  $\delta_{\text{H}}$  7.58 (d,  $J = 8.5$  Hz, H3/5) and 7.49 (d,  $J = 8.5$  Hz, H2/6). In the  $^{13}\text{C}$  NMR spectrum (Figure S4, supplementary material) the signal observed at

$\delta_C$  193.5 can be attributed to a  $\alpha$ ,  $\beta$ -unsaturated carbonyl group, The olefinic carbons are observed at  $\delta_C$  143.9 (C $\beta$ ), and 118.9 (C $\alpha$ ), and the signals referring to the carbons present in ring A are observed at  $\delta_C$  163.6 (C-2'), 136.5 (C-4'), 129.6 (C-6'), 120.6 (C-1'), 119.9 (C-3') and 118.7 (C-5'). In addition, the signals at  $\delta_C$  133.2 (C-1), 129.4 (C-2/6) and 129.8 (C-3/5) refer to the carbons in ring B, highlighted by the carbon signal that is linked to the chlorine atom at  $\delta_C$  136, 9 (C-4).

### 3.1.3 (E)-1-(2-hydroxyphenyl)-3-phenylprop-2-en-1-one (A3)

In the spectrum of  $^1\text{H}$  NMR (Figure S5, supplementary material) the signals at  $\delta_H$  7.60 (d,  $J = 15.5$  Hz, H  $\alpha$ ) and 8.02 (d,  $J = 15.5$  Hz, H $\beta$ ) were clearly attributed to olefinic protons. The higher coupling value shows that the two olefinic protons are in *trans*-position. The signals at  $\delta_H$  8.00 (d,  $J = 8.2$  Hz, H6'), 7.13 (m, H4'), 7.12 (m, H3'), and 7.02 (t,  $J = 7, 6$  Hz, H5') refer to aromatic hydrogens in ring A. The signals at  $\delta_H$  7.72-7.78 (m, H2/6), 7.59-7.61 (m, H3/5) and 7.53 (m, H4) refer to aromatic hydrogens of ring B. In the  $^{13}\text{C}$  NMR spectrum (Figure S6, supplementary material) there is the sign referring to carbonyl  $\alpha$ ,  $\beta$  unsaturated at  $\delta_C$  193.8. The olefinic carbons  $\alpha$  and  $\beta$  are observed at  $\delta_C$  145.4 and 118.9, respectively. The signals at  $\delta_C$  163.6 (C-2'), 136.2 (C-4'), 130.9 (C-6'), 120.2 (C-1'), 120.0 (C-3') and 118.7 (C-5') are the signals referring to the carbons present in ring A, and the signals at  $\delta_C$  136, 4 (C-4), 134.7 (C-1), 129.0 (C -2/6) and 129.7 (C-3/5) refer to the carbons in ring B.

### 3.1.4 (E)-1-(2-hydroxyphenyl)-3-(4-methoxyphenyl)prop-2-en-1-one (A4)

The spectrum of  $^1\text{H}$  NMR (Figure S7, supplementary material) displayed one singlet signal at  $\delta_H$  3.87 attributed to presence of one methoxy group (-CH<sub>3</sub>) at C4 position. The signals attributed to olefinic protons, were clearly observed at 7,54 (d,  $J = 15,5$  Hz, H $\alpha$ ) and 7,91 (d,  $J = 15,6$  Hz, H $\beta$ ), the higher coupling value shows that the two olefinic protons are in *trans*-position. The signs at  $\delta_H$  7.88-7.93 (m, H6'), 6.94-7.04 (m, H5'), 7.49-7.57 (m, H4'), and 7.02 (d,  $J = 8.3$  H3') refer to aromatic hydrogens in ring A, and the signs at  $\delta_H$  7.64 (d,  $J = 8.7$ , H2/6) and 6.95 (d,  $J = 8, 5$ , H3/5) refer to the aromatic hydrogens of the B ring. In the  $^{13}\text{C}$  NMR spectrum (Figure S8, supplementary material) there is the signal referring to carbonyl  $\alpha$ ,  $\beta$  unsaturated at  $\delta_C$  193.8. The olefinic carbons  $\alpha$  and  $\beta$  are observed at  $\delta_C$  145.5 and 118.9, respectively. The signals at  $\delta_C$  163.7 (C-2'), 136.3 (C-4'), 130.7 (C-6'), 120.3 (C-1'), 117.8 (C-3') and 118.7 (C-5') are the signals referring to the carbons present in ring A, and the signals at  $\delta_C$  162.2 (C-4), 129.7 (C-1), 127.5 (C -2/6) and 114.7 (C-3/5) refer to the carbons in ring B. In addition, the signal referring to the methoxy group carbon can be observed at  $\delta_C$  55.6.

### 3.1.5 (2E, 4E)-1-(2-hydroxyphenyl)-5-phenylpenta-2,4-dien-1-one (A5)

In the spectrum of  $^1\text{H}$  NMR (Figure S9, supplementary material) can be observed signals that have been attributed to the presence of two double bonds at  $\delta_{\text{H}}$  7.70 and 7.37 (d,  $J = 14.7$ ; 15.6 Hz,  $\text{H}\alpha$ ), 7.72 and 7.40 (d,  $J = 14.1$ ;14.8 Hz,  $\text{H}\beta$ ) were clearly attributed to olefinic protons, that higher coupling value shows that protons are in trans-position. The signals at  $\delta_{\text{H}}$  7,83-7,86 (m,  $\text{H6}'$ ), 7.46-7.51 (m,  $\text{H4}'$ ), 6,93 (t,  $J = 8.1$  Hz,  $\text{H5}'$ ) and 7.03 (t,  $J = 8.5$  Hz,  $\text{H3}'$ ) refer to aromatic hydrogens in ring A. The signals at  $\delta_{\text{H}}$  7.52 (d,  $J = 7.5$  Hz,  $\text{H2} /6$ ), 7.38 (d,  $J = 7.4$  Hz,  $\text{H3}/5$ ) and 7.43 (m,  $\text{H4}$ ) refer to aromatic hydrogens of ring B. In the  $^{13}\text{C}$  NMR spectrum (Figure S10, supplementary material) there is a resonance referring to carbonyl  $\alpha$ ,  $\beta$  unsaturated at  $\delta_{\text{C}}$  193.9. The four olefinic carbons are observed at  $\delta_{\text{C}}$  127.3 and 127.0 ( $\text{C}\alpha$ ), and 145.7 and 143.1( $\text{C}\beta$ ). The signals at  $\delta_{\text{C}}$  163.7 ( $\text{C-2}'$ ), 136.1 ( $\text{C-4}'$ ), 129.6 ( $\text{C-6}'$ ), 120.2 ( $\text{C-1}'$ ), 118.7 ( $\text{C-3}'$ ), and 118.9 ( $\text{C-5}'$ ) are the signals referring to the carbons present in ring A, and the signals at  $\delta_{\text{C}}$  136, 4 ( $\text{C-1}$ ), 127.6 ( $\text{C-2}/6$ ) and 129.6 ( $\text{C-3}/5$ ) refer to the carbons in ring B.

### 3.1.6 (E)-3-(2-fluorophenyl)-1-(2-hydroxyphenyl)prop-2en-1-one (A6)

In the spectrum of  $^1\text{H}$  NMR (Figure S11, supplementary material) the signals at  $\delta_{\text{H}}$  7.77 and 8.00 (d,  $J = 15.6$  Hz) are attributed to two doubles referring to the hydrogens  $\alpha$ , unsaturated  $\beta$ , whose coupling constant confirms the stereochemistry *E* of the double bond. The signals at  $\delta_{\text{H}}$  7.91 (d,  $J = 8.0$  Hz,  $\text{H6}'$ ), 7.49 (d,  $J = 7.1$  Hz,  $\text{H4}'$ ), 7.03 (d,  $J = 8.4$  Hz,  $\text{H3}'$ ) and 6.96 (d,  $J = 8.0$  Hz,  $\text{H5}'$ ) refer to aromatic hydrogens in ring A, and the signals at  $\delta_{\text{H}}$  7.62-7.68 (m,  $\text{H3}$ ), 7,39-7.42 (m,  $\text{H4}$ ), 7.21-7.24 (m,  $\text{H5}$ ) and 7,15-7.18 (m,  $\text{H6}$ ) refer to the aromatic hydrogens of ring B. In the  $^{13}\text{C}$  NMR spectrum ((Figure S12, supplementary material)) there is the sign referring to carbonyl  $\alpha$ ,  $\beta$  unsaturated at  $\delta_{\text{C}}$  193.9. The olefinic carbons  $\alpha$  and  $\beta$  are observed at  $\delta_{\text{C}}$  124.8 and 138.4, respectively. The signals at  $\delta_{\text{C}}$  163.8 ( $\text{C-2}'$ ), 136.7 ( $\text{C-4}'$ ), 129.9 ( $\text{C-6}'$ ), 120.10 ( $\text{C-1}'$ ), 118.8 ( $\text{C-3}'$ ) and 119.1 ( $\text{C-5}'$ ) there are the signals referring to the carbons present in ring A, and the signals at  $\delta_{\text{C}}$  160.3 ( $\text{C2}$ ), 130, 3 ( $\text{C-4}$ ), 130.3 ( $\text{C6}$ ), 124.7 ( $\text{C5}$ ), 123.0 ( $\text{C1}$ ) and 116.4 ( $\text{C3}$ ) refer to the carbons in ring B.

## 3.2. Vibrational analysis

The chalcones **A1-A6** possess respectively, 26, 29, 29, 33, 33, and 29 atoms, and since they are nonlinear molecules, we can conclude that they have respectively, 72, 81, 81, 93, 93, and 72 vibrational modes. The assignment of the vibrational modes for some Raman and infrared bands of the chalcones **A1-A6** is given in Table 1. There are some variations in the positions and in the intensities of the spectral bands in these chalcones. They occur due to changes in the B-ring

substitution pattern, where, in the chalcone **A1** the B-ring corresponds to the furan ring, and in the chalcones **A2**, **A3**, and **A4**, the B-ring corresponds to the phenyl ring with the modifications in 4-position, which contains, respectively, a chloride atom, a hydrogen atom, and an ethoxy group. It is also noted spectral changes due to the elongation of the enone chain that links the two aromatic rings of the chalcone **A6**.

The experimental Raman spectra of polycrystalline samples of the chalcones **A1-A6** are shown in Figure 1, and the experimental infrared absorbance spectra of the chalcones **A1-A6** are presented in the Supplementary Material on Figure S13. There is a good match between the experimental Raman wavenumbers and experimental infrared wavenumbers. The low symmetry which these chalcones present, they belong to the  $C_1$  point group, favors this good agreement between Raman and infrared wavenumbers.

The ATR-FTIR spectra of these chalcones (Figures S14-S19 on the supplementary material) give away characteristic  $-C=O$  stretching at  $1638-1689\text{ cm}^{-1}$  and  $-C=C-$  stretching at  $1444-1488\text{ cm}^{-1}$ , respectively. Additional  $-C=C-$  and  $-C-H$  stretching at  $1555-1581\text{ cm}^{-1}$  and  $3042-3060\text{ cm}^{-1}$  had established the occurrence of aromatic rings. In compound **A1**, two bends at  $1020$  and  $1225\text{ cm}^{-1}$  confirmed the presence of the furfuryl ring. The C-F str. peak at  $1296\text{ cm}^{-1}$  in compound **A6** confirmed the presence of the C-F group at the aromatic ring. Characteristic C-Cl str. The peak in IR spectra of compound **A2** recognized the presence of the C-F group in the para position of the aromatic ring.

The chalcones **A1-A6** show Raman and IR bands with weak intensities in the range from  $3200-2700\text{ cm}^{-1}$ , which correspond to the stretching modes of the O-H and C-H groups of these molecules. The stretching modes of the hydroxyl were observed only in the infrared absorbance spectra of the chalcones **A3**, **A4**, and **A5**, respectively, at  $3513\text{ cm}^{-1}$ ,  $3453\text{ cm}^{-1}$ , and  $3519\text{ cm}^{-1}$ . Comparing the hydroxyl stretching modes of the chalcones **A3** and **A5**, it is observed only a small variation in their wavenumbers. Therefore, the elongation of the enone chain does not significantly affect this vibrational mode.

It is known that the carbonyl stretching modes of chalcones are conjugated with the  $C=C$  stretching mode [9, 27]. The Raman bands of the chalcones **A1-A6** associated with the mixture of the carbonyl stretching modes with the  $C=C$  stretching modes possess very weak intensities. Notwithstanding, they appear with medium intensities in the infrared absorbance spectra of the chalcones **A3**, **A4**, and **A6**, respectively, at  $1689\text{ cm}^{-1}$ ,  $1672\text{ cm}^{-1}$ , and  $1692\text{ cm}^{-1}$ .

**Table 1.** Experimental wavenumbers ( $\text{cm}^{-1}$ ) and normalized Raman intensity (in arbitrary units) for some Raman bands of the six chalcones, and assignment of their vibrational modes.

Vibrational modes	For each Raman band the position of the wavenumber [in unit of $\text{cm}^{-1}$ ] and normalized Raman intensity [in arbitrary unit] are given in the above and below lines, respectively.						For each infrared band the position of the wavenumber [in unit of $\text{cm}^{-1}$ ] and normalized Raman intensity [in arbitrary unit] are given in the above and below lines, respectively.					
	A1	A2	A3	A4	A5	A6	A1	A2	A3	A4	A5	A6
$\nu$ O-H									3513	3453	3519	
									0.14	0.08		
$\nu$ C=O + $\nu$ C <sub>2</sub> =C <sub>2</sub>	1681	1690	1686	1678	1678	1696	1677	1691	1689	1672	1674	1692
	0.04	0.02	0.04	0.04	0.02	0.03	0.04	0.09	0.24	0.11	0.05	0.18
$\nu$ C=C + $\nu$ C-C	1625	1638	1638	1629	1629	1642	1638	1638	1637	1633	1632	1639
	0.44	0.25	0.46	0.52	0.46	0.31	0.68	0.76	0.87	0.66	0.71	0.92
$\nu$ C=C	1617	1618	1615	1616	1615	1613	1620	1624	1619	1613	1611	1611
	0.28	0.23	0.40	1.00	0.84	1.00	0.39	0.42	0.43	0.45	0.41	0.59
$\square$ C-C-Cl		1011						1011				
		0.11						0.45				
$\square$ C-C-C			1000	997	997				999	1004	1003	
			0.55	0.32	0.33				0.29	0.75	0.78	
$\square\square$ C-O-C	930						930					
	0.11						0.37					
$\square$ C-C-F						818						814
						0.34						0.46

**Nomenclature for the atoms:** C = Carbon; O = Oxygen; H = Hydrogen. **Nomenclature for the vibrational modes:**  $\square$  = bending;  $\square$  = stretching.

The changes in the B-ring substitution pattern also lead to modifications in the positions and in the intensities of the Raman bands of the chalcones **A1-A6**, in the wavenumber region between  $1642 \text{ cm}^{-1}$  and  $1611 \text{ cm}^{-1}$  where are localized the bands originating from the C-C and C=C stretching modes. Comparing these modes for chalcones **A3** and **A5**, it is noted that elongation of the enone chain leads to overlapping of these bands occurring with an increase of the intensity of the band of lower wavenumber.

The vibrational modes in the chalcones **A2** and **A6** are very differentiated at almost Raman spectra, either in their intensities or in the position of their wavenumbers, showing that the electronegativity of the chloride and fluorine atoms significantly affect the molecular polarizability. The bands appearing in the Raman and infrared spectra at  $1011 \text{ cm}^{-1}$  correspond to C-C-Cl bending mode, while the bands appearing in the Raman and infrared spectra, respectively, at  $818 \text{ cm}^{-1}$  and  $814 \text{ cm}^{-1}$  correspond to C-C-F bending mode. In the Raman spectra of the chalcones **A3**, **A4**, and **A5**, respectively, at  $1000 \text{ cm}^{-1}$ ,  $997 \text{ cm}^{-1}$ , and  $997 \text{ cm}^{-1}$  are observed C-C-C bending

modes. The Raman and infrared bands at  $930\text{ cm}^{-1}$  are associated with the C-O-C bending mode of the chalcone **A1**.

The vibrational modes below  $100\text{ cm}^{-1}$  are associated with external modes. Only three bands below  $100\text{ cm}^{-1}$  are observed in the Raman spectra of the chalcones **A1-A5**, and they are located for these chalcones, respectively, at  $97, 80$  and  $71\text{ cm}^{-1}$ ,  $89, 83$  and  $71\text{ cm}^{-1}$ ,  $91, 69$  and  $59\text{ cm}^{-1}$ ,  $91, 75$  and  $66\text{ cm}^{-1}$  and  $92, 75$  and  $65\text{ cm}^{-1}$ . Whereas only two bands below  $100\text{ cm}^{-1}$  are observed in the Raman spectrum of the chalcone **A6**, which are located at  $77$  and  $66\text{ cm}^{-1}$ .

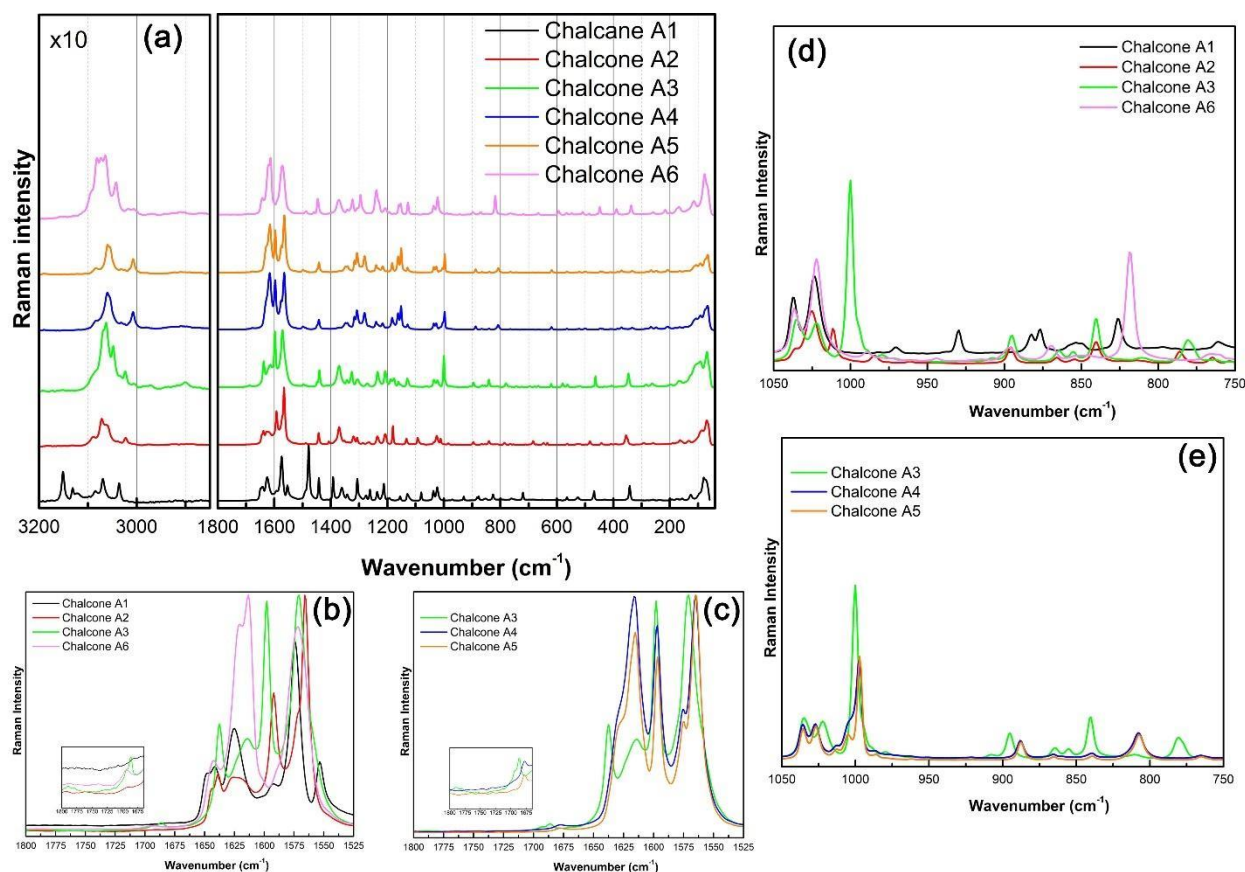


**Fig. 1.** (a) FT-Raman of the six synthesized chalcones. Zoom of some Raman bands at different temperatures in the spectral range; (b) Raman bands for chalcones A1-A3 and A6 in the region  $1800 - 1525\text{ cm}^{-1}$ ; (c) Raman bands for chalcones A3, A4 and A5 in the region  $1800 - 1525\text{ cm}^{-1}$ ; (d) Raman bands for chalcones A1-A3 and A6 in the region  $1050 - 750\text{ cm}^{-1}$ ; (e) Raman bands for chalcones A3, A4 and A5 in the region  $1050 - 750\text{ cm}^{-1}$ .

### 3.3. Electronic properties

The calculated HOMO and LUMO frontier molecular orbitals for chalcones **A1-A6** obtained at B3LYP/6-311G(d,p) level of theory are presented in Figure 2 and Figure 3, respectively. The HOMO (electron donor) in all the six chalcones are mainly localized over their aromatic B-rings, and in their enone chains, only in the chalcone **A6** the electronic density of this frontier molecular orbital also is found over the aromatic A-ring. It is still observed the difference in the electron density located over the hydroxy group. It is higher for chalcone 6 than for the other

chalcones. It is known that the electronic density is taken as the measurement of the hydrogen bond strength. Therefore, it is expected that the hydrogen bond formed of the hydroxy group of the chalcone **6** is more stronger those of other chalcones [28].

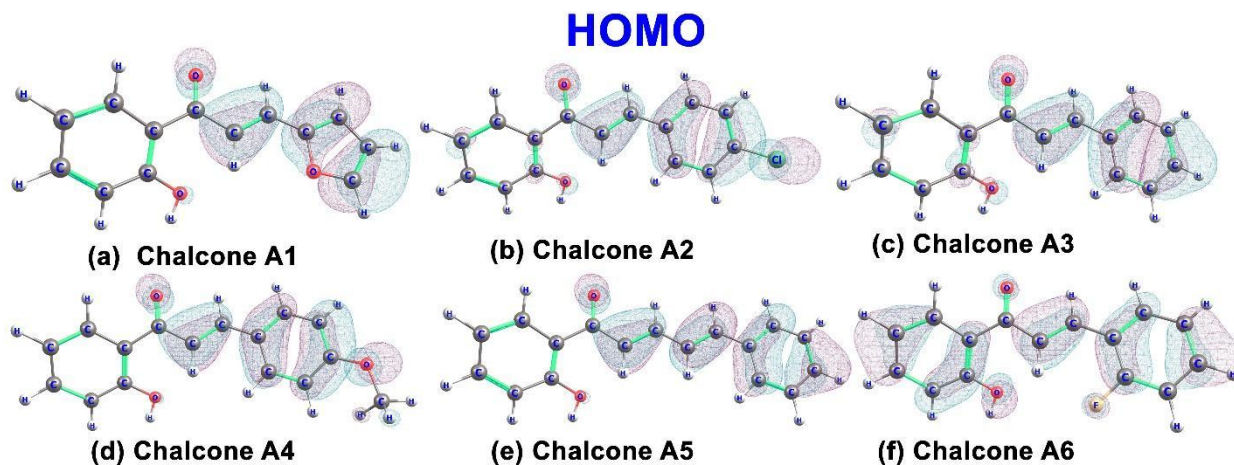


Fig. 2. HOMO of the chalcones A1-A

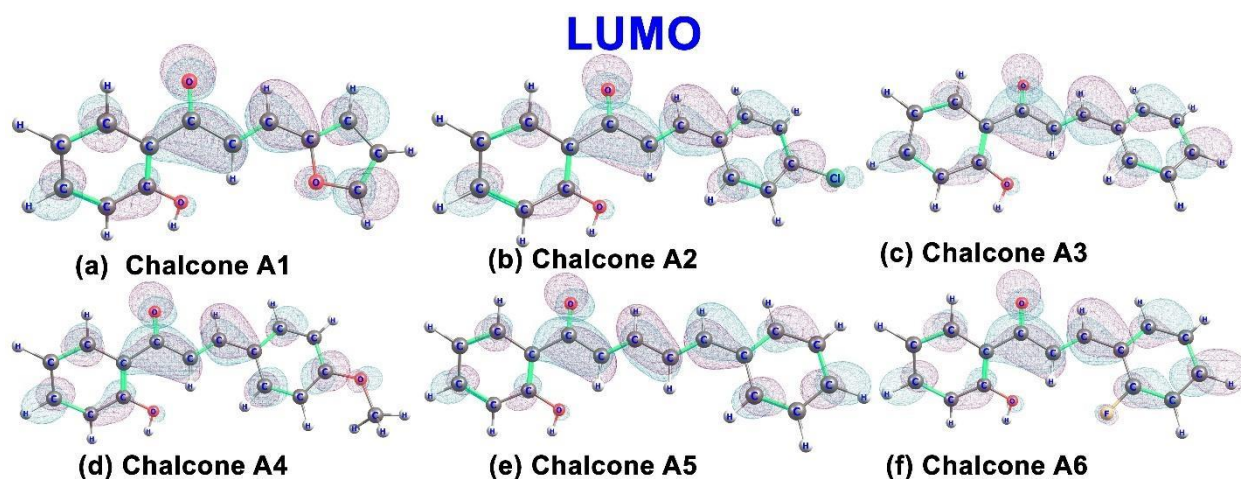


Fig. 3. LUMO of the chalcones A1-A

The LUMO (electron acceptor) orbital is mainly localized over the carbon atoms aromatic rings, as well as, by the oxygen atoms in all the six chalcones, with the exception of the methyl group of chalcone **A4**. The LUMO for chalcones **A2** and **A6** also are localized, respectively, over the chloride and fluorine atoms. The frontier molecular orbitals are important parameters that characterize the reactivity of chemical compounds. Through them it is possible to calculate the molecular descriptors: energy gap ( $\Delta E = E_{\text{LUMO}} - E_{\text{HOMO}}$ ) [29], ionization energy ( $I = -E_{\text{HOMO}}$ ) [30], electron affinity ( $A = -E_{\text{LUMO}}$ ) [30], chemical potential ( $\mu = -(I + A)/2$ ) [31, 32], electronegativity ( $\chi = -\mu$ ) [31, 32], global hardness ( $\eta = (I - A)/2$ ) [33-35], the global softness ( $S = 1/\eta$ ) [36], electrophilicity index ( $\omega = \mu^2/2\eta$ ) [37], global nucleophilicity index ( $\Omega = 1/\omega$ ) [38], and the maximum charge transfer index ( $\Delta N_{\text{max}} = -(I+A)/(I-A)$ ) [37, 39, 40]. In Table 2 is presented these molecular descriptors for the chalcones **A1-A6**. It is observed in this table that the values for the energy gap, global hardness, global nucleophilicity index, and the maximum charge transfer

index are smaller in the chalcone **A5** than in the other chalcones, indicating that it is more reactive than the other chalcones, consequently, it presents greater susceptibility to accept electronic density. and better electrophilic character. As it is expected, due to presence of the chloride and fluorine atoms, respectively in the chalcones **A2** and **A6**, their values of electronegativity are greater than those observed in the other chalcones. They also present greater values of ionization energy. The values of the dipole moments for chalcones **A1-A6** determined from DFT calculations were in Debye (D) unit, respectively, 3.94 D, 4.56 D, 4.13 D, 5.75 D, 4.86 D, and 3.33 D. Therefore, the chalcone **A4** is more most polarized than the other chalcones.

**Table 2.** Quantum chemical parameters for the optimized geometries of the chalcones A1-A6.

Compound	$E_{\text{HOMO}}$ (eV)	$E_{\text{LUMO}}$ (eV)	$\Delta E$ (eV)	$I$ (eV)	$A$ (eV)	$\mu$ (eV)	$\mu$ (eV)	$\mu$ (eV)	$S$ (1/eV)	$\mu$ (eV)	$\mu$ (1/eV)	$\mu N_{\text{max}}$
Chalcone <b>A1</b>	-6.17	-2.36	3.81	6.17	2.36	-4.27	4.27	1.91	0.52	4.77	0.21	-1.12
Chalcone <b>A2</b>	-6.56	-2.53	4.03	6.56	2.53	-4.55	4.55	2.02	0.50	5.12	0.20	-1.13
Chalcone <b>A3</b>	-6.50	-2.38	4.12	6.50	2.38	-4.44	4.44	2.06	0.49	4.78	0.21	-1.08
Chalcone <b>A4</b>	-6.02	-2.21	3.81	6.02	2.21	-4.12	4.12	1.91	0.52	4.44	0.23	-1.08
Chalcone <b>A5</b>	-6.09	-2.52	3.57	6.09	2.52	-4.31	4.31	1.79	0.56	5.19	0.19	-1.02
Chalcone <b>A6</b>	-6.59	-2.42	4.17	6.59	2.42	-4.51	4.51	2.09	0.48	4.87	0.21	-1.08

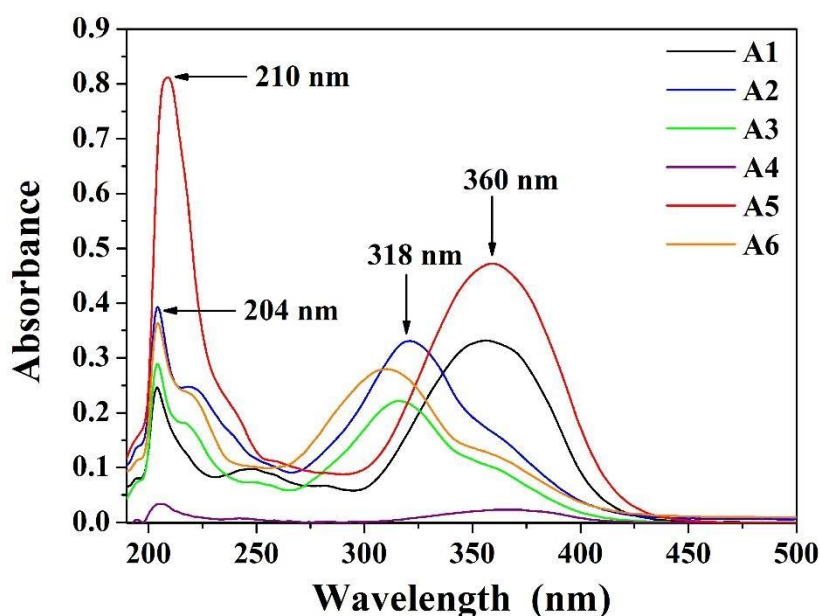


**Fig. 4.** Experimental UV-Vis spectra of the chalcones A1-A6 in the region 190 – 240 nm

The experimental spectra of UV absorption of the chalcones A1-A6 are shown in Figure 4, and the comparative between the experimental and theoretical spectra of UV absorption spectra are



given in Figure S20 in the supplementary material. In Table 3 is shown the electronic absorption spectral data (experimental and theoretical) for the three singlet states of these chalcones. The calculated maximum wavelengths, which correspond to the electronic transitions of the first singlet states for the chalcones A1-A6 are respectively at 379 nm (2.27 eV), 365 nm (3.40 eV), 361 nm (3.43 eV), 390 nm (3.18 eV), 384 nm (3.23 eV), and 365 nm (3.40 eV). It is possible to verify that the substitution of heteroatoms, in-ring B, significantly alter their spectroscopic properties, mainly for the first and second singlet states. For instance, for the first singlet state the electronic transitions are from HOMO to the LUMO for A1, A4 and A5 chalcones, and from HOMO-2 to the LUMO for A2 and A3 chalcones, and from HOMO-4 to the LUMO for A6 chalcone. It is also noted, which all the electronic transitions of the third singlet state of the chalcones A1-A6 are from the HOMO-1 to the LUMO; however, are also observed differences in the absorption wavelengths and oscillator strengths of them.

**Table 3.** Electronic absorption spectral data (experimental and theoretical) for three singlet states of the chalcones A1-A6.

Singlet states	Chalcones	Experimental		TD-DFT/B3LYP/6-311++G(d,p)				
		$\lambda$ (nm)	E (eV)	$\lambda$ (nm)	E (eV)	<i>f<sub>os</sub></i>	Electronic Transitions	% Major Contributions
S1	A1	379	3.27	370	3.35	0.57944	HOMO → LUMO	67
	A2	365	3.40	366	3.39	0.55396	HOMO-2 → LUMO	61
	A3	361	3.43	364	3.41	0.60196	HOMO-2 → LUMO	72
	A4	390	3.18	373	3.32	0.67256	HOMO → LUMO	90
	A5	384	3.23	389	3.18	0.65891	HOMO → LUMO	87
	A6	365	3.40	334	3.70	0.55766	HOMO-4 → LUMO	62
S2	A1	356	3.48	364	3.40	0.58811	HOMO-2 → LUMO	69
	A2	323	3.84	364	3.40	0.55441	HOMO → LUMO	61
	A3	316	3.92	359	3.45	0.61299	HOMO → LUMO	75
	A4	363	3.42	359	3.45	0.62517	HOMO-2 → LUMO	78
	A5	360	3.44	372	3.32	0.61807	HOMO-2 → LUMO	76
	A6	312	3.97	307	4.03	0.67428	HOMO → LUMO	91
S3	A1	333	3.72	345	3.60	0.60010	HOMO-1 → LUMO	72
	A2	298	4.16	337	3.68	0.59324	HOMO-1 → LUMO	70
	A3	292	4.25	330	3.75	0.61057	HOMO-1 → LUMO	75
	A4	350	3.54	340	3.64	0.67276	HOMO-1 → LUMO	91
	A5	333	3.72	358	3.46	0.66140	HOMO-1 →	87

							LUMO	
	A6	289	4.29	287	4.31	0.66876	HOMO-1 → LUMO	89

$f_{os}$  = oscillator strength, H = highest occupied molecular orbital, L = lowest unoccupied molecular orbital.

## 4 Antimicrobial Evaluation

### 4.4.1 Antimicrobial activity

The MIC of the chalcones **A1-A6** against the strains *Staphylococcus aureus* RN4220, K4414, 1199B, and K2068 are given in Table 4. These results are considered as not clinically relevant and indicate that chemical substitutions did not contribute to become chalcones active against the strains tested. Recently, it was reported that isomeric chalcones derived from natural acetophenone also did not show intrinsic activity at clinically relevant concentrations [10, 15].

**Table 4.** MIC of the six synthesized compounds.

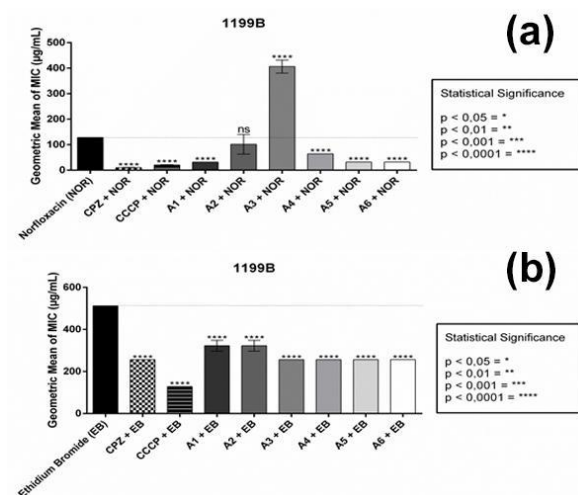
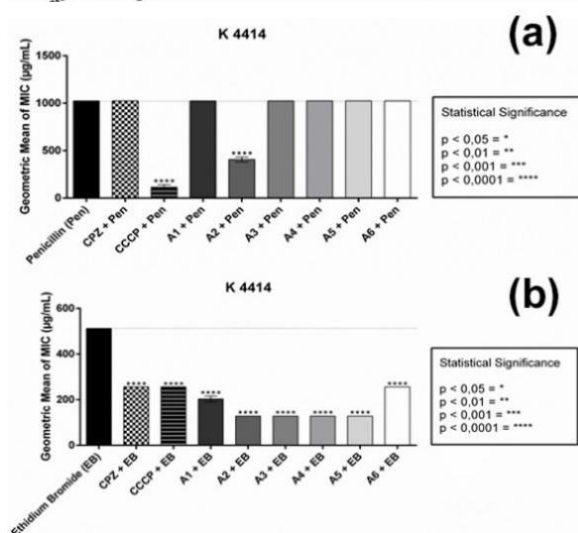
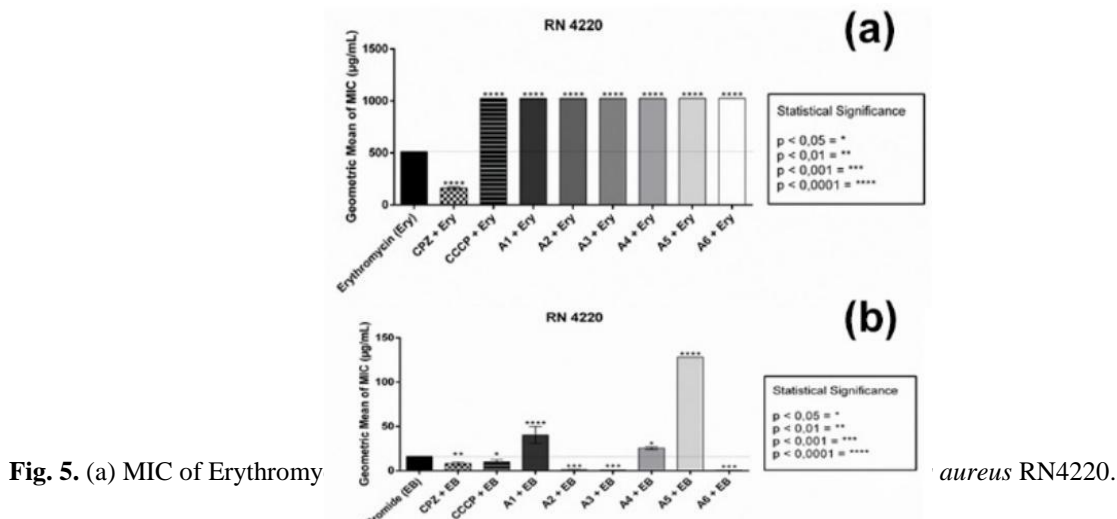
Chalcones	(MIC in $\mu\text{g} / \text{mL}$ ) Bacterial Strains			
	RN 4220	K 4414	1199B	K2068
A1	645	1024	1024	1024
A2	1024	1024	1024	1024
A3	1024	1024	1024	1024
A4	1024	1024	1024	1024
A5	1024	1024	1024	1024
A6	813	1024	1024	1024

### 4.4.2 Modulating effect of antibiotic activity and Modulating effect of ethidium bromide activity.

Resistance to antibiotics is a phenomenon that limits therapeutic options for treatment of bacterial infections, representing a threat to public health [13]. Reversion of the antibiotic resistance by natural or synthetic compounds could be an interesting alternative [41]. The chalcones tested were not able to attenuate the resistance to Erythromycin against RN4220, only the chalcone A2 was able to attenuate the resistance to Penicillin against K4414, all chalcones except A2 and A3 were able to attenuate the resistance to Norfloxacin against 1199B and, all chalcones were able to attenuate the resistance to Ciprofloxacin against K2068 suggesting that chalcones are modulating agents of antibiotics-resistance in *S. aureus*, probably acting as NorA inhibitors (Figures 5a, 6a, 7a and 8a) Once similar results were obtained for chlorpromazine, used here as an efflux pump inhibitor standard.

The chalcone A2 showed the best modulating effect reducing the MIC values for Penicillin (Figure 6a). This result indicates that modulating effect was influenced by introduction of a chlorine atom at C4 position on ring B. The analogs A1, A4, A5 and A6 reduced the Norfloxacin MIC

(Figure 7a) indicating that modulating effect was influenced by introduction of the furanic ring (A1), methoxy group at C4 position (A4), a second double bond (A5), and a fluorine atom at C2 position (A6).



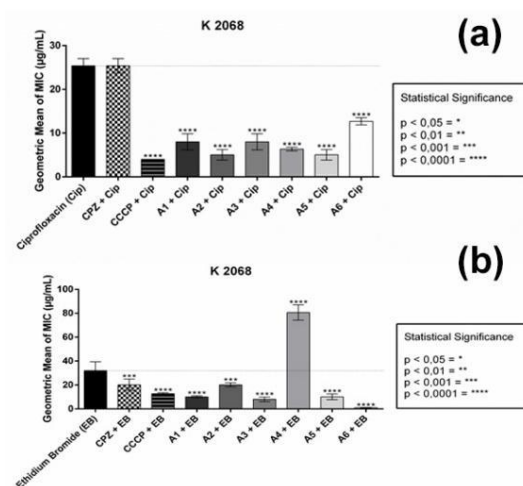


**Fig. 8.** (a) MIC of Ciprofloxacin, and (b) MIC of EB against the strain *Staphylococcus aureus* K2068.

All chalcones reduced the ciprofloxacin MIC (Figure 8a), the chalcones A2 and A5 showed the best results. It is known that the substitution of heteroatom or functional group in a molecular structure leads to modifications in its biological activity [42].

EtBr has been considered as a good marker to assess occurrence of efflux inhibition because active efflux is the only mechanism of resistance known to this NorA substrate [43]. Thus, strains were also treated with EtBr in combination or not with chalcones to assess if their modulating effect of Norfloxacin-resistance could be related to NorA inhibition. Results showed that chalcones A2, A3, and A6 were able to reduce MIC values of EtBr against RN4220 (Figure 5B), chalcones A1 to A5 were able to reduce MIC values of EtBr against K4414 (Figure 6B), chalcones A1 to A6 were not able to reduce MIC values of EtBr against SA1199B (Figure 7B), and only chalcones A1, A3, A5, and A6 were able to reduce MIC values of EtBr against K2068, the reduction of MIC values of EtBr suggesting a possible action as NorA inhibitors.

Modulating effect of Norfloxacin-resistance of chalcones have already been reported. A previous study assessed the modulating effect of natural chalcones isolated from *A. brachypoda* flowers in both Norfloxacin- and EtBr-resistance [44]. On the other hand, the presence of halogens such as fluor and chlorine is compatible with a good modulating effect of Fluoroquinolone-resistance [45], as well as verified for chalcones A2 and A6 tested in the present study. The influence of halogen-atom substitution in the molecular structure can lead to beneficial modifications in case of biological activity due to the formation of specific  $\sigma$ -hole (positive electrostatic potential) of halogen-atom and the carbonyl oxygen atom of amino acid residues [46]. Another study showed that hydroxylated chalcone proved to have a significant synergistic effect with Ciprofloxacin against the Methicillin-resistant *S. aureus* (MRSA) ATCC 43300 [14, 47, 48], corroborating the role of hydroxychalcones as enhancers of the modulating effect.

## 5. Predicted physicochemical and pharmacokinetics properties

In Table 5, the physical-chemical properties that determine the bioavailability of an oral drug are listed, such as ionization coefficient (pKa), partition coefficient (log P) and distribution (log D) and topological polar surface area (TPSA). As a rule, lipophilic and unloaded compounds are better absorbed in the intestine and, therefore, have a higher molecular fraction bioavailable for penetration into biological barriers and for transport through cell membranes [49-52]. The calculated values of pKa for the A1-6 analogues in the order of 7.19 indicate that, at physiological pH, the chemical balance moves towards the formation of the loaded species, where the phenol ionized group is the main micro-species, reaching a concentration around 61% (Figure 9). As a consequence, the compounds presented a decrease in lipophilicity, with log D values at pH 7.4 organized in the following order of permeability: A2 > A5 > A6 > A3 > A4 > A1 (Figure 10), with high percentages of absorption, varying between 97-98.8%. The lower TPSA values in the order of 40.13 Å<sup>2</sup> indicate the best cellular permeability conditions associated with A2, A3, A5 and A6 compounds, where the permeability potentials in Caco2 cells were evaluated between log Papp 1.35-1.65x10<sup>-6</sup> cm/s. Such behavior occurs due to the absence of polar atoms (N or O) in the aromatic substitution region of analogs A2, A3, A5 and A6, resulting in a decrease in polarity and leading to an easier of passive cell permeation of substances (Table 5).

**Table 5.** Predicted ADMET properties of the chalcone analogs **A1-A6**.

<b>Properties</b>	<b>A1</b>	<b>A2</b>	<b>A3</b>	<b>A4</b>	<b>A5</b>	<b>A6</b>
pKa	7.191	7.194	7.194	7.194	7.196	7.194
log P	3.297	4.841	4.237	4.079	4.764	4.379
log D <sub>7.4</sub>	2.884	4.430	3.826	3.668	4.354	3.968
TPSA	53.270	40.130	40.130	49.360	40.130	40.130
<b>Absorption</b>						
Caco2 permeability (log Papp in 10 <sup>-6</sup> cm/s)	1.261	1.357	1.509	1.334	1.484	1.653
Intestinal absorption (human, % Absorbed)	98.344	97.461	98.87	97.981	98.086	98.008
P-glycoprotein substrate	No	Yes	Yes	No	Yes	No
P-glycoprotein I inhibitor	No	No	No	No	No	No
<b>Distribution</b>						
VDss (human, log L/kg)	0.086	0.305	0.29	-0.035	0.346	0.126
Fraction unbound (human, Fu)	0.222	0.012	0.018	0.02	0	0.014
BBB permeability (log BB)	0.112	0.064	0.09	-0.057	-0.001	-0.037
CNS permeability (log PS)	-2.137	-1.328	-1.326	-2.12	-1.268	-1.323
<b>Metabolism</b>						
CYP2D6 substrate	No	No	No	No	No	No
CYP3A4 substrate	No	Yes	Yes	Yes	Yes	Yes
<b>Excretion</b>						
Total Clearance (log ml/min/kg)	0.342	-0.095	0.266	0.334	0.272	0.212
<b>Toxicity</b>						
AMES toxicity	Yes	Yes	No	Yes	Yes	Yes
hERG I inhibitor	No	No	No	No	No	No
Oral Rat Acute Toxicity (LD <sub>50</sub> , mol/kg)	2.24	2.247	2.048	1.736	1.983	2.179
Hepatotoxicity	No	No	No	No	No	No

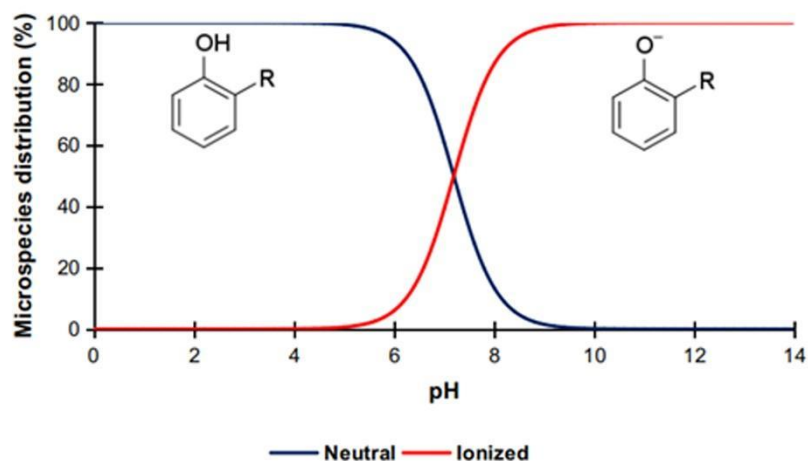


**Fig. 9.** Microspecies distribution of the chalcone analogs A1-A6 with de pH variation.

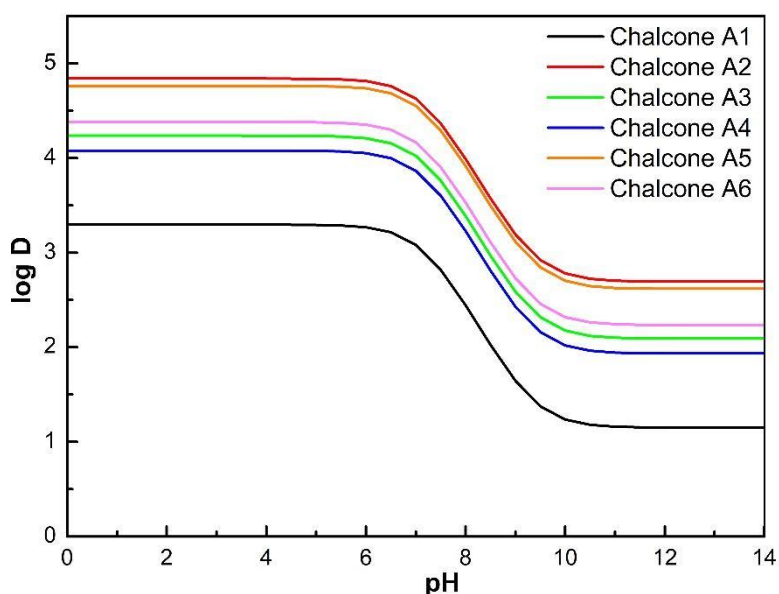


**Fig. 10.** Distribution coefficient (log D) of the chalcone analogs A1-A6 with the pH variation

Another factor that interferes with the bioavailability of the drug are the interactions with the proteins of transport and efflux, such as glycoprotein-P (Pgp). Potential inhibitor compounds of intestinal Pgp have their efflux diffculted, resulting in a decrease of the free molecular fraction in the blood [52, 53]. The prediction showed that the A2, A3 and A5 analogues are potential substrates of Pgp, resulting in the highest distribution volumes (VD<sub>ss</sub>) evaluated between log L/kg 0.29-0.34, in which only the A5 analog did not show a molecular fraction unlinked to plasma proteins, as a result of its side chain being made up of a long unsaturated hydrocarbon chain, where the delocalized  $\pi$  electrons result in a nucleophilic region capable of covalently bonding with these

proteins, thus limits its bioactivity and its molecular fraction distributed to biological barriers such as the blood-brain barrier (BBB). The calculated values of log BB between -0.05 and 0.11 suggest that the compounds have moderate permeability in BBB, which indicates that they are active substances in the central nervous system (CNS), highlighting the compounds A2 and A3, which are pumped out of the BBB because they are substrates of Pgp, and do not generate toxic risk by residual accumulation of the drug in adjacent blood (Table 5).

By means of interactions with the metabolizing isoenzymes of cytochrome P450 CYP450 drugs it is possible to predict structural modifications that favor the excretion of the drug. As the main precursor of this process, CYP3A4 is responsible for the O-dealkylation reactions of these drugs, constituting more water-soluble radicals favorable to excretion [54-56]. The enzyme and protease inhibition scores < 0.02 suggest that Chalcones A1-A6 have a low inhibition potential in biological receptors (Table 6). In this prediction, Chalcones A2-A6 are potential substrates of CYP3A4, which indicates that the biotransformation suffered by these compounds are easily metabolized and excreted chemicals, highlighting the highest total release potential (log ml/min/kg) in the order of A1 > A4 > A5 > A3 > A6 > A2. The ease of excretion of substances A1 and A4 results from the oxygenated aromatic substitutions, constituting more water-soluble chemical entities, where the substitution of the methoxy type of analogue A4 is more susceptible to O-demethylation reactions by the CYP3A4 isoenzyme (Table 5).

The mutagenic activity of oral drugs has led to emphasis on the development of new therapeutic substances. Since this activity results in tumorigenicity, the interactions with the main intracellular biological targets can be fundamental in the determination of this class of toxicity [57, 58]. The bioactivity score of less than 0.02 associated with binding of **A1-A6** analogues to G-protein coupled receptor (GPCR) indicates that isolated administration of these compounds can result in carcinogenicity, with strong contribution from the nucleophilic receptor made up of carbonyl in the vicinity of unsaturation in the six analogs, at the same time that the substances presented low ion channel modulating activity (Table 6). Thus, the predicted minimum oral dose values of LD50 between 1.73-2.24 mol/kg for the analogues do not present hepatic or cardiotoxic risk, but the prediction of AMES toxicity showed that the A3 analog is the only compound among the others in this study that does not present carcinogenic risk (Table 5).

**Table 6.** Predicted bioactivity of the chalcone analogs **A1-A6** through multi target classes.

Properties	A1	A2	A3	A4	A5	A6
GPCR ligand	-0.69	-0.24	-0.31	-0.24	-0.13	-0.26
Ion channel modulator	-0.66	-0.10	-0.10	-0.18	-0.18	-0.09
Kinase inhibitor	-0.98	-0.44	-0.49	-0.39	-0.31	-0.50
Nuclear receptor ligand	-0.76	-0.33	-0.38	-0.24	-0.27	-0.31
Protease inhibitor	-0.96	-0.44	-0.46	-0.38	-0.23	-0.42
Enzyme inhibitor	-0.38	-0.07	-0.06	-0.07	0.10	-0.07

## 6. Molecular docking

The best poses of all compounds are shown in Figure 11. Their binding energies were -6.4, -7.4, -7.0, -7.2, -7.5 and -7.2 kcal/mol for molecules A1 through A6, respectively. As can be seen from the figure, the chalcones A1, A2, A4, and A6 cluster together on the same region of the binding site. They interact with essentially the same residues making contacts with residues Leu218, Glu222, Phe306, Phe16, Ile136, Ile141, Gly248, and Asn137. As can be seen on Figure 12 a, b, d and f, there are also  $\pi$ - $\pi$  interactions with Phe140 and Phe303. For the A1, the distances to these residues are 3.93 Å and 4.88 Å, respectively. As A1, A2, A4 and A6 cluster together, these distances vary very little: the chalcone-to-Phe140 distance varies from 3.90 to 3.93 Å, while the distance to Phe303 is in the range of 4.82 to 4.88 Å. It's also worth mentioning that these chalcones interact with residue Ile244 through  $\pi$ -alkyl. These interactions are exemplified in the 2D Protein-Ligand interaction diagram for the A1 compound, which is provided as Figure S21 in the supplementary material. The A5 compound binds to a different portion of the binding site. There are contacts with residues Glu222, Leu218, Thr336, Ser337, Gln51, and Ile12, as well as  $\pi$ - $\pi$  stacking interactions with Phe140 and Phe16, with distances of 3.78 and 4.33 Å, respectively. Compound A5 also interacts with Asn340 through hydrogen bonds of similar lengths: 2.84 and 2.86 Å, as can be seen in Figure 12e. Compound A3 binds in a cavity formed by residues Met109, Gln51, and Ile15. It makes short contacts with residues Phe306, Arg310, Asn340, Thr336, Ile15, Ile 12, Phe47, Gln51, and Leu218. Its hydroxyphenyl ring is positioned such that it interacts with the phenyl ring of Phe16 through a  $\pi$ - $\pi$  T-shaped interaction of 4.7 Å.  $\pi$ -alkyl interactions with Met109 and Ile19 are also present. 2D ligand-protein interaction diagrams for A5 and A3 are provided as Figures S22 and S23, respectively, in the supplementary material. Docking the norfloxacin antibiotic to the NorA model (Figure S24) reveals that all six compounds could hinder the binding of norfloxacin to the NorA efflux pump, so, in theory, all six compounds could act as competitive inhibitors. This is, indeed, what one can infer from Figure 6b, as all six compounds reduced the MIC of the EtBr. The antagonistic effect of A3 and norfloxacin observed in Figure 6a is probably due to a different mechanism altogether, such as the reduction of permeability of the bacterial membrane, increasing the MIC of norfloxacin.

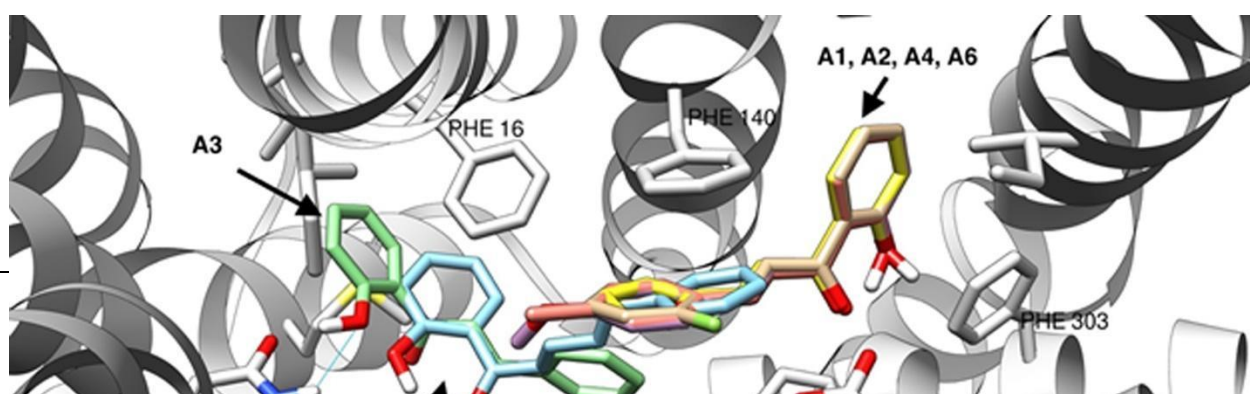




**Fig. 11.** Best poses for the six synthesized chalcones, A1 (yellow), A2 (orange), A3 (light green), A4 (pink), A5 (light blue) and A6 (brown) on the binding site of the NorA model.

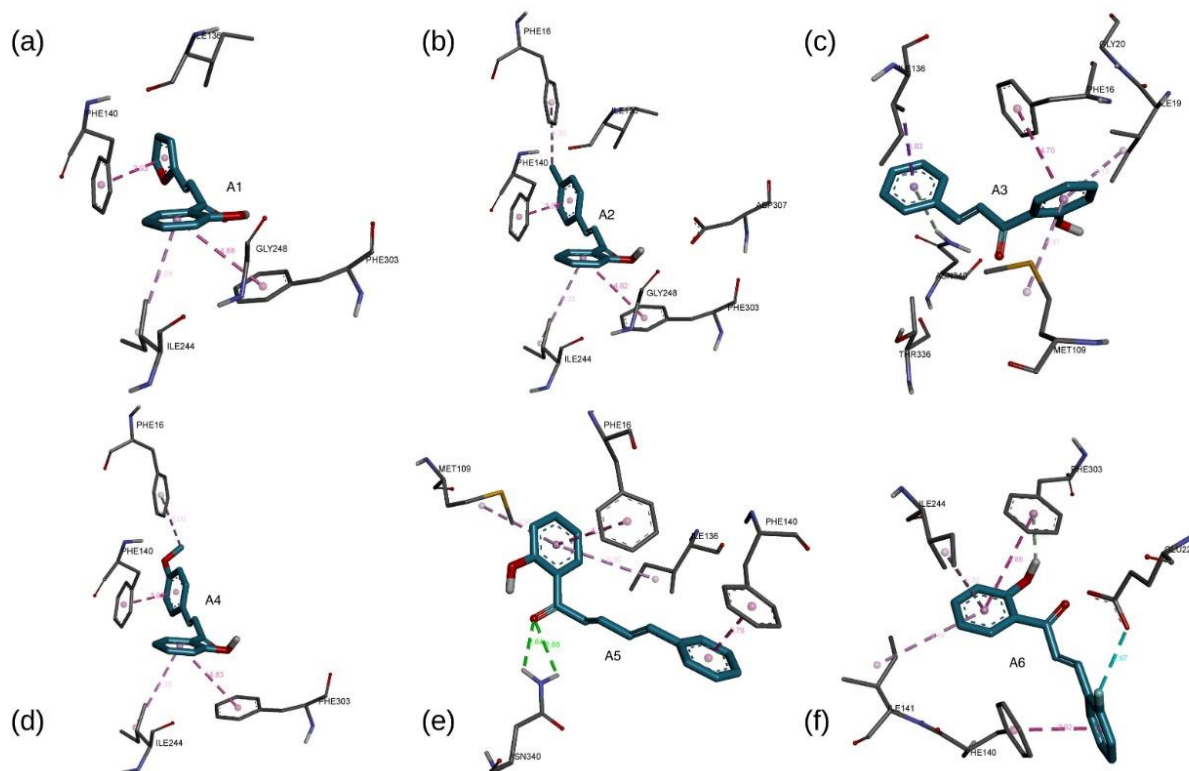


**Fig. 12.** Best poses for the six synthesized chalcones one the binding site of the model and its most important interactions.  $\pi$ - $\pi$  interactions are depicted in bright pink, while  $\pi$ -alkyl are in light pink. Hydrogen bonds are depicted in green and the fluorine bonding is in light blue.

## Conclusion

The  $^1\text{H}$  NMR data showed two diagnostic doublets in the spectrum around  $\delta$  7.37–7.77 ( $J$ = 14.0- 15.6 Hz) and  $\delta$  7.02–8.0 ppm ( $J$ = 14.8- 15.6 Hz) for -CO-CH= ( $\alpha$ -H) and =CH- ( $\beta$ -H), respectively, other protons exhibited additional resonance signals typically present in each compound such as the methoxy group in compound A4 at 3.87 (s) and the doublet signal observed at 6.85 with  $J$ = 3.4 Hz confirmed the furfuryl ring in compound A1. In the  $^{13}\text{C}$  NMR the signals around 118.5-127.3 and 136.1-145.7 confirmed  $\text{C}\alpha$  and  $\text{C}\beta$  unsaturated carbons, and an absorption

of ketone (C=O) around 193.4-193.9. The spectroscopic analysis by ATR-FTIR, FT-Raman and UV-Vis showed that modifications in-ring B leads to modifications in the intensities of the vibrational modes and alter the electronic properties of synthesized chalcones. The MIC values obtained for compounds were upper than 1000 µg/mL which are considered as not clinically relevant. However, the chalcones were able to attenuate the resistance to penicillin against K4414 (A2), Norfloxacin against 1199B (A1, A4, A5, and A6), and ciprofloxacin against K2068 (A1-A6) suggesting that compounds are modulating agents of antibiotics-resistance in *S. aureus*. This result indicates that the modulating effect demonstrated were influenced by introduction of a furanic ring (A1), chlorine atom and methoxy group at C4 position (A2 and A4), a second double bond (A5), and a fluorine atom at C2 position (A6). ADMET analysis predicts that absence of polar atoms (N or O) in the aromatic substitution region of analogs A2, A3, A5 and A6 resulting an easier of passive cell permeation of substances. The A5 analog has a nucleophilic region capable of covalently bonding with plasma proteins, and the ease of excretion of substances A1 and A4 results from the oxygenated aromatic substitutions. The molecular docking reveals that binding energies were -6.4, -7.4, -7.0, -7.2, -7.5 and -7.2 kcal/mol for chalcones A1 through A6, respectively, and all six compounds could hinder the binding of norfloxacin to the NorA efflux pump. Thus, this study adds new evidence and highlights that synthesized chalcones can potentially be used to develop compounds with antibiotic modifying activity.

### Acknowledgments

We thank the financial support from CNPq, CAPES, and FUNCAP. Jayze da Cunha Xavier acknowledges financial support from program of the government of India “Research Training Fellowship for Developing Country Scientist” (RTF- DCS)” DCS/2019/000192. We acknowledge Centro Nacional de Processamento de Alto Desempenho (CENAPAD) of the Federal University of Ceará (UFC) for the use of the *Gaussian09* software package, and the Northeastern Center for the Use and Application of Nuclear Magnetic Resonance (CENAUREM) for the NMR measurements. F.W.Q. Almeida-Neto thanks CNPq for his grant. H.S. Santos acknowledges financial support from the PQ/BPI-FUNCAP (Grant BP4-0172-00075.01.00/20), A.M.R. Teixeira acknowledges financial support from CNPq (Grant 305719/2018-1).

### References

- [1] J. O’Neill, Tackling Drug-Resistant Infections Globally: Final Report and Recommendations, Review on Antimicrobial Resistance:, DOI (2016).
- [2] H.M. Nguyen, C.J. Graber, Limitations of antibiotic options for invasive infections caused by methicillin-resistant *Staphylococcus aureus*: is combination therapy the answer?, *J. Antimicrob. Chemother.*, 65 (2010) 24-36. <https://doi.org/10.1093/jac/dkp377>.
- [3] D.P. Levine, Vancomycin: A History, *Clin. Infect. Dis.*, 42 (2006) S5-S12. <https://doi.org/10.1086/491709>.

- [4] A. García-Fernández, S. Gallina, S. Owczarek, A.M. Dionisi, I. Benedetti, L. Decastelli, I. Luzzi, Emergence of Ciprofloxacin-Resistant Salmonella enterica Serovar Typhi in Italy, PLoS One, 10 (2015) e0132065. <https://doi.org/10.1371/journal.pone.0132065>.
- [5] V. de Lastours, F. Chau, C. Roy, B. Larroque, B. Fantin, Emergence of quinolone resistance in the microbiota of hospitalized patients treated or not with a fluoroquinolone, J. Antimicrob. Chemother., 69 (2014) 3393-3400. <https://doi.org/10.1093/jac/dku283>.
- [6] D.E. Payne, B.R. Boles, Emerging interactions between matrix components during biofilm development, Curr. Genet., 62 (2016) 137-141. <https://doi.org/10.1007/s00294-015-0527-5>.
- [7] M.K.A. Ferreira, A.W. Silva, A.L. Santos, K.V.B. Sales, E.M. Marinho, J.N.M. Cardoso, M.M. Marinho, P.N. Bandeira, F.E.A. Magalhaes, E.S. Marinho, J.E.S.A. Menezes, H. S. Santos, Chalcones reverse the anxiety and convulsive behavior of adult zebrafish. *Epilepsy Behav*, 117 (2021) 107881. <https://doi.org/10.1016/j.yebeh.2021.107881>.
- [8] J.C. Xavier, F.W.Q. Almeida-Neto, P.T. Silva, E.S. Marinho, M.K.A. Ferreira, F.E.A. Magalhaes, C.E.S. Nogueira, P.N. Bandeira, J.E.S.A. Menezes, A.M.R. Teixeira, H. S. Santos, Structural characterization, electronic properties, and anxiolytic-like effect in adult zebrafish (*Danio rerio*) of cinnamaldehyde chalcone. *J. Mol. Struct.*, 1222 (2020) 128954. <https://doi.org/10.1016/j.molstruc.2020.128954>
- [9] A.M.R. Teixeira, H.S. Santos, P.N. Bandeira, M.S.S. Juliao, P.T.C. Freire, V.N. Lima, B.G. Cruz, P.T. da Silva, H.D.M. Coutinho, D.M. Sena, Structural, spectroscopic and microbiological characterization of the chalcone 2E-1-(2'-hydroxy-3',4',6'-trimethoxyphenyl)-3-(phenyl)-prop-2-en-1-one derived from the natural product 2-hydroxy-3,4,6-trimethoxyacetophenone, 1179 (2019) 739-748. <https://doi.org/10.1016/j.molstruc.2018.11.075>.
- [10] T.S.d. Freitas, J.d.C. Xavier, R.L.S. Pereira, J.E. Rocha, D.F. Muniz, P.T. da Silva, J.P. da Hora, H.S. dos Santos, P.N. Bandeira, C.E.S. Nogueira, A.M.R. Teixeira, H.D.M. Coutinho, Direct antibacterial and antibiotic resistance modulatory activity of chalcones synthesized from the natural product 2-hydroxy-3,4,6-trimethoxyacetophenone, *FEMS Microbiol. Lett.*, 367 (2020). <http://dx.doi.org/10.1093/femsle/fnaa124>.
- [11] M.N. Uddin, M.N.H. Knock, M. Uzzaman, M.M.H. Bhuiyan, A.F.M. Sanaulah, W. Shumi, H.M. Sadrul Amin, Microwave assisted synthesis, characterization, molecular docking and pharmacological activities of some new 2'-hydroxychalcone derivatives, *J. Mol. Struct.*, 1206 (2020) 127678. <https://doi.org/10.1016/j.molstruc.2020.127678>.
- [12] P.T. Da Silva, J. Da Cunha Xavier, T.S. Freitas, M.M. Oliveira, H.D.M. Coutinho, A.L.A.B. Leal, H.M. Barreto, P.N. Bandeira, C.E.S. Nogueira, D.M. Sena, F.W.Q. Almeida-Neto, E.S. Marinho, H.S. Santos, A.M.R. Teixeira, Synthesis, spectroscopic characterization and antibacterial evaluation by chalcones derived of acetophenone isolated from *Croton anisodontus* Müll.Arg.. *J. Mol. Struct.*, 1226 (2021) 129403. <https://doi.org/10.1016/j.molstruc.2020.129403>
- [13] J. da Cunha Xavier, F.W.d.Q. Almeida-Neto, P.T. da Silva, A.P. de Sousa, E.S. Marinho, M.M. Marinho, J.E. Rocha, P.R. Freitas, A.C.J. de Araújo, T.S. Freitas, C.E.S. Nogueira, P. de Lima-Neto, P.N. Bandeira, A.M.R. Teixeira, H.D.M. Coutinho, H.S. dos Santos, Structural characterization, DFT calculations, ADMET studies, antibiotic potentiating activity, evaluation of efflux pump inhibition and molecular docking of chalcone (E)-1-(2-hydroxy-3,4,6-trimethoxyphenyl)-3-(4-methoxyphenyl)prop-2-en-1-one, 1227 (2021) 129692. <https://doi.org/10.1016/j.molstruc.2020.129692>.
- [14] L.M. Rezende-Junior, L.M. de Sousa Andrade, A.L. Alves Borges Leal, A.B. de Souza Mesquita, A.L. Portela de Araujo dos Santos, J.d.S. Lima Neto, J.P. Siqueira-Junior, C.E. Sampaio Nogueira, G.W. Kaatz, H.D. Melo Coutinho, N. Martins, C.Q. Rocha, H.M. Barreto, Chalcones Isolated from Arrabidaea brachypoda Flowers as Inhibitors of NorA and MepA Multidrug Efflux Pumps of *Staphylococcus aureus*, *Antibiotics-Basel*, 9 (2020). <https://doi.org/10.3390/antibiotics9060351>.
- [15] P.T. Silva, T.S. Freitas, D.M. Sena, Jr.; , P.N. Bandeira, M.S.S. Julião, E.S. Marinho, A.A.C. Alcanfor, E.M. Marinho, P. Lima-Neto, C.E.S. Nogueira, H.D.M. Coutinho, A.L.A.B. Leal, H.M. Barreto, N. Martins,

Rodrigues Teixeira, A. M.; H.S. Santos, Structural, Vibrational and Electrochemical Analysis and Antibacterial Potential of Isomeric Chalcones Derived from Natural Acetophenone, *Applied Sciences*, 10 (2020) 4713. <http://dx.doi.org/10.3390/app10144713>.

[16] M.J. Frisch, G.W. Trucks, H.B. Schlegel, G.E. Scuseria, M.A. Robb, J.R. Cheeseman, G. Scalmani, V. Barone, B. Mennucci, G.A. Petersson, H. Nakatsuji, M. Caricato, X. Li, H.P. Hratchian, A.F. Izmaylov, J. Bloino, G. Zheng, J.L. Sonnenberg, M. Hada, M. Ehara, K. Toyota, R. Fukuda, J. Hasegawa, M. Ishida, T. Nakajima, Y. Honda, O. Kitao, H. Nakai, T. Vreven, J.A. Montgomery Jr., J.E. Peralta, F. Ogliaro, M.J. Bearpark, J. Heyd, E.N. Brothers, K.N. Kudin, V.N. Staroverov, R. Kobayashi, J. Normand, K. Raghavachari, A.P. Rendell, J.C. Burant, S.S. Iyengar, J. Tomasi, M. Cossi, N. Rega, N.J. Millam, M. Klene, J.E. Knox, J.B. Cross, V. Bakken, C. Adamo, J. Jaramillo, R. Gomperts, R.E. Stratmann, O. Yazyev, A.J. Austin, R. Cammi, C. Pomelli, J.W. Ochterski, R.L. Martin, K. Morokuma, V.G. Zakrzewski, G.A. Voth, P. Salvador, J.J. Dannenberg, S. Dapprich, A.D. Daniels, Ö. Farkas, J.B. Foresman, J.V. Ortiz, J. Cioslowski, D.J. Fox, Gaussian 09, Gaussian, Inc., Wallingford, CT, USA, 2009.

[17] B.E. KSOZ, R. ERTAN, Chemical and Structural Properties of Chalcones I, *Fabad J. Pharm. Sci.*, 36 (2011) 232-242.

[18] F.C. Chahar, P.E. Alvarez, C. Zampini, M.I. Isla, S.A. Brandán, Experimental and DFT studies on 2',4'-dihydroxychalcone, a product isolated from *Zuccagnia punctata* Cav. (Fabaceae) medicinal plant, *J. Mol. Struct.*, 1201 (2020) 127221. <https://doi.org/10.1016/j.molstruc.2019.127221>.

[19] CLSI – Clinical and Laboratory Standards Institute Performance standards of antimicrobial disk susceptibility test: Ninth Informational Supplement. NCCLS document M100-S9. , Wayne, PA: NIH, 2008, pp. 120-126.

[20] R.S. Almeida, P.R. Freitas, A.C.J. Araújo, I.R. Alencar Menezes, E.L. Santos, S.R. Tintino, T.F. Moura, J.R. Filho, V.A. Ferreira, A.C.A. Silva, L.E. Silva, W. do Amaral, C. Deschamps, M. Iriti, H.D. Melo Coutinho, GC-MS Profile and Enhancement of Antibiotic Activity by the Essential Oil of *Ocotea odorífera* and Safrole: Inhibition of *Staphylococcus aureus* Efflux Pumps, *Antibiotics*, 9 (2020). <https://doi.org/10.3390/antibiotics9050247>.

[21] P. Csizmadia, MarvinSketch and MarvinView: Molecule Applets for the World Wide Web, DOI [https://doi.org/10.3390/ecsoc-3-01775\(1999\)](https://doi.org/10.3390/ecsoc-3-01775(1999)). <https://doi.org/10.3390/ecsoc-3-01775>.

[22] D.E.V. Pires, T.L. Blundell, D.B. Ascher, pkCSM: Predicting Small-Molecule Pharmacokinetic and Toxicity Properties Using Graph-Based Signatures, *J. Med. Chem.*, 58 (2015) 4066-4072. <https://doi.org/10.1021/acs.jmedchem.5b00104>.

[23] B.N. Ames, E.G. Gurney, J.A. Miller, H. Bartsch, Carcinogens as Frameshift Mutagens: Metabolites and Derivatives of 2-Acetylaminofluorene and Other Aromatic Amine Carcinogens, *Proceedings of the National Academy of Sciences*, 69 (1972) 3128. <https://doi.org/10.1073/pnas.69.11.3128>.

[24] A. Waterhouse, M. Bertoni, S. Bienert, G. Studer, G. Tauriello, R. Gumienny, F.T. Heer, T.A P. de Beer, C. Rempfer, L. Bordoli, R. Lepore, T. Schwede, SWISS-MODEL: homology modelling of protein structures and complexes, *Nucleic Acids Res.*, 46 (2018) W296-W303. <https://doi.org/10.1093/nar/gky427>.

[25] M.M. Oliveira, H.S. Santos, H.D.M. Coutinho, P.N. Bandeira, P.T. da Silva, T.S. Freitas, J.E. Rocha, J.C. Xavier, F.F. Campina, C.R.S. Barbosa, J.B. Araújo Neto, R.L.S. Pereira, M.M.C. Silva, D.F. Muniz, A.M.R. Teixeira, V.M. Frota, T.H.S. Rodrigues, A.M. Amado, M.P.M. Marques, L.A.E. Batista de Carvalho, C.E.S. Nogueira, Spectroscopic characterization and efflux pump modulation of a thiophene curcumin derivative, *J. Mol. Struct.*, 1215 (2020) 128291. <https://doi.org/10.1016/j.molstruc.2020.128291>.

[26] O. Trott, A.J. Olson, AutoDock Vina: Improving the speed and accuracy of docking with a new scoring function, efficient optimization, and multithreading, *J. Comput. Chem.*, 31 (2010) 455-461. <https://doi.org/10.1002/jcc.21334>.

- [27] T.R. Garcia, T.S. de Freitas, H.S. dos Santos, P.N. Bandeira, M.S.S. Julião, J.E. Rocha, C.E.S. Nogueira, R.L.S. Pereira, A.C.H. Barreto, P.T.C. Freire, H.D.M. Coutinho, A.M.R. Teixeira, Structural, vibrational and electrochemical analysis and antibiotic activity study of chalcone (2E)-1-(3',-methoxy-4',-hydroxyphenyl)-3-(3-nitrophenyl)prop-2-en-1-one, *J. Mol. Struct.*, 1216 (2020) 128358. <https://doi.org/10.1016/j.molstruc.2020.128358>.
- [28] D. Dimić, D. Milenković, J. Ilić, B. Šmit, A. Amić, Z. Marković, J. Dimitrić Marković, Experimental and theoretical elucidation of structural and antioxidant properties of vanillylmandelic acid and its carboxylate anion, *Spectrochim. Acta A Mol. Biomol. Spectrosc.*, 198 (2018) 61-70. <https://doi.org/10.1016/j.saa.2018.02.063>.
- [29] R.G. Pearson, Hard and soft acids and bases, *JACS*, 85 (1963) 3533-&. <http://dx.doi.org/10.1021/ja00905a001>.
- [30] T. Koopmans, Über die Zuordnung von Wellenfunktionen und Eigenwerten zu den Einzelnen Elektronen Eines Atoms, *Phy*, 1 (1934) 104-113. [https://doi.org/10.1016/S0031-8914\(34\)90011-2](https://doi.org/10.1016/S0031-8914(34)90011-2).
- [31] H. Chermette, Chemical reactivity indexes in density functional theory, *J. Comput. Chem.*, 20 (1999) 129-154. [http://dx.doi.org/10.1002/\(SICI\)1096-987X\(19990115\)20:1<129::AID-JCC13>3.0.CO;2-A](http://dx.doi.org/10.1002/(SICI)1096-987X(19990115)20:1<129::AID-JCC13>3.0.CO;2-A).
- [32] R.P. Iczkowski, J.L. Margrave, Electronegativity, *JACS*, 83 (1961) 3547-3551. <https://doi.org/10.1021/ja01478a001>.
- [33] R.G. Pearson, Recent advances in the concept of hard and soft acids and bases, *J. Chem. Educ.*, 64 (1987) 561. <https://doi.org/10.1021/ed064p561>.
- [34] J.F. Janak, Proof that  $\partial E/\partial n_i = \epsilon_i$  in density-functional theory, *PhRvB*, 18 (1978) 7165-7168. <https://doi.org/10.1103/PhysRevB.18.7165>.
- [35] L. Von Szentpály, Studies on electronegativity equalization: Part 1. Consistent diatomic partial charges, *J. Mol. Struct.-THEOCHEM*, 233 (1991) 71-81. [https://doi.org/10.1016/0166-1280\(91\)85055-C](https://doi.org/10.1016/0166-1280(91)85055-C).
- [36] W.T. Yang, R.G. Parr, Hardness, softness, and the Fukui function in the electronic theory of metals and catalysis, *Proc. Natl. Acad. Sci. U.S.A.*, 82 (1985) 6723-6726. <https://doi.org/10.1073/pnas.82.20.6723>.
- [37] R.G. Parr, L.v. Szentpály, S. Liu, Electrophilicity Index, *JACS*, 121 (1999) 1922-1924. <https://doi.org/10.1021/ja983494x>.
- [38] P.K. Chattaraj, S. Giri, S. Duley, Update 2 of: Electrophilicity Index, *Chem. Rev.*, 111 (2011) PR43-PR75. <https://doi.org/10.1021/cr100149p>.
- [39] R.G. Parr, R.G. Pearson, Absolute Hardness - Companion Parameter To Absolute Electronegativity, *JACS*, 105 (1983) 7512-7516. <https://doi.org/10.1021/ja00364a005>.
- [40] R.G. Pearson, Absolute electronegativity and hardness correlated with molecular orbital theory, *Proceedings of the National Academy of Sciences*, 83 (1986) 8440. <https://doi.org/10.1073/pnas.83.22.8440>.
- [41] M.M.R. Siqueira, P.d.T.C. Freire, B.G. Cruz, T.S. de Freitas, P.N. Bandeira, H. Silva dos Santos, C.E.S. Nogueira, A.M.R. Teixeira, R.L.S. Pereira, J.d.C. Xavier, F.F. Campina, C.R. dos Santos Barbosa, J.B.d.A. Neto, M.M.C. da Silva, J.P. Siqueira-Júnior, H. Douglas Melo Coutinho, Aminophenyl chalcones potentiating antibiotic activity and inhibiting bacterial efflux pump, *Eur. J. Pharm. Sci.*, 158 (2021) 105695. <https://doi.org/10.1016/j.ejps.2020.105695>.
- [42] E.H. Avdović, D.S. Dimić, J.M. Dimitrić Marković, N. Vuković, M.Đ. Radulović, M.N. Živanović, N.D. Filipović, J.R. Đorović, S.R. Trifunović, Z.S. Marković, Spectroscopic and theoretical investigation of the potential anti-tumor and anti-microbial agent, 3-(1-((2-hydroxyphenyl)amino)ethylidene)chroman-2,4-dione, *Spectrochim. Acta A Mol. Biomol. Spectrosc.*, 206 (2019) 421-429. <https://doi.org/10.1016/j.saa.2018.08.034>.

- [43] G.W. Kaatz, S.M. Seo, L. Brien, M. Wahiduzzaman, T.J. Foster, Evidence for the Existence of a Multidrug Efflux Transporter Distinct from NorA in *Staphylococcus aureus*, *Antimicrob. Agents Chemother.*, 44 (2000) 1404. [10.1128/AAC.44.5.1404-1406.2000](https://doi.org/10.1128/AAC.44.5.1404-1406.2000).
- [44] J. Davies, D. Davies, Origins and Evolution of Antibiotic Resistance, *Microbiol. Mol. Biol. Rev.*, 74 (2010) 417. <https://doi.org/10.1128/MMBR.00016-10>.
- [45] V.K. Gupta, R. Gaur, A. Sharma, J. Akther, M. Saini, R.S. Bhakuni, R. Pathania, A novel bi-functional chalcone inhibits multi-drug resistant *Staphylococcus aureus* and potentiates the activity of fluoroquinolones, *Bioorg. Chem.*, 83 (2019) 214-225. <https://doi.org/10.1016/j.bioorg.2018.10.024>.
- [46] E.H. Avdović, D.S. Dimić, M. Fronc, J. Kožisek, E. Klein, Ž.B. Milanović, A. Kesić, Z.S. Marković, Structural and theoretical analysis, molecular docking/dynamics investigation of 3-(1-m-chloridoethylidene)-chromane-2,4-dione: The role of chlorine atom, *J. Mol. Struct.*, 1231 (2021) 129962. <https://doi.org/10.1016/j.molstruc.2021.129962>.
- [47] T. Thanh-Dao, D. Tuong-Ha, T. Ngoc-Chau, N. Trieu-Du, H. Thi-Ngoc-Phuong, T. Cat-Dong, T. Khac-Minh, Synthesis and anti Methicillin resistant *Staphylococcus aureus* activity of substituted chalcones alone and in combination with non-beta-lactam antibiotics, *Biorg. Med. Chem. Lett.*, 22 (2012) 4555-4560. <https://doi.org/10.1016/j.bmcl.2012.05.112>.
- [48] D. Bozic, M. Milenkovic, B. Ivkovic, I. Cirkovic, Antibacterial activity of three newly-synthesized chalcones & synergism with antibiotics against clinical isolates of methicillin-resistant *Staphylococcus aureus*, *Indian J. Med. Res.*, 140 (2014) 130-137.
- [49] T. Hay, R. Jones, K. Beaumont, M. Kemp, Modulation of the Partition Coefficient between Octanol and Buffer at pH 7.4 and pKa to Achieve the Optimum Balance of Blood Clearance and Volume of Distribution for a Series of Tetrahydropyran Histamine Type 3 Receptor Antagonists, *Drug Metab. Disposition*, 37 (2009) 1864. <https://doi.org/10.1124/dmd.109.027888>.
- [50] N. Perisic-Janjic, R. Kaliszan, P. Wiczling, N. Milosevic, G. Uscumlic, N. Banjac, Reversed-Phase TLC and HPLC Retention Data in Correlation Studies with in Silico Molecular Descriptors and Druglikeness Properties of Newly Synthesized Anticonvulsant Succinimide Derivatives, *Mol. Pharm.*, 8 (2011) 555-563. <https://doi.org/10.1021/mp100373d>.
- [51] C.A. Lipinski, Lead- and drug-like compounds: the rule-of-five revolution, *Drug Discovery Today: Technologies*, 1 (2004) 337-341. <https://doi.org/10.1016/j.ddtec.2004.11.007>.
- [52] D.F. Veber, S.R. Johnson, H.Y. Cheng, B.R. Smith, K.W. Ward, K.D. Kopple, Molecular properties that influence the oral bioavailability of drug candidates, *J. Med. Chem.*, 45 (2002) 2615-2623. <https://doi.org/10.1021/jm020017n>.
- [53] E.C.M. de Lange, P.G.M. Ravenstijn, D. Groenendaal, T.J. van Steeg, Toward the prediction of CNS drug-effect profiles in physiological and pathological conditions using microdialysis and mechanism-based pharmacokinetic-pharmacodynamic modeling, *The AAPS Journal*, 7 (2005) E532-E543. <https://doi.org/10.1208/aapsj070354>.
- [54] B. Meunier, S.P. de Visser, S. Shaik, Mechanism of Oxidation Reactions Catalyzed by Cytochrome P450 Enzymes, *Chem. Rev.*, 104 (2004) 3947-3980. <https://doi.org/10.1021/cr020443g>.
- [55] M. Louet, C.M. Labbé, C. Fagnen, C.M. Aono, P. Homem-de-Mello, B.O. Villoutreix, M.A. Miteva, Insights into molecular mechanisms of drug metabolism dysfunction of human CYP2C9\*30, *PLoS One*, 13 (2018) e0197249. <https://doi.org/10.1371/journal.pone.0197249>.
- [56] Y.-A. Cho, J.-S. Choi, J.-P. Burm, Effects of the antioxidant baicalein on the pharmacokinetics of nimodipine in rats: a possible role of P-glycoprotein and CYP3A4 inhibition by baicalein, *Pharmacol. Rep.*, 63 (2011) 1066-1073. [https://doi.org/10.1016/S1734-1140\(11\)70624-7](https://doi.org/10.1016/S1734-1140(11)70624-7).

[57] M. Olivo, R. Bhuvaneswari, S.S. Lucky, N. Dendukuri, P. Soo-Ping Thong, Targeted Therapy of Cancer Using Photodynamic Therapy in Combination with Multi-faceted Anti-Tumor Modalities, *Pharmaceuticals*, 3 (2010). <https://doi.org/10.3390/ph3051507>.

[58] D. D'Eliseo, F. Velotti, Omega-3 Fatty Acids and Cancer Cell Cytotoxicity: Implications for Multi-Targeted Cancer Therapy, *J. Clin. Med.*, 5 (2016). <https://doi.org/10.3390/jcm5020015>.

### 10.1 GENERAL ASPECTS OF SCIENTIFIC PRODUCTION

The use of chalcone (E) -1- (2-hydroxy-3,4,6-trimethoxyphenyl) -3- (4-methoxyphenyl) prop-2-en-1-one can be used as a pharmacological tool for the treatment of anxiety disorders in ZFa. There was a reduction in the number of line crossings in the Petri dish by the animals, without showing a toxic effect until 96 h due to the anxiolytic effect in the doses (20 and 40 mg/kg; 20  $\mu$ L; IP), confirmed by the predominant permanence in the clear area by fish similar to diazepam (40 mg /kg; 20  $\mu$ L; IP). The blockade of flumazenil on the anxiolytic effect of chalcone, in turn, necessarily has a direct relationship of action to receptors in the GABAergic system. And the docking showed high-affinity energy, in the order of - 8.1 Kcal /mol and an RMSD of 1.312.

Its molecular structure was confirmed by chemical calculations through the linear correlation between experimental and theoretical changes. The electronic characterization identifies the regions of the electronic density of the donor (nucleophilic) and receptor (electrophilic). Based on the criteria based on the rules of Lipinski and Veber. its active ingredient as oral medicine and low applications with plasma proteins. The studies also conclude that this chalcone is highly probable as an inactive drug in the CNS, there is no risk of toxicity to the nervous and respiratory system, being a good candidate for oral medication. In addition, the indefinite microbiological tests that chalcone can be used as a possible inhibitor of the MepA efflux pump and a basis for the design of substances with an antibiotic effect.

Electronic properties were also used to identify the nucleophilic and electrophilic regions of chalcone (2E, 4E)-1-(2-hydroxy-3,4,6-trimethoxyphenyl)- 5-phenylpenta-2,4-dien-1-one synthesized from two natural products. NMR, infrared, UV-vis spectroscopic analysis, and quantum chemistry calculations confirmed a molecular structure of chalcone. The experimental and calculated results were also in agreement and confirmed its anxiolytic effect in the adult zebrafish.

The results of the microbiological tests induced that this chalcone can be used as a possible inhibitor of the MepA efflux pump and base for the design of substances with antibiotic modifying activity. The combined action of EPI and antibiotics as their



substrates can keep a higher percentage of drugs within the cell, making existing anti-staphylococcal agents more effective.

Of the 6 chalcones identified as A1, A2, A3, A4, A5, and A6 tested in combination with antibiotics, A2 was able to attenuate penicillin resistance against K4414, (A1, A4, A5, and A6) to norfloxacin against 1199B and (A1 -A6) to ciprofloxacin against K2068, suggesting that these compounds are modulating agents of antibiotic resistance in *S. aureus*. Therefore, it is more efficient against 1199B and K2068. All were efficient in two of the three strains with the exception of the A3, which only mitigated the resistance against a K2068. Despite the syntheses of chalcones not dissipated of relevant clinical antibacterial activity, compared to the strains tested, synergistic results when associated with antibiotics and ethidium bromide, inducing a reduction in the minimum inhibitory concentration and inhibitory effects of the Qac A/B norA and mepA efflux pumps.

An ADMET analysis predicts the absence of polar atoms (N or O) in the aromatic substitution region for chalcones A2, A3, A5, and A6, making polarity decrease and leading to easier passive cell permeability of substances, which may have influenced the good results of these chalcones. They presented a good pharmacokinetic profile and favorable interaction energy, establishing several lines with no protein ligand, where the in silico data were similar to the microbiological data.

## 10.2 GENERAL CONCLUSION

Chalcones have multiple biological activities in both prokaryotes and eukaryotes. Its relatively simple structure allows its manipulation in the synthesis of new compounds to potentiate pre-existing bioactivities. The coupling together with the study of the extrusion activity makes the molecule broad, a possible execution in the actions of the molecule, and the coupling characteristics of its receptors. With the characterization of the chalcones after synthesis, it was possible by spectroscopic techniques and computational calculations of quantum chemistry to confirm the antimicrobial potential by the microdilution technique, to prove the efflux pump action and to confirm the antinociceptive capacity in the respective tested chalcones. the chalcones are propitious to form new active compounds probably due to the altered portions making a promising structure-activity relationship.

These studies can be improved, simplified and made economically viable using computational calculations and molecular docking to predict their action before other tests. In this work we also visualized which chalcones would do better and were confirmed with further microdilution analyses. That is, the results of the anxiolytic and antimicrobial activity of chalcones confirm their potential as molecules or prototypes for the synthesis of new pharmacological agents. The combination of efflux pump inhibitors (EPP) and antibiotics may make them more effective compared to using the antibiotic alone. (...) Molecular docking studies of chalcones with target proteins expressed the same result in antimicrobial activity and we were able to confirm the computational predictions in silico to assess drug similarity. With that, we finished the work with all our goals achieved. However, broader investigations of its pharmacokinetic properties and toxicity should be carried out. Because with a synergism it is possible to use antibiotics in low doses to help reduce toxicity.

### 10.3 OUTLOOK FOR FUTURE RESEARCH

As a perspective, one should understand the best regions of the molecule if the best and predict which of them will obtain better results from an acetophenone-based body as prototypes for future explorations regarding antimicrobials derived from semi-synthetic and synthetic chalcones.

In the future, computational calculations, in addition to a previous study avoiding future expenses with expensive analyzes, it is possible to focus the study on predictive results and it is hoped with docking to visualize this interaction or mechanism of *Staphylococcus aureus* in order to elucidate it.

The zebrafish is a fundamental alternative to decrease the tests with mammals, to fully study how several stages of its development more quickly in the study of chalcones also with anxiolytic action, the focus of this study.

However, the main gap in this area of research is the scarcity of clinical trials. With them, the results of the research reach pharmacies and the population's consumption to fight bacterial diseases and anxiety.

CAMPELO, M.J.M. et al. Synthesis, crystal structure, vibrational spectra and theoretical calculations of quantum chemistry of a potential antimicrobial Meldrum's acid derivative. **Journal of Molecular Structure**. v.1146. p.828-836, Out. 2017

CLSI. Methods for Dilution Antimicrobial Susceptibility Tests for Bacteria that Grow Aerobically, Approved Standard. 9th ed. Wayne, **PA: Clinical and Laboratory Standards Institute**. CLSI document M07-A9. 2012.

COUTINHO H. D. M. et al. Enhancement of the antibiotic activity against a multiresistant *Escherichia coli* by *Mentha arvensis* L. and chlorpromazine, **Chemotherapy**. v.54, n.4, p. 328. 2008.

CSIZMADIA P. MarvinSketch and MarvinView: Molecule Applets for the World Wide Web.in Proceedings of the 3rd International Electronic Conference on Synthetic Organic Chemistry. **MDPI: Basel**, Switzerland, p.1–30 Nov.1999.

ELIZABETH A. HARVIE, A.H. Neutrophils in host defense: new insights from zebrafish. **J Leukoc Biol**. v.98, n.4, p.523–537. Fev. 2015.

HOLLER, J.G. et al. Chalcone inhibitors of the NorA efflux pump in *Staphylococcus aureus* whole cells and enriched everted membrane vesicles. **Bioorganic & Medicinal Chemistry**. v.20, n.14, p. 4514–4521. Jul. 2012.

KALUEFF A.V. et al. Anxiolytic-like effects of noribogaine in zebrafish, *Behav. Brain Res*. v.330, p. 63–67. Jul. 2017.

KATZ, M. L. et al. Where have all the antibiotic patents gone? **Nature biotechnology**. v. 24, n. 12, p. 529-1531. Dec. 2006.

LIVERMORE, D. M. Minimising antibiotic resistance. **The Lancet infectious diseases** v. 5, n. 7, p. 450-459. Jul. 2005.

MAGALHÃES, F.E.A. et al. Adult Zebrafish (*Danio rerio*): an alternative behavioral model of formalina-induced nociception. **Revista Zebrafish**. v. 14, n. 5, p. 422-429. Oct. 2017.

POOLE, K. Efflux pumps as antimicrobial resistance mechanisms. **Annals of Medicine**. v. 39, n. 3, p. 162–176. Jul. 2007.

RAMMOHAN A. et al. Chalcone synthesis, properties and medicinal applications: a review. **Environmental Chemistry Letters**. vol. 18, n. 2, p. 433-458 Jan, 2020.

- RITTER, M. et al. Green Synthesis of Chalcones and Microbiological Evaluation. **J. Braz. Chem Soc.** v. 26, n. 6, p. 1201-1210. Jun. 2015.
- SCHLEGEL A. Studying non-alcoholic fatty liver disease with zebrafish: a confluence of optics, genetics, and physiology. **Cell Mol Life Sci.** v. 69, n. 23, p. 3953-3961. Jun. 2012.
- SCOTTI, L. et al. Docking Studies for Multi-Target Drugs **Current Drug Targets.** v. 18, n. 5, p. 592-604. Abr. 2017.
- SNEDDON L.V. Evolutions of nociception and pain: evidence from fish models, **Phil. Trans. B347.** p. 1785-1793. Sep. 2019.
- SRIVALLI, K.M, LAKSHMI PK. Overview of P-glycoprotein inhibitors: a rational outlook. **Brazilian Journal of Pharmaceutical Sciences.** v. 48, n. 3, p. 353-67. Sep. 2012.
- STEWART, A. M. et al. Developing zebrafish models of autism spectrum disorder (ASD). **Progress in Neuro-Psychopharmacology and Biological Psychiatry,** v. 50, p. 27-36. Abr. 2014
- TAYLOR, J.C. et al. Novel zebrafish-based model of nociception, **Physiol. Behav.** v. 174, p. 83-88. May. 2017.
- TROTT O, OLSON AJ. AutoDock Vina: Improving the speed and accuracy of docking with a new scoring function, efficient optimization, and multithreading. **J. Comput. Chem.** p. 455-461. 2009
- UTCHARIYAKIAT, I. Efficacy of cinnamon bark oil and cinnamaldehyde on anti-multidrug resistant *Pseudomonas aeruginosa* and the synergistic effects in combination with other antimicrobial agents. **BMC Complement. Altern. Med.** v. 16, n. 1, p. 158. Jun. 2016.
- VAZ, R.J. et al. The challenges of in silico contributions to drug metabolism in lead optimization. **Expert Opinion on Drug Metabolism & Toxicology.** v. 6, n. 7, p. 851–861. Jun. 2010.
- YADAV, P. et al. Design, synthesis, characterization, antimicrobial evaluation and molecular modeling studies of some dehydroacetic acid-chalcone-1, 2, 3-triazole hybrids. **European Journal of Medicinal Chemistry.** v. 155, p. 263-274, Apr. 2018.
- ZHUANG, C. et al. Chalcone: A Privileged Structure in Medicinal Chemistry. **Chem Rev.** V. 7, N. 12, p. 7762–7810. May. 2017.

### **Structural characterization, DFT calculations, ADMET studies, antibiotic potentiating activity, evaluation of efflux pump inhibition and molecular docking of chalcone (*E*)-1-(2-hydroxy-3,4,6-trimethoxyphenyl)-3-(4-methoxyphenyl)prop-2-en-1-one**

Jayze da Cunha Xavier<sup>a</sup>, Francisco Wagner Queiroz Almeida-Neto<sup>b</sup>, Priscila Teixeira da Silva<sup>a</sup>, Amanda Pereira de Sousa<sup>f</sup>, Emmanuel Silva Marinho<sup>c</sup>, Márcia Machado Marinho<sup>g</sup>, Janaina Esmeraldo Rocha<sup>a</sup>, Priscila Ramos Freitas, Ana Carolina Justino de Araújo<sup>a</sup>, Thiago Santiago Freitas<sup>a</sup>, Carlos Emídio Sampaio Nogueira<sup>a,e</sup>, Pedro de Lima-Neto<sup>b</sup>, Paulo Nogueira Bandeira<sup>f</sup>, Alexandre Magno Rodrigues Teixeira<sup>a</sup>, Henrique Douglas Melo Coutinho<sup>a</sup>, Hércio Silva dos Santos<sup>a,d,f4\*</sup>

<sup>a</sup>Department of Biological Chemistry, Regional University of Cariri, Crato, CE, Brazil,

<sup>b</sup>Group of Theoretical Chemistry, Department of Analytical Chemistry and Physical Chemistry, Federal University of Ceará, Fortaleza, CE, Brazil

<sup>c</sup>Group of Theoretical Chemistry and Electrochemistry, State University of Ceará, Campus FAFIDAM, Limoeiro do Norte, CE, Brazil.

<sup>d</sup>Science and Technology Center, Postgraduate Program in Natural Sciences, State University of Ceará, Fortaleza, CE, Brazil

---

<sup>4\*</sup>Corresponding author. Postgraduate Program in Biological Chemistry, Department of Biological Chemistry, Regional University of Cariri, Campus Pimenta II, CEP: 63.100-000, Crato, CE, Brazil. E-mail addresses: [helciodossantos@gmail.com](mailto:helciodossantos@gmail.com)

<sup>e</sup>Department of Physics, Regional University of Cariri, Juazeiro do Norte, CE, Brazil.

<sup>f</sup>Center for Exact Sciences and Technology - Chemistry Course, Vale do Acaraú

University, Sobral, CE, Brazil

<sup>g</sup>Iguatu Faculty of Education, Science and Letters (Fecli), Ceará State University,  
Iguatu, Ceará, Brazil

**Figure S1.**  $^1\text{H}$  NMR spectrum ( $\text{CDCl}_3$ , 500 MHz) of chalcone (E) -1- (2-hydroxy-3,4,6-trimethoxyphenyl) -3- (4-methoxyphenyl) prop-2-en-1-one

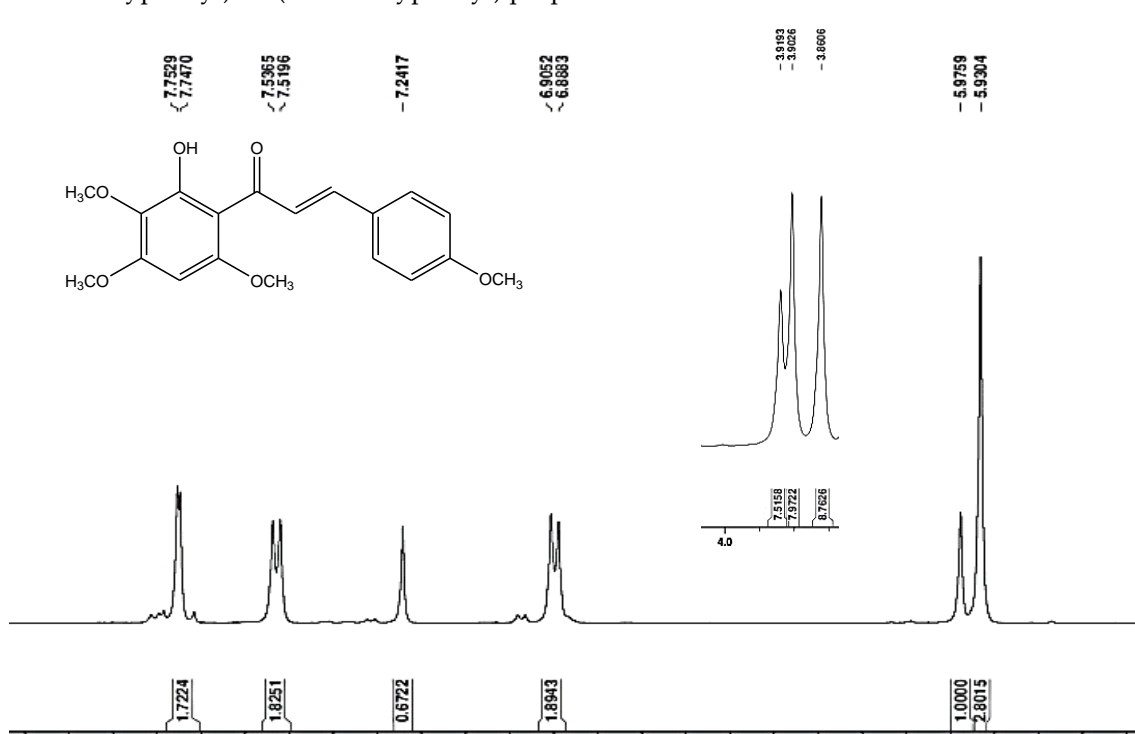


**Figure S2.**  $^{13}\text{C}$  NMR ( $\text{CDCl}_3$ , 125 MHz) spectrum of (E) -1- (2-hydroxy-3,4,6-trimethoxyphenyl) -3- (4-methoxyphenyl) prop-2-en-1-one.

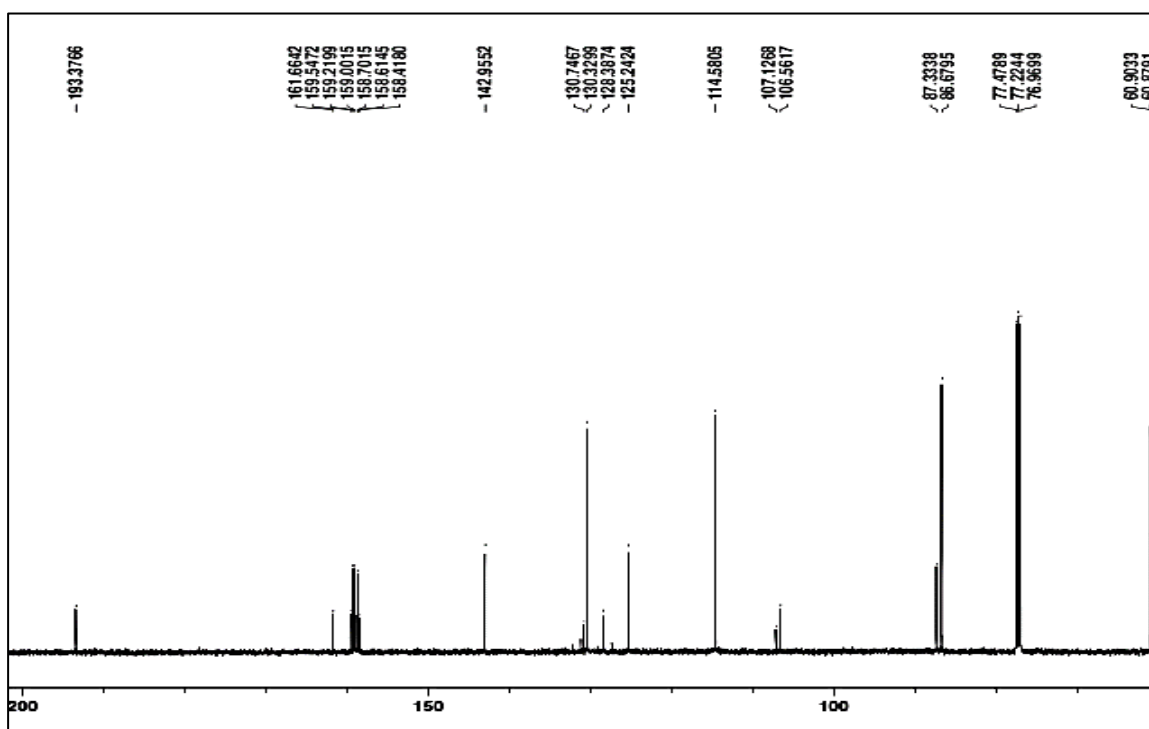


**Figure S3.** Linear fitting of the experimental and theoretical chemical shifts for the structural characterization of the title chalcone.

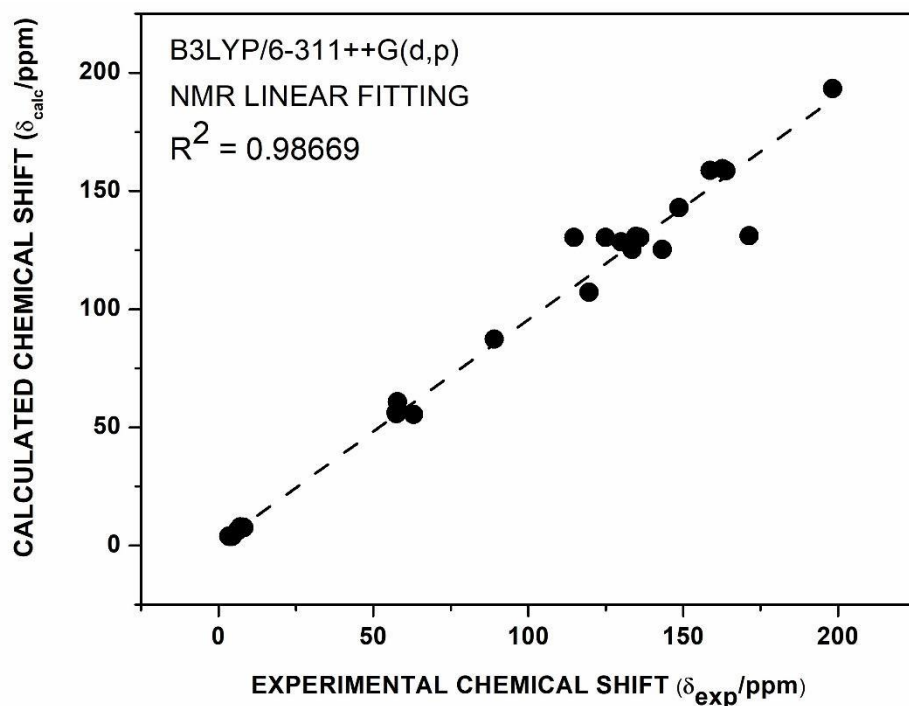
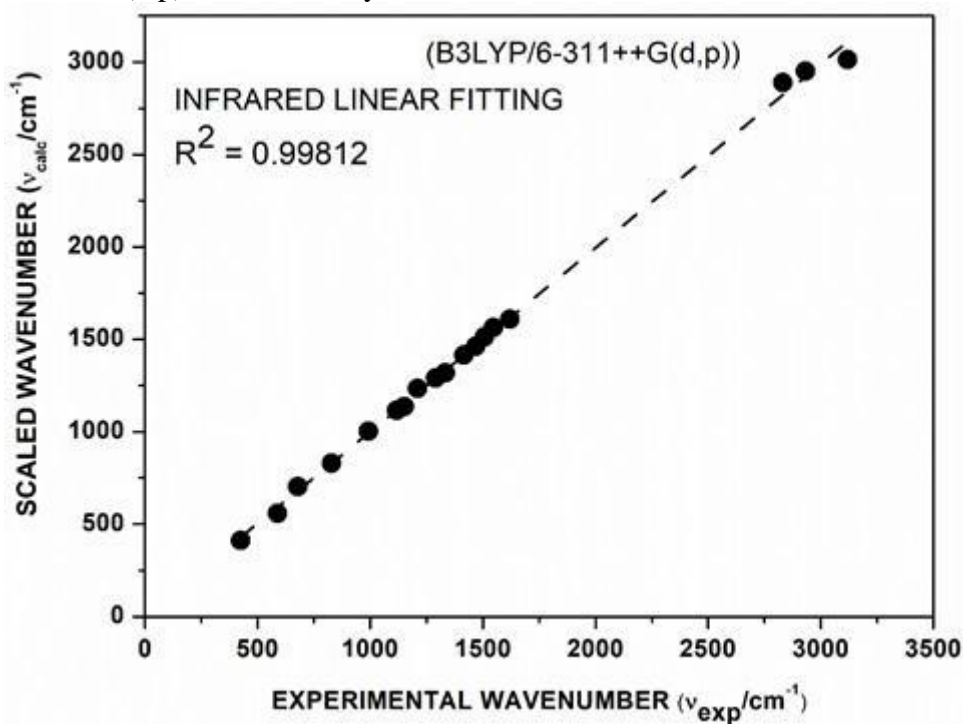


**Figure S4.** Linear fitting using the experimental and calculated wavenumbers calculated at B3LYP/6-311++G(d,p) level of theory of the title chalcone.



## Structural characterization, electronic properties, and anxiolytic-like effect in adult zebrafish (*Danio rerio*) of cinnamaldehyde chalcone

Jayze Cunha Xavier<sup>a</sup>, Francisco Wagner Queiroz Almeida-Neto<sup>b</sup>, Priscila Teixeira da Silva<sup>a</sup>, Emmanuel Silva Marinho<sup>c</sup>, Maria Kueirislene Amâncio Ferreira<sup>d</sup>, Francisco Ernani Alves



Magalhães<sup>d,g</sup>, Carlos Emídio Sampaio Nogueira<sup>a,e</sup>, Paulo Nogueira Bandeira<sup>f</sup>, Jane Eire Silva Alencar de Menezes<sup>d</sup>, Alexandre Magno Rodrigues Teixeira<sup>a</sup>, Hécio Silva dos Santos<sup>a,d,f,5\*</sup>

<sup>a</sup>Department of Biological Chemistry, Regional University of Cariri, Crato-CE, Brazil,

<sup>b</sup>Group of Theoretical Chemistry, Department of Analytical Chemistry and Physical Chemistry, Federal University of Ceará, Fortaleza, CE, Brazil

<sup>c</sup>Group of Theoretical Chemistry and Electrochemistry, State University of Ceará, Campus FAFIDAM, Limoeiro do Norte, CE, Brazil.

<sup>d</sup>Science and Technology Center, Postgraduate Program in Natural Sciences, State University of Ceará, Fortaleza, CE, Brazil

<sup>e</sup>Department of Physics, Regional University of Cariri, Juazeiro do Norte-CE, Brazil. <sup>f</sup>Center for Exact Sciences and Technology - Chemistry Course, Vale do Acaraú University, Sobral, CE, Brazil

<sup>5\*</sup>State University of Ceará, Department of Chemistry, Laboratory of Natural Products Bioprospecting and Biotechnology, CECITEC Campus, Tauá, CE, Brazil.

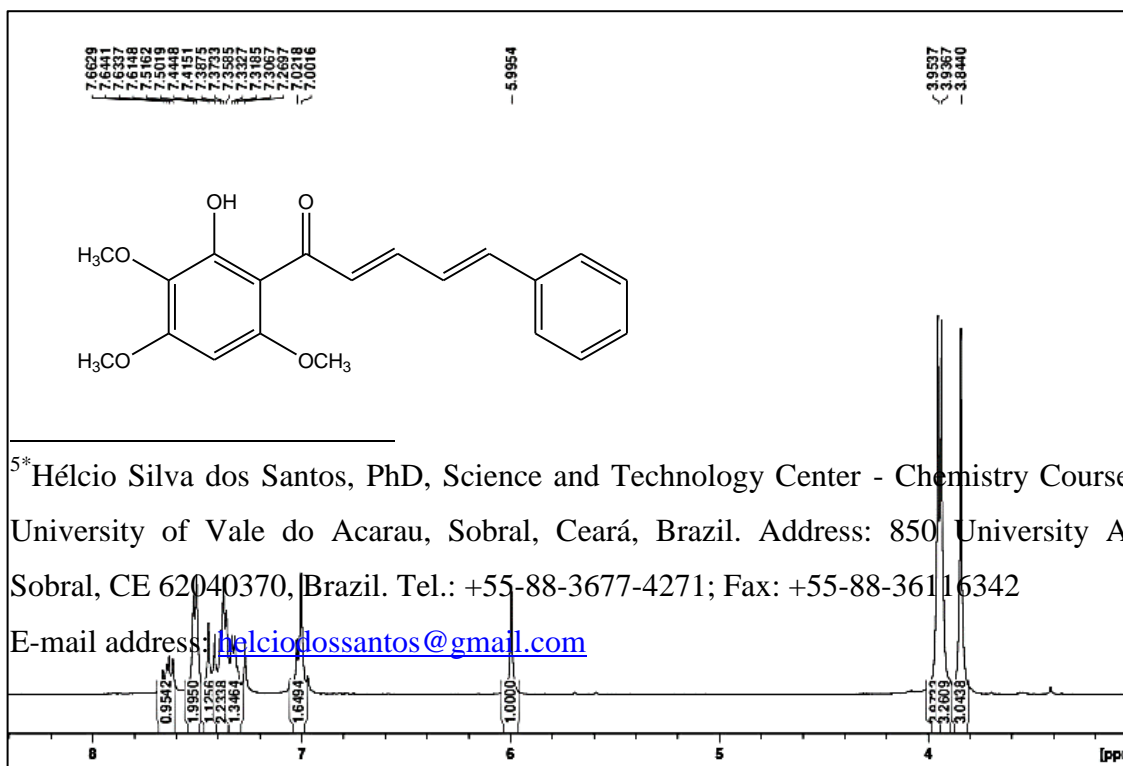


Figure S1.  $^1\text{H}$  NMR spectrum ( $\text{CDCl}_3$ , 500 MHz) of chalcone ( $2E, 4E$ )-1-(2-hydroxy-3,4,6-trimethoxyphenyl)-5-phenylpenta-2,4-dien-1-one

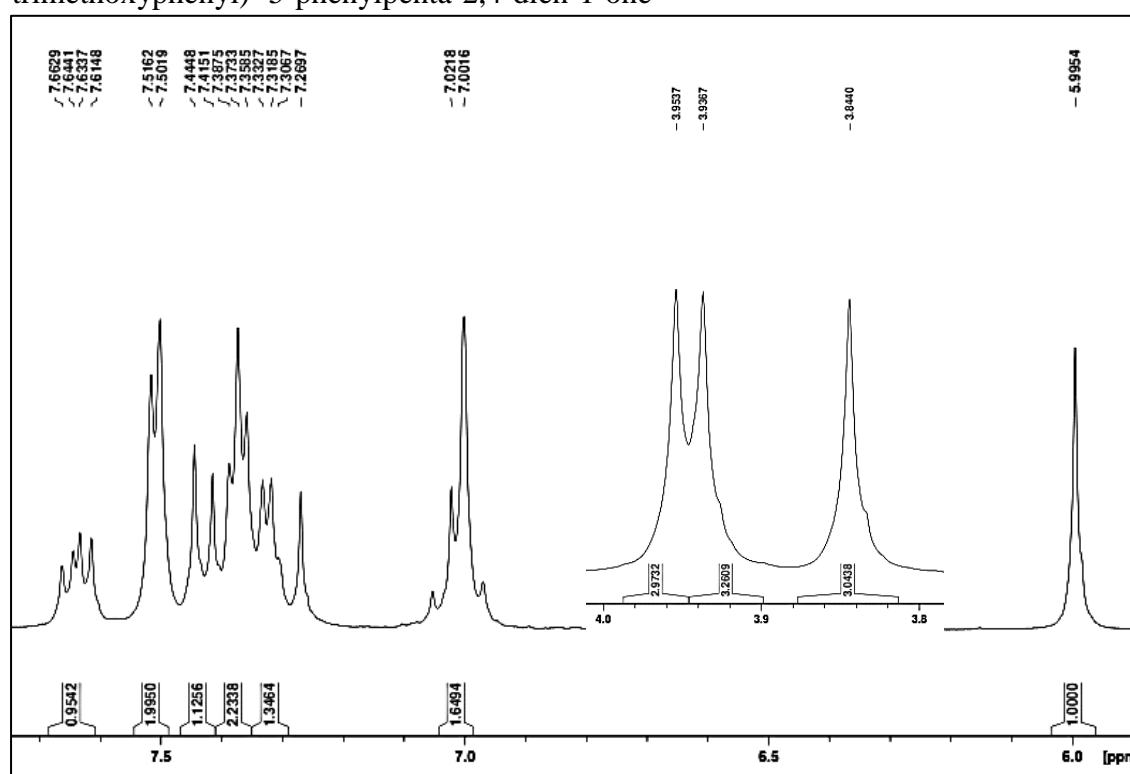


Figure S2. Expansion of the  $^1\text{H}$  NMR spectrum ( $\text{CDCl}_3$ , 500 MHz) of Chalcona ( $2E, 4E$ )-1-(2-hydroxy-3,4,6-trimethoxyphenyl)-5-phenylpenta-2,4-dien-1-one

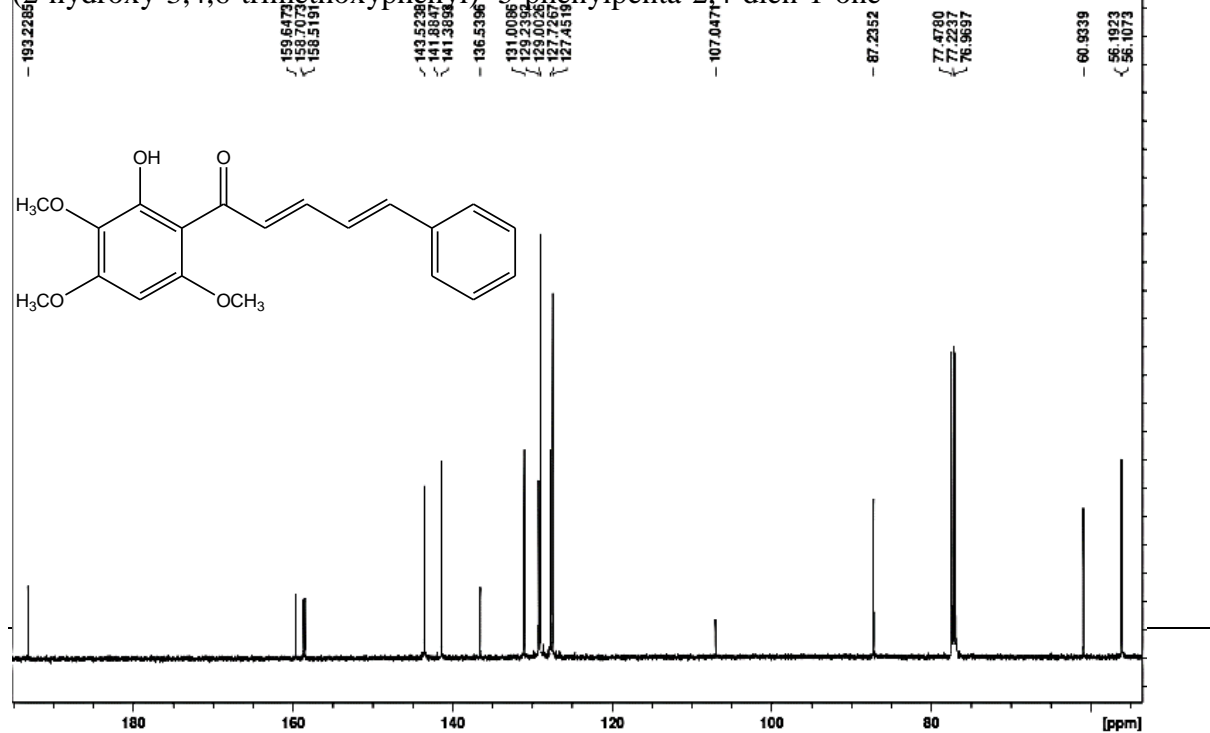


Figure S3.  $^{13}\text{C}$  NMR ( $\text{CDCl}_3$ , 125 MHz) spectrum of Chalcona (*2E*, *4E*) -1- (2-hydroxy-3,4,6-trimethoxyphenyl) -5-phenylpenta-2,4-dien-1-one

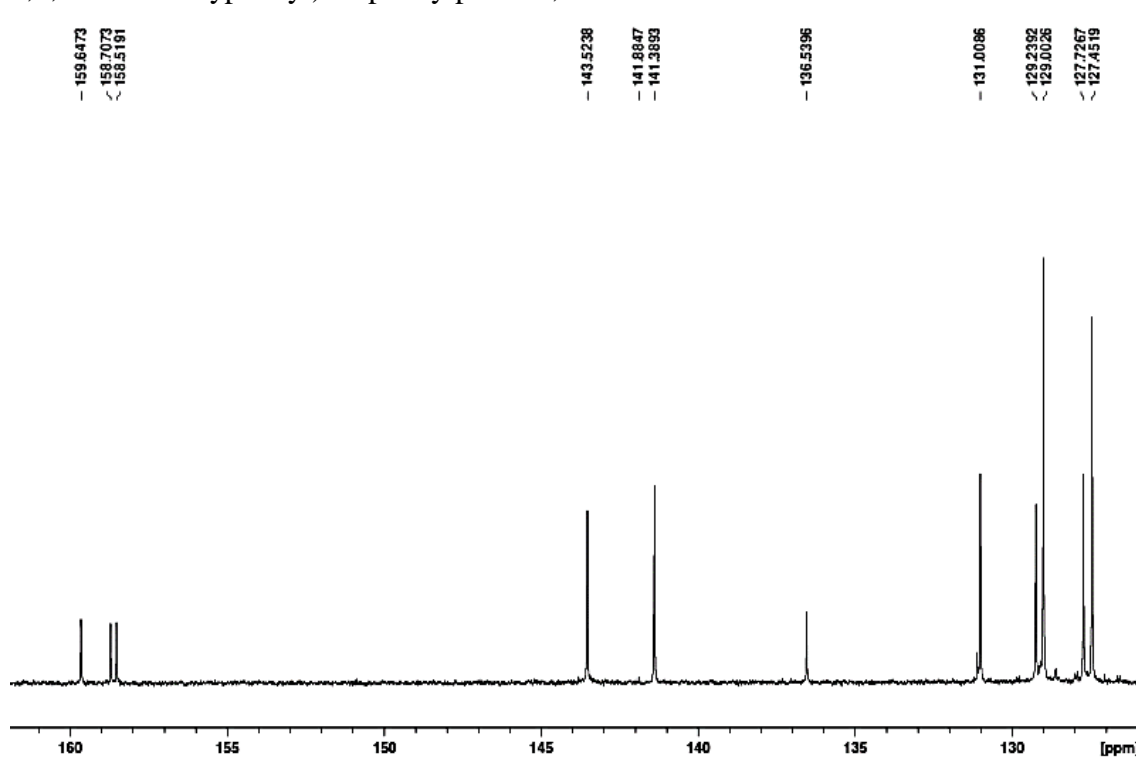


Figure S4. Expansion of the NMR  $^{13}\text{C}$  ( $\text{CDCl}_3$ , 125 MHz) spectrum of Chalcona (*2E*, *4E*) -1- (2-hydroxy-3,4,6-trimethoxyphenyl) -5-phenylpenta-2,4-dien-1-one

## **Spectroscopic analysis by NMR, FT-Raman, ATR-FTIR, and UV-Vis, evaluation of antimicrobial activity, and *in silico* studies of chalcones derived from 2-hydroxyacetophenone**

Jayze da Cunha Xavier<sup>a</sup>, Francisco W.Q. de Almeida-Neto<sup>h</sup>, Janaina E. Rocha<sup>a</sup>, Thiago S. Freitas<sup>a</sup>, Priscila R. Freitas<sup>a</sup>, Ana C.J. de Araújo<sup>a</sup>, Priscila.T. da Silva<sup>b</sup>, Carlos E.S. Nogueira<sup>a,d</sup>, Paulo N. Bandeira<sup>b</sup>, Marcia M. Marinho<sup>c</sup>, Emmanuel S. Marinho<sup>f</sup>, Nitin Kumar<sup>c</sup>,

Antonio C.H. Barreto<sup>g</sup>, Henrique D.M. Coutinho<sup>a</sup>, Murilo S.S. Julião<sup>b</sup>, Hécio S. dos Santos<sup>a,b</sup>, Alexandre M.R. Teixeira<sup>a,d6\*</sup>

<sup>a</sup> Department of Biological Chemistry, Regional University of Cariri, CE, Brazil.

<sup>b</sup> Center for Exact Sciences and Technology, Chemistry Course, Vale do Acaraú University, Sobral, CE, Brazil.

<sup>c</sup> KR Mangalan University, Sohna Road, Gurugram, India

<sup>d</sup> Department of Physics, Regional University of Cariri, Juazeiro do Norte, CE, Brazil

<sup>e</sup> State University of Ceará, Faculty of Education, Science and Letters of Iguatu Iguatu, CE, Brazil.

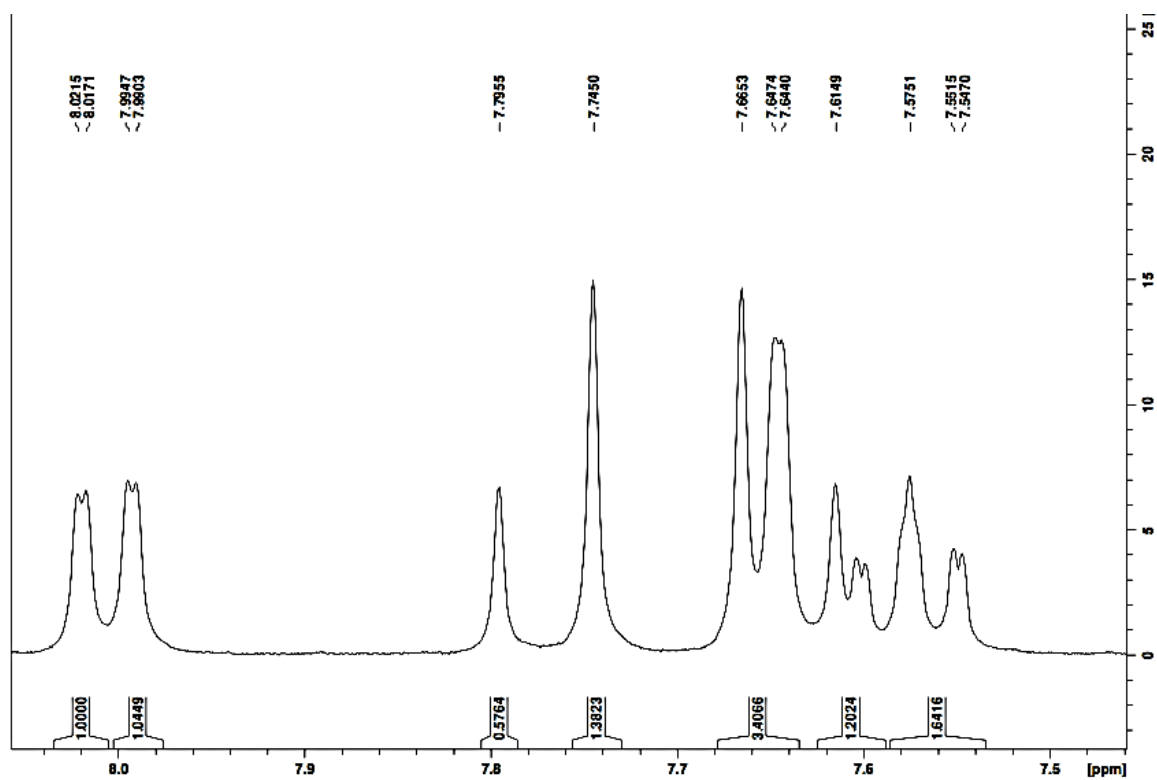
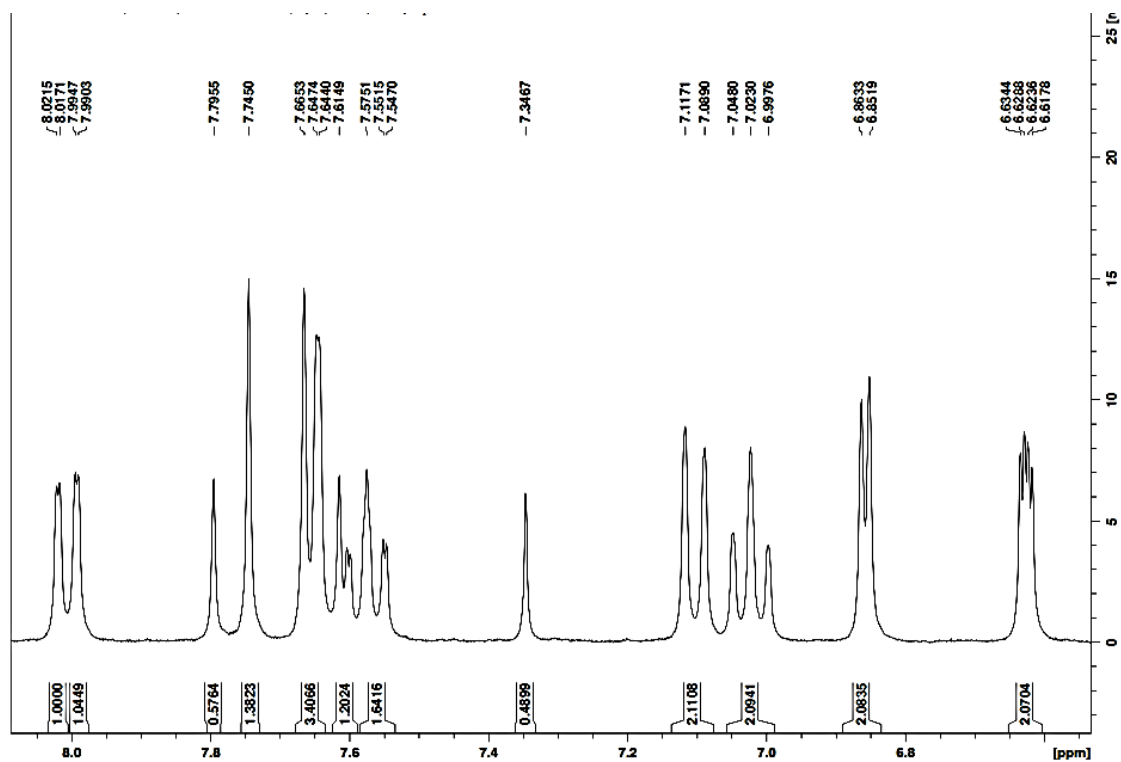
<sup>f</sup> State University of Ceará, Faculty of Philosophy Dom Aureliano Matos, Limoeiro do Norte, CE, Brazil

<sup>g</sup> Department of Physics, Federal University of Ceará, Fortaleza, CE, Brazil.

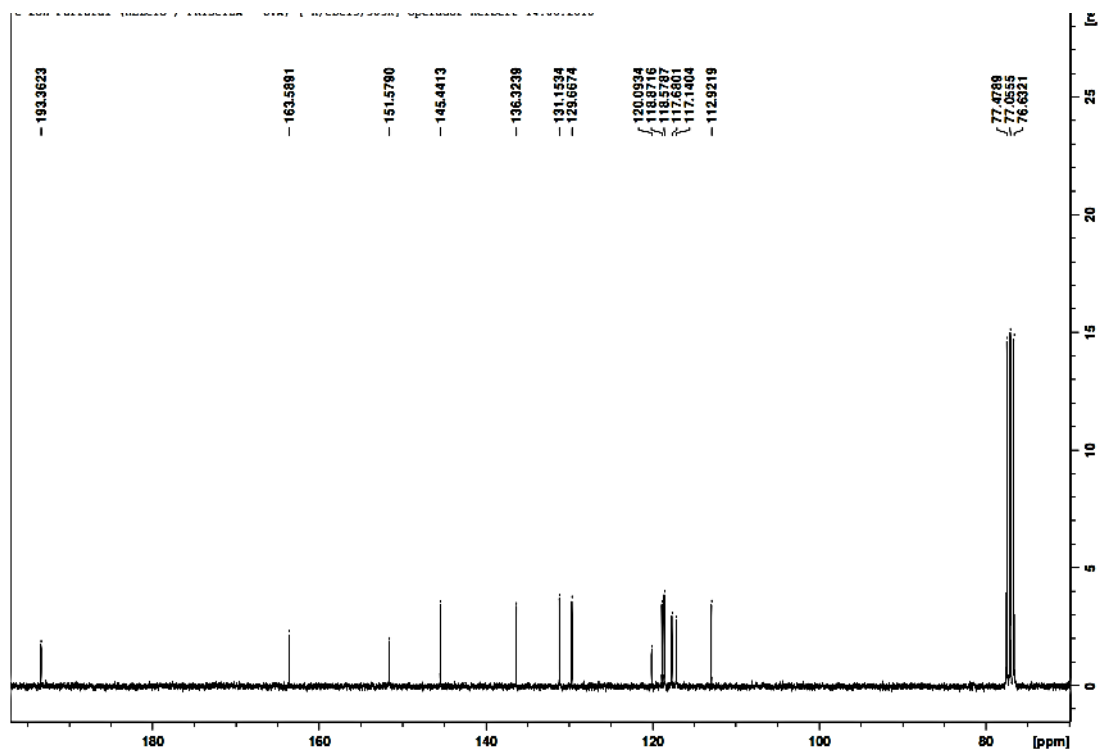
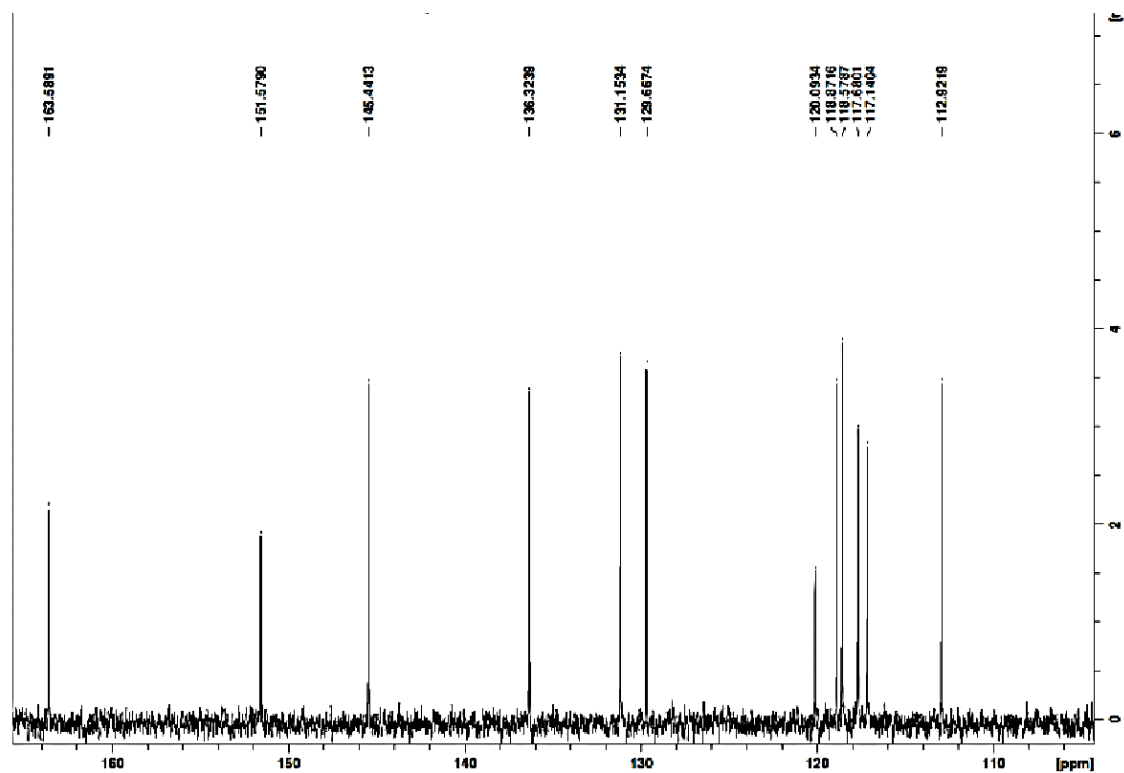
<sup>h</sup> Department of Analytical Chemistry and Physical Chemistry, Federal University of Ceará, Fortaleza, CE, Brazil

---

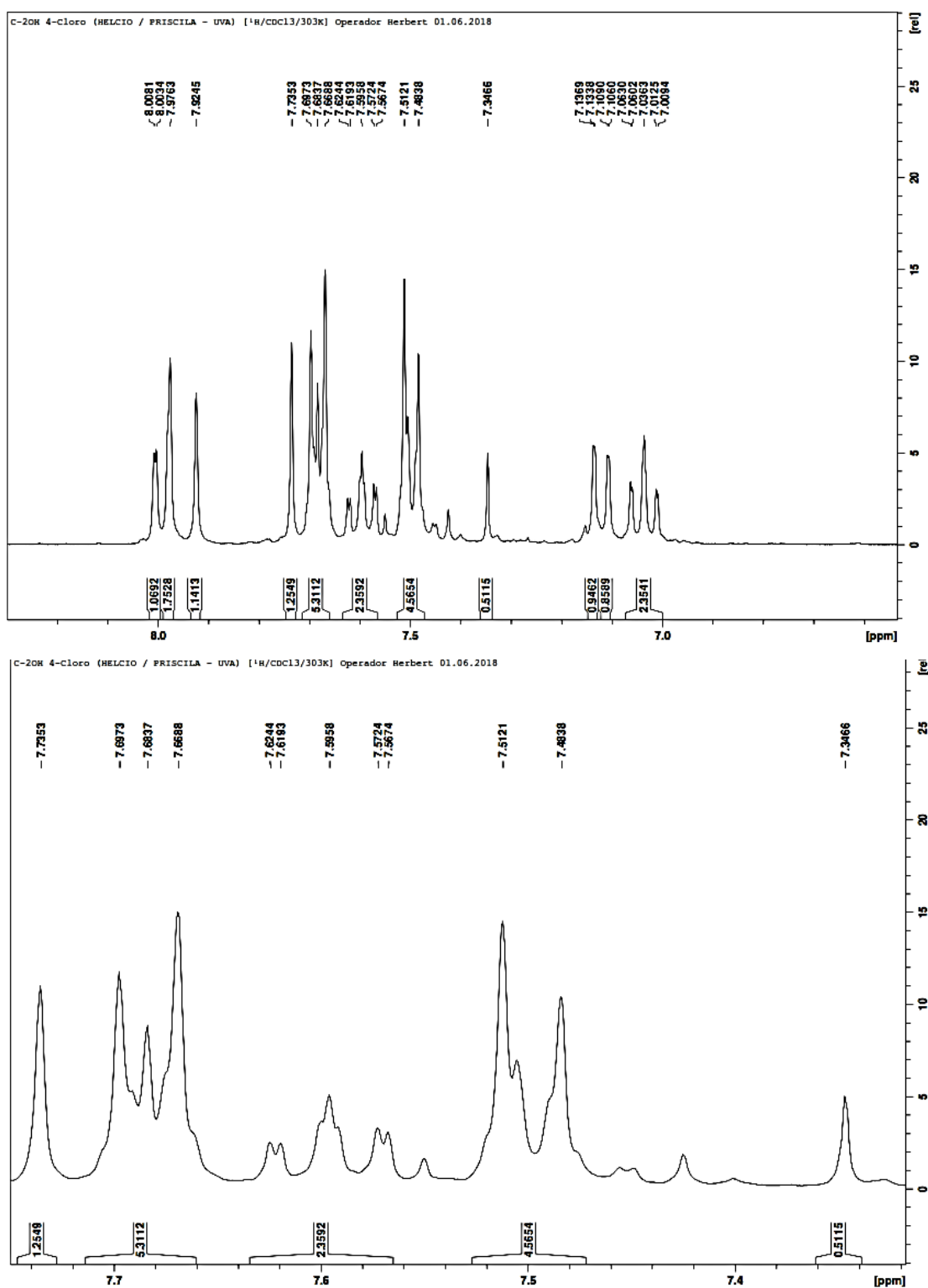
<sup>6\*</sup> Corresponding author. Postgraduate Program in Biological Chemistry, Department of Biological Chemistry, Regional University of Cariri, Campus Pimenta II, CEP: 63.100-000, Crato, CE, Brazil. E-mail addresses: [alexandre.teixeira@urca.br](mailto:alexandre.teixeira@urca.br)



**Figure S1 (a).** Spectrum of  $^1\text{H}$ NMR ( $\text{CDCl}_3$ , 500 MHz) of chalcone(*E*)-3-(furan-2-yl)-1-(2-hydroxyphenyl)prop-2-en-1-one (**A1**).



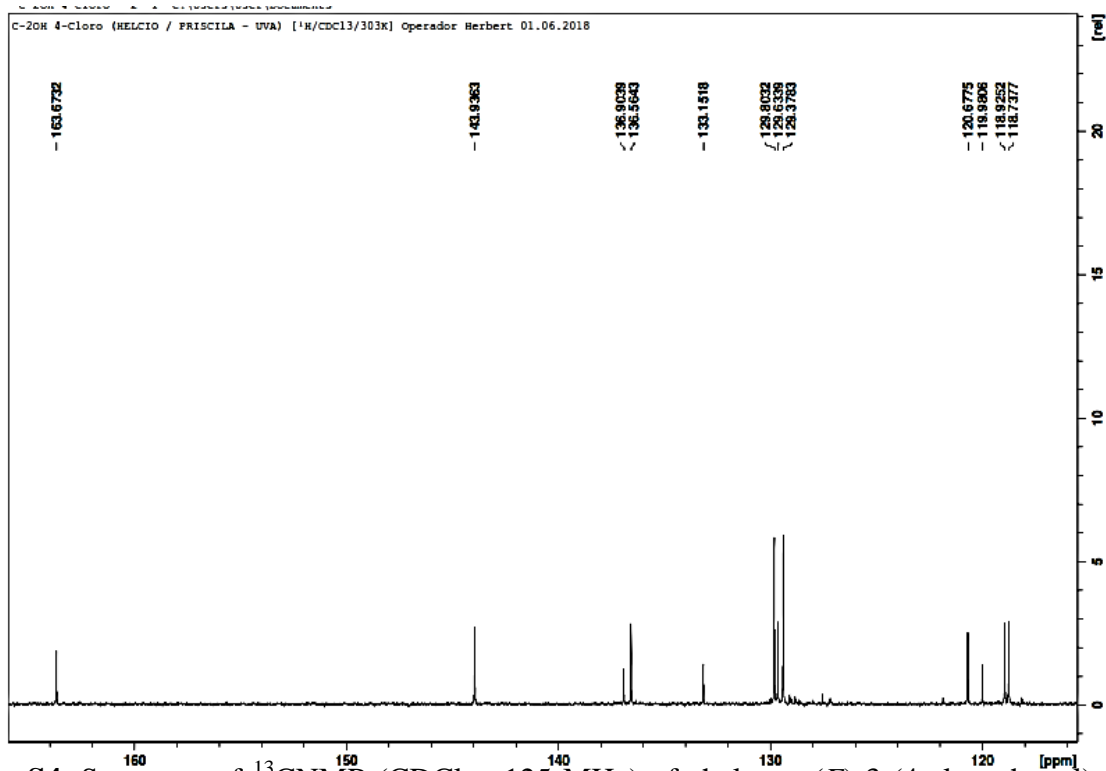
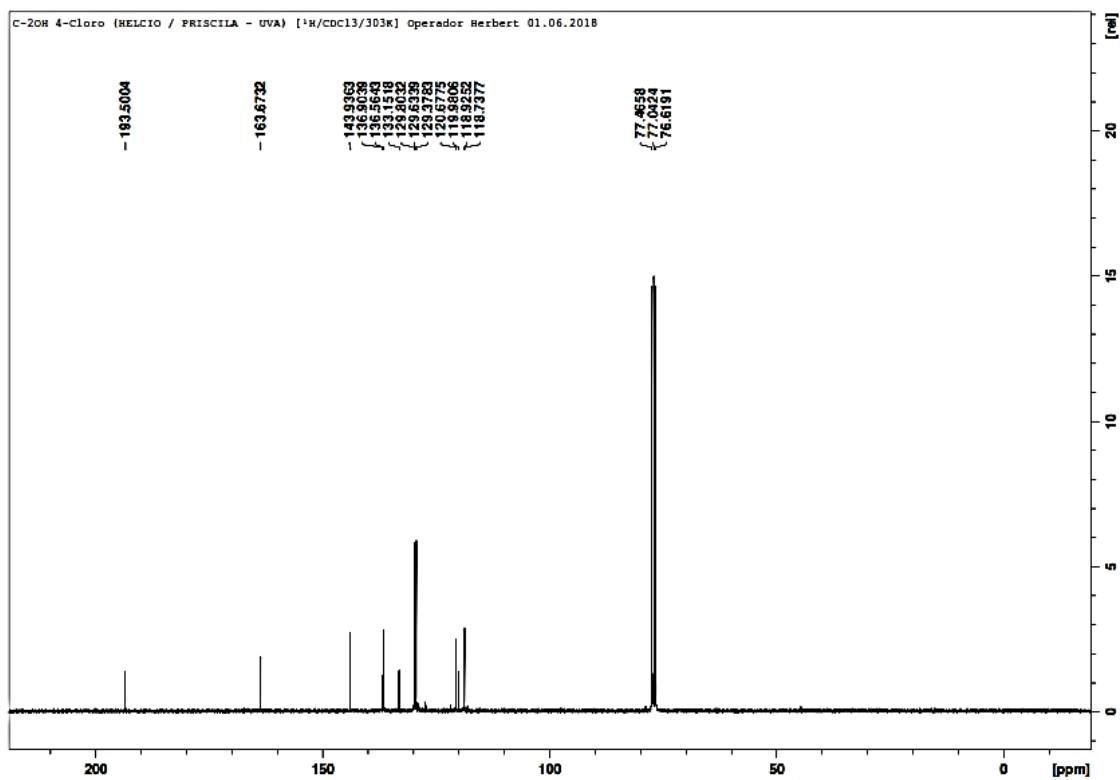
**Figure S2.** Spectrum of  $^{13}\text{C}$ NMR ( $\text{CDCl}_3$ , 125 MHz) of chalcone(*E*)-3-(furan-2-yl)-1-(2-hydroxyphenyl)prop-2-en-1-one (**A1**).



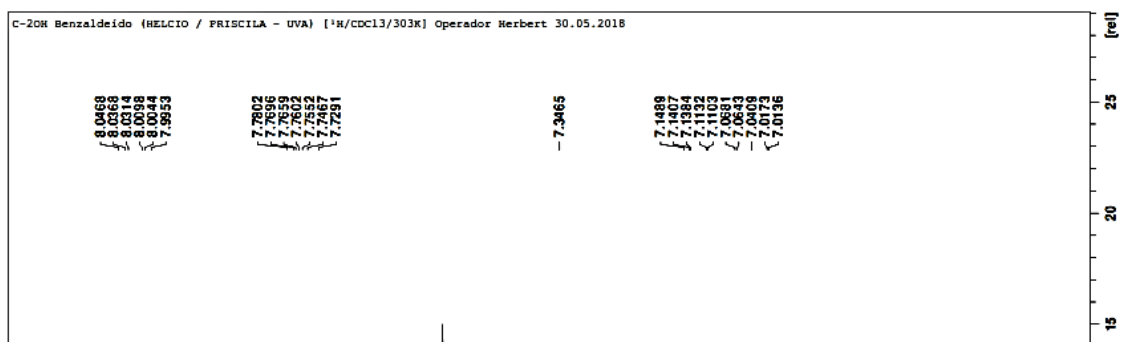
**Figure S3.** Spectrum of <sup>1</sup>HNMR (CDCl<sub>3</sub>, 500 MHz) of chalcone (*E*)-3-(4-chlorophenyl)-1-(2-hydroxyphenyl)prop-2-en-1-one (**A2**).







**Figure S4.** Spectrum of <sup>13</sup>CNMR (CDCl<sub>3</sub>, 125 MHz) of chalcone (*E*)-3-(4-clorophenyl)-1-(2-hydroxyphenyl)prop-2-en-1-one (**A2**).



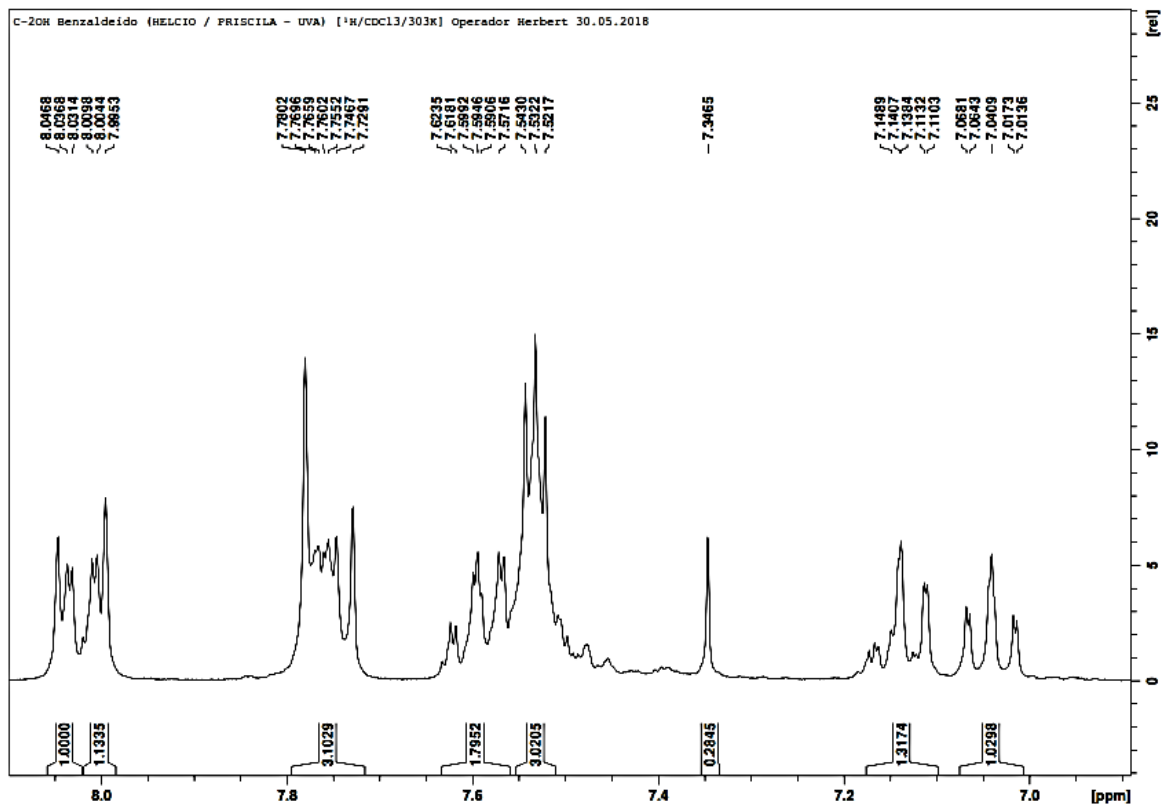


**Figure S5.** Spectrum of <sup>1</sup>HNMR (CDCl<sub>3</sub>, 500 MHz) of chalcone (*E*)-1-(2-hydroxyphenyl)-3-phenyl prop-2-en-1-one (**A3**).

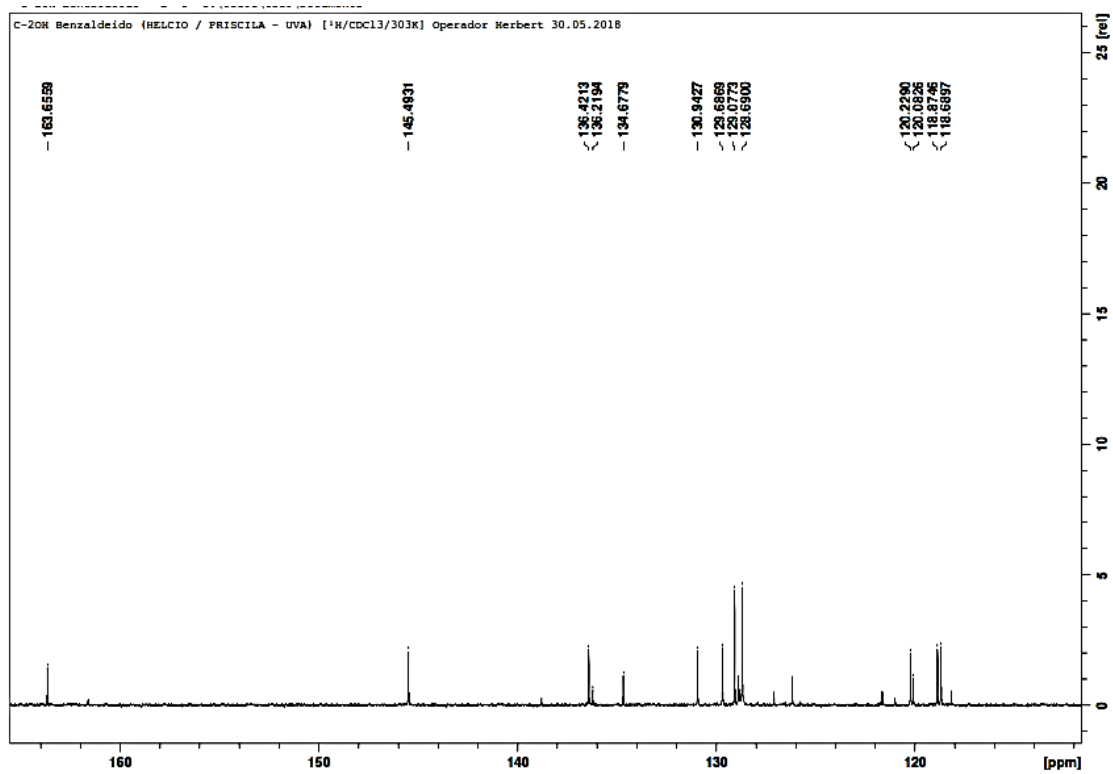
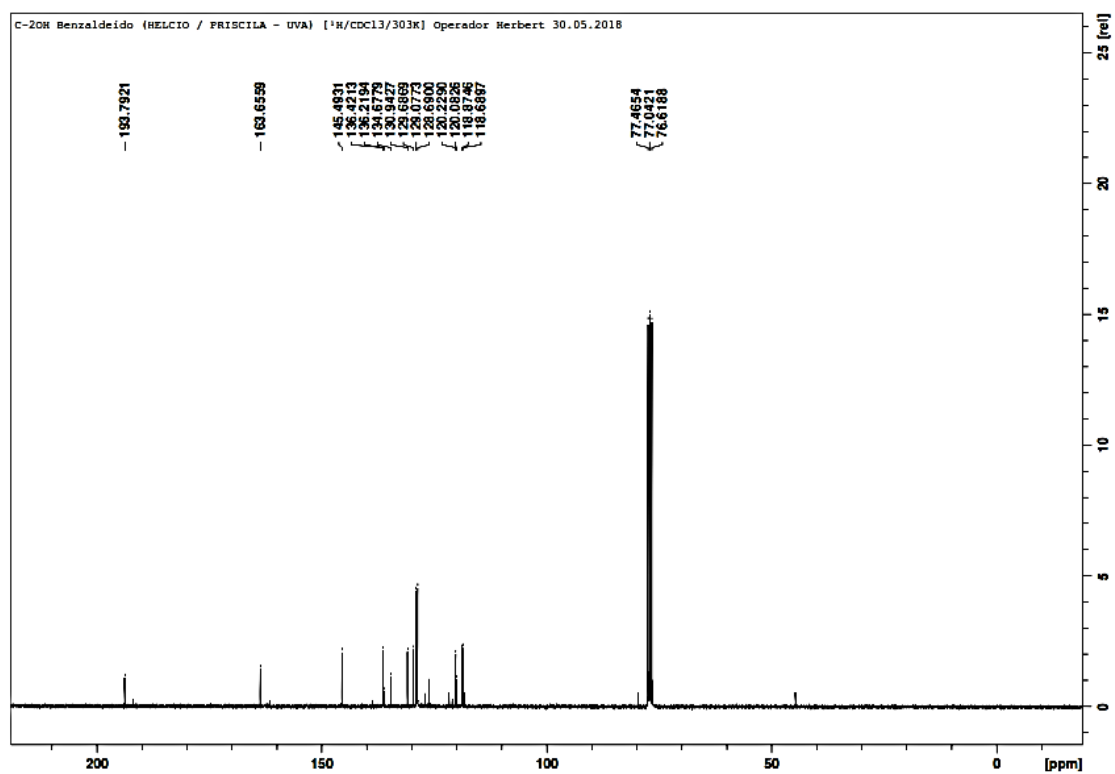


**Figure S6.** Spectrum of <sup>13</sup>CNMR (CDCl<sub>3</sub>, 125 MHz) of chalcone (*E*)-1-(2-hydroxyphenyl)-3-phenyl prop-2-en-1-one (**A3**).

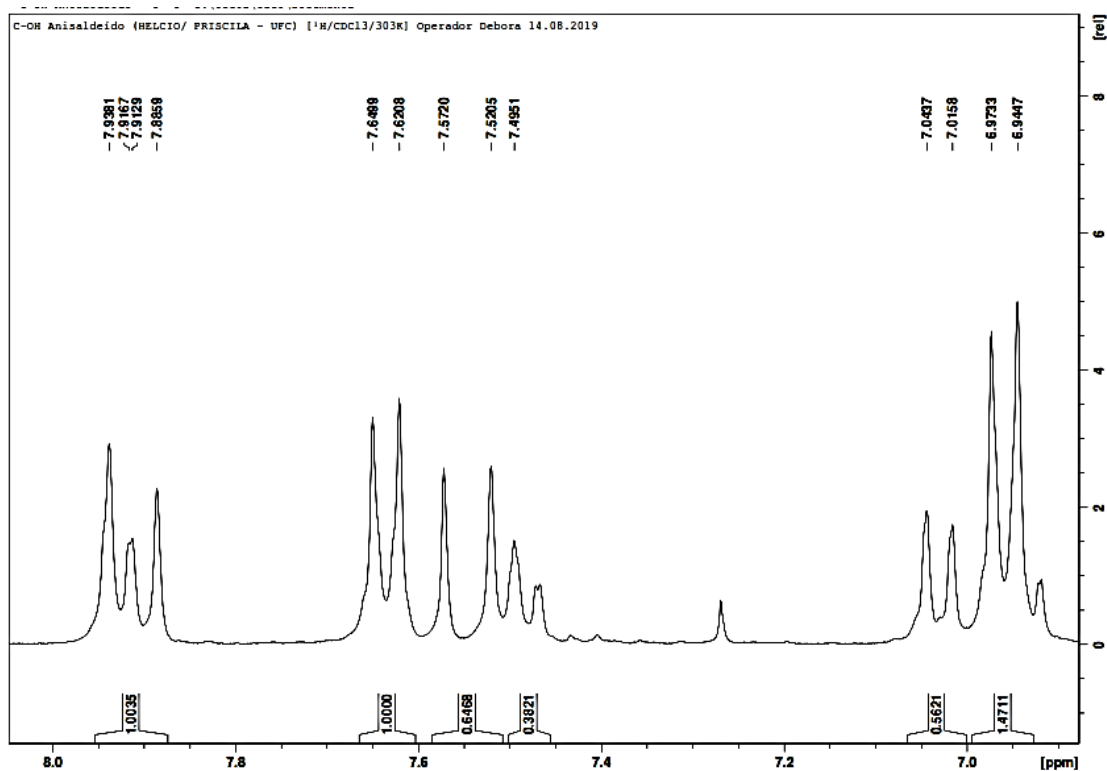
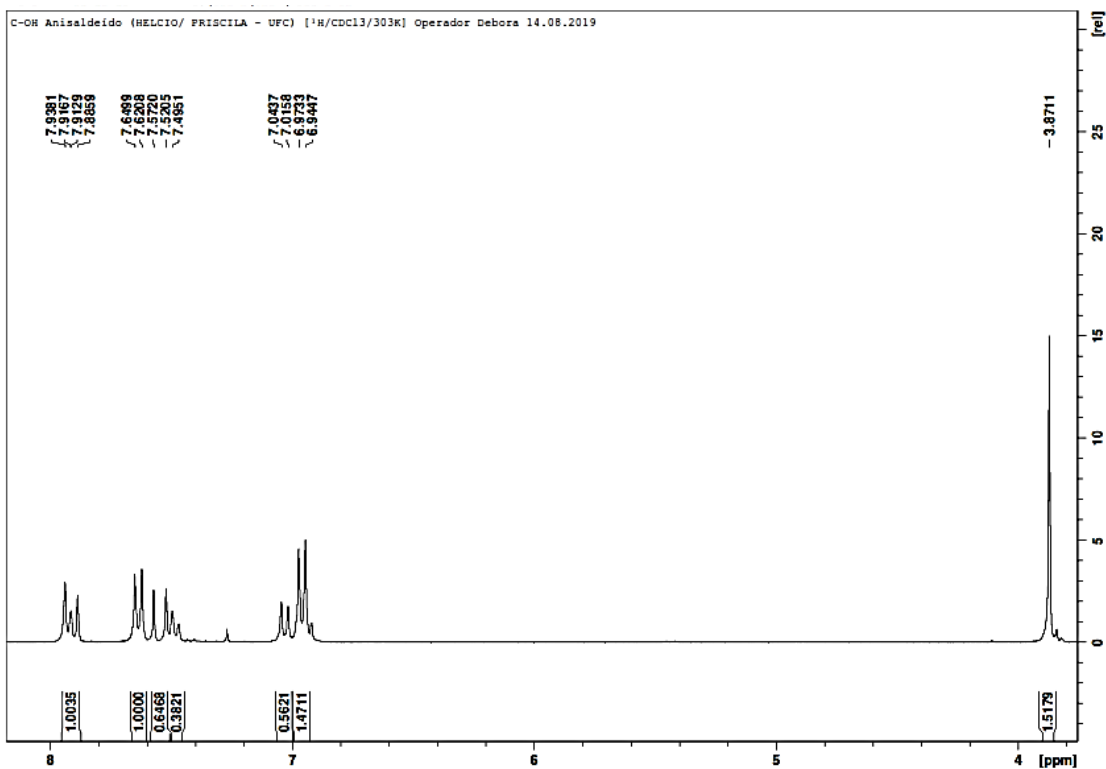


**Figure S7.** Spectrum of <sup>1</sup>HNMR (CDCl<sub>3</sub>, 500 MHz) of chalcone (*E*)-1-(2-hydroxyphenyl)-3-(4-methoxyphenyl)prop-2-en-1-one (**A4**).

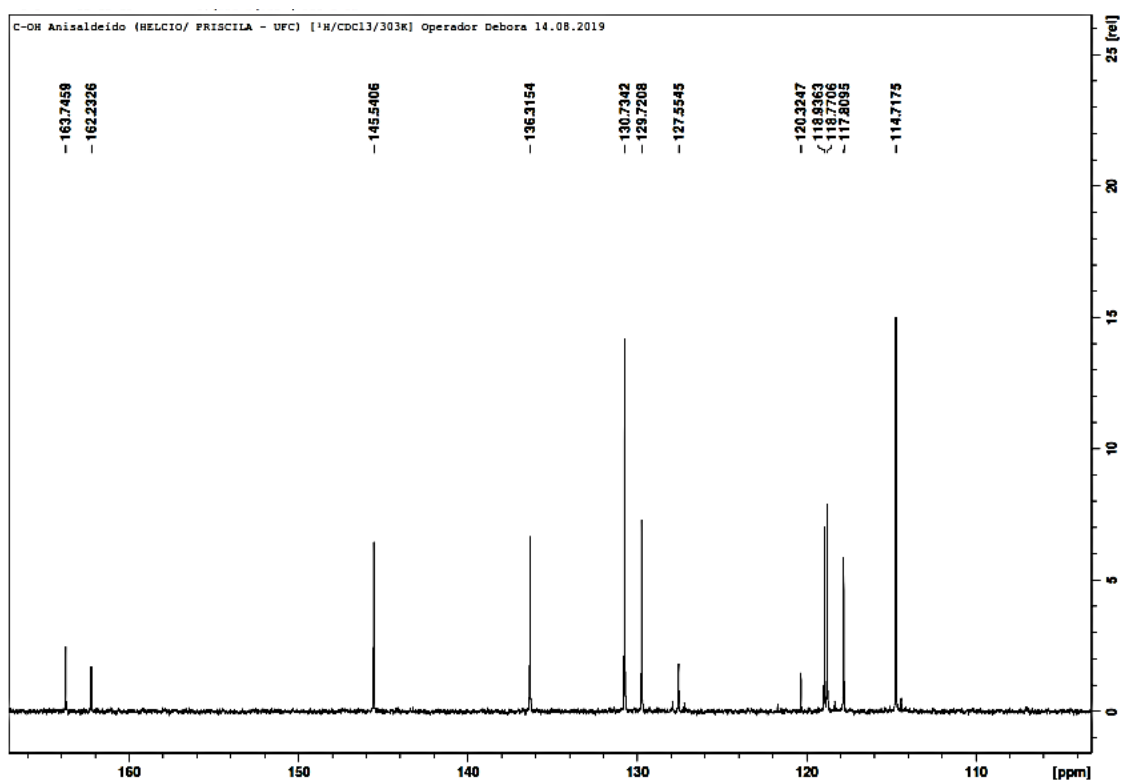
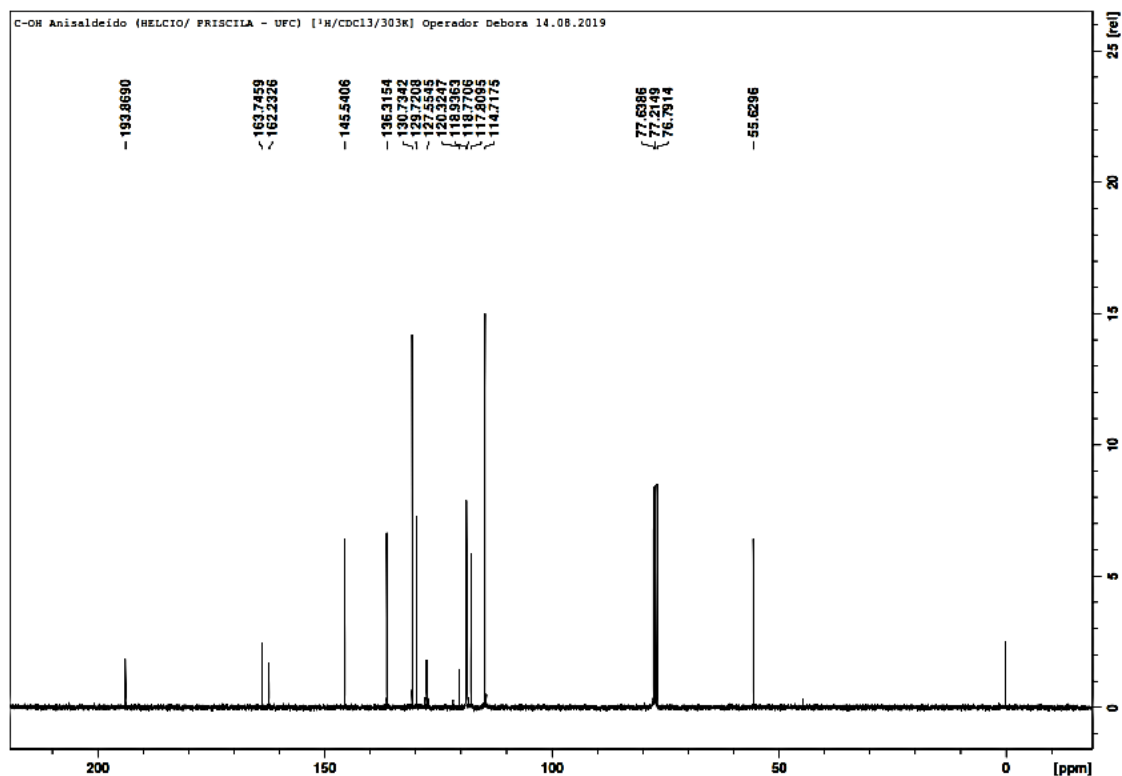


**Figure S8.** Spectrum of <sup>13</sup>CNMR (CDCl<sub>3</sub>, 125 MHz) of chalcone (*E*)-1-(2-hydroxyphenyl)-3-(4-methoxyphenyl)prop-2-en-1-one (**A4**).

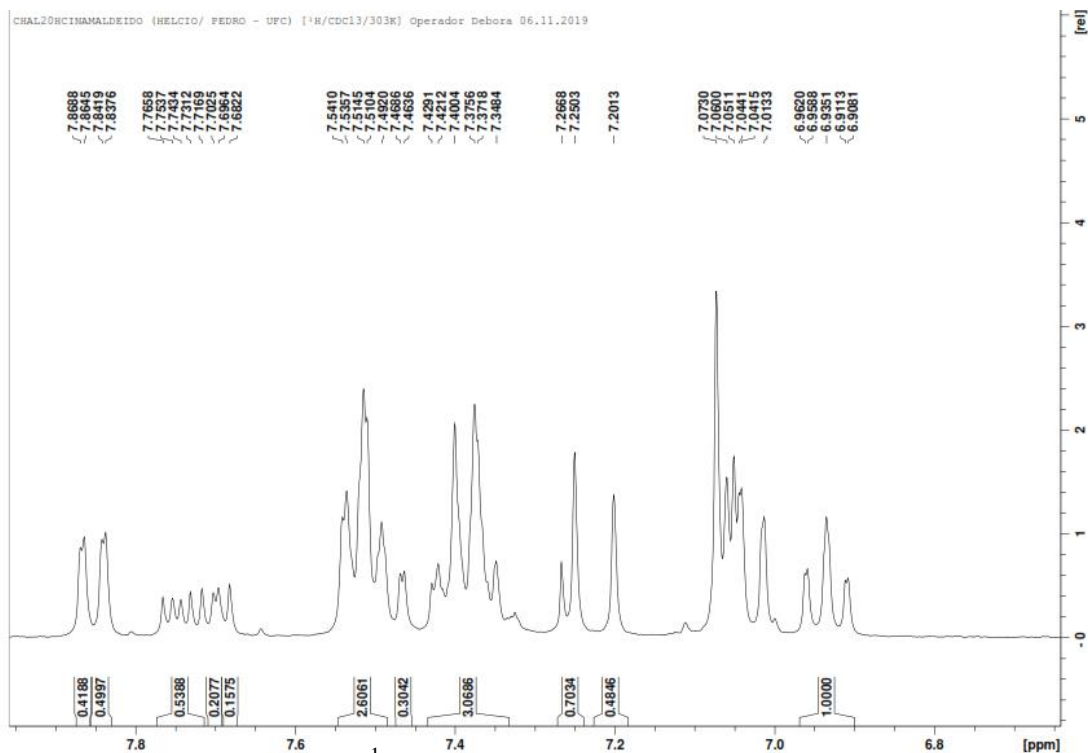
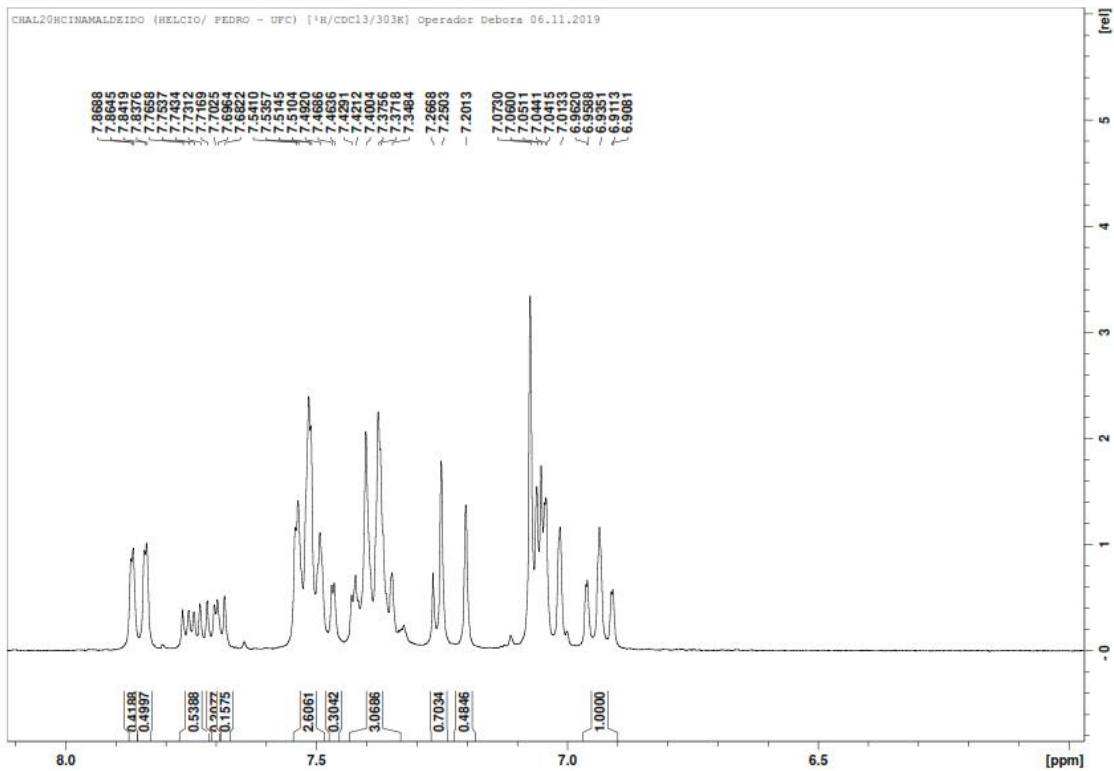


**Figure S9.** Spectrum of  $^1\text{H}$ NMR ( $\text{CDCl}_3$ , 500 MHz) of chalcone ( $2E$ ,  $4E$ )-1-(2-hydroxyphenyl)-5-phenylpenta-2,4-dien-1-one (**A5**).

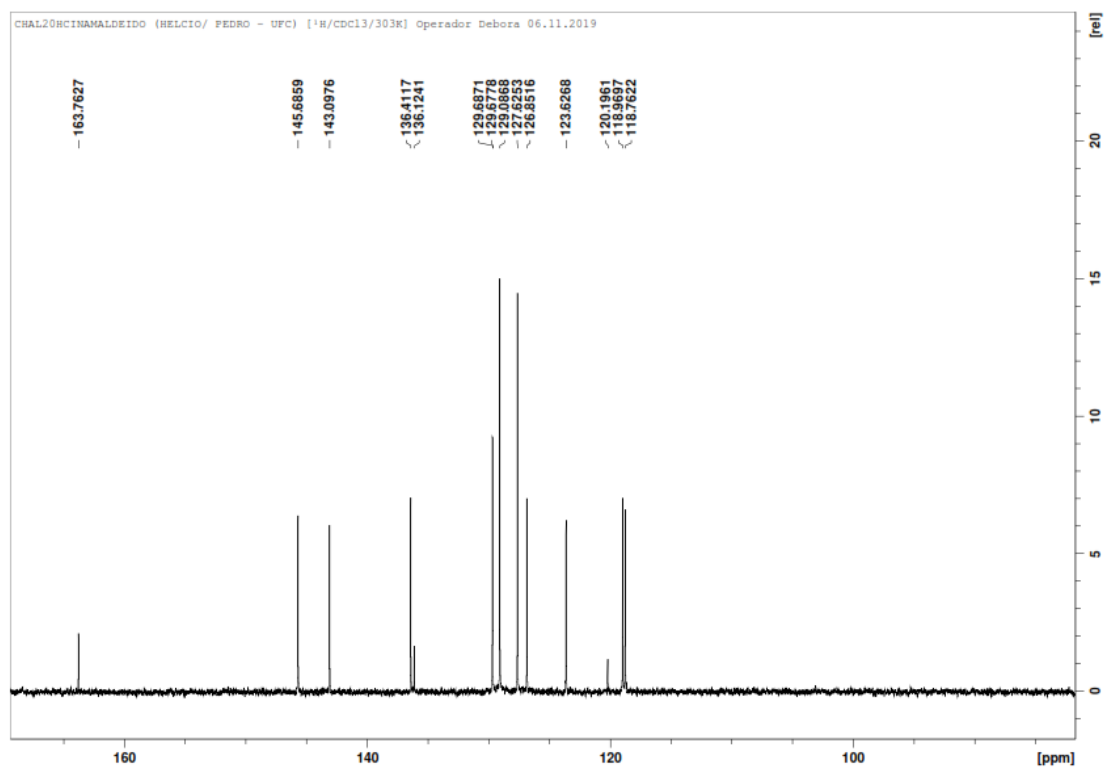
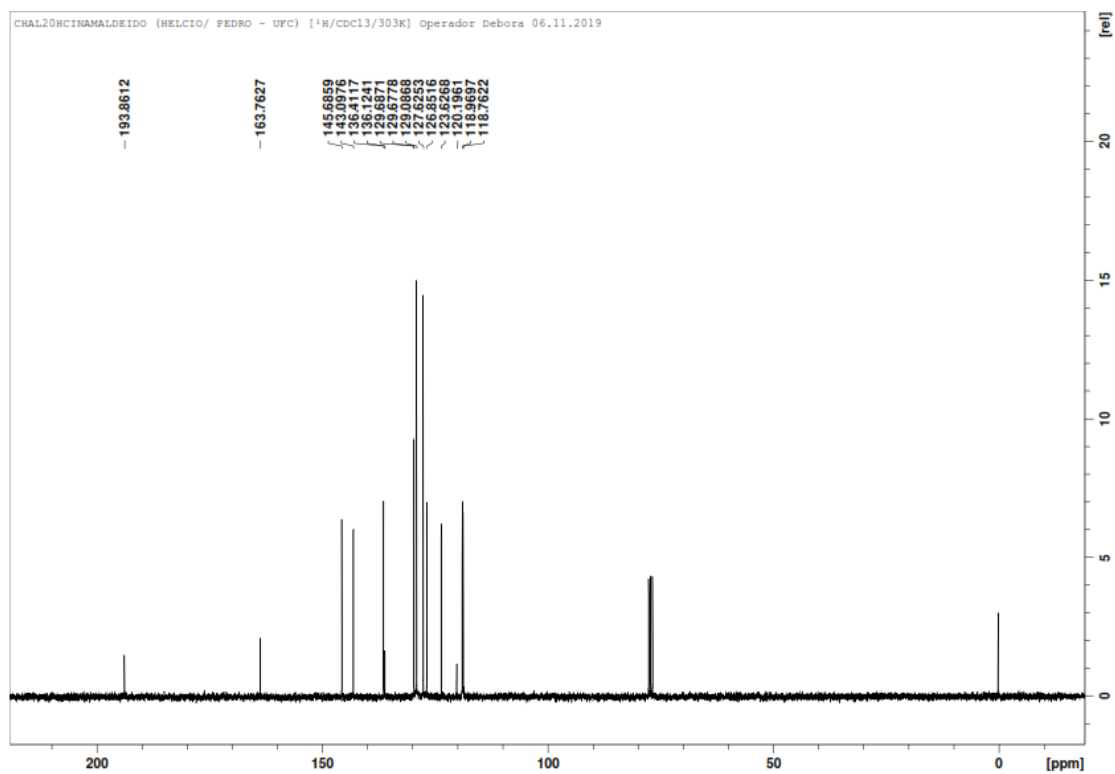


**Figure 10.** Spectrum of  $^{13}\text{C}$ NMR ( $\text{CDCl}_3$ , 125 MHz) of chalcone (*2E*, *4E*)-1-(2-hydroxyphenyl)-5-phenylpenta-2,4-dien-1-one (**A5**).

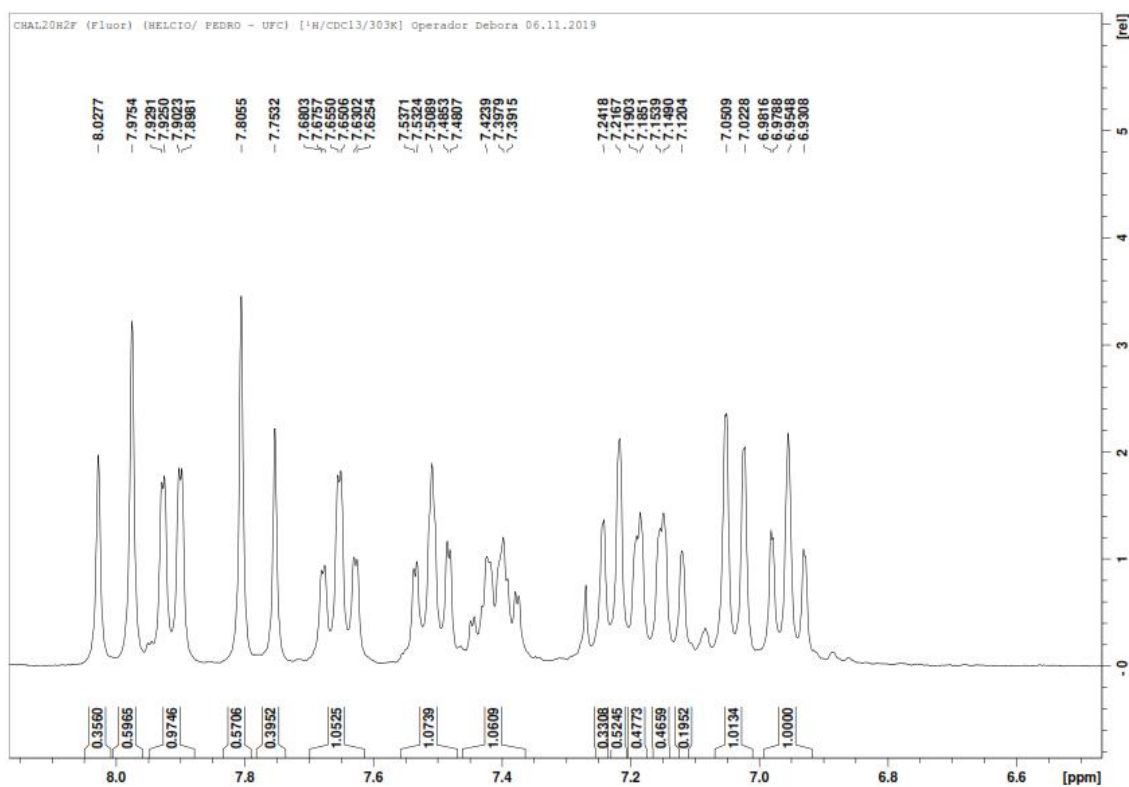
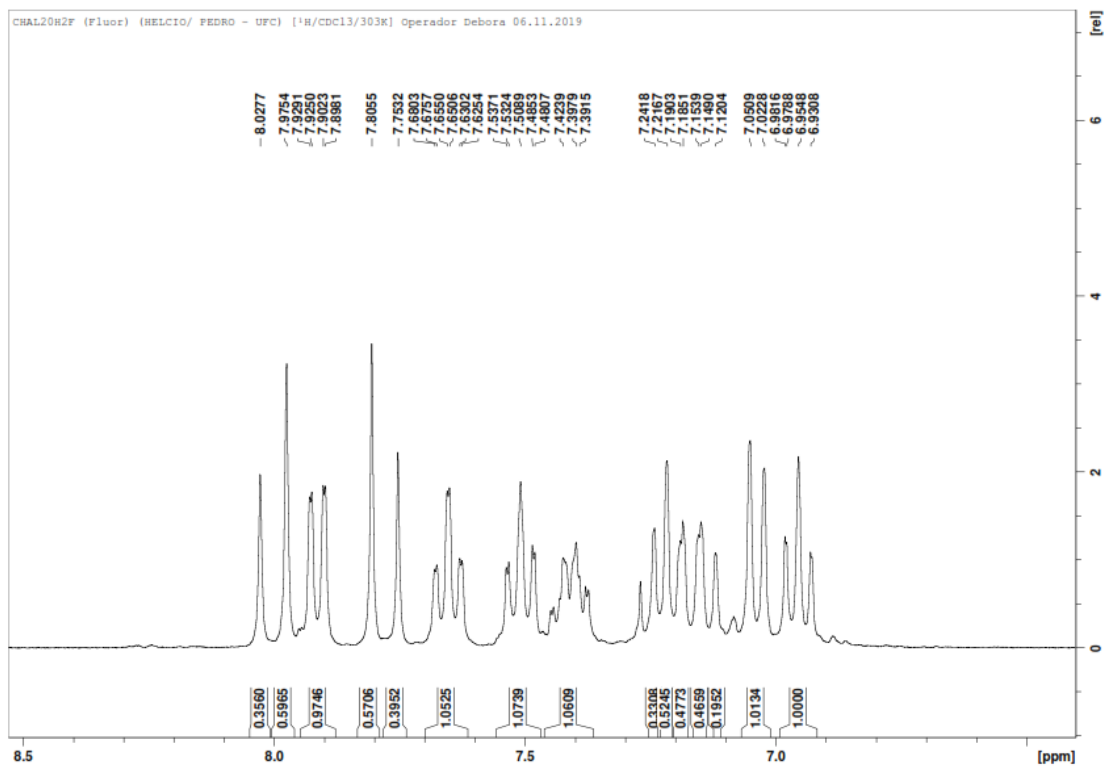


**Figure S11.** Spectrum of <sup>1</sup>H NMR (CDCl<sub>3</sub>, 500 MHz) of chalcone (*E*)-3-(2-fluorophenyl)-1-(2-hydroxyphenyl)prop-2-en-1-one (**A6**).





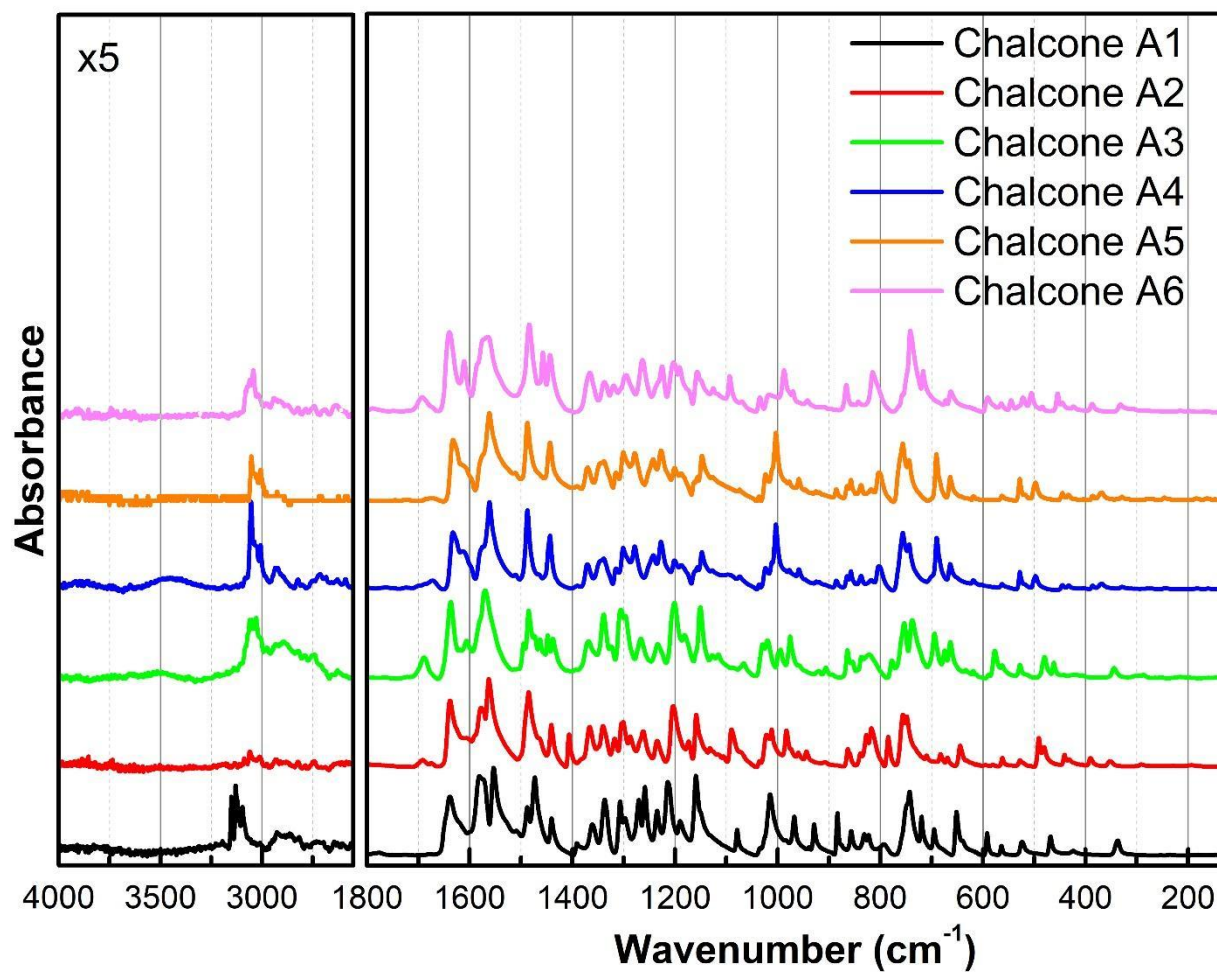


**Figure S13.** Comparative of the ATR-FTIR spectra of the chalcones A1-A6.

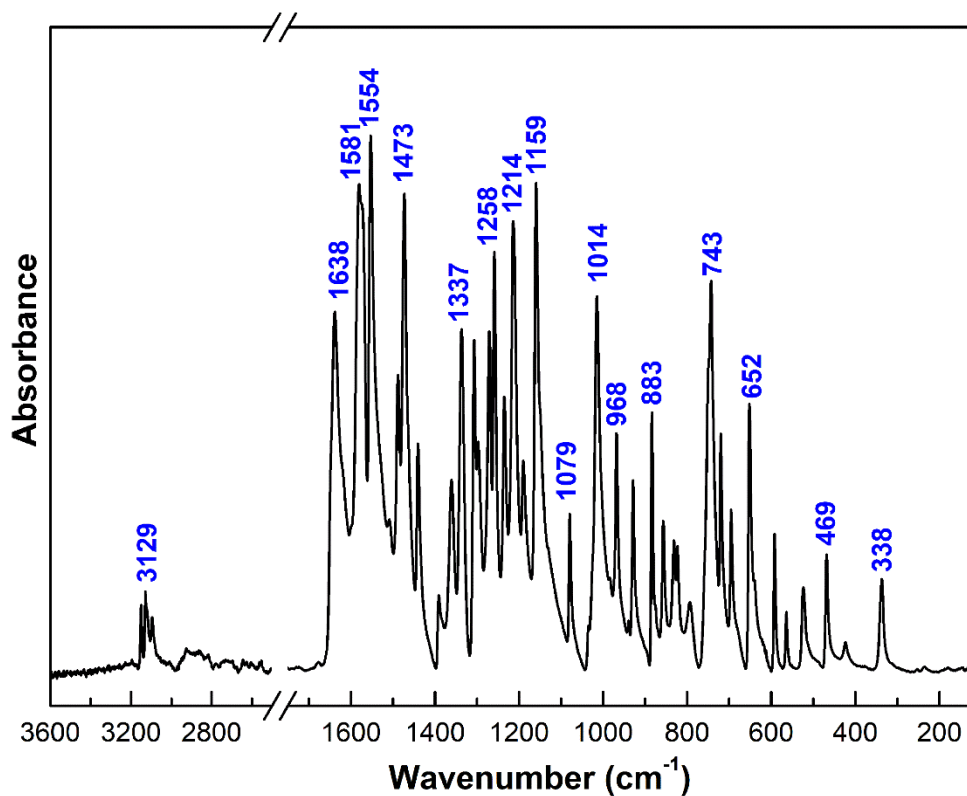


Figure S14. ATR-FTIR spectrum of A1

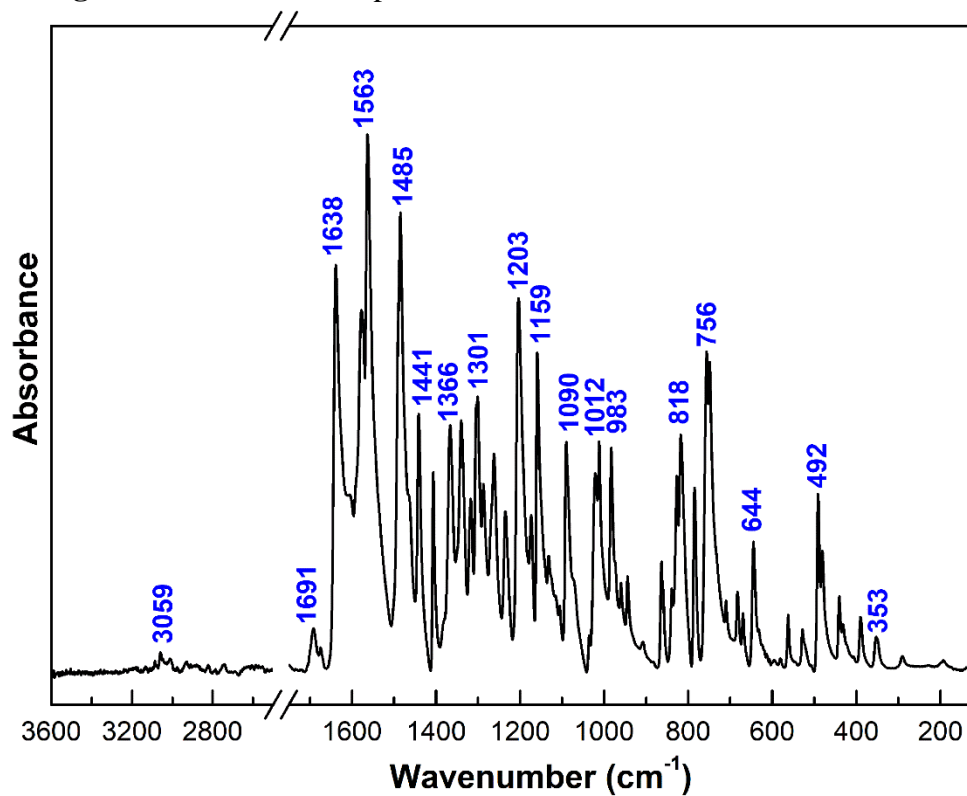


Figure S15. ATR-FTIR spectrum of A2.

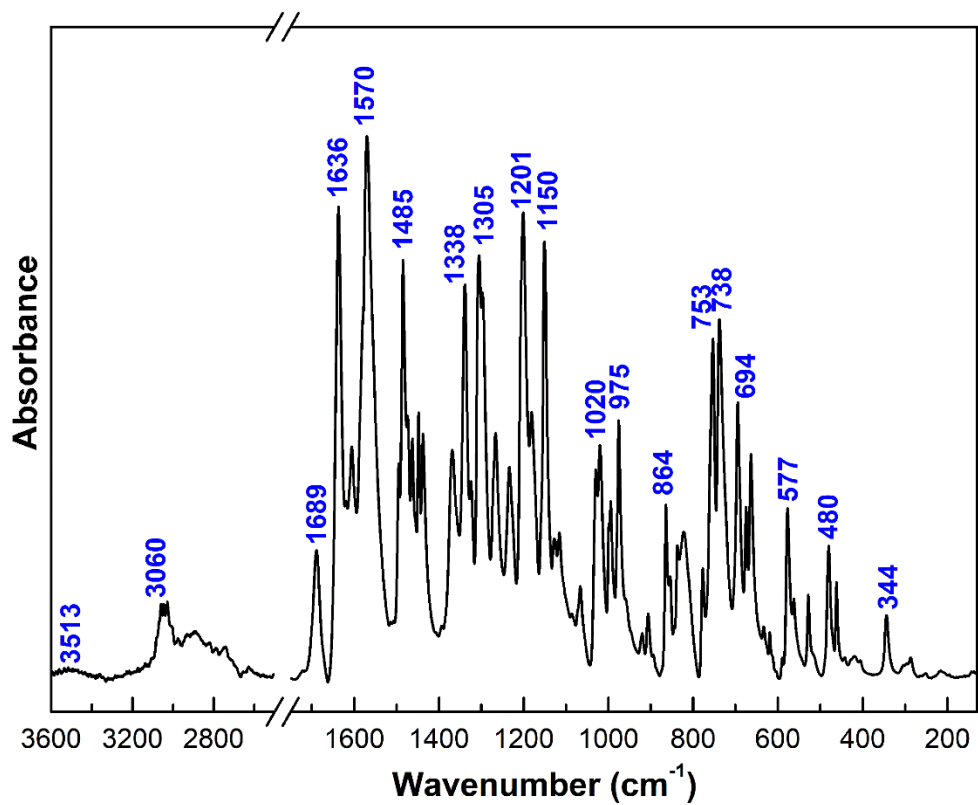


Figure S16. ATR-FTIR spectrum of A3

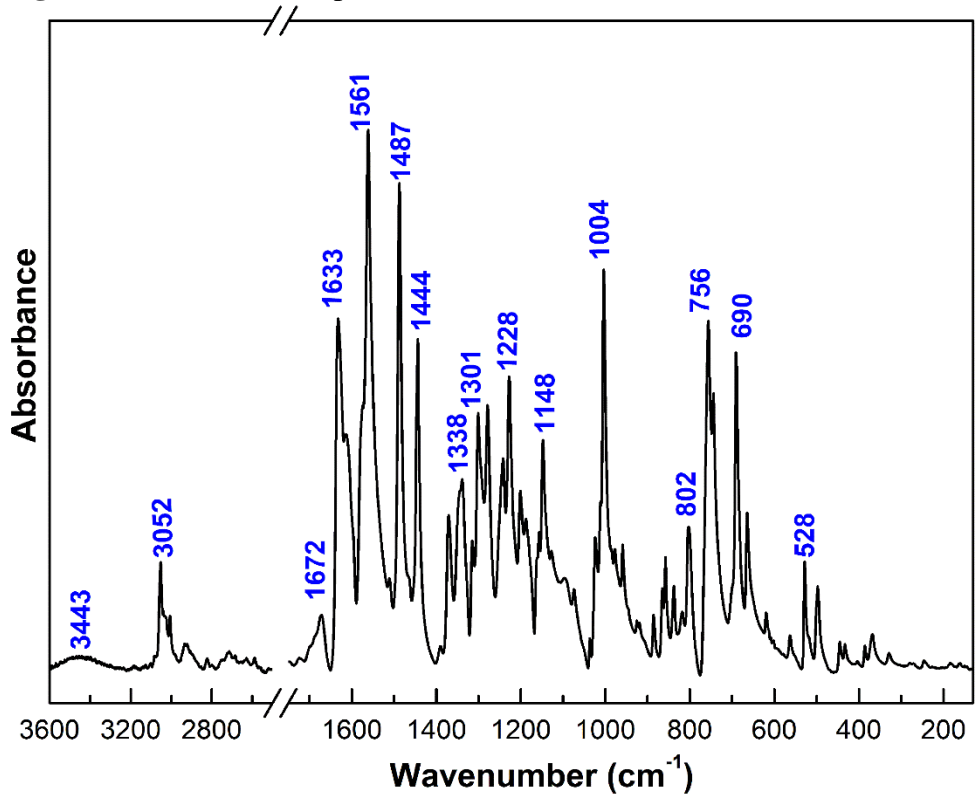


Figure S17. ATR-FTIR spectrum of A4.

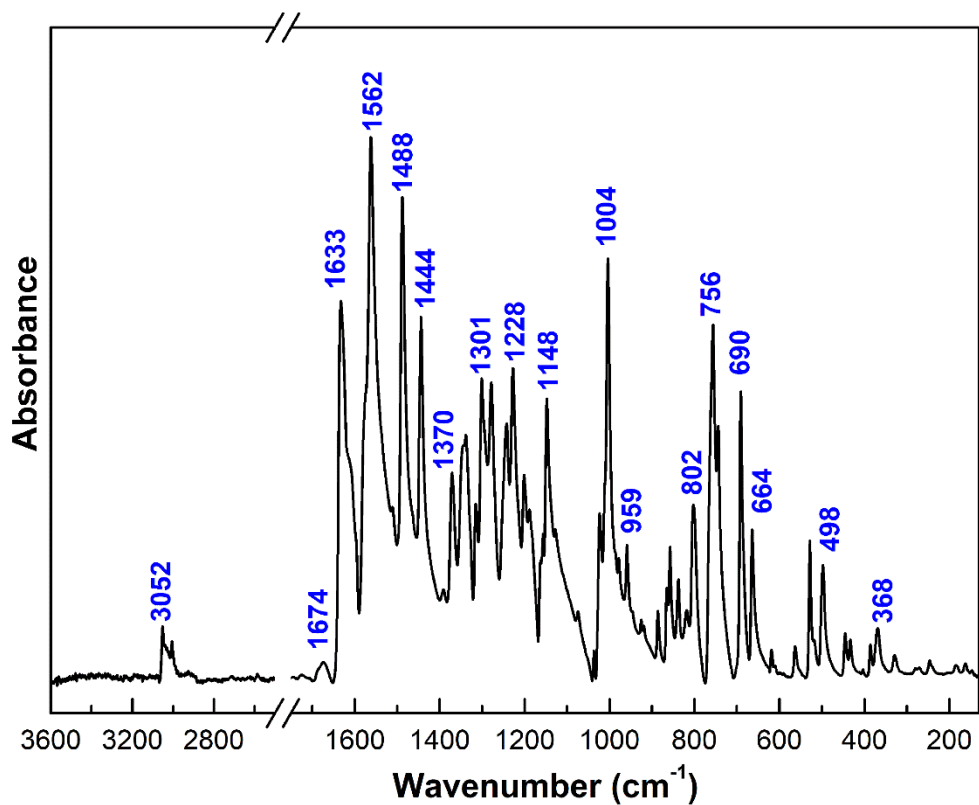


Figure S18. ATR-FTIR spectrum of A5.

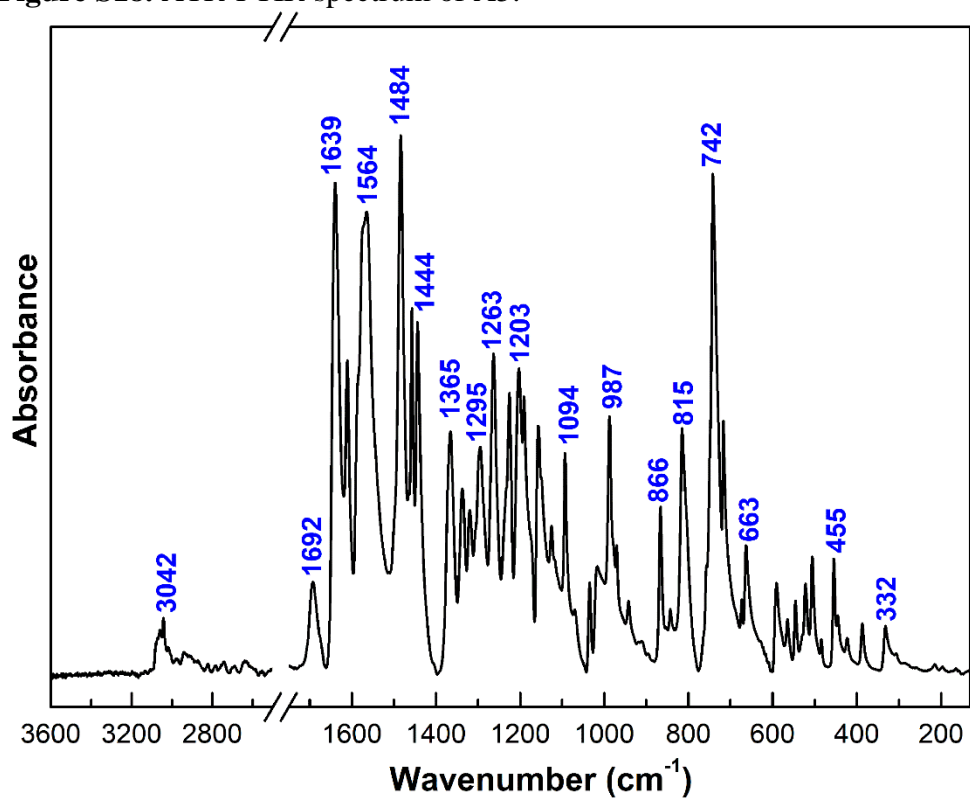
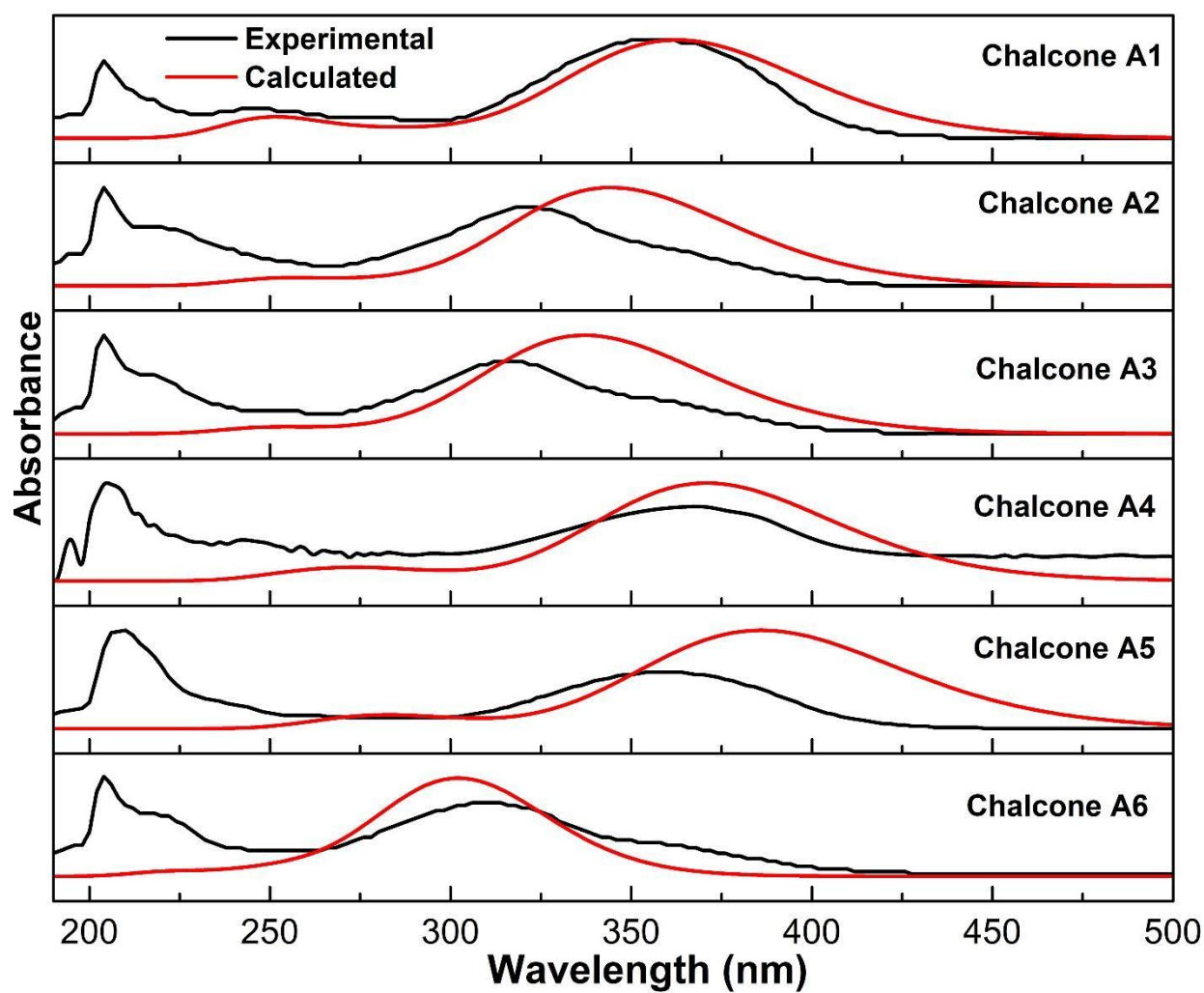
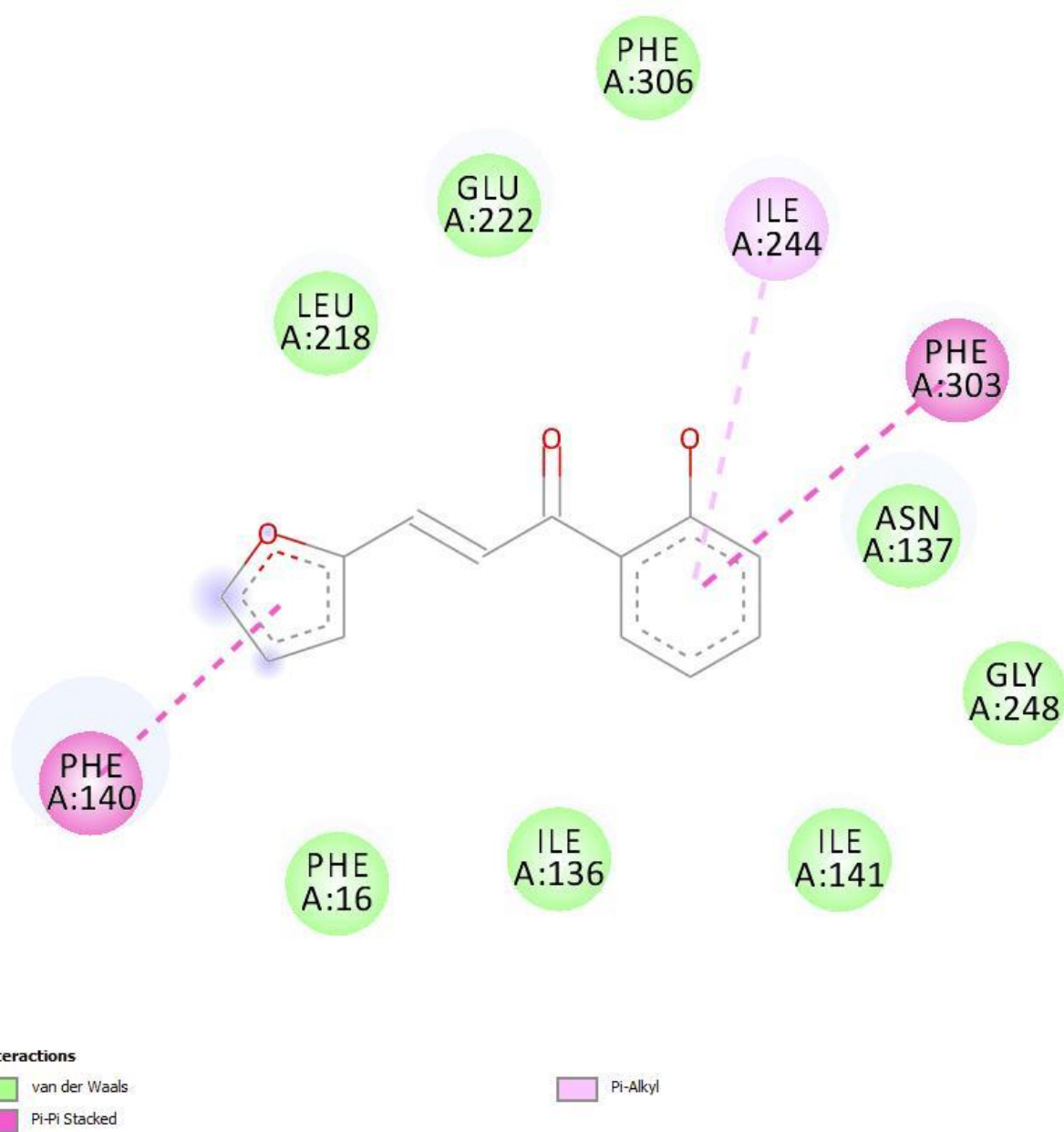


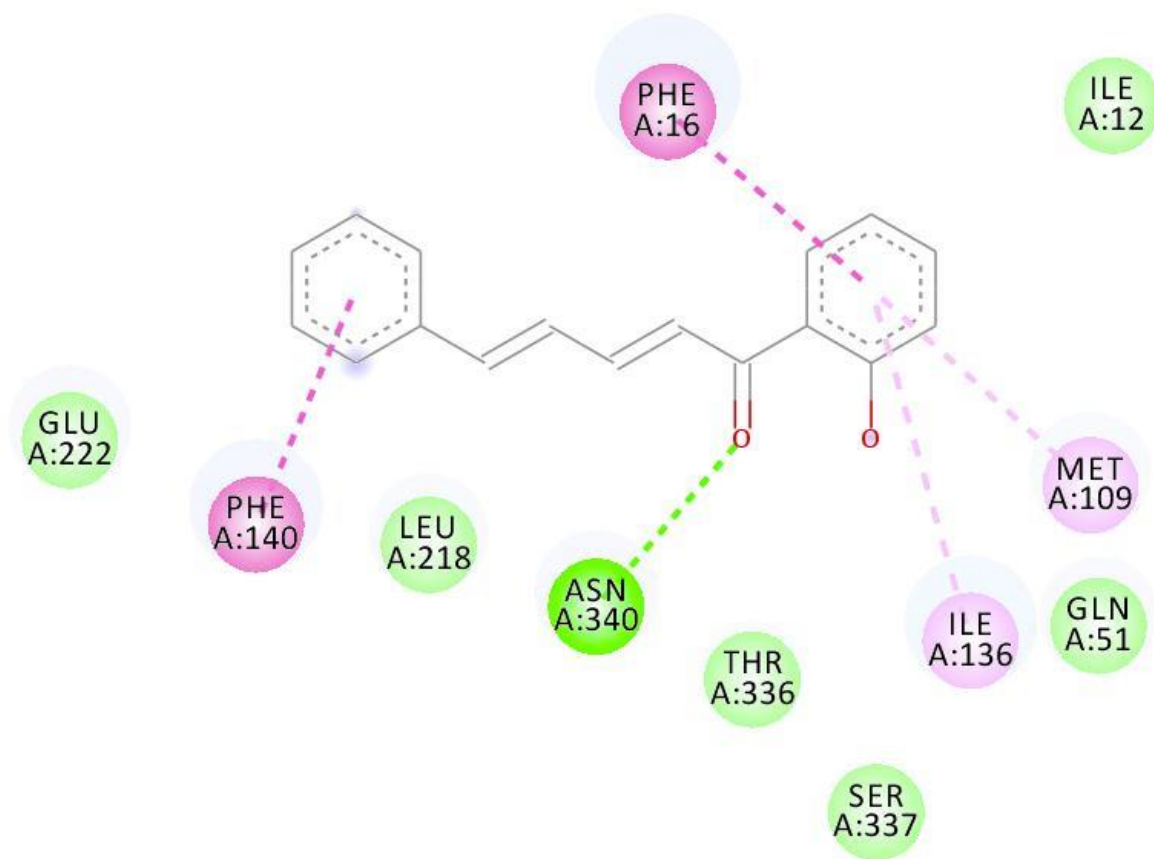
Figure S19. ATR-FTIR spectrum of A6



**Figure S20.** Comparative of the experimental and theoretical ATR-FTIR spectra of the chalcones A1-A6.



**Figure S21.** 2D ligand-protein interaction diagram of A1 and the NorA model



**Interactions**

van der Waals

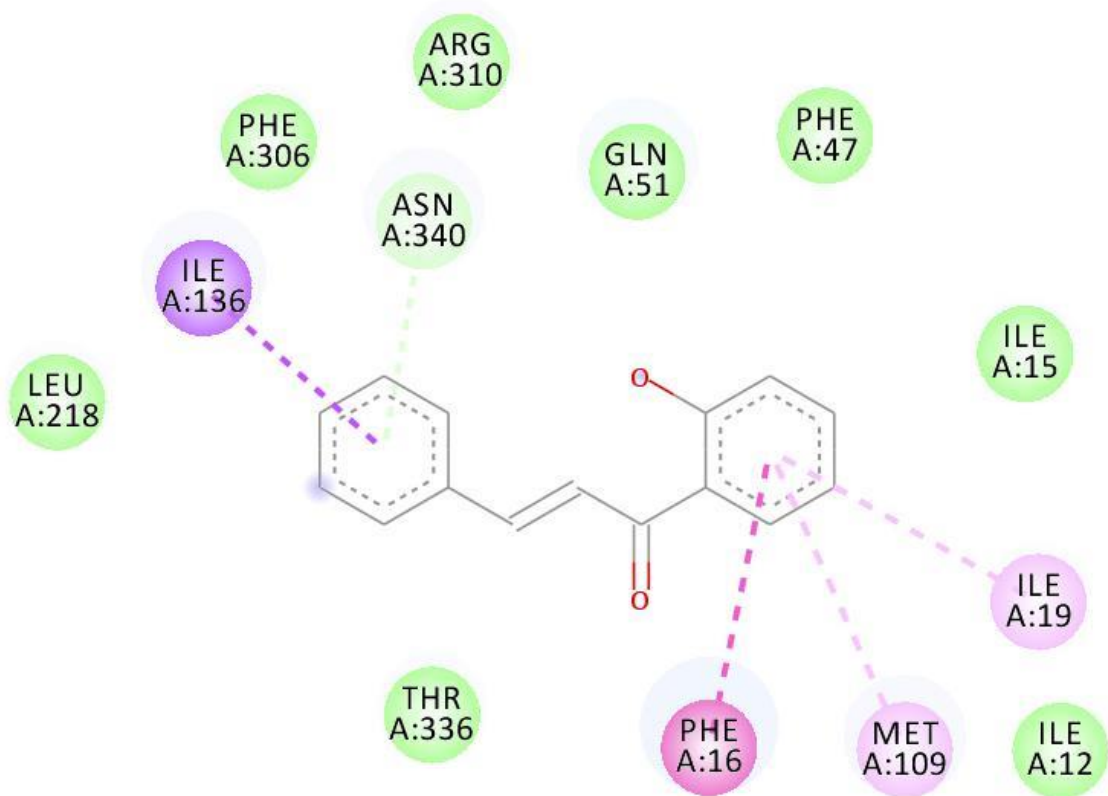
Conventional Hydrogen Bond

Pi-Pi Stacked

Pi-Alkyl

**Figure S22.** 2D ligand-protein interaction diagram of A5 and the NorA model





**Interactions**

- van der Waals
- Pi-Donor Hydrogen Bond
- Pi-Sigma

- Pi-Pi T-shaped
- Pi-Alkyl

**Figure S23.** 2D ligand-protein interaction diagram of A3 and the NorA model

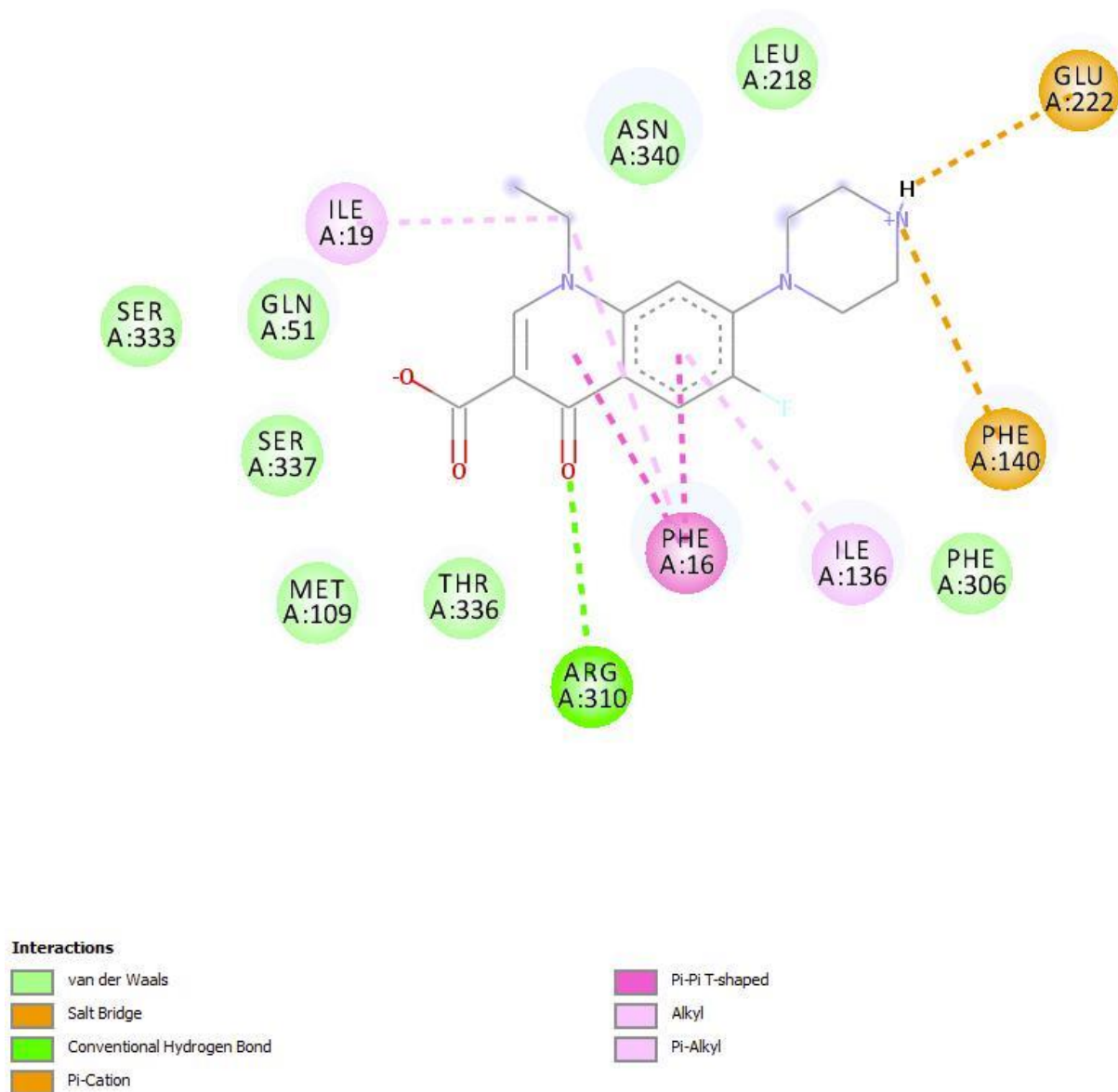


**Figure S24.** 2D ligand-protein interaction diagram of norfloxacin and the NorA model

**Table S1.**  $^1\text{H}$  NMR and  $^{13}\text{C}$  data from chalcone (*E*)-3- (furan-2-yl) -1- (2-hydroxyphenyl) prop-2-en-1-one in  $\text{CDCl}_3$ . The chemical shifts in  $^{\text{TM}}\text{C}$  e  $^{\text{TM}}\text{H}$  are in ppm.

C	$\delta_C$	$\delta_H$
1'	120.1	
2'	163.6	
3'	117.6	7.10 (d, $J = 8.4$ Hz)
4'	131.2	7.54-7.79 (m)
5'	118.8	7.02 (t, $J = 7.5$ Hz)
6'	129.6	8.00 (d, $J = 11.2$ Hz)
C=O	193.4	
1	151.6	
2		
3	112.9	6.85 (d, $J = 3.4$ Hz)
4	117.1	6.62(dd, $J = 8.3; 2.6$ Hz)
5	145.4	7.54-7.79 (m)
C $_{\alpha}$	118.5	7.56 (d, $J = 14.0$ Hz)
C $_{\beta}$	136.1	8.00 (d, $J = 15.6$ Hz)

**Table S2.**  $^1\text{H}$  NMR and  $^{13}\text{C}$  data from chalcone (*E*)-3-(4-chlorophenyl)-1-(2-hydroxyphenyl) prop-2-en-1-one in  $\text{CDCl}_3$ . The chemical shifts in  $^{\text{TM}}\text{C}$  e  $^{\text{TM}}\text{H}$  are in ppm.

C	$\delta_C$	$\delta_H$
1'	120.6	
2'	163.6	
3'	119.9	7.12 (d, $J = 8.3$ Hz)
4'	136.5	7.66-7.73 (m)
5'	118.7	7.03 (t, $J = 7.5$ Hz)
6'	129.6	8.00 (d, $J = 11.2$ Hz)
C=O	193.5	
1	133.2	
2/6	129.4	7.49 (d, $J = 8.5$ Hz)
3/5	129.8	7.58 (d, $J = 8.5$ Hz)
4	136.9	
C $_{\alpha}$	118.9	7.59 (d, $J = 15.5$ Hz)
C $_{\beta}$	143.9	7.95 (d, $J = 15.5$ Hz)

**Table S3.**  $^1\text{H}$  NMR and  $^{13}\text{C}$  data from chalcone (*E*)-1-(2-hydroxyphenyl)-3-phenylprop-2-en-1-one prop-2-en-1-one in  $\text{CDCl}_3$ . The chemical shifts in  $^{\text{TM}}\text{C}$  e  $^{\text{TM}}\text{H}$  are in ppm.

C	$\delta_C$	$\delta_H$
1'	120.2	
2'	163.6	
3'	120.0	7.12 (m)
4'	136.2	7.13 (m)
5'	118.7	7.02 (t, $J = 7.6$ Hz)
6'	130.9	8.02 (d, $J = 8.2$ Hz)
C=O	193.8	

1	134.7	
2/6	129.0	7.72-7.78 (m)
3/5	129.7	7.59-7.61 (m)
4	136.4	7.53 (m)
C <sub>α</sub>	118.9	7.60 (d, <i>J</i> = 15.5 Hz)
C <sub>β</sub>	145.4	8.02 (d, <i>J</i> = 15.5 Hz)

**Table S4.** <sup>1</sup>H NMR and <sup>13</sup>C data from chalcone (*E*)-1-(2-hydroxyphenyl)-3-(4-methoxyphenyl) prop-2-en-1-one in CDCl<sub>3</sub>. The chemical shifts in <sup>TM</sup><sub>C</sub> e <sup>TM</sup><sub>H</sub> are in ppm.

C	δ <sub>C</sub>	δ <sub>H</sub>
1'	120.3	
2'	163.7	
3'	117.8	7.02 (d, <i>J</i> = 8.3 Hz)
4'	136.3	7.49-7.57 (m)
5'	118.7	6.94-7.04 (m)
6'	130.7	7.88-7.93 (m)
C=O	193.8	
1	129.7	
2/6	127.5	7.64 (d, <i>J</i> = 8.7)
3/5	114.7	6.95 (d, <i>J</i> = 8.5)
4	162.2	
C <sub>α</sub>	118.9	7.54 (d, <i>J</i> = 15.5 Hz)
C <sub>β</sub>	145.5	7.91 (d, <i>J</i> = 15.6 Hz)
OCH <sub>3</sub>	55.6	3.87 (s)

**Table S5.** <sup>1</sup>H NMR and <sup>13</sup>C data from chalcone (*2E,4E*)-1-(2-hydroxyphenyl)-5-phenylpenta-2,4-dien-1-one in CDCl<sub>3</sub>. The chemical shifts in <sup>TM</sup><sub>C</sub> e <sup>TM</sup><sub>H</sub> are in ppm.

C	δ <sub>C</sub>	δ <sub>H</sub>
1'	120,2	
2'	163,7	
3'	118,7	7,03 (d, <i>J</i> = 8,5 Hz)
4'	136,1	7,46-7,51 (m)
5'	118,9	6,93 (t, <i>J</i> = 8,1 Hz)
6'	129,6	7,83-7,86 (m)
C=O	193,9	
1	136,4	
2/6	127,6	7,52 (d, <i>J</i> = 7,5 Hz)
3/5	129,6	7,38 (d, <i>J</i> = 7,4 Hz)
4	129,7	7,43 (m)
C <sub>α</sub>	127,3	7,70 (d, <i>J</i> = 14,7 Hz)

C <sub>β</sub>	145,7	7,72 (d, J = 14,1 Hz)
C <sub>α</sub>	127,0	7,37 (d, J = 15,6 Hz)
C <sub>β</sub>	143,1	7,40 (d, J = 14,8 Hz)
C	δ <sub>C</sub>	δ <sub>H</sub>
1'	120.1	
2'	163.8	
3'	118.8	7.03 (d, J = 8.4 Hz)
4'	136.7	7.49 (t, J = 7.1 Hz)
5'	119.1	6.96 (t, J = 8.0 Hz)
6'	129.9	7.91 (d, J = 8.0 Hz)
C=O	193.9	
1	123.0	
2	160.3	
3	116.4	7.62-7.68 (m)
4	130.3	7.39-7.42 (m)
5	124.7	7.21-7.24 (m)
6	130.3	7.15-7.18 (m)
C <sub>α</sub>	124.8	7.77 (d, J = 15.6 Hz)
C <sub>β</sub>	138.4	8.00 (d, J = 15.6 Hz)

**Table S6.** <sup>1</sup>H NMR and <sup>13</sup>C data from chalcone (*E*)-3-(2-fluorophenyl)-1-(2-hydroxyphenyl)prop-2-en-1-one in CDCl<sub>3</sub>. The chemical shifts in <sup>TM</sup><sub>C</sub> e <sup>TM</sup><sub>H</sub> are in ppm.